BRNO UNIVERSITY OF TECHNOLOGY
VYSOKÉ UČENÍ TECHNICKÉ V BRNĚ

FACULTY OF CHEMISTRY
FAKULTA CHEMICKÁ

INSTITUTE OF MATERIALS SCIENCE
ÚSTAV CHEMIE MATERIÁLŮ

MACRO-CONCENTRATED ELEMENTS RECOVERY FROM COAL COMBUSTION PRODUCTS
SEPARACE MAJORITNÍCH PRVKŮ Z VEDLEJŠÍCH ENERGETICKÝCH PRODUKTŮ

DOCTORAL THESIS
DIZERTAČNÍ PRÁCE

AUTHOR
AUTOR PRÁCE
Ing. Michal Marko

SUPERVISOR
ŠKOLITEL
doc. Ing. Tomáš Opravil, Ph.D.

BRNO 2024

BRNO UNIVERSITY OF TECHNOLOGY | FACULTY OF CHEMISTRY

Doctoral Thesis Assignment

Number of thesis:	FCH-DIZ0243/2023	Academic year: 2023/24
Institute	Institute of Materials Science	
Student:	**Ing. Michal Marko**	
Study programme:	Chemistry, Technology and Properties of Materials	
Study field:	Chemistry, Technology and Properties of Materials	
Head of thesis:	**doc. Ing. Tomáš Opravil, Ph.D.**	

Title of Doctoral Thesis:

Macro-concentrated elements recovery from coal combustion products

Doctoral Thesis assignment:

The main goal of this work is to find ways to achieve the maximum efficiency of the process of separating major (macro-concentrated) elements from coal combustion products. This will be achieved by researching the appropriate methods and procedures used in traditional commodity processing industries, such as hydrometallurgical processes. Furthermore, various techniques and possibilities of ash modification, either high-temperature or fluidised-bed ashes, will be explored and clarified to achieve high efficiency in the entire separation process.
The key parameter for assessing the suitability of experimentally designed solutions will be the leachability parameter (dissolution into solution) of aluminum, iron and titanium.

Deadline for Doctoral Thesis delivery: 31. 7. 2024

Doctoral Thesis is necessary to deliver to a secretary of institute in the number of copies defined by the dean. This assignment is part of Doctoral Thesis.

Ing, Michal Marko Student	doc. Ing. Tomáš Opravil, Ph.D. Head of thesis	doc. Ing. František Šoukal, Ph.D.. Head of institute

In Brno, 1. 9. 2023

prof. Ing. Michal Veselý, CSc.
Dean

ABSTRACT

This doctoral thesis focuses on the convergence of two widely debated subjects – the utilisation of secondary raw materials and the availability of appropriate raw materials as a potential material base for the upcoming decades. The study delves into the utilisation of coal combustion products, especially ashes.

As a result of their chemical composition, ashes from coal combustion represent considerable potential in the area of profit, especially aluminium, but also iron and titanium (marked as macro-concentrated elements in this work due to their predominant concentration). Experimental activity has confirmed that to achieve selective leachability of aluminium, iron or titanium, using any one-step direct leaching method is not suitable. Therefore, the input material must now be modified - i.e., chemically activated using high-temperature modification reactions.

Substances containing calcium components, such as calcium carbonate or chloride, have been demonstrated to be effective agents in the modification of fly ash. The use of carbonate alone as a modifying agent has been shown to increase the leachability of Al from high-temperature fly ash by up to 20 times, and the modified material exhibits auto-disintegrating properties. On the other hand, the sequence of modification reactions with calcium chloride results in a further doubling of the effectiveness of Al leaching compared to carbonate one. However, the material activated by chloride does not exhibit auto-disintegrating properties.

Nevertheless, research has demonstrated that the combination of these agents can be utilised concurrently, resulting in an aluminium leachability exceeding 95 % when a proper ratio is maintained, along with auto-disintegration.

Based on the optimization of the modification process, i.e., the ratio and type of modifier, the high-temperature reaction regime and the extraction process using sulphuric acid, a universal method was developed. This method was applied to more than 30 different types of fly ashes with very satisfactory results in the selective leachability of aluminium, iron, and titanium up to 99 %.

KEYWORDS

Raw material base, coal combustion products, fly ash, fly ash utilisation, macro-concentrated elements recovery from fly ash.

ABSTRAKT

Tato dizertační práce je věnována průniku dvou celosvětově diskutovaných témat – využití sekundárních produktů a zajištění vhodných surovin a postupů v nalezení surovinové základny pro následující dekády. Práce se zabývá uplatněním vedlejších energetických produktů, zejména pak popílků.

V důsledku svého chemického složení představují popílky pocházející ze spalování uhlí nemalý potenciál v oblasti zisku zejména hliníku, ale dále i železa a titanu (v této práci díky své převažující koncentraci označeny jako majoritní prvky). Experimentální činnost potvrdila, že k dosažení selektivní vyluhovatelnosti hliníku, železa či titanu není vhodné užití jakékoliv jednokrokové metody přímého loužení. Vstupní materiál je proto nyní nutné modifikovat – tzn. chemicky aktivovat pomocí vysokoteplotních modifikačních reakcí.

Bylo prokázáno, že jako vhodná činidla v modifikaci popílku mohou sloužit látky na bázi vápenatých složek – zejména pak uhličitan či chlorid vápenatý. Užití samotného uhličitanu jako modifikačního činidla představuje zvýšení vyluhovatelnosti hliníku z vysokoteplotních popílků až 20násobně, a modifikovaný materiál jeví schopnost auto-disintegrace Sled modifikačních reakcí s chloridem vápenatým vede k dalšímu násobení efektivity vyluhování hliníku v porovnání s předchozím typem modifikace. Avšak materiál aktivovaný pomocí chloridu pozbývá auto-disintegrační vlastnosti. Bylo prokázáno, že lze obě tato činidla použít dohromady a při vhodném poměru je zachována vysoká míra vyluhovatelnosti hliníku přes 95 %, tak i auto-disintegrace.

Na základě optimalizace procesu modifikace, tedy poměru a typu činidla, režimu vysokoteplotní reakce, procesu extrakce s využitím kyseliny sírové, byla vytvořena univerzální metoda. Ta byla aplikována na více než 30 různých druzích popílků s velm vysokými výsledky vyluhovatelností hliníku, železa i titanu až 99 %.

KLÍČOVÁ SLOVA

Surovinová základna, vedlejší energetické produkty, popílky, využití popílků, zisk majoritních prvků

MARKO, Michal. *Macro-concentrated elements recovery from coal combustion products.* Brno, 2024. Doctoral thesis. Brno University if Technology, Faculty of Chemistry, Institute of Materials Science. Head of thesis doc. Ing. Tomáš Opravil, Ph.D.

DECLARATION

I, the signatory below, affirm that this doctoral thesis has been meticulously crafted solely by my own efforts, drawing from the findings of my personal research. Every reference has been duly acknowledged, with no AI intervention in the content creation process, only for an enhanced English review. This doctoral thesis is the intellectual possession of the author and is under the jurisdiction of the Faculty of Chemistry at Brno University of Technology. Any commercial utilisation must receive authorization from all; the author, the supervisor and the dean of the Faculty of Chemistry.

PROHLÁŠENÍ

Já, níže podepsaný tímto prohlašuji, že uvedenou dizertační práci jsem vypracoval samostatně, pečlivě, čerpáním výsledků z vlastního výzkumu. Všechny použité literární zdroje byly řádně odcitovány a umělá inteligence nebyla použita pro generování jakéhokoli obsahu této práce, pouze pro korekci jazyka. Dizertační práce je z hlediska obsahu majetkem autora a Fakulty chemické VUT v Brně a může být využita ke komerčním účelům jen se souhlasem autora, vedoucího práce a děkana FCH VUT.

.....

Ing. Michal Marko

PODĚKOVÁNÍ

Rád bych tímto poděkoval vedoucímu disertační práce doc. Ing. Tomáši Opravilovi, Ph.D. a školitelům specialistům Ing. Evě Bartoníčkové, Ph.D. a doc. Ing. Františku Šoukalovi, Ph.D. za ochotu, odbornou pomoc při realizaci experimentů, vyhodnocování výsledků a následné interpretace dosažených dat. Dále pak všem pracovníkům Centra materiálového výzkumu za měření pomocí analytických metod. V neposlední řadě však patří dík mojí manželce a celé rodině za to, že mi po celou dobu studia a zejména pak při sepisování práce byli oporou.

CONTENT

1 INTRODUCTION

Coal, a pivotal energy source in human history, has evolved from a heat producer to a key player in electricity generation. Its role in the industrial revolution and the technological advancements of our modern society is undeniable. However, the benefits of coal combustion come with a significant environmental cost. The process generates several by-products, including slag, fly ash, bottom ash, and the more recent energy-gypsum from flue gas desulphurisation.

Ash from coal combustion was traditionally seen as a byproduct with no valuable purpose for an extended period. Nevertheless, during the latter half of the 20th century, there was a concerted push to explore potential applications for this industrial residue, particularly as an additive in various sectors, including cement manufacturing, concrete production, brick making, and the development of refractory materials. This material was also adopted in remedial materials, metallurgy, and road construction, as well as as a raw material for alkaline activation.

In recent years, some scientific research has focused on exploring the potential of utilising fly ash as a source of raw materials, especially for element recovery. Researchers frequently experiment with innovative techniques and strategies to extract valuable and scarce elements that can be utilised in various industrial processes. Connecting the utilisation of fly ash with the search for appropriate raw materials and production methods for future raw material bases could serve as high entropy oxides (catalysts, semiconductors, etc.). This could potentially address the overflowing ash landfills and storage sites while promoting raw material neutrality and self-sufficiency, particularly in the realm of aluminium and, to some extent, in the cases of iron and titanium. Such an approach may yield numerous advantages, such as reducing reliance on raw material imports, enhancing economic efficiency, and contributing to environmental conservation.

This study examines the utilisation of fly ash as a potential source of raw materials, specifically aluminium, titanium, and iron. The research focuses on exploring innovative methods and technologies to efficiently and economically extract these raw materials from fly ash. The objective is to address the issue of coal waste and create new opportunities for acquiring valuable raw materials that can support sustainable development and enhance raw material self-sufficiency. Consequently, this research could significantly contribute to addressing a critical present and future challenge. The findings of this study have the potential to find broad applications in various industries and foster the advancement of novel up-scaling technologies and processes for raw material recovery from waste.

2 THEORETICAL BACKGROUND

The theoretical part of this dissertation thesis delves into secondary energy products as a possible source of raw materials, underscoring the significance of covering subjects like energy origins, combustion methods, flue gas desulphurisation, and other pertinent technologies. These conversations are vital as they directly correlate to the attributes of secondary energy products, their responsiveness, possible uses, and numerous other facets.

The terminology employed in this research pertains to the distribution of element concentrations in the tested samples - macro signifying concentrations exceeding 1 %, and micro representing concentrations under 1 %.

2.1 Energy sources and combustion technology

This section provides a comprehensive analysis of the fundamental raw materials used to generate electricity in the Czech Republic and various other nations worldwide. It also delves into the prevalent combustion techniques and technologies employed in contemporary coal-fired power stations. It is crucial to recognise that the characteristics of the resulting by-products are intricately linked to both the secondary fuel combusted and the specific combustion method utilised.

2.1.1 Coal

Coal combustion, also known as coal firing, is the oldest and most extensively utilised technique for generating electricity. Coal, a fossil fuel, is a heterogeneous, colloidal, solid sedimentary rock originating from converting organic matter through biochemical decomposition. Subsequently, this process was accompanied by the deposition of layers, impeding air access and resulting in charred coal formation. [1, 2]

Regarding energy sources, coal is assigned a value called the combustible fraction. This value is defined as the total amount of all combustible elements present in the coal, which is determined by measuring the weight loss during the complete combustion of a sample. Combustible elements can be categorised into two types: solid and volatile. Natural coal contains both mentioned components, but the solid state is represented in several hundred times higher proportion. Physical and chemical properties, composition and carbon content in coal depend mainly on the time and conditions of the carbonisation process (anthracite 90–95 % C, bituminous/black coal 80–90 % C, sub-bituminous/brown coal 70 % C, lignite 60 % C, peat 50 % C). The quality of coal depends on the content of combustibles, ash, and water. The water content of coal has a direct impact on its calorific value, as it is closely linked to the coal's carbonisation level. Ash-forming materials are of the most significant importance for studying non-combustible residues, of which 95 % are formed by three primary groups of minerals – clays (aluminosilicates), sulfides and carbonates. [2–5] The composition of minerals determines the final properties of produced fly ash (FA). An overview of the most essential minerals occurring together with coal is summarised in tables 1 and 2.

The mines in the Cheb, Sokolov, North Bohemian, and Zittau basins in the Czech Republic are primary sources of brown coal, with significant reserves that have been exploited for decades. The coal extracted from these mines is primarily used by power plants in the Czech Republic to generate electricity and heat for residential and industrial use. The composition of brown coal from these basins typically consists of around 70 % combustibles, 10–15 % water, 5–10 % sulfides and carbonates, and about the same amount of other mineral groups. [1, 4]

Table 1 Overview of the main minerals occurring in coal deposits (part 1.) [1, 6]

Group	Mineral	Chemical composition
Clays	Kaolinite	$Al_2O_3 \cdot 2SiO_2 \cdot H_2O$
	Halloysite	$Al_2O_3 \cdot 2SiO_2 \cdot 4H_2O$
	Illite	$K_2O \cdot 2Al_2O_3 \cdot 6SiO_2 \cdot 2H_2O$
	Montmorillonite	$AlSi_2O_5(OH) \cdot nH_2O$
Sulphides	Pyrite and Marcasite	FeS_2
	Pyrhotine	Fe_5S_6 až $Fe_{16}S_{17}$

Table 2 Overview of the main minerals occurring in coal deposits (part 2.) [1, 6]

Group	Mineral	Chemical composition
Carbonates	Calcite	$CaCO_3$
	Dolomite	$CaMg(CO_3)_2$
	Ankerite	$(Ca,Mg,Fe,Mn)(CO_3)_2$
	Siderite	$FeCO_3$
Halogenides	Halite	NaCl
	Sylvite	KCl
Accessory minerals	Quartz	SiO_2
	Gypsum	$CaSO_4 \cdot 2H_2O$
	Orthoclase	$KAlSi_3O_8$
	Biotite	$K(Mg,Fe)_3(AlSi_3O_{10})(OH)_2$
	Diaspore	$Al_2O_3 \cdot H_2O$
	Cyanite	$Al_2O_3 \cdot SiO_2$
	Apatite	$9CaO \cdot 3P_2O_5 \cdot CaF_2$

2.1.2 Biomass

Another type of fuel used to generate electricity is biomass. Biomass can be defined as a viable option for heating purposes through combustion. Essentially, it refers to solid or liquid organic matter originating from natural sources. This valuable resource can be acquired through intentional production methods or by-products of activities such as forestry, food production, or agricultural processing. [7]

In the power industry, solid biomass is burned mainly for technological reasons, so new combustion boilers do not have to be built completely; existing granulation boilers can be used with slight modification. The thermal utilisation of solid biomass is significantly impacted by the composition of its components, including their physical attributes, such as particle size, bulk

density, moisture content, gross calorific value, and chemical composition. These factors are closely linked to the specific components employed in the process. [8]

Biomass primarily consists of potassium, sulphur, chlorine, and silica as its main elements. Potassium is commonly found in an organic form within biomass, and it undergoes vaporisation and decomposition during combustion. This process leads to oxides, hydroxides, chlorides, and sulfates forming. These substances have low melting points and tend to condense on surfaces such as walls, tubes, and fly ash particles. Consequently, they contribute to the occurrence of slagging and fouling. [8, 9]

In the Czech Republic, like in other European nations, the biomass utilised in power and heating plants consists of a diverse mixture primarily composed of ligno-cellulosic plants. This assortment encompasses woody plants such as trees, shrubs, wood chips, forest waste, cereals like straw, grasses, and a combination of household biowaste. Additionally, small amounts of residues from oleaginous or starch-sugar plants are incorporated. [10]

2.1.3 Conventional combustion technology of raw materials

The combustion/firing of solid fuels in an oxidising atmosphere can be described as a heterogeneous process between the reaction surface of the fuel and the gaseous phase. This process can be defined in a simplified way as an exothermic reaction of carbon with oxygen. In the case of complete combustion, carbon dioxide, water vapour and a large amount of thermal energy are produced. However, coal mined in the mines contains various impurities that cause undesirable products such as sulphur oxides, nitrogen oxides, fly ash and slag. [1, 4]

The treatment of coal prior to combustion can significantly impact the combustion process and technology. Before being fired, the coal undergoes various treatments to enhance its performance. These treatments involve mixing the components of the coal batch with the fuel, grinding it into smaller grains, adjusting the water content, and reducing the levels of mineral substances and pyritic sulphur. These pre-combustion treatments aim to optimise the combustion process and improve the overall efficiency of the technology used. [3–6]

Coal combustion is currently responsible for about 40 % of the electricity production worldwide. Notably, countries like South Africa and China heavily rely on coal combustion, with rates ranging from 75 % to 95 %. On the other hand, European countries use combustion processes to a lesser extent, with a maximum utilisation of 40 %, where coal combustion makes up half of the overall combustion methods. [11, 12]

High-temperature combustion

The classical high-temperature combustion process is based on the firing of lump or granulated fuels. The temperature of the combustion process reaches up to 1,500 °C in the case of the combustion of high-quality and high-calorific coal, 1,000–1,300 °C in the case of alternative fuels and biomass. Based on the equipment construction design equipment, diverse types of combustion systems in basic can be distinguished. [1, 3, 13]

Grate firing.

In grate boilers, lump fuel is burned in a solid layer. Grate firing is the oldest type of classic fireplaces and no new ones are being built for coal combustion nowadays, but they are still in operation. Grate boilers burn lump fuel in a solid layer [13].

The grate is responsible for establishing and sustaining the appropriate thickness and permeability of the fuel layer. It also guarantees the provision of air for ideal combustion and captures solid remnants post-combustion. The fuel within the boiler undergoes distinct stages, including drying, degassing, combustion of volatile combustibles, ignition of the solid combustible layer, combustion of the solid phase, and cooling of solid residues. Combustion in grate boilers occurs in both the layer on the grate (solid carbon) and the area above the fuel layer (emitted volatile combustibles). [13, 14] This process is shown in Fig. 1. Possible constructions of grate boilers are summarised in Fig. 2.

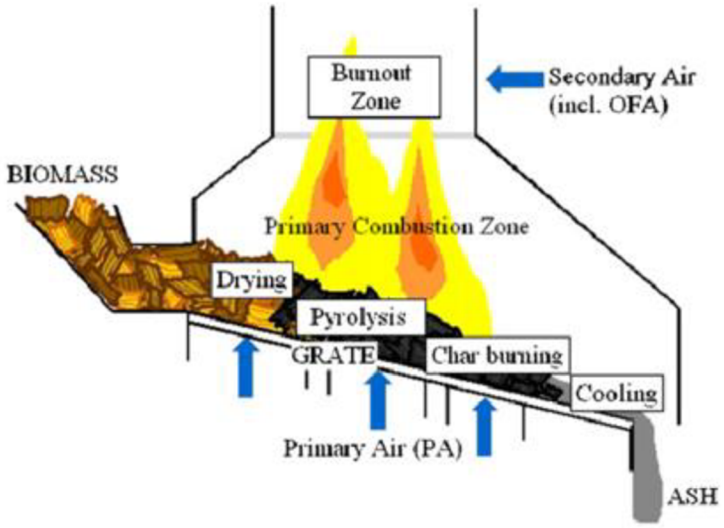

Fig. 1 Stages of fuel combustion in the grate fireplace [14]

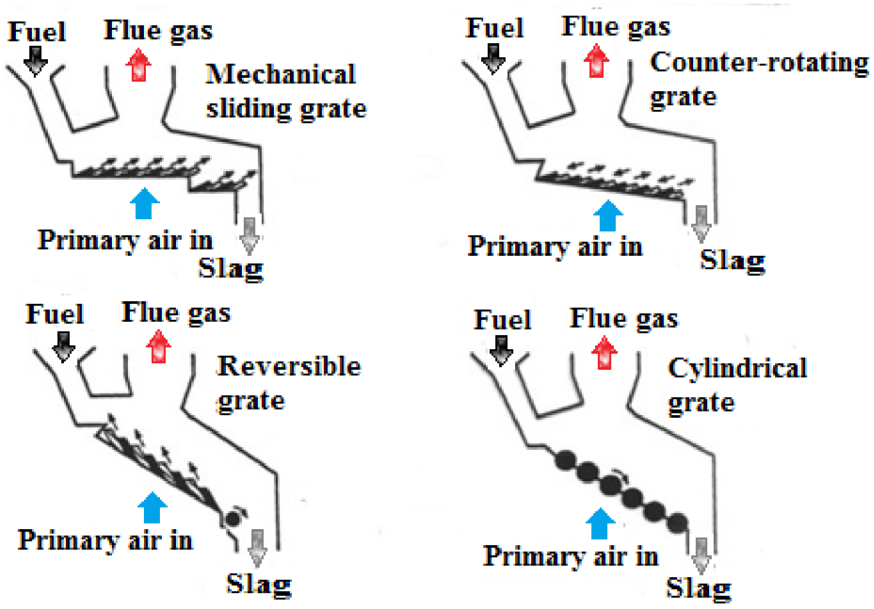

Fig. 2 Grate boilers construction [13]

Pulverised fuel firing

Pulverised coal-fired boilers, also known as powder boilers, are specifically engineered to combust coal powder with a maximum grain size of 1 mm (typically around 100 μm). Grinding the solid fuel significantly enhances the particle's surface area by a factor of 100 to 1,000. These fine fuel grains are then injected with heated combustion air through several burners into the lower part of the furnace. This alteration results in a heightened and more effective combustion process. Consequently, powder boilers exhibit significantly greater efficiency compared to grate systems. However, these devices have a drawback due to their expensive initial cost, which is attributed to the requirement of acquiring grinding equipment for fuel granulometry adjustment. Additionally, they also contribute to a high level of flue gas pollution caused by fly ash, necessitating the use of more advanced electrostatic precipitator technology for separation. From a technological standpoint, two categories of powder boilers can be identified. [15–16]

Granulating boilers are primarily used to burn lesser-value fuels, such as lower-quality bituminous or sub-bituminous coal and biomass. These boilers are designed to not exceed the ash melting point/temperature. Thus, the non-combustible fraction is melted only on the top layer of the particles and gathers into agglomerates. Approximately 10–20 % of the ash accumulates into this product; the rest must be separated in filters. [4, 13, 17]

Powder boilers of the second category operate on the principle of melting. In this particular design, the temperatures of the ash flow are deliberately surpassed to enable its continuous discharge. This construction is suitable only for high-calorie fuels – bituminous coal and anthracite. The smelting product is boiler (power plant) slag, formed by melting 40–70 % of the generated fly ash. [13, 16, 18]

2.1.4 Fluidised-bed combustion

Fluidised-bed boilers burn fuels in a fluidised-bed and can be used to burn a wide range of fuels, including those with low calorific value and also fuels with large amounts of quenching compounds (lower quality sub-bituminous coal, lignite, biomass). The fluidised-bed could be described as a dispersed system resulting from gas flow through a layer of particles loosely poured onto the porous bottom (fluidised-bed). Fluidised-bed combustion provides several advantages – the ability to burn fuel directly with the desulphurisation agent in the same space while achieving optimal desulphurisation efficiency. Furthermore, the lower combustion temperature (700–900 °C) prevents the sintering of ash residues, and at the same time, a significant reduction of NO_x in the flue gas in comparison with classical combustion is achieved. Fluidisation technology can be used not only in the combustion process but also in several processes where it is necessary to ensure contact between solids and gases (absorbers, catalysts, etc.). [13, 19, 20]

In practice, it is possible to come into contact with boilers burning fuel in a stationary or circulating fluidised-bed. In the first type of combustion equipment, a fluidised-bed with a constant height is formed. Spent fuel particles (fly ash) are lighter and are carried out from the base level above, until they exceed the flight limit and are carried together with the flue gases to the filters. Some particles may agglomerate, gradually falling below the bed, from where they are then discharged. [13, 21]

In circulating fluidised-bed boilers, the particles are constantly above the flight threshold and are separated by a cyclone system and returned to the combustion part of the boiler. In practice, one fuel particle passes through the entire system 10–15 times before it burns out and is trapped on the last filter. The higher number of cycles has a positive effect on better combustion as well as for more efficient desulphurisation and reduction of NO_x content. Circulating bed boilers are, therefore, generally more efficient and also have lower temperature differences than boilers with a stationary layer. The combustion efficiency in these boilers varies around 95 %. [13, 20, 21]

The fluidised-bed combustion diagram is shown in the following figure:

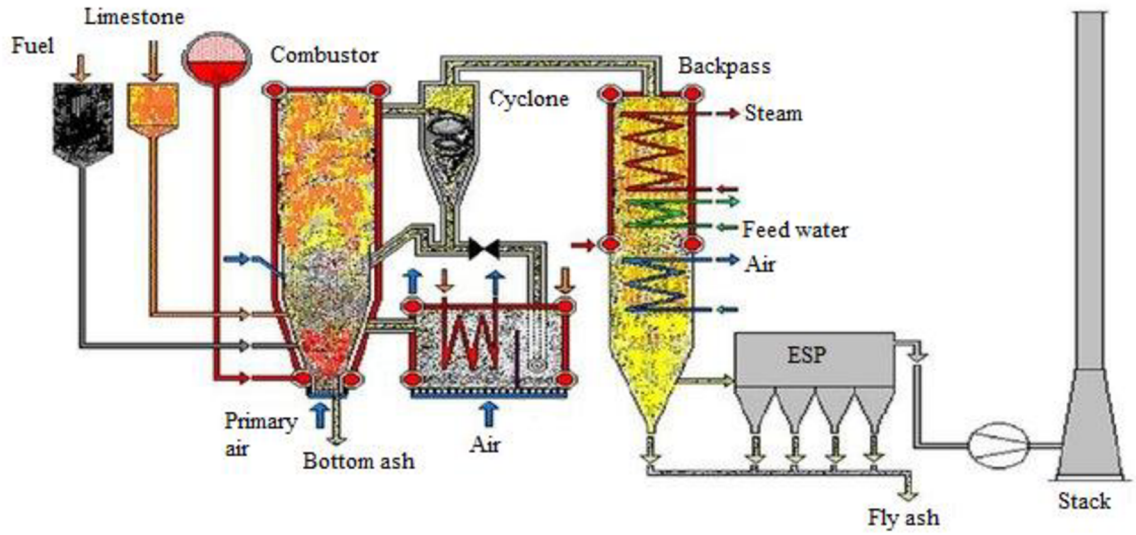

Fig. 3 Fluidised-bed combustion scheme [22]

2.1.5 Flue gas desulphurisation

The presence of elevated levels of sulphur, esp. in lignite fuels, requires the implementation of desulphurisation techniques during combustion processes. Desulphurisation can be achieved through both physical and chemical means, with chemical processes being the most prevalent. Among these, methods involving the reaction of sulphur dioxide with lime or limestone are commonly utilised. Flue gas desulphurisation methods are typically categorised into two main types based on the environment in which they occur – dry and wet methods. [13, 23]

Dry methods

In the process of dry flue gas desulphurisation, the interaction between gaseous sulphur dioxide and a solid sorbent occurs. This sorbent can be introduced into the fuel supply, combustion chamber, or flue in a controlled manner. Subsequently, the flue gas desulphurisation proceeds in accordance with specific chemical equations. (1)–(3).

$$CaCO_3 \xrightarrow{750\ °C} CaO + CO_2, \tag{1}$$

$$CaO + SO_2 \longrightarrow CaSO_3, \tag{2}$$

$$CaSO_3 + {}^1/_2\, O_2 \longrightarrow CaSO_4. \tag{3}$$

This reaction is exclusively conducted under specific circumstances. These circumstances entail the utilisation of desulphurisation agent particles with a remarkably small size and their efficient dispersion throughout the entire combustion area. Since the desulphurisation product is generated on the surface of the particles, it forms a diffusion barrier that hinders any subsequent reaction within the particles. [24, 25]

The utilisation of this method is limited to combustion processes with temperatures not exceeding 1,000 °C due to the thermal stability of the resulting anhydrite. Beyond this temperature threshold, the anhydrite undergoes decomposition, leading to the release of SO_2. Due to this limitation, the dry flue gas desulphurisation method is used exclusively for fluidised-

bed boilers. To achieve optimum process efficiency, it is necessary to dose the desulphurisation agent in a 20 % excess of an equimolar amount of sulphur dioxide. [26]

Wet methods

Wet techniques are the predominant methods utilised, constituting roughly 80% of desulphurisation tools. Wet-cantered apparatuses are situated adjacent to sizable boilers, boasting elevated efficiency and dependability, minimal operational expenses, and straightforward handling. The desulphurisation process occurs external to the combustion chamber and the flue, occurring right before the flue gases are discharged into the chimney, and is founded on the interaction between SO_2 and limewater (less frequently) or a limestone-water suspension, as delineated in chemical reactions. (4)–(8).

$$Ca(OH)_2 + SO_2 \longrightarrow CaSO_3 + H_2O, \tag{4}$$

$$CaSO_3 + 2H_2O + {}^1/_2\, O_2 \longrightarrow CaSO_4 \cdot 2H_2O, \tag{5}$$

$$CaCO_3 + SO_2 + H_2O \longrightarrow Ca(HSO_3)_2 + CO_2, \tag{6}$$

$$Ca(HSO_3)_2 + {}^1/_2\, O_2 + 2H_2O \longrightarrow CaSO_4 \cdot 2H_2O + H_2SO_3, \tag{7}$$

$$Ca^{2+} + HSO_3{}^- + OH^- + H_2O + {}^1/_2\, O_2 \longrightarrow CaSO_4 \cdot 2H_2O. \tag{8}$$

In order of the described principle to work successfully, it is necessary to maintain an acidic pH scale in the range of 3.5–5.0 in the aqueous suspension of the desulphurisation plant. The resulting product of desulphurisation – energy-gypsum precipitated from solution and is further processed in various construction industry branches. [26–28]

The device is designed chiefly counter currently, where the flue gases from the separators are blown from below into the layer of medium, which is added by showering from above, as described in Fig. 4. [29]

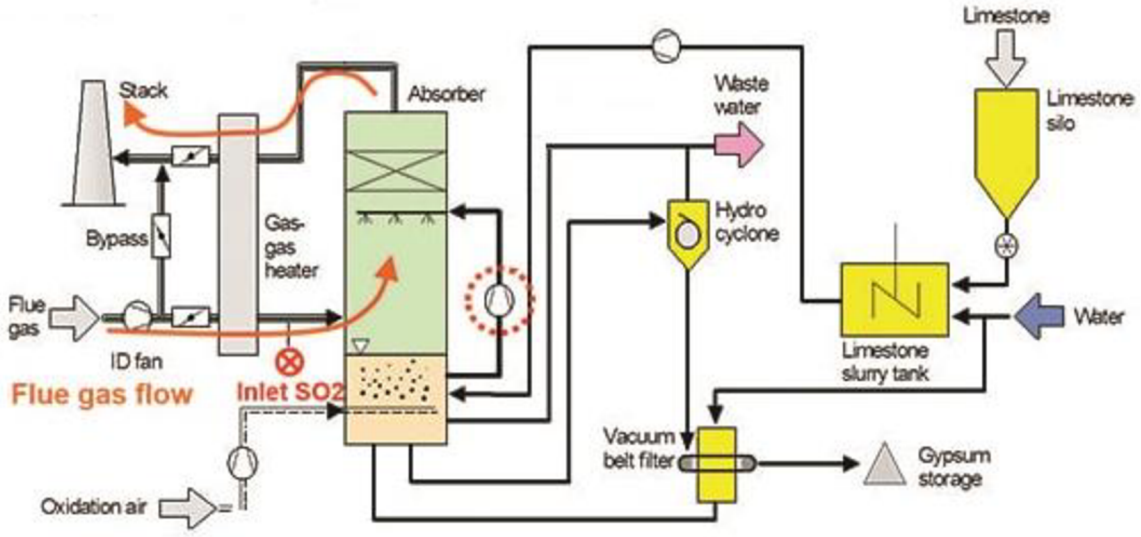

Fig. 4 Wet limestone scrubbing flue gas desulphurisation scheme [29]

2.1.6 Flue gas denitrification

The combustion of coal results in the production of flue gas, which contains various nitrogenous gases, commonly referred to as NO_x. The presence of NO_x in the environment and the air poses a significant threat to life. To address this issue, the resulting flue gases undergo denitrification. In the majority of thermal power plants and heating plants, denitrification is achieved through a method known as selective non-catalytic reduction (SNCR). This method offers a more straightforward and more cost-effective approach to reducing the concentration of NO_x in the flue gas. There are three primary options for SNCR, which involve reacting with an aqueous solution of ammonia, urea, or the cyanourea method, as described by the following equations (9)–(10):

$$4NH_4OH + 4NO + O_2 \longrightarrow 4N_2 + 10H_2O, \tag{9}$$

$$NH_2CONH_2 + 2NO + {}^1\!/_2\, O_2 \longrightarrow 2N_2 + 2H_2O + CO_2. \tag{10}$$

Effective regulation of this reaction necessitates careful monitoring of both temperature and oxygen levels in the flue gas, with the most favourable efficiency observed within the temperature range of 760 to 1,050 °C. However, at higher temperatures and increased oxygen levels, the activation of reaction (11) in the system leads to an undesirable consequence of elevated NO_x content in the flue gas. [30]

$$4NH_3 + 5O_2 \longrightarrow 4NO + 6H_2O. \tag{11}$$

As a consequence of flue gas denitrification through the use of SNCR, the characteristics of the generated CCPs are altered, primarily due to a direct chemical reaction or adsorption on ammonia on their surface. This leads to the presence of ammonia in the resulting FA, with levels reaching up to 1,000 ppm. Subsequently, ammonia, known as ammonium slip, may be released from FA during its use in the concrete industry. Another impact, particularly on HTFA, is observed in its particle morphology, as FA following SNCR exhibits variances in shape, such as reduced sphericity, potential partial disintegration of particles, or cracking of their surfaces. [31, 32]

2.2 Coal combustion products

In addition to the heat obtained by burning fossil or alternative fuels, a relatively large number of secondary materials are produced – non-combustible components, fuel treatment products, and desulphurisation of combustion equipment. The Czech Republic alone produces approximately 14 million tons of these energy by-products per year, of which about 10 million tons of fly ash. The EU's annual production is more than 100 million metric tons. Worldwide, a year production of FA reaches 500 mil tons and 280 mil tons of other CCPs, such as flue gas desulphurisation products, slag, etc. [33, 34]

2.2.1 Fly ash

In general, fly ash is the primary and, consequently, the most extensively distributed and manufactured secondary energy by-product/coal combustion product (CCP). Very simply, fly ash can be defined as an inorganic solid-state non-combustible product of the combustion process which is captured from flue gases in mechanical or electrical separators. In the field of real estate, the definition of fly ash becomes more complex. Fly ash can be differentiated based on the combustion processes into classical types, including *high-temperature* and *fluidised-bed* fly ash, which can be further categorised as fly ash, boiler slag, or cinder. To ensure a comprehensive depiction of ash, it is imperative to acknowledge that certain variants, particularly fluidised-bed ash, encompass diverse byproducts resulting from desulphurisation and denitrification procedures alongside the uncombusted fraction of fuel and other compounds. Generated by the technology of combustion, flue gas cleaning or storage. It is usually a relatively fine (3–200 μm) powder material, in colour with shades of brown to dark grey. The morphology and chemical composition depend on the type of coal and the type and design of the combustion device, desulphurisation and denitrification process, storage, etc. [1, 35]

Physical properties

The fly ash is made up of very fine, mostly spherical particles. The particle size depends on the type and fineness of the fuel burned. Depending on the type of combustion process, up to 30 FA particles can be formed from each fuel grain. The grain size of fly ash could be pretty diverse – most particle size lies in the 1–150 μm range. Moreover, FA generally also contains sub-micron particles and even particle clusters – cenospheres and unburned fuel residues can be up to 300–500 μm in size. These agglomerates occur, for example, due to exceeding the flow temperature. Thus, the glass melts on the surface of the grains and joins them after subsequent cooling. Another mechanism of formation of these aggregates may be the consequence of flue gas desulphurisation (bonding with the emerging energy-gypsum) or deposition in waste ponds. [36–38]

The specific surface area of the particles is related to the particle size of the fuel and the type of combustion, and it reaches about 400–700 $m^2 \cdot kg^{-1}$ (Blaine), 500–9,000 $m^2 \cdot kg^{-1}$ (BET). Due to fuel granulometry, fluidised-bed fly ash has a larger surface area than high-temperature

combustion residues. The size of the specific surface area also depends on the amount of unburnable content. In the case of alternative fuels and biomass, the raw material is much more porous than the resulting fly ash. [39, 40]

High-temperature fly ash (HTFA), especially, is characterised by its spherical particles with a minimum of pores coated with glass. In contrast, fluidised-bed filter ash (FFA) forms irregular shape particles with a significant pore content and a rugged surface. The ash grains can be hollow or full of smaller grains. [41]

Examples of the morphology and differences between high-temperature and fluidised-bed ash observed via scanning electron microscope are shown in the images in Fig. 5.

a b

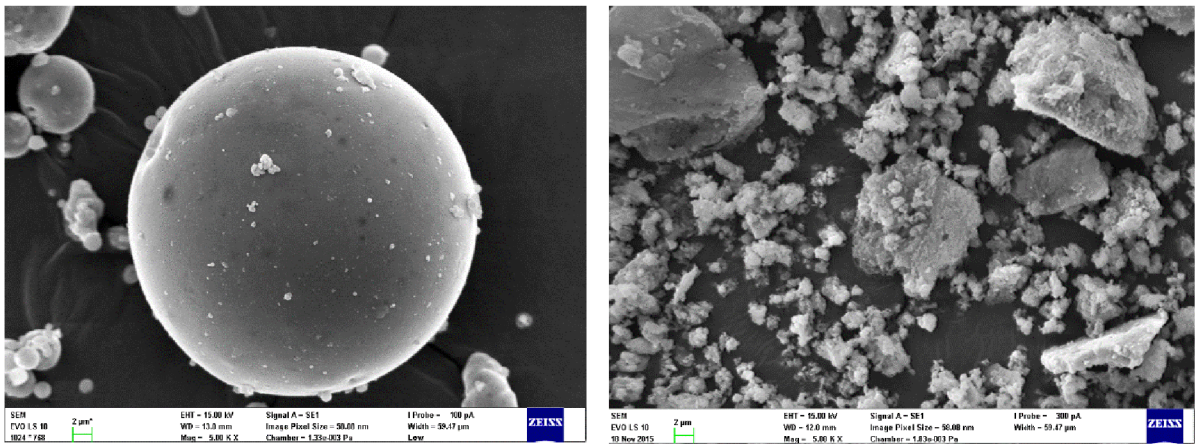

Fig. 5 Image of HTFA grain (a) and FFA (b) morphology

The granularity of fly ash is one of the main factors influencing the majority of physical and chemical properties – density, specific surface area, susceptibility, etc. The density of fly ash is in the range of 1,900–2,600 kg·m^{-3}, for high-temperature combustion fly ash the average is around 2,200 kg·m^{-3}, and for fluidised-bed ash it is around 2,600 kg·m^{-3}. The bulk density of these materials varies in the range of 500–1,000 kg·m^{-3}, most often around 750 kg·m^{-3}. [1, 38–41]

Chemical properties

The chemical nature of the burned fuels and possible chemical reactions during combustion gives the chemical composition of fly ash. The diversity of the phase composition and the content of the amorphous, sometimes called glassy, phase arises due to the passage of particles through different oxidation and reduction zones and the course of melting, agglomeration, condensation and sublimation processes. However, the particles pass through the high-temperature zone only briefly, so melting occurs only on their surface. [1, 42]

The approximate chemical composition of fly ash from the production of the Czech power plants adjusted to oxide form (determined by XRF) is summarised in tables 4–5.

Table 3 Composition of sub-bituminous coal FA from the Czech Republic (major elements) [43]

Type of FA	*Chemical content (wt. %)*				
	SiO_2	**Al_2O_3**	**Fe_2O_3**	**TiO_2**	**CaO**
High-temperature	45.8–54.2	20.3–33.1	4.7–19.6	1.3–3.8	0.8–10.0
Fluidised-bed filter	29.1–33.9	16.3–22.4	7.2–8.1	1.3–5.4	22.8–32.4
Fluidised-bed bottom	30.2–33.5	15.1–22.2	3.5–7.3	1.2–5.5	25.5–29.1

Table 4 Composition of sub-bituminous coal FA from the Czech Republic (minor elements) [43]

Type of FA	*Chemical content (wt. %)*				
	MgO	**K_2O**	**Na_2O**	**SO_3**	**P_2O_5**
High-temperature	0.6–1.3	1.1–2.7	0.3–1.3	0.2–2.9	0.13–0.32
Fluidised-bed filter	0.9–1.0	0.7–1.4	0.4–0.7	5.2–8.8	0.19–0.31
Fluidised-bed bottom	0.5–0.8	0.7–1.6	0.2–0.3	7.8–16.1	0.14–0.26

As can be seen from the results in the tables above, the main difference in chemical composition between HTFA and FBA is appreciable in the content of CaO and SO_3, which corresponds to the sum of the amount of desulphurisation product and the unreacted proportion of lime. Fly ash with a lower calcium content (high-temperature) usually achieves lower loss on ignition compared to fluidised-bed combustion residues. [44] This difference may be due to the small amount of unburnable content, but the reactions occurring during the annealing have the largest share in the loss. In the case of fluidised-bed ash, the excess limestone is decomposed during ignition and, as well as the clay minerals and gypsum that are present too. [45–47]

The crystallisation and the formation of the amorphous phase influence the mineralogical composition of fly ash. The quantity of the crystalline phase is closely linked to the presence of ferric, aluminium and other metal components, as well as the alkali content in the fly ash. On the other hand, the amount of amorphous phase is determined by the overall content of glass-forming components, with SiO_2 being the primary component. Three different types of particles can be distinguished in the residue. The first type, referred to as type A, is composed of unburned coal particles, also called black carbon particles. These type A particles usually account for approx. 2–5 wt. % of the fly ash and give it its characteristic grey colour. Type B particles are formed through a chemical reaction that occurs during the combustion process, thereby giving rise to various crystalline or amorphous phases. On the other hand, type C particles are those that have experienced a chemical transformation due to their storage, such as surface carbonation, hydration, and other similar processes. [48]

Another significant difference between high-temperature and fluidised-bed bed fly ash occurs in the mineralogical composition. More stable minerals and possibly high-temperature modifications are formed at high-temperature FA. According to the calcium content, HTFA can be divided into two groups. The low-calcium group contains crystalline minerals such as β-quartz SiO_2, mullite $Al_6Si_2O_{13}$, silimanite Al_2SiO_5, hematite Fe_2O_3 a magnetite Fe_3O_4. The

high-calcium group contains β-quartz and cristobalite SiO_2, tricalcium aluminate $Ca_3Al_2O_6$, aluminosulfate $Ca_4Al_6SO_3O_{13}$, anhydrite $CaSO_4$, free lime CaO, periclase MgO, calcite $CaCO_3$, siderite $FeCO_3$ and others. [45, 49, 50]

On the other hand, FBA is characterised by the presence of $CaSO_4$ anhydrite, unreacted free lime CaO and undecomposed calcite $CaCO_3$ due to flue gas desulphurisation technology. Furthermore, fluidised-bedashes contain quartz SiO_2, hematite Fe_2O_3, magnetite Fe_3O_4, albite $NaAlSi_3O_8$, anatase TiO_2, gehlenite $Ca_2Al[AlSiO_7]$ and others. Long-term storage can hydrate the fly ash with atmospheric moisture to $Ca(OH)_2$ portlandite. Under particular circumstances like prolonged storage at significant depths within the landfill under increased temperatures, the formation of somewhat surprising by-products like ettringite. $Ca_6Al_2(SO_4)_2(OH)_{12}\cdot 26H_2O$ or tobermorite $Ca_3Si_6O_{16}(OH)_2\cdot 2H_2O$ could take place. [46, 49, 50]

Pozzolanic activity of fly ash

Pozzolans are refined natural or synthetic materials that consist of active silica and alumina but lack the capacity for any hydraulic reaction. Combined with calcium hydroxide and water, they undergo a chemical reaction (12) to produce insoluble compounds with cementitious characteristics. The pozzolanic reaction primarily occurs due to the presence of amorphous silica and alumina components. The pozzolanic activity of fly ash is defined in terms of the reactions of its main components; SiO_2 and $A1_2O_3$ with $Ca(OH)_2$ to form CSH and CAH phases, as shown in more detail in Fig. 6.

$$\left|\begin{matrix}SiO_2\\Al_2O_3\end{matrix}\right| (\text{active}) + Ca(OH)_2 \xrightarrow{H_2O} \left|\begin{matrix}C-S-H\\C-A-S-H\\C_4AH_{13}\\C_2AH_8\\C_3AS_3-C_3AH_6\end{matrix}\right|. \qquad (12)$$

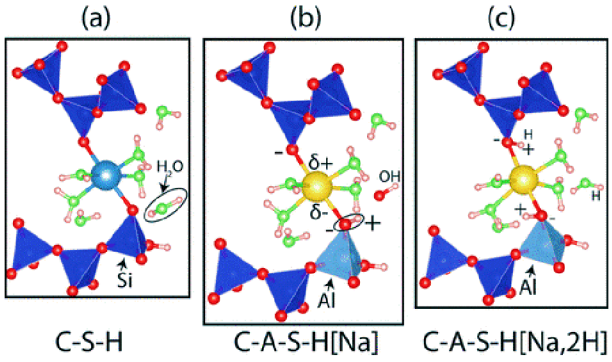

Fig. 6 Formation of CSH and CASH gel; taken from [51]

Naturally occurring pozzolans are mostly volcanic ashes in the form of solidified rocks, e.g., tuff. Fine grinding of tuff produces a long-used material called trass. One of the most important pozzolanic materials from synthetic production is fly ash. [51– 53]

The fly ash acquires its pozzolanic properties because the high-calcium porous solution of the fresh binder putty disrupts the surface of the glassy particles from which silica and alumina are gradually leached. These components then form C-S-H gel-type hydration products similar

to Portland cement hydration. [54, 55] Pozzolanic activity of fly ash occurs in the additive and production of mixed cements or alkali-activated systems. These applications will be described later in other chapters.

2.2.2 Energy-gypsum

Energy-gypsum or flue gas-gypsum is another CCP generated through the wet process of flue gas desulphurisation. This particular type of gypsum is commonly associated with the traditional combustion of coal in power plants. A comprehensive explanation of the process responsible for forming energy-gypsum can be found in chapter 2.1.5. Flue gas-gypsum is known for its exceptional purity and high dihydrate content, distinguishing it from natural gypsum. While natural gypsum is commonly found in a dry, crushed form, energy-gypsum is created through desulphurisation processes using the wet limestone washing method, resulting in a moist, fine-grained powder with a surface moisture content ranging from 8 % to 12 %. The primary distinctions lie in the physical characteristics such as grain size, crystal structure, and bulk density. Flue gas-gypsum predominantly consists of very fine β-hemihydrate. Energy-gypsum may contain other impurities that are not commonly found in natural gypsum. These are mainly chlorides, fluorides, soluble Mg and Na salts, and unreacted $CaCO_3$. [56, 57]

Energy-gypsum is primarily utilised in the cement sector as an additive, constituting approximately 5 wt. %, to effectively control the initial solidification process of cement. To cater to this specific application, energy-gypsum must be in a lump form, necessitating prior briquetting. Besides its role in regulating cement setting, energy-gypsum finds industrial applications in manufacturing diverse gypsum and plaster variants, drywall or gypsum fibre boards, and highly malleable coatings. [58, 59]

The conditions of the relevant standard are placed on the energy-gypsum for the production of gypsum products and plasters. Table 5 summarises the list of allowable values for these applications.

Table 5 Requirements for gypsum products [59]

Determined component	Permissible value
$CaSO_4 \cdot 2H_2O$	min. 95 wt. %
Moisture	max. 10 wt. %.
MgO	0.1
Cl^-	0.01
Na_2O	0.06 wt. %.
SO_2	0.25 wt. %.
pH	5–9
Colour	90 % whiteness
Odor	neutral
Toxicity	none

2.3 The present and prospective uses of fly ash

Fly ash is classified as one of the commonly produced by-products, with attempts to utilise it commencing in the 1950s. The chemical composition of fly ash is notably diverse, contingent upon the coal type combusted and the desulphurisation technique employed. Discrepancies in mineral composition, particle size distribution, specific surface area, and bulk density arise from the various combustion plant configurations and temperatures utilised. This extensive range of characteristics of fly ash poses challenges in establishing a universal method of application. Currently, specific varieties of fly ash are integrated into construction materials, adsorbents, serve as fillers, among other functions. [1, 46].

Although the effort to use fly ash worldwide is increasing, approximately 50 % of ash production is currently processed in Europe and the North American continent, Asia and South America reach up to 30 % ash processing capacity, and Africa around 20 %. [60–63] for this reason, a large amount of ash is still deposited permanently. Despite the effort to achieve carbon neutrality and not to produce other CCP, there is still a vast mass of materials in these landfills that would be suitable to be implemented or evaluated by some suitable and valuable process.

The central part of used FA is as a supplement material in cement and concrete production, structural fills, solidification, etc. [61] The share of current applications for the use of fly ash is summarised in the following chart:

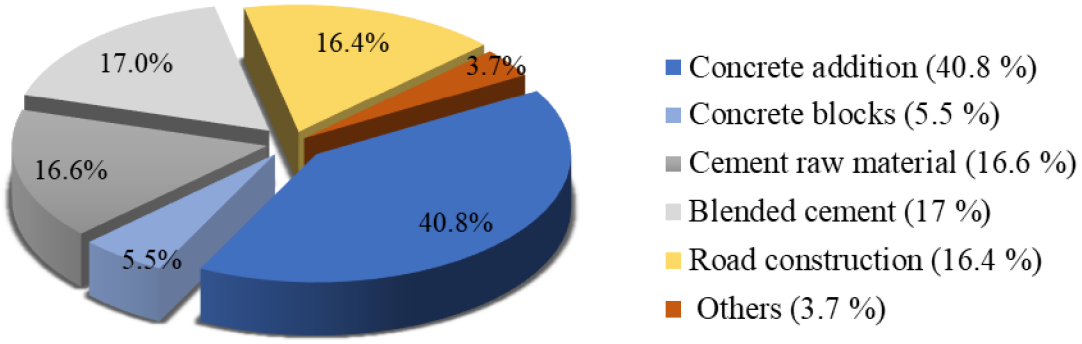

Fig. 7 Current use of fly ash in the Europe [61]

2.3.1 Cement and supplementary cementitious materials

The major part of utilised fly ash (over 80 %) has been applied in concrete and other building materials from mixed cements, supplementary cementitious material, and road base material to special applications such as non-freezing surfaces of highways and airport runways or in the production of antibacterial screeds for water management applications. [46, 64]

2.3.2 Cement and concrete addition

In the Czech Republic and other European nations, the utilisation of fly ash in cement is governed by the ČSN EN 197–1 standard. As per this standard, "FA for use in concrete" is denoted as a finely ground substance comprising predominantly of spherical particles produced through the combustion of anthracite, bituminous, or sub-bituminous coal. FA for use in concrete exhibits pozzolanic characteristics, with a minimum of 25 % active SiO_2, a maximum of 10 % reactive lime content, and a maximum loss on ignition of 7 %. [64, 65]

The addition of fly ash to cement has a positive effect on, for example, the liquefaction of cement or concrete slurry. This property is carried out due to the spherical grains of the high-temperature fly ash, which create a ball-bearing effect in the mixture and facilitate the rearrangement of the grains of the mixture. This consequence makes it possible to reduce the water coefficient by 0.03–0.07 while achieving the same fluidity. Therefore, the addition of fly ash has a positive effect on the rheological properties of the slurry due to the increase in flowability – making pouring, pumping, transport and compaction of the final product easier. [64]

The pozzolanic activity of fly ash in traditional Portland cement systems causes the active SiO_2 and Al_2O_3 content to react with the by-product of cement hydration, $Ca(OH)_2$ – portlandite. This chemical reaction results in a reduction of portlandite content within the cement mixture an increase in the density of the hydration products, consequently enhancing the durability of the final composite to the corrosive environment (weak acid solutions, increased chlorides and sulfates concentration, alkalis, as well as carbonation) and, with optimal addition, it brings a positive effect on increasing final mechanical properties, such as compressive and flexural strength of concrete systems. [46, 64, 66]

2.3.3 Low-energy cement production

Various research groups have explored the potential of utilising HTFA and FBA in the manufacturing process of belitic cement as a means to reduce carbon dioxide emissions associated with cement production. Belite, which is the predominant phase in traditional Portland cement, plays a crucial role in providing long-term strength despite its slow hydration process within the first few days to weeks. Incorporating hydration accelerators, typically calcium chloride-based, in these systems has been found to enhance initial strengths and expedite the hydration process. Chemically, belite is primarily composed of dicalcium silicate (C_2S). [67]

Belitic cements are mainly used in poor and developing countries. Belite is produced by the clinkerization process in a solid state at a temperature over 800 °C in a rotary kiln. To form belite, the reaction of two molar equivalents of free lime with one molar silica equivalent is needed. Belite has five allotropic forms: α, α^H, α^L, β and γ. Only αs and β modifications mentioned show hydraulic activity. For this reason, the metastable phase β should be rapidly cooled below 500 °C. [67, 68]

Belitic cement production, which relies on coal combustion products, typically involves the utilisation of both high-temperature and fluidised-bed fly ash. Specifically, low-calcium fly ash and high-calcium fly ash are combined to create the desired mixture. The starting material consists of fly ash with a higher concentration of reactive calcium. Energy-gypsum is commonly employed to adjust the composition, particularly the enrichment of the mixture with reactive calcium oxide (CaO). Subsequently, the appropriate mixture is heated in a rotary or shaft furnace, reaching temperatures of 1,000–1,200 °C. The composition of these cements varies considerably. Thus, the quality does not appear to be suitable for applications in civil engineering. [69–71]

2.3.4 Alkali-activated systems

The utilisation of by-products through alkali activation has emerged as a significant field of study due to the potential to produce cost-effective and environmentally friendly cement-like construction materials. Alkali activation of waste materials involves a chemical process that enables the conversion of glassy structures into highly compact and well-cemented composites. Fly ash, containing SiO_2 and Al_2O_3, has also been found to be applicable in contemporary cement-less hybrid binders based on alkali-activated systems. These binders primarily consist of alkali-activatable substances, such as latent hydraulic pozzolans (e.g., fly ash, slag, metakaolin) and alkaline activators (e.g., hydroxide solutions, strong and weak acids salts, etc.). The treatment of fly ash or blast furnace slag with highly alkaline mixtures in an aqueous medium triggers the activation of these raw materials, resulting in the formation of hydration products similar to those formed during the hydration of Portland cement. Nevertheless, this process's precise reaction mechanism has yet to be fully elucidated. [72–74]

Hydration products of alkali-activated fly ash-based systems could be crystalline hydrosodalite $Na_6[AlSiO_4]_6 \cdot 8H_2O$ or amorphous (more common) sodalite $Na_6[AlSiO_4]$, or herschlite. It is thus the formation of (C)NS(A)H gel in the system $Na_2O–Al_2O_3–SiO_2–H_2O$ and $Na_2O–CaO–Al_2O_3–SiO_2–H_2O$. These materials often achieve high initial strengths (up to 40 MPa after 24 hours). In addition, they are more environmentally friendly, as they can be largely based on the application of by-products from production (fly ash, slag, waste sludge from alkaline production), which ultimately means a reduction in CO_2 production by about 60–65 % per kilogram in comparison to Portland cement production. [73–75]

Various authors dealing with this issue have concluded that geopolymers based on FA can achieve very good mechanical properties, durability, are easy to manufacture and storage. FA pozzolanic activity and partial latent hydraulicity are evaluated particularly positively. However, later research has shown a relatively fundamental difficulty of these materials, namely their large shrinkage over time, which often leads to the disintegration of the sample. [72, 74, 75]

2.3.5 Light-weight filler

Fly ash primarily consists of hollow particles, leading to a reduction in bulk density. These hollow, inert, spherical particles, known as FA cenospheres, are enveloped by a glassy phase and are predominantly composed of silica and alumina. The chemical constituents present in cenospheres vary in proportions, influencing their texture and overall chemical makeup. The specific composition of cenospheres is influenced by factors such as furnace temperature, coal type, and base minerals. In addition to chemical composition, gas formation from mineral components at high-temperatures plays a crucial role in cenosphere formation. The gas atmosphere within the cavities of cenospheres also contributes to the formation process. The bulk density of cenospheres is determined by the thickness of the shell and the diameter, typically ranging from 0.4 to 0.8 g·cm^{-3} and 100 to 300 μm in diameter. [76, 77]

The separation of cenospheres from the mixture of produced FA can be achieved through both dry and wet methods. The wet separation process involves flotation, gravity separation, and magnetic separation. Flotation, the most commonly used method, utilises a heavy fluid with a higher density than the cenospheres. As a result, the cenospheres float, and the diameter size of each particle determines their position. On the other hand, the dry method of cenosphere separation relies on the fluidisation effect and surpasses the flight limit. Unlike the wet process, this approach does not require the use of any chemicals and is known to be faster. However, it should be noted that fractionation does not yield a precise division. [77, 78] The instrumentation scheme of basic types of separation is given in Fig. 8.

Because cenospheres reach such low sizes and bulk densities, they have found their application as a filler in some types of inorganic materials, such as mortars and concrete. In the case of using cenospheres as filler, the weight of the products is significantly reduced. Another positive effect is increasing mechanical and degradation resistance in various environments. Although the nominal strength decreases when using a foamed filler (hollow particles with a brittle shell do not also reach a higher modulus of strength than conventional aggregates), after recalculating the strength concerning the weight of the material, light-weight samples achieve better results. [79]

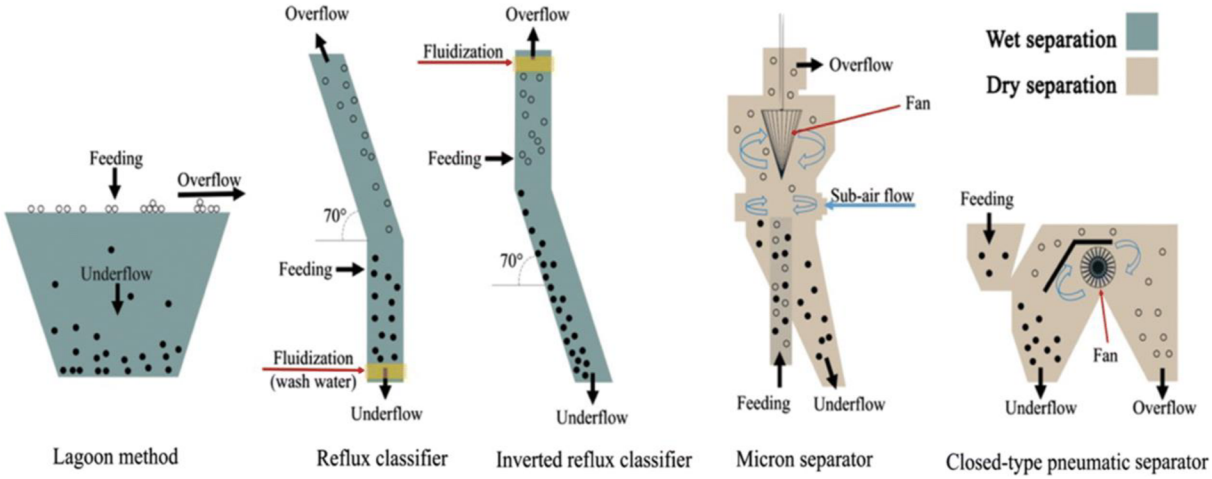

Fig. 8 Methods for separating cenospheres [77]

Another option for bribing fly ash is the production of lightweight aggregate. One of these species is produced in the Czech Republic under the name Agloporite. Agloporite is a light-weight synthetic porous aggregate produced by sintering of coal or anthracite fly ash and other corrective admixtures. It is suitable for the production of insulating concrete as well as for structural concrete. Reinforced concrete and pre-stressed structural elements can also be produced from a particularly strong agloporite. Agloporite is mainly created in 4–8 and 8–16 mm fraction, with bulk density of 1.15–1.25 $g \cdot cm^{-3}$ and compressive strength between 5–9 MPa. [80]

The possibility of application of crushed agloporite in lightweight mortars and their resistance to degradation was investigated together with the partial cement replacement with fly ash in these systems. The results of this research yielded better than expected, when the strengths based on the weight of the product surpassed traditional aggregates and no degradation processes took place under the action of chlorides and sulfates even after several months. [81]

2.3.6 Ceramics materials

Refractory materials

Due to the phase and chemical composition of high-temperature fly ash, and especially the presence of mullite as one of a number of refractory materials, these solid coal combustion residues may be suitable for applications in thermally stressed materials. Various experiments of implementation of FA in refractory materials were carried out.

Using FA in these materials leads to a reduction of produced carbon dioxide and partial savings of required raw materials. Refractory materials are materials resistant to high temperatures, typically 1,100– 1,500 °C. These products are mostly dense, inert and chemically very stable. Of course, the use of by-products as a raw material for refractory materials production has a partial negative effect on their basic properties. [82]

Mullite fittings

Mullite is a highly utilised refractory material in numerous industries for a variety of linings and thermally stressed components. There is a growing interest in developing alternative methods for mullite production using cost-effective materials like kaolinite and sillimanite. Due to the fact that the ashes of high-temperature coal combustion show the presence of mullite and at the same time also contain a sufficient amount of reactive alumina and silica, there is a great effort to produce mullite shaped parts based on these secondary energy products.

The fittings are manufactured through the alkali-activation of fly ash using highly alkaline sodium hydroxide solutions (with an ideal concentration of 100 $g \cdot l^{-1}$) at elevated temperatures of approximately 100 °C over an extended period. This process mirrors the production of alkali activated materials. During the activation, amorphous SiO_2 and also a small amount of amorphous Al_2O_3 dissolve and at the same time precipitates of *P*-zeolite $Na_6Al_6Si_{10}O_{32} \cdot 12H_2O$

and hydroxysodalite $Na_8Al_6Si_6O_{24}(OH)_2 \cdot 4H_2O$ are formed. The activated material is afterwards partially washed with water and moldings of the desired shapes are extruded, which are then fired at 1,300 °C. [83]

Another paper dealt with the same topic using a part of clay as a raw material and HTFA, sodium silicate as well as research above. In this study, mullite based bricks were produced using hydrogen peroxide as a foaming agent. Then, after 24 hours of foaming and 12 hours of drying at room temperature, the samples were fired at 900–1,100 °C to form the final product. Afterwards, physical, mechanical and chemical properties, as well as heat resistance and heat conductivity were tested. All results have met European standards for building thermal insulation bricks and this process is suitable for use in practice. Compressive strength reached up to 6 MPa, bulk density 0.50 $g \cdot cm^{-3}$, thermal conductivity 0.098 $W \cdot m^{-1} \cdot K^{-1}$ (100 °C) and 0.163 $W \cdot m^{-1} \cdot K^{-1}$ (600 °C) with the maximum temperature of 1,250 °C. [83, 84]

Ceramic filters

High-temperature fly ash can be utilised in the production of various ceramic materials. By reacting high-temperature fly ash with a suitable ball at temperatures ranging from 1000 to 1200 degrees, partial sintering can occur, resulting in the formation of a dense ceramic material. These ceramics exhibit notable mechanical strength, corrosion resistance, cavitation resistance, and minimal shrinkage. Additionally, they possess heat resistance and remain stable through repeated heating and cooling cycles due to their elemental and phase composition, primarily consisting of mullite. [85]

The utilisation of ceramic materials extends beyond the mere manufacturing of dense products, encompassing the production of items with specific porosity or cavities. These specialised products are commonly employed in processes such as the purification of hot gases. The high heat resistance and non-flammability of this material are attributed to its aluminium, titanium, silicon, and magnesium content, allowing for the production of materials like mullite or cordierite through optimal production techniques. Ceramic filters based on HTFA are commonly used due to the presence of mullite, although FBA can also be utilised. Fly ash offers advantages in particle size distribution, with large grains of around 50 μm, small grains ranging from 3-5 μm, and medium fractions of 15-25 μm, enabling effective sintering. Additionally, the glassy phase in fly ash promotes solid-phase reactions and grain wetting. The production process involves adjusting the fly ash composition, firing at temperatures exceeding 1,050 °C, and controlled cooling to crystallize mullite or cordierite. The firing process must be carefully managed to retain a portion of the glass phase for the subsequent production stage. In the second stage, organic combustibles are added to the sintered fly ash, followed by firing at 850 °C to create small cavities through controlled decomposition. The number and size of cavities can be controlled by adjusting the organic content, firing temperature, and dwell time at 850 °C. [86]

2.3.7 Other and special applications

The subsequent chapter outlines the potential applications of FA in unique, presently less prevalent, or peripheral circumstances. However, considering their significance, these applications might assume a more substantial role in the future than they currently do.

Carbon nanotubes

Extensive research has been carried out in recent decades on carbon materials to investigate their chemical and physical properties, methods of preparation, and applications of newly discovered structures such as fullerenes, carbon nanotubes, carbon nanofibers, graphene, carbon nanoparticles, and cubic nanocarriers.

Carbon nanotubes, as previously mentioned, serve as excellent conductors of electric current due to their zero-resistance structure, which does not increase with the length of the fibre tubes. These materials show promise for use in superconductors. Initially, the production of carbon nanotubes was economically unfeasible until it was found that they could be produced from fly ash rich in free carbon, primarily generated in biomass-fired power plants, with minor adjustments to the production process.

When used as fillers in nanocomposite materials, carbon nanotubes have a significant positive impact on both mechanical properties (such as modulus of elasticity, abrasion resistance, and strength) and physical properties (including conductivity) even with a small addition of approximately 5 % by weight. Nanotubes can be synthesised through low-pressure deposition in steam gas at elevated temperature and pressure, with a reaction time of several hours to create a carbon co-precursor and as a by-product of acetylene synthesis. This mixture is then blown onto the catalyst using an overpressure of inert gas (argon), with a small amount of fly ash potentially serving as the catalyst. The tubes grow on the enclosed silicon sheet under a maximum pressure of 1 Pa at a temperature of 650 °C. The progression of the reaction can be visually monitored as the colour of the mixture changes from initial grey to final black, indicating an increase in the proportion of tubes on the catalyst and plate. [87, 88]

This procedure can be used both for the industrial production and for laboratory preparation of nanotubes, with possible single-layer (SWCNT – "*single wall carbon nano tubes*") and multi-layer (MWCNT – "*multi wall carbon nano tubes*") outcome products. The differences in their structures are shown in Fig. 9.

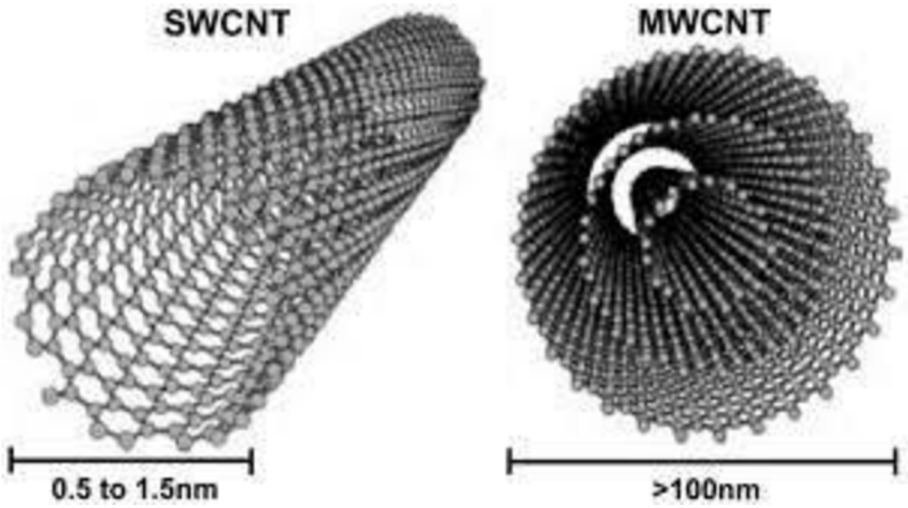

Fig. 9 Model of SWCNT and MWCNT [89]

Adsorbents

Due to its chemical composition and morphology, fly ash from coal combustion can be used as a cost-effective adsorbent after chemical or thermal activation. For example, fly ash with an unburned carbon content of around 5–7 % can be used for desulphurisation, but the economic aspect of such a process is very unfavourable. A far better way to use fly ash for desulphurisation and denitrification of combustion processes is to activate it with concentrated calcium hydroxide. The substrate treated in this way can be used, most notably in dry adsorption devices, achieving efficiencies of up to 90 % in one stage. This process has found application in some foreign power plants such as Ebetsu, Amtoh Atsuma, etc. [46]

In addition to the adsorption of SO_x and NO_x, fly ash is also partially used to capture gaseous organic substances or vapours of organic solvents (toluene, xylenes, benzene, etc.). In this application, the thermal activation of fly ash is used, and the formation of agglomerates also has a positive effect on the absorption efficiency. Today, these fly ash sorbents are used mainly in cheaper facilities with low output. [46, 90]

Fly ash also has potential use in wastewater management due to its chemical composition, porosity, particle distribution and specific surface area. The mild to moderately alkaline nature of the fly ash itself helps to neutralise wastewater, and adjusting the pH to the alkaline or acidic range increases the possibility of separating some toxic or heavy metals. In several studies and technological applications in south and south-west Africa, India, and some Mid-East develop ing countries, it has been shown that the FA adsorbent brings a quite positive effect on the removal of both heavy metals (Cd, Pb) and metals dangerous for the environment (Cu, As, Cr) as well. Heavy metal ions can be separated in the pH range 6–8. The latter group can then be removed in the acidic pH range 3–4. Although these absorbents do not have a very good process efficiency, they are often the only available option due to their very low acquisition cost and operating costs in these countries. An overview of separable metal ions, including adsorption capacities (A_c) and experimental conditions, is summarised in table below. [46, 90, 91]

Table 6 Summary of adsorption capacities for individual water pollutants [46]

	A_c (mg·g^{-1})	T (°C)		A_c (mg·g^{-1})	T (°C)
Zn^{2+}	5	25	**Cr^{3+}**	50–100	20–40
Cd^{2+}	200	25	**Cr^{6+}**	1–2	20
Pb^{2+}	440	25	**Hg^{2+}**	11	30–60
Cu^{2+}	200	25	**As^{3+}**	10	25
Ni^{2+}	9–14	30–60	**As^{5+}**	8–28	20

At a time when the pollution of groundwater and wastewater with heavy metals, organic solvents and pesticides is increasing, it is necessary to look for affordable measures with favorable performance, especially in less developed countries of the world. In this regard, the use of cheap and functional fly ash adsorbents is to be considered. [90]

2.3.8 Potential source of raw materials

Some types of power plant fly ash are significantly similar in their chemical composition to many raw materials used for the production of aluminium, titanium and iron. However, it is also necessary to consider the representation of minor elements, which can be rare commodities such as lithium, germanium, cerium, samarium, and others.

Separation of up to 99 % of the aluminium components present from both high-temperature and fluidised-bed ashes was achieved. Currently, the research deals with the issue of streamlining the leaching process and the possibilities of activating the fly ash to achieve the most suitable ratio of the amount of separated aluminium in a single-stage extraction in sulphuric acid and the total material and energy costs of the process. [46]

Aluminium

Aluminium is found in fly ash in relatively complicated and less reactive minerals such as refractory materials mullite $Al_6Si_2O_{13}$, andalusite, kyanite and sillimanite Al_2SiO_5, albite $NaAlSi_3O_8$, gehlenite $Ca_2Al[AlSiO_7]$, rarely as Al_2O_3. A suitable extraction method is chosen according to the predominant form of occurrence. FA typically contains about 20–35 wt. % of alumina. [1]

Aluminium extraction technology, resp. fly ash alumina recovery can be divided into acidic, basic and acid-basic methods. Acid processes are based on the FA leaching in mineral acids, such as sulphuric, hydrochloric, nitric, hydrofluoric acid, or mixture. These processes are mainly based on analytical possibilities of sample decompositions using different types of leaching. Although these methods are relatively simple in instrumentation and inexpensive for the chemicals used, they mostly require the use of acid-resistant equipment and technology and generally do not achieve optimal efficiency at all. Alkaline methods are based on sintering fly ash with various substances – with limestone, or with limestone and soda ash- and subsequent product processing in several ways on Al_2O_3. [1, 46]

Titanium

Titanium is partially bound inside fly ash in the crystalline form such as rutile, ilmenite, perovskite ($CaTiO_3$), but occurs mainly in the amorphous phase of Si-Al-Ti-Fe-O, Al-Si-K-Fe-Ti-O, Al-Si-Ti-O in a range of 0.5–2 wt. %. This matrix can only be broken down chemically. Minerals containing iron are weakly magnetic. Hydrometallurgical processes can be used for the separation of titanium, as well as separation by leaching with some cultivated strains of bacteria – bio hydrometallurgical processes. [1]

Iron

In fly ash, iron is found mainly in oxide minerals, characterised by a high magnetic susceptibility value and tends to be weakly to strongly magnetic. Magnetic properties could be used further in separation from other minerals. In addition, iron also occurs as a structure of titanium minerals (ilmenite, ilmenorutile). Part of the iron is also in metallic form or in the amorphous form in a silicate matrix. [1]

Rare elements present in fly ash.

In addition to the macro-concentrated elements themselves, fly ash can contain many other components, which, in some cases, are very rare in the order of ppm units up to tenths of a percent. Given their natural deposits and ways of obtaining them, fly ash could be an essential precursor for their production in the future.

The content of rare elements in fly ash depends on the location of the mined coal. Globally, based on analyses of fly ash from around the world, the coal elements of the lanthanide group La, Ce, Pr, Nd, Sm, Eu, Gd, Tb, Dy, Ho, Er, Tm, Yb, Lu can be represented in ppm (summarised in the following table). [92]

Table 7 Representation of lanthanides in coal and fly ash (ppm) [92]

	La	**Ce**	**Pr**	**Nd**	**Sm**	**Eu**	**Gd**	**Tb**	**Dy**	**Ho**	**Er**	**Tm**	**Yb**	**Lu**
Bituminous	11	23	3.4	12	2.2	0.43	2.7	0.31	2.1	0.57	1	0.3	1	0.2
Sub-bit.	10	22	3.5	11	1.9	0.5	2.6	0.32	2	0.54	0.85	0.31	1	0.19
FA	69	130	20	67	13	2.5	16	2.1	14	4	5.5	2	6.2	1.2

In some types of coal or fly ash, other rare metals and semi-metals Ga, Ge, Sb, Te, Se in the order of several hundredths to tenths of a percent may also locally occur. These elements are typical for only a few mineral veins, especially in black coal. The worldwide average in coal and fly ash is summarised in the following table. [93]

Table 8 Content of Ga, Ge, Sb, Se (ppm) in different types of coal [93]

	Ga	Ge	Se	Sb
Bituminous	6.0	2.4	1.6	1.5
Sub-bituminous	5.5	2.0	1.0	1.1
FA (BC)	36	18	10	8
FA (S-BC)	29	11	7.6	6

From the 1960s until the 1980s, germanium was obtained from Czech bituminous coal fly ash from the Pilsen and Kladno basins and brown coal fly ash from the Sokolov region. Currently, coal deposits in the Czech Republic are depleted of this element. However, germanium reserves in Czech fly ash are estimated at several thousand tons. Currently, only a few companies from the United Kingdom and Russia are involved in the recovery of germanium from fly ash. [93, 94]

Other minor elements represented in fly ash can also be noble, precious and heavy metals such as Ir, Pt, Pd, Cu, Ag, Au, Be, Sb, Cs, Pb, Cd, etc. Some valuable commodities contained in fly ash in the ppm range can be elements such as Y, Hf, Ta, W, V, Re, Os and many others. [95] Due to their rarity and particular uses, these metals are precious. The content of elements mentioned above in FA and C is summarised in Table 9 and 10.

Table 9 Content of precious and heavy metal elements (ppm) in coal and fly ash [93, 95, 96]

	Au+Pt	Ag	Cu	Ir	Pb	Cd
Bituminous	0.0461	0.100	42	1	55	1.5
Sub-bituminous	0.0059	0.09	38	0.8	37	1.2
FA (BC)	0.189	0.59	214	3.2	180	5
FA (S-BC)	0.069	0.63	178	2.5	92	3

Table 10 Content of V, W, Y and U (ppm) in coal and fly ash [93, 95]

	V	W	Y	U	Mo
Bituminous	28	0.99	8.2	1.9	2.2
Sub-bituminous	22	1.2	8.6	2.9	2.1
FA (BC)	170	7.8	57	15	14
FA (S-BC)	140	6	44	16	15

2.4 Macro-concentrated elements recovery

The following section presents and summarises the most recognised and promising approaches for the recovery of macro-concentrated elements from FA. This overview highlights the methods suitable for high-temperature FA and fluidised-bed FA, with a specific focus on their utilisation for the different types of fly ash produced in the Czech Republic.

In essence, these techniques can be categorised into two distinct groups: extraction and sintering methods. The former primarily involves the dissolution and leaching of fly ash using different extraction agents; in contrast, the latter encompasses a range of high-temperature modifications and activation of the fly ash, followed by leaching.

2.4.1 Extraction methods

Different techniques are employed to extract metals or their oxides from fly ash. These methods involve directly leaching the power plant fly ash or using pretreated material using mineral acids, hydroxides, or other media. The extraction process occurs under different conditions, such as elevated temperatures, boiling, or autoclaving.

Extraction into acidic solutions

The commonly employed technique is known as “direct acid leaching” in the realm of acidic surroundings. Extraction reagents such as sulphuric acid, hydrochloric acid, nitric acid, and their different proportions and strengths combinations, can be utilised. Considering the cost of these acids, sulphuric acid is predominantly favoured for leaching purposes. However, it is essential to note that the effectiveness of direct leaching varies depending on the specific characteristics of the fly ash, thus making it unsuitable as a universally applicable method. [97, 107]

Sulphuric acid leaching

Another possibility to increase the efficiency of direct leaching with sulphuric acid is to improve the extraction temperature up to the solvent's boiling point. For high-temperature fly ash rich in aluminium, when kept at a temperature of about 200 °C and under the action of concentrated sulphuric acid, it is possible to dissolve up to 90 % of the fly ash mass at an optimal 5/1 weight ratio of medium to fly ash. [108, 109]

An extensive study on the possibility of recovering aluminium from fly ash by using sulphuric acid on untreated material was addressed by Seidel and Zimmels [110], who addressed this issue depending on acid concentration, liquid to solid phase ratio, temperature and extraction time. They also investigated the effect of the amount of free calcium ions reacting with the medium and the formation of a reaction by-product – gypsum. The resulting gypsum is precipitated on the surface of the fly ash grains and thus forms a diffusion-resistant layer that prevents further mass transfer during extraction. The sequence of reactions in the dissolution of individual ions into the solution was described by the sequence of the following reactions (13)–(20).

$$H_2SO_4 \longleftrightarrow SO_4^{2-} + 2H^+, \quad (13)$$

$$MO + 2H^+ \longleftrightarrow M^{2+} + H_2O \ (M = Ca, Mg, \ldots), \quad (14)$$

$$J_2O + 2H^+ \longleftrightarrow 2J^+ + H_2O \ (J = Na, K, \ldots), \quad (15)$$

$$Al_2O_3 + 6H^+ \longleftrightarrow 2Al^{3+} + 3H_2O, \quad (16)$$

$$Al^{3+} + 3H_2O \longleftrightarrow Al(OH)_3 \downarrow + 3H^+, \quad (17)$$

$$Fe_2O_3 + 6H^+ \longleftrightarrow 2Fe^{3+} + 3H_2O, \quad (18)$$

$$Fe^{3+} + 3H_2O \longleftrightarrow Fe(OH)_3 \downarrow + 3H^+, \quad (19)$$

$$Ca^{2+} + SO_4^{2-} \longleftrightarrow CaSO_4 \downarrow. \quad (20)$$

However, this model greatly simplifies the extraction situation to the case of equal ion concentration. In practice, soluble aluminium, iron and sodium sulfates are also formed. Furthermore, theoretical knowledge considers only the reaction of simple oxide forms, which cannot be achieved in practice with high-temperature fly ash, where the majority source of aluminium is mullite ($3Al_2O_3 \cdot 2SiO_2$) and amorphous phase. Based on the comparison of experimental data and theoretical assumptions, they concluded that a heterogeneous non-catalytic auto-inhibitory reaction causes this fact. In this experiment, the concentration of aluminium, or in some cases of iron, grows logarithmically until an equilibrium is achieved in the form of insoluble extraction products covering the surface of the grains and forming a diffusion barrier. The value of the equilibrium Al concentration in the solution depends entirely on the amount of free calcium ions and the concentration of the extracting agent. With increasing reaction temperature, the course of the curve becomes steeper, and the maximum is reached in a shorter time interval. However, the maximum concentration also depends on the concentration of other dilute content, the concentration of the leaching agent and the solid/liquid ratio. [110, 111]

Many authors have dealt with methods of direct leaching of FA. In most cases, the experiments did not achieve the leachability of Al at room temperature higher than 50 % in the case of classical HTFA [112]. The same leaching efficiency, but selectively only for dissolving aluminium, can be achieved by the action of dilute sulphuric acid at the boiling point of the solvent at an extraction time of 4–6 hours. This experiment was then carried out for FBA (bottom and filter) with selectively dissolving up to 95 % of Al. [113] Researchers have carried out the digesting of HTFA in sulphuric acid solutions at high temperatures over 120 °C [114]. They came out with similar results to Al's dissolution.

Hydrochloric acid

The investigation and characterisation of the leaching process of fly ash in a hydrochloric acid environment under varying conditions of elevated temperature, medium concentration, excess medium, and other factors were also addressed. Several authors' accounts of their experiments are rooted in the traditional analytical framework of the breakdown of inorganic materials, thus

detailing the impacts of hydrochloric acid, particularly on the leaching of alkaline ions like alkali metals and alkaline earth metals, as well as potentially other non-noble metals. Another study, such as that conducted by Huang et al. [115], focused on assessing the leachability of different elements from fly ash using hydrochloric acid at various pH levels. The general finding was that as the pH level approaches neutrality, the leachability of heavy and base metals diminishes. Additionally, their research suggests that beyond a L/S ratio of 20, there is no significant increase in leachability with further increases in the ratio. The findings of this research can be briefly summarised in the two graphs presented below:

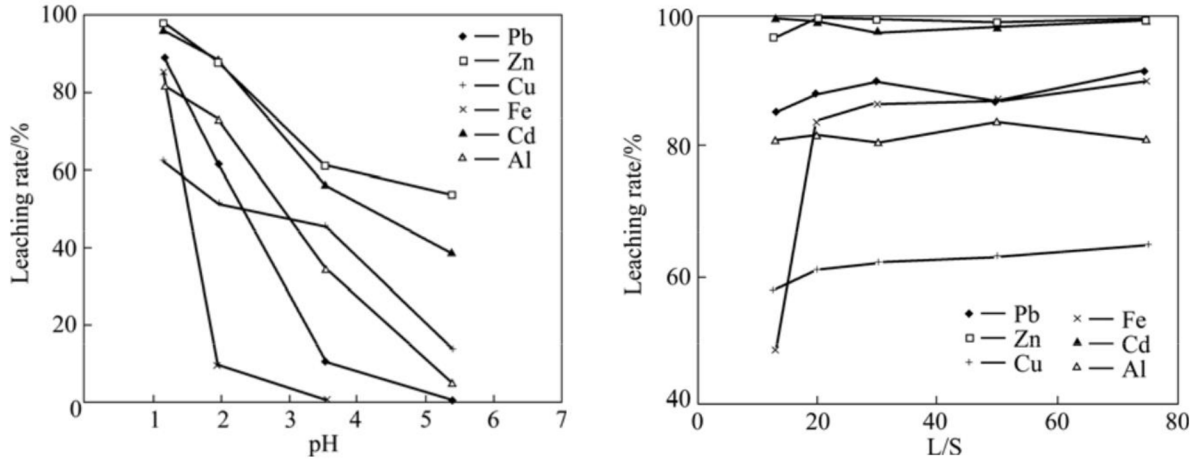

Fig. 10 Leachability of elements depending on the pH of the solution (left) and the L/S ratio (right) [115]

The researchers in these investigations [116, 117] reached a similar conclusion regarding the effectiveness of hydrochloric acid, mainly when applied at temperatures exceeding 100 degrees Celsius and allowed to react for a duration of 4 to 6 hours. This method yielded noteworthy outcomes in terms of the leaching of rare metals and elements such as Nd, Er, Eu, Tb, Dy, and others, with optimal results observed at acid concentrations ranging from 0.2 to 2 M. When utilising acid concentrations of up to 7 M and a relatively high liquid-to-solid ratio, it was possible to dissolve as much as 85 % of the iron content. However, this approach proved to be less effective for the extraction of Al or Ti.

The extraction of aluminium from ash, which holds promise for industrial utilisation, involves using the autoclaving technique under elevated temperatures. By subjecting the ash to temperatures of 210 °C and applying immense pressure, it becomes feasible to extract up to 90 % of aluminium through the action of hydrochloric acid with concentrations of 10–35 %. [118] Nevertheless, implementing this method proves to be highly challenging, particularly in laboratory settings, primarily due to the difficulties in attaining the required operating pressures and ensuring effective anti-corrosion treatment of the equipment.

2.4.2 Sintering methods

Sintering methods, in the experimental part, and results further, such as high-temperature modification or activation, for separating aluminium are particularly suitable for high-temperature fly ash with a higher Al_2O_3 content. The essence of sintering methods is reacting with an alkali oxide or carbonate in the solid phase to form more easily separable aluminates or aluminosilicates.

Sintering with limestone

The sintering of fly ash rich in aluminium with limestone or anhydrous lime is based on the original "*Pedersen process"* used to produce crude iron pigment using calcium-aluminate slags from a mixture of bauxite, iron ore, coal and limestone.

The first step of the process is the magnetic separation of the fly ash, followed by the subsequent addition of calcium carbonate or quicklime. The sintering temperature can be variably changed between 1,100 and 1,400 °C. The firing results in the formation of calcium aluminate phases analogous to the production of aluminium cement.

The aim of the firing is to prepare the maximum amount of dodecacalcium heptaaluminate (mayenite) $12CaO{\cdot}7Al_2O_3$ ($C_{12}A_7$) and the by-product of dicalcium silicate $2CaO{\cdot}SiO_2$ (C_2S) from mullite, possibly also from the present glass phase and quartz. Other possible products of the sintering method are tricalcium aluminate $3CaO{\cdot}Al_2O_3$ (C_3A) and monocalcium aluminate $CaO{\cdot}Al_2O_3$ (CA). However, these two phases are much less soluble than $C_{12}A_7$. The solid-state reactions follow the equations (21)–(27).

$$CaCO_3 \longrightarrow CaO + CO_2, \tag{21}$$

$$7(3Al_2O_3{\cdot}2SiO_2)+64CaO \longrightarrow 3(12CaO{\cdot}7Al_2O_3)+14(2CaO{\cdot}SiO_2), \tag{22}$$

$$3Al_2O_3 \cdot 2SiO_2 + 13CaO \longrightarrow 3(3CaO \cdot Al_2O_3) + 2(2CaO \cdot SiO_2), \tag{23}$$

$$3Al_2O_3 \cdot 2SiO_2 + 5CaO \longrightarrow 3(CaO \cdot Al_2O_3) + 2(2CaO \cdot SiO_2), \tag{24}$$

$$2CaO + SiO_2 \longrightarrow 2CaO \cdot SiO_2, \tag{25}$$

$$CaO + Fe_2O_3 \longrightarrow CaO \cdot Fe_2O_3, \tag{26}$$

$$CaO + TiO_2 \longrightarrow CaO \cdot TiO_2. \tag{27}$$

The resulting C_2S transforms at a temperature of 500 °C from a monoclinic β–modification to an orthorhombic γ–modification, which is associated with an increase in phase volume by 11 %. This modification conversion positively affects the resulting granulometry, as the material decomposes into small particles. This method of production is, therefore, partially self-disintegrating.

After cooling the material to temperatures of about 100–150 °C, the resulting mixture of $C_{12}A_7$ (C_3A and CA), C_2S and unreacted fraction can be separated by leaching in a sodium hydroxide solution at 170 °C for several hours. $C_{12}A_7$ is entirely soluble in this medium, C_3A and CA are significantly less soluble, and the remaining sintering products dissolve only in

miniscule amounts. Subsequent filtration can, therefore, desilicate the mixture. Any dissolved residual silicate can be further separated by the addition of a suspension of $Ca(OH)_2$ to form insoluble calcium aluminosilicates. However, this reaction is not very suitable industrially, especially due to the reduced yield of Al_2O_3. The course of leaching and desilication could be better described by the following equations (28)–(32):

$$12CaO \cdot 7Al_2O_3 + 12Na_2CO_3 + 5H_2O \longrightarrow 14NaAlO_2 + 12CaCO_3 + 10NaOH, \tag{28}$$

$$3CaO \cdot Al_2O_3 + 3Na_2CO_3 + 2H_2O \longrightarrow 2NaAlO_2 + 3CaCO_3 + 4NaOH, \tag{29}$$

$$CaO \cdot Al_2O_3 + Na_2CO_3 \longrightarrow 2NaAlO_2 + CaCO_3, \tag{30}$$

$$2CaO \cdot SiO_2 + 2Na_2CO_3 \longrightarrow 2CaCO_3 + 2NaOH + Na_2SiO_3, \tag{31}$$

$$2CaO \cdot SiO_2 + 2NaOH + H_2O \longrightarrow 2Ca(OH)_2 + Na_2SiO_3. \tag{32}$$

In the liquid phase, sodium aluminate $NaAlO_2$ is formed, depending on the pH scale. Sodium aluminate can be further hydrolysed, and a curtain amount of $Al(OH)_3$ (gibbsite) precipitated. Precipitated gibbsite typically aggregates into various agglomerates. The addition of dispersants such as polyethylene glycol or polyvinyl alcohol can easily control undesirable agglomeration. Al(OH)3 is precipitated from the solution by bubbling through CO_2 to form sodium carbonate, which is then returned to the production process. So, most of the used sodium carbonate is regenerated. Precipitation proceeds through equations as follows (33)–(35). [97–100]

$$2NaAlO_2 + CO_2 + 3H_2O \longrightarrow Na_2CO_3 + 2Al(OH)_3, \tag{33}$$

$$NaOH + CO_2 \longrightarrow Na_2CO_3 + H_2O, \tag{34}$$

$$2Al(OH)_3 \longrightarrow Al_2O_3 + 3H_2O. \tag{35}$$

The diagram of the possibility of the optimal production process is described in Fig. 11.

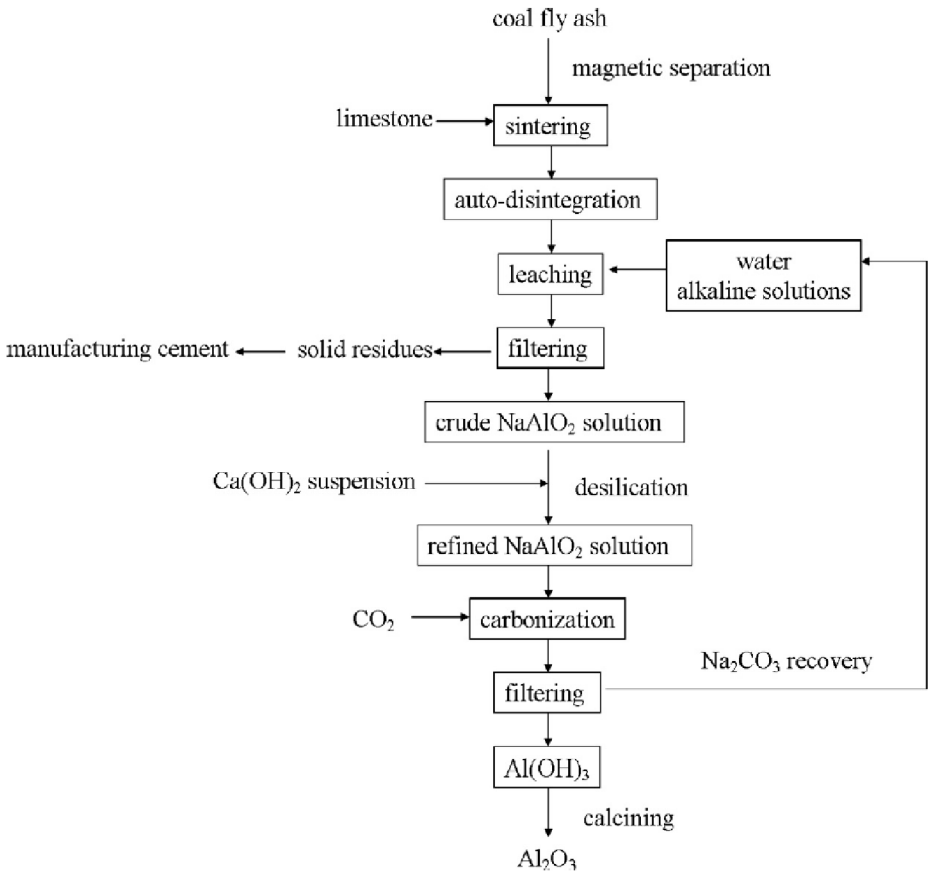

Fig. 11 Limestone sintering process [98]

Sintering with soda and limestone

An alternative to the first mentioned method, resp. combination of the two sintering methods discussed above is to add soda ash (Na_2CO_3) to the primary sintering mixture. Sintering of the material with soda ash and limestone was initially used to purify bauxite ore from silicon and iron compounds, and this procedure can also be applied to high-temperature fly ash rich in aluminium. [97]

In essence, this is a part of modifying the sintering process with limestone. The addition of soda ash to the firing mixture facilitates the formation of the melt, significantly shortening the sintering process. At the same time, the formation of $NaAlO_2$ occurs during firing at 1,100–1,400 °C. The reactions of the sintering stage of the process are described by reactions (36)–(40).

$$CaCO_3 \longrightarrow CaO + CO_2, \tag{36}$$

$$Al_2O_3 + Na_2CO_3 \longrightarrow 2NaAlO_2 + CO_2, \tag{37}$$

$$3Al_2O_3 \cdot 2SiO_2 + 4CaO + 3Na_2CO_3 \longrightarrow 2(2CaO \cdot SiO_2) + 6NaAlO_2 + 3CO_2, \tag{38}$$

$$Fe_2O_3 + Na_2CO_3 \longrightarrow Fe_2O_3 \cdot Na_2O + CO_2, \tag{39}$$

$$2CaO + SiO_2 \longrightarrow 2CaO \cdot SiO_2. \tag{40}$$

The by-product also formed in this process, C2S, is the same as mentioned in the previous sintering method. Another difference compared to sintering with limestone is only the course of leaching in the separation of C_2S from $NaAlO_2$. In the case of the addition of soda to the sintering mixture, the subsequent leaching in water can only be carried out. In the case of a low degree conversion of $NaAlO_2$ formation, leaching the mixture in a soda ash solution is necessary as in the previous method. [97, 99–101] The reactions of the leaching stage of the process are summarised by equations (41) and (42).

$$Na_2FeO_4 + 4H_2O \longrightarrow 2NaOH + Fe_2O_3 + 3H_2O, \tag{41}$$

$$NaAlO_2 + 2H_2O \longrightarrow Na^+ + [Al(OH)_4]^-. \tag{42}$$

The possible product of this kind of sintering reaction and the influence of calcium and iron ions on the product during sintering were discussed by Liu et al. [102]. They published that in the case of low calcium and iron content, the primary product of the sintering reaction is sodium aluminosilicate rather than sodium aluminate. After donating the system with more than 10 wt. % of Ca, the sodium aluminate and calcium aluminate phases had appeared. The presence of iron ions provides sodium ironate $Na_2Fe_2O_4$ creation and also sodium and calcium aluminates stabilisation.

Sintering with calcium chloride

One of the possibilities of activating high–temperature fly ash for subsequent acid leaching is its sintering with anhydrous calcium chloride. $CaCl_2$ anhydride is a vital drying agent with a melting point of 775 °C and a boiling point of up to 1,935 °C. [103]

In this method, HTFA is sintered with the addition of $CaCl_2$ (optimised agent addition 100 % of fly ash weight) in a muffle furnace at a temperature of 900–1,000 °C for at least 60 minutes. Subsequently, the sintering product is allowed to cool freely in air to room temperature, thereby partially auto-disintegration the material is done. The process of auto-disintegration, sometimes also referred to as self-disintegration of the material, can be described as a phenomenon resulting in the spontaneous mechanical decomposition of a compact material into a particulate system. This occurs with significant volume changes in the material due to thermal crystallisation, rapid cooling, or a chemical reaction. The unreacted calcium chloride is removed from the product by washing it with distilled water (possibly diluted with 0.1 M hydrochloric acid) and drying. The chemistry of fly ash sintering to form the main product $C_{12}A_7$ is described by equations as follows (43)–(45).

$$3Al_2O_3 \cdot 2SiO_2 + 6CaCl_2 + SiO_2 + 6H_2O \longrightarrow 3(2CaO \cdot Al_2O_3 \cdot SiO_2) + 12HCl, \tag{43}$$

$$3SiO_2 + 3CaCl_2 + Fe_2O_3 + 3H_2O \longrightarrow 3CaO \cdot Fe_2O_3 \cdot 3SiO_2 + 6HCl, \tag{44}$$

$$7(3Al_2O_3 \cdot 2SiO_2) + 36CaCl_2 + 36H_2O \longrightarrow 3(12CaO \cdot 7Al_2O_3) + 14SiO_2 + 72HCl. \tag{45}$$

This method is intended to provide higher efficiency and shorten the time of the leaching process. According to the authors' experimental results, it is possible to achieve an efficiency of alumina extraction of up to 95 % by leaching in dilute sulphuric acid solutions at room temperature for 1–2 hours. At the same time, titanium leachability and iron separation are increased. The course of leaching is described by reactions (46) and (47).

$$3CaO \cdot Fe_2O_3 \cdot 3SiO_2 + 6H_2SO_4 \longrightarrow 3CaSO_4 \downarrow + 3H_4SiO_4 \downarrow + Fe_2(SO_4)_3, \quad (46)$$

$$12CaO \cdot 7Al_2O_3 + 33H_2SO_4 \longrightarrow 12CaSO_4 \downarrow + 7Al_2(SO_4)_3 + 33H_2O. \quad (47)$$

The formed calcium sulfate and silicic acid are insoluble in the medium and therefore can be removed from the mixture together with the unreacted fraction by filtration. [104]

Ammonia sintering

Another possibility to FA chemical and phase modification to obtain macro-concentrated elements is sintering with ammonium salts. Ammonium sulfate was found after the experiments as the best source of ammonia ions to this reaction. The proper conditions to this process based on experimental results of [105, 106] were 280–500 °C and 1–3 hours. Above 280 °C the ammonia starts to be released from ammonium sulphate and over 500 °C. The ammonium aluminium sulphate starts to decompose forming aluminium sulphate and ammonia. After sintering, the mixture is cooled slowly to laboratory temperature, and it is advisable to grind the sinter. While lowering the particle size to less than 15 μm, the efficiency of the next leaching process increases 2–3 times. Sintering product ammonium aluminium sulphate could be then decomposed by leaching in both strong acid and alkali solutions. The sintering and leaching process could be described by equations as follows:

$$4(NH_4)_2SO_4 + Al_2O_3 \longrightarrow NH_4Al(SO_4)_2 + 6NH_3 + 3H_2O, \quad (48)$$

$$2NH_4Al(SO_4)_2 + H_2SO_4 \longrightarrow (NH_4)_2SO_4 + Al_2(SO_4)_3 + H_2, \quad (49)$$

$$2NH_4Al(SO_4)_2 + 10NaOH \longrightarrow 2NH_4OH + 2NaAlO_2 + 4Na_2SO_4 + 4H_2O. \quad (50)$$

The leachability of Al can reach up to 90 °% via extraction in an acid solution. The acidic form of leaching is preferred, especially due to the regeneration of the modifying agent and to avoid the formation of sodium aluminosilicate, which could form a reaction product in alkali leaching.

2.4.3 Combined and other methods

Other methods can also be used to activate fly ash for individual commodity recovery. These are mostly based on modifying various traditional methods of producing important and strategic commodities.

Alkaline desilication of fly ash

In the case of desilicated or partially desilicated fly ash, the molar ratio Al_2O_3/SiO_2 increases in the range of 1.6–2.0. The material treated in this way can be a suitable raw material for the processes described in Chapter 2.4.1 and thus significantly increase their efficiency and usability.

The desilication can be performed by leaching the sintered fly ash in a medium composed of soda ash and sodium hydroxide. The optimised solution for leaching in industry contains 5 g Na_2CO_3 and 15 g NaOH per litre of medium. This reaction experimentally assessed the fly ash to medium ratio as 1 to 15. The leaching is carried out at 85 °C for at least 15 minutes while stirring the mixture. Otherwise, this method does not appear to be selective for diluting silicon content only. Even some aluminium components are diluted by this method, too, as shown in the following equations (51)–(52). [120–122]

$$2NaOH + SiO_2(\text{amorphous}) \longrightarrow Na_2SiO_3 + H_2O, \tag{51}$$

$$10Na_2SiO_3 + Al_2O_3(\text{amorphous}) + 19H_2O \longrightarrow Na_6Al_6Si_{10}O_{32} \cdot 12H_2O + 14NaOH. \tag{52}$$

The pre-treated ash then undergoes sintering, which is performed either in powder or shaped pellets. Limestone or lime is added to the fly ash in a C/S molar ratio of 2 and soda ash in a N/FA ratio of 1. Physical or chemical activation of the FA is recommended to improve the efficiency of the desilication process. Physical/mechanical activation is based on milling to lower the particle size, while chemical activation mainly uses pre-leaching in an acid solution to open the structure. [120–122]

Thermal chlorination

One of the possibilities for obtaining titanium from fly ash is chlorination carried out at high temperatures and increased pressure in excess chlorine. The method can only be applied to materials separated from iron compounds. It is also suitable for application on fly ash with a non-combustion content of more than 5–7 %, when adding further reduction agents to the reaction mixture is unnecessary. Thermal chlorination method process is similar to the chlorination method of TiO_2 production from raw materials.

The fly ash is chlorinated by this method in a closed reactor at a pressure of more than 15 atm. at a temperature of 900–1,100 °C for several hours by several times the excess of chlorine gas to form titanium tetrachloride, which reacts to TiO_2 by the subsequent oxolysis process. Using more demanding and sophisticated final methods, it is possible to prepare titanium metal using the mentioned method. [123, 124]

The method is not very economically viable; however, if it is applied to a solid filtered after sintering and leaching of fly ash in processes for aluminium separation and C2S flushing, the by-product may contain about 85 % TiO2, and this method seems interesting.

2.5 Possibilities of selective precipitation of dissolved content from acidic solutions

Finely ground fly ash is leached at laboratory or increased temperatures in a solution of sulphuric acid for several hours, which gradually converts into a solution of toxic and also valuable elements, including Al and Ti (Fe, Si, As, Cd, Hg, Pb) from the solid phase. The undissolved residue of the raw material sediments can be easily filtered from the leachate. The individual metals can be selectively precipitated by the addition of 25 % ammonia solution to form not entirely stoichiometric sulfate-aqua-ammonium complexes. This is a very selective method, as the pH range determining the flocculation of the individual complexes has a sufficiently wide interval, so that no complexes with double cations are formed. The size of the flakes can be modified and controlled by the addition of alkalis during precipitation. For example, sodium and potassium hydroxides can be used as precipitants, but the resulting flakes of the complexes are much smaller and tend not to agglomerate much, on the other hand, their use makes it possible to form very fine structures which can reach sub-micron dimensions after subsequent annealing. [113, 125]

2.5.1 Titanium and aluminium

Titanium precipitates at pH 2.05, aluminium at pH = 6.5 and the remaining and toxic elements (heavy metals, rare elements) only at pH 8.5 and higher. This method is therefore completely selective for titanium and aluminium and relatively economically viable. Using separation, metals in their oxide form can be obtained by short annealing with the gradual release of ammonia and sulphur dioxide, which can then be returned to the production process of the leaching and precipitation medium. To increase efficiency, bacteria of the genus *Rhodococcus* adsorbed on magnetite can also be introduced into the pH 2.05 solution. During biomagnetic separation, bacteria move from the magnetite to the Ti-containing material. [125]

2.5.2 Techniques for extracting rare elements

In this chapter, leaching methods for separating selected components in fly ash will be further evaluated in detail. Liquid extraction methods are currently the most widespread possibilities for obtaining rare or expensive elements, especially for their versatility and simple industrial applicability. In this regard, suitable literature summarising the dissolution of these elements as a function of pH was selected.

Evaluating the effect of pH on the amount of dissolved elements in a given medium is critical to creating a comprehensive process for separating components from fly ash.

Antimony

Antimony is most often found in coal or fly ash in the form of sulfides or silicates. If the antimony accompanies the pyrite present, the antimony can be obtained from the fly ash in a relatively straightforward manner, for example by leaching methods in an acidic medium, where it is dissolved in pH < 5 together with the iron released by thermal decomposition of the

pyrite. As the pH decreases, the leachability of antimony increases. Alkaline pH values do not give favourable results when transferring antimony into solution.

However, if the antimony is bound in the form of silicates, then Sb is entirely insoluble in all acidic and some alkaline solvents. A significant increase in leachability occurs only from pH ≥ 12.5.

Therefore, the total leachability of antimony depends on the ratio of sulfides and silicates in the coal or the fly ash itself. The results of foreign authors of the experimental implementation of the dissolution of antimony from fly ash show that using an acidic medium can transfer up to 36 % of the Sb present, while only about 12 % using an alkaline agent. However, it is necessary to consider that the tested fly ash samples showed a large variability in composition. [126–128]

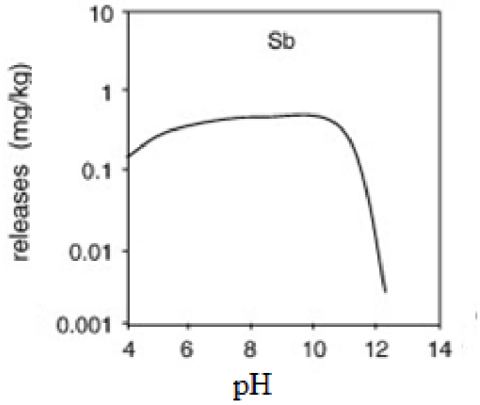

Fig. 12 Leachability of antimony depending on pH [126]

Barium a beryllium

Barium is present in fly ash in the form of variably soluble compounds such as carbonates (less usual) or sulfates. With regard to the combustion process, the typical presence of Ba in carbonates is due to the low temperature and thus the less calorific fuels burned in the fluidised-bed. In high-temperature fly ash Ba is usually not contained mainly due to the subsequent desulphurisation of flue gases by the wet method, when Ba precipitates and crystallises together with gypsum. The solubility of barium compounds does not show significant changes concerning the pH of the solution, most compounds are barely soluble to insoluble. The leachability of Ba into solution is also affected by the presence of calcium ions, where a competitive reaction to sulfate occurs. Barium sulfate is insoluble and therefore precipitates from solution in the form of an anhydrous salt, in some cases it may precipitate from solution in the form of double sulfate together with strontium. The possibilities of obtaining Ba from fly ash, when its characteristic representation is in tens of ppm with regard to its solubility, do not seem to be economically and procedurally advantageous. Evaluation of Ba content has only informative character in combustion by-products (fly ash, energy-gypsum) in order to determine their possible toxicity, etc. [126, 129]

Beryllium, one of the lightest elements in the periodic table, is very difficult to determine in fly ash or other materials. At the same time, Be is currently a strategic element, especially in application areas in *X*-ray lamps. Be is almost insoluble in the pH range of 6 and above. Even in an acidic environment, the equilibrium concentrations of Be reach values of only up to tens of ppm. [126, 130]

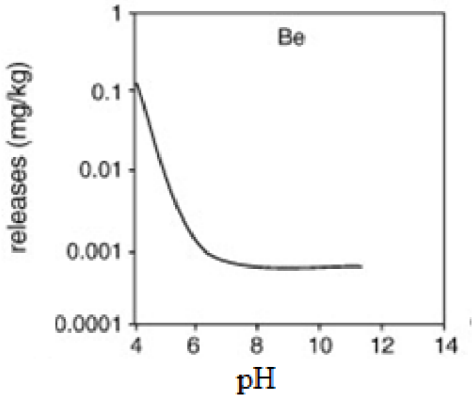

Fig. 13 Leachability of beryllium depending on pH [126]

Cadmium, mercury, caesium, molybdenum, arsenic

The leachability of these elements, depending on the extracting agent, is very important, especially in the areas of workplace safety and environmental protection. Due to the fact that these are relatively dangerous poisons, it is necessary to determine the components of all separation products. During leaching, significant solubility changes occur in this group of elements. With increasing pH the leachability of Cd gradually decreases, does not change significantly for mercury, and increases for molybdenum and arsenic. [126]

Cadmium and mercury are most often trapped on the surface of fly ash grains, while caesium and molybdenum are more often contained in the grain matrix and resist leaching in the initial stages. As soon as the physical and chemical properties of the aluminosilicate matrix of the grain change, there is a significant increase in the leachability of these components as well. The value of the maximum equilibrium concentration of Cs in solution based on experimental data [131] can be considered as 1 ppm, as it did not exceed this value during a wide range of experimental conditions.

The pH-dependent curve of molybdenum solubility shows that the highest leaching of Mo occurs under conditions from neutral to slightly alkaline. At pH = 12, there is a significant decrease in its solubility. This phenomenon can therefore be used in applications leading to the separation of Mo from solution. [126] Possibilities of obtaining molybdenum from fly ash, resp. to be exact, Ogata et al. [132] studied different types of solutions by combined leaching in hydrochloric acid and sodium hydroxide in the presence of gibbsite. In the first phase, the fly ash was treated with hydrochloric acid, and gibbsite was added to the solution with pH = 2. Under these conditions, precipitation of molybdenum ions occurred. Gibbsite was used as a nucleating agent to precipitate Mo on its surface. After completion of the precipitation, the

mixture was calcined at 400 °C to yield molybdenum oxide. The selective separation of Mo from gibbsite was then done by the action of a solution of NaOH, whereby the aluminium component has been dissolved.

Arsenic is most commonly found in coal as a substituted impurity in pyrite. During the combustion process, As is decomposed, volatilised and subsequently condensed on the surface of the grains. In this respect, As compounds in fly ash are prone to easy leaching, especially in the pH range of 7–10. In acidic and alkaline environments, leaching into the solution hardly occurs. The pH of the fly ash itself also contributes to this phenomenon. In the case of acid fly ash, arsenic can be released, for example, in concrete product applications, where the action of an alkaline porous solution results in the formation of readily soluble compounds. Furthermore, the leaching of As is affected by the presence of calcium ions. With increasing concentration of Ca^{2+} ions, calcium arsenate $Ca_3(AsO_4)_2$ is formed, which is classified as a carcinogen, and at pH ≥ 11.5, ettringite (contaminated with As) precipitates and the amount of As in solution decreases rapidly. [126, 133]

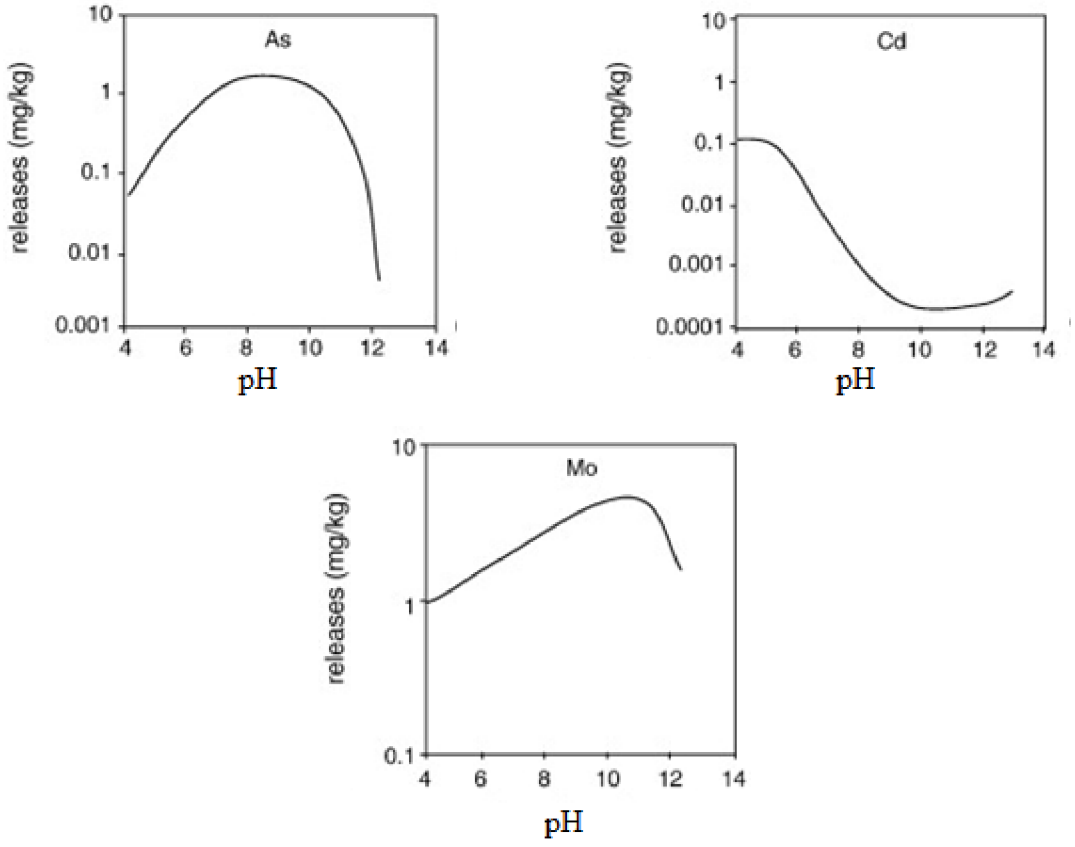

Fig. 14 Leachability of arsenic, cadmium and molybdenum depending on pH [126]

Chromium

The low proportion of chromium in the fly ash does not indicate the future use of this material as a potential source of Cr. Cr^{VI} is another element with an adverse effect on living organisms. This oxidative state is known for its carcinogenic and mutagenic nature. In coal, chromium occurs in the form of Cr^{III} as an impurity in illite. During the combustion process, Cr is released,

and its oxidation and reduction reactions take place. It is oxidised due to increased temperature and excess oxygen from trivalent to hexavalent and reduced due to the formation of SO_2. Cr^{VI} then contains approximately 5% of the total chromium content in the fly ash. In particular, hexavalent chromium is very soluble in aqueous solutions. It thus poses a potential risk of contamination of other products from fly ash, as well as during fly ash processing in different areas of industry (concreting, ceramics, etc.). Overall, chromium can be described as a well-leachable element, both in a strongly acidic and alkaline environment, as shown by the leaching curve in Fig. 15. [126]

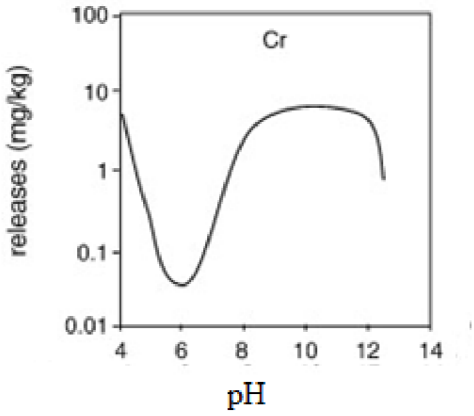

Fig. 15 Leachability of chromium depending on pH [126]

Lithium, rubidium

Rubidium, like other alkalis, forms readily soluble salts. Although fly ash, with its rubidium content of tens to hundreds of ppm, is not the most suitable by-product for its profit, in tandem with profit from other components, it can be an exciting alternative. The formation of readily soluble chlorides is characteristic, even in aqueous media. Rubidium can then be selectively precipitated from aqueous extracts as hydroxide and further processed, for example, by calcination. Furthermore, Ru can also be obtained from acidic or alkaline extracts. For the highest leachability, it is appropriate to use a hydrochloric acid solution. [126, 134]

Increased emphasis is placed on lithium applications, especially in the areas of sophisticated materials and electronics. Lithium, the third lightest element of the periodic table, is exceedingly difficult to determine qualitatively and quantitatively using commonly available analyses. Research teams in the USA had studied the acquisition of lithium from energy by-products since the 1970s when several patented technologies were created. The basis of all proven methods is using a neutral or weakly acidic leachate and the subsequent selective precipitation of the desired lithium compound. These can be hydroxides (alkalisation of the solution up to pH = 13), carbonates (introduction of CO_2 gas into the acidified solution). In particular, the method of bubbling the solution with CO_2 appears to be very economically viable and easily feasible experimentally. In total, it is possible to separate up to 90 % of the Rb present from the fly ash. [134–136]

Germanium, gallium

Germanium and gallium can be described as strategic elements, especially in the developing areas of semiconductors, electronics and special ceramics. In the earth's crust, they most often accompany zinc compounds, and therefore are most often obtained from by-products of Zn production and processing. However, Ge and Ga can also be relatively abundant in some types of coal. Since the 1970s, many methods have been tried to separate these two components, especially from black coal fly ash. Most methods are based on acid leaching and subsequent selective separation of dissolved components. Arroyo et al., for example, have dealt with this method in their work [137, 138]. Germanium, together with gallium, was separated from the fly ash using acidic, alkaline and complexing agents. The highest yields of Ge (up to 90 %) were achieved by using the complexing agent catechol in the process according to the following figure:

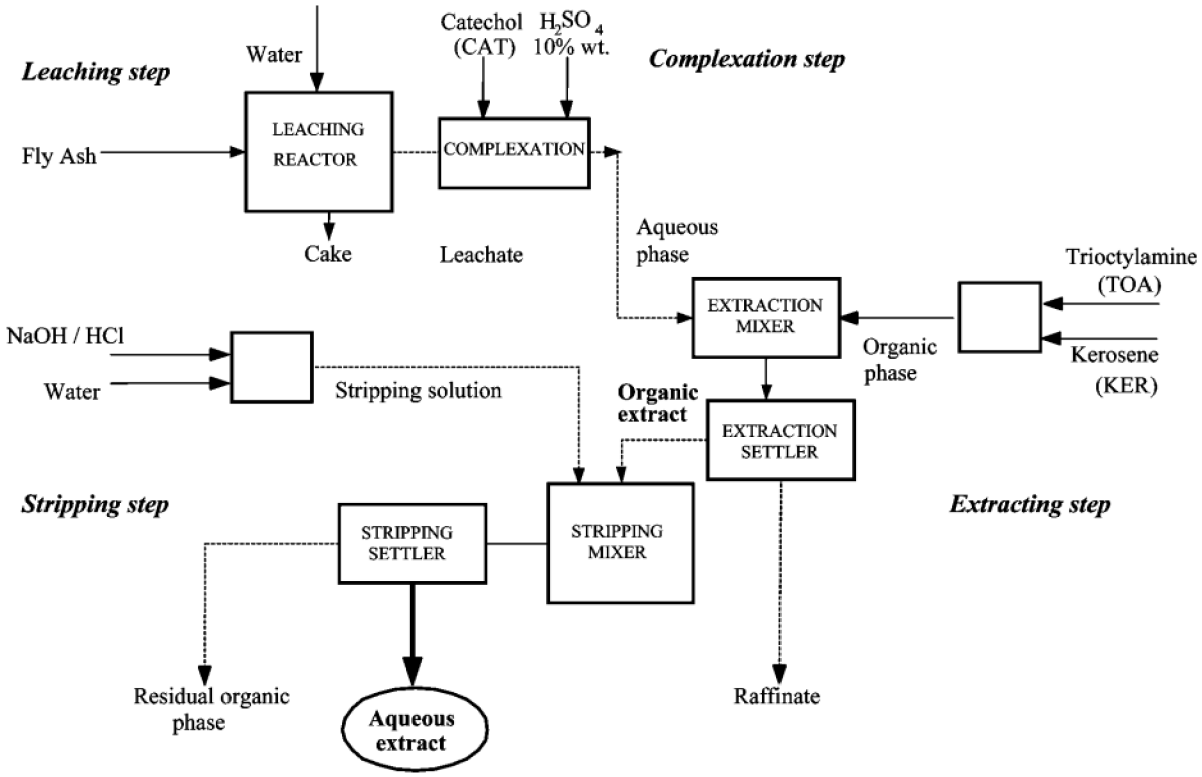

Fig. 16 Scheme of the hydrometallurgical process of Ge and Ga recovery using complexing agent [137]

As seen above, regarding the chemical reagents used and the total number of steps, this complex process can hardly be implemented. For this reason, a series of experiments based on simple leaching and precipitation with acidic and alkaline solutions were performed. The leachability of Ge in these media is 60–98 % after 30 min of extraction (60 % 1 M H_2SO_4, 82 % 1 M HCl and 98 % 1 M NaOH). With increasing extraction time, leachability increases, but only in a single percentage. A certain amount of Ga, Mo and Sb is also present in these solutions. Therefore, for efficient separation of Ge from fly ash, it is suitable to use strongly acidic ($pH \leq 1$) or strongly alkaline ($pH \geq 12$) solutions.

Another possibility for obtaining Ge and Ga is the already patented technology (USA 1986) based on the physical properties of these two elements. The process is based on sublimation at temperatures of 700–900 °C, trapping and cooling vapours. Up to 90 % of Ga can be separated in this process. However, in terms of energy requirements, the use of this method is very debatable. [134]

Precious metals

Elements such as Au, Ag, Pt, Ir, Rh can be included in this group. Precious metals such as gold (Au) and silver (Ag) have many applications in industry, jewellery and medicine. Some Au compounds are used as anti-inflammatory drugs, e.g., in treating rheumatoid arthritis. Ag compounds are then used in the treatment of infections and disinfectants. Gold is also increasingly used in electronic devices and Ag is used in photography, industry and solders.

Methods for separating this whole group of elements have been developed and applied since the late 1990s. Many of them have been patented, especially in the USA. These patents most often use combustion processes combined with acid leaching. In the first phase, fly ash rich in these precious metals is burned with high-quality coal to melt the grains. Subsequently, these extracts are leached in an environment of 30 % HNO_3 and the leachate is further electrolysed. These elements are then separated from the leachate on the base of electromobility or using selective reagents. Silver is separated by adding a solution of HCl, Rh, Ir, and others, which can then be selectively precipitated using KOH, resp. $NaBH_4$. Pd can be separated by an insoluble $PdCl_2(NH_3)_2$ complex, i.e. HCl additions and NH_4OH flocculation. Alternatively, the Pd can be separated by the action of organic reagents. Pt can also be obtained by a combination of HCl and ammonia such as $(NH_4)_2PtCl_6$. [134] All these products can then be calcined to oxides, possibly using an electric arc furnace or carboreduction to elemental metals. [138]

Selenium, tellurium, thallium

Selenium occurs abundantly in coal with a higher content of other minerals. The primary sources of selenium in coal are sulfides and organic compounds. During the combustion process, many reactions occur, and selenium often substitutes iron in its oxides. For this reason, Se is contained in the fly ash matrix. In the case of alkaline fly ash with a higher lime content, $CaSeO_3$ can then be formed, which is then concentrated on the surface of the fly ash particles. The pH value strongly influences the leachability of selenium, and it passes into solution in both acidic and basic environments. At $pH \geq 2$, stable selenic acid is formed, which is stable in this environment and remains in solution. Above this value is a gradual formation of hydrogen selenites, which, due to the increase in pH, have a higher absorption on the surface of the ash grains. Subsequently, the solubility of the compounds decreases up to the alkaline range, where at pH = 12, there is a sudden change in solubility. [126, 134, 139]

The experimental data of Wang et al. [139], who studied the solubility of Se compounds in fly ash as a function of pH, indicate the possibility of separation of this element using both acidic and alkaline media. It also depends on the ratio of the oxidation states of Se^{IV} and Se^{VI},

where the lower oxidation state can be more effectively converted into solution, and at the same time the effect of pH of the extractant used is more pronounced, as shown in the Fig. 17.

Up to 70 % of selenium compounds from black and brown coal fly ash were experimentally leached by combining leaching in nitric acid and sodium hydroxide.

Tellurium and thallium occur in fly ash only in minimal amounts, while their content usually increases with coal quality. These elements are most often present in the surface layers of fly ash grains; they occur sporadically in the matrix. In practice, they usually accompany the occurrence of selenium and are soluble in strongly acidic environments. However, their total leachability across a wide range of experimental conditions did not exceed 10 %.

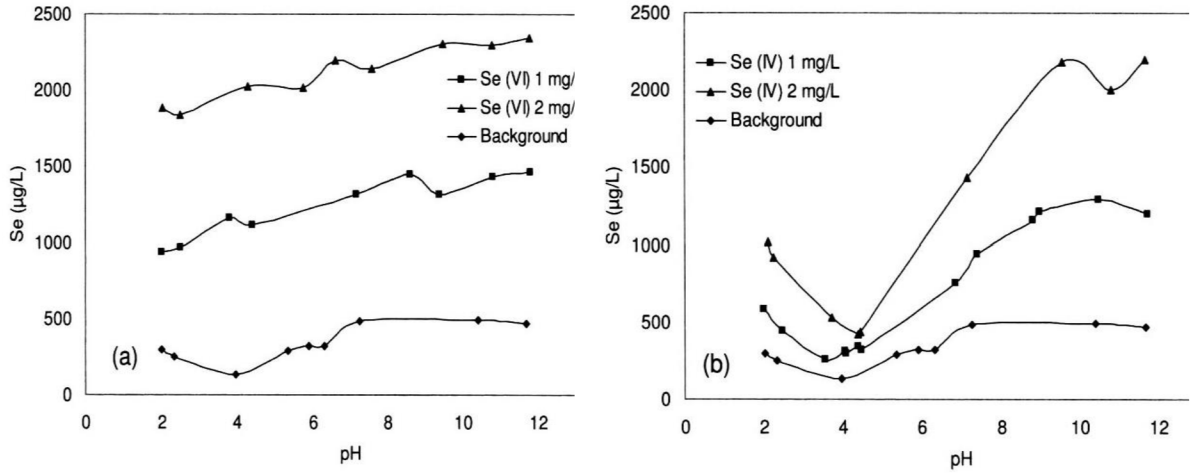

Fig. 17 Comparison of the effect of pH on solubility changes of S Se^{IV} (right) and Se^{VI} (left) [139]

Tungsten, vanadium

Tungsten is relatively non-volatile; hexavalent tungsten (WVI) is very thermodynamically stable in fly ash, and its leachability is almost non-existent. W can form water-soluble compounds such as scheelite ($CaWO_4$) in alkaline fly ash with a higher calcium content. Tungsten is not subject to dissolution at pH ≤ 5 (less than 1 %). Calcium, sodium, potassium, or other alkalis metal tungstates dissolve in the neutral pH range. In an alkaline environment, up to 2–24 % of the tungsten present can be extracted. [126, 131] In terms of the presence of tungsten in the fly ash and not very satisfactory leachability, the use of fly ash as a source of W is unlikely.

Vanadium is currently used in both iron and non-iron alloys due to increased tensile strength, hardness and other mechanical properties. It is also used as a catalyst or in progressive vanadium redox batteries. Vanadium is abundantly obtained from coal and its residues. Some methods of recovering V from fly ash and other coal residues have been patented in the past. In summary, these are leaching and precipitation mechanisms, in some cases supplemented by combustion. In these processes, acid leaching of the material and subsequent precipitation using NaOH solution and calcination of the intermediate to V_2O_5 is most often used. These techniques lead to efficient separation of up to 98 % of the V present, but a significant excess of extraction

medium significantly disadvantages the whole process. Xiang et al. and Vitolo et al. dealt with the possibilities of direct leaching and incineration with subsequent leaching. [140, 141]

The former dealt with the conversion of V into solution using sulphuric acid. He discusses optimising leaching conditions, such as the used reagent's temperature, time, and concentration. Based on these parameters, the highest efficiency of extraction V into the solution was achieved using 6 M H_2SO_4, at a temperature of 90 °C and a reaction time of 3–5 hours. Under these conditions, up to 96 % of the vanadium present was dissolved. The latter uses a three-stage process, in which in the first step the fly ash activated by sintering at a temperature of 650–1,150 °C is leached in a sulphuric acid medium (3 M) and then oxidative precipitation occurs with $NaClO_3$. The resulting V_2O_5 is then subsequently cleaned of contaminants several times. According to this method, the resulting amount of extracted vanadium from fly ash reached 83 %.

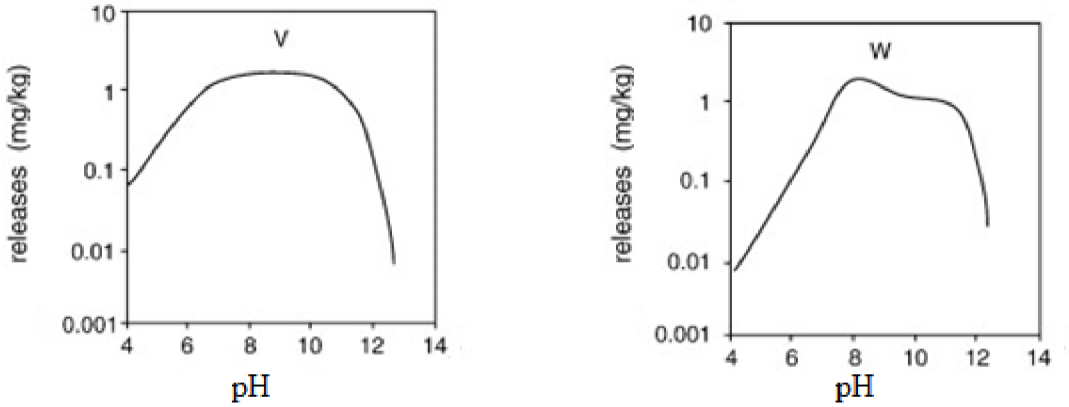

Fig. 18 Leachability of tungsten and vanadium depending on pH [126]

Yttrium, lanthanides, radioactive elements

Radioactive elements have extensive industrial and scientific applications despite their nature, risks, and difficult preservation. Most coal ores contain impurities of natural radioactive elements. The most represented are U, Ra, Th. Most research is based on acidic leaching methods and subsequent selective separation from solutions. Promising leachability was achieved using all mineral acids, where the number of extracted elements, U, Th and Ra, exceeded 90 %. This fact is especially important in the application of solid residues after leaching but also in the possible contamination of selective separation products. [134] One of the complex procedures for the separation of radioactive elements from fly ash was discussed by Maslov et al. [142]. They achieved the best results by leaching the fly ash in 8 M H_2SO_4 with the addition of 10 % HF. Subsequently, the individual groups of elements were separated from each other using a commercial anion exchanger using 2 M HCl as an eluent. The separation efficiency in their case was 99 % for U and 97 % for other radioactive elements. At the same time, no radioactive isotopes or their transformation products were detected in the solid residue after extraction. Diagram and individual groups of extracted elements are summarised in the following figure:

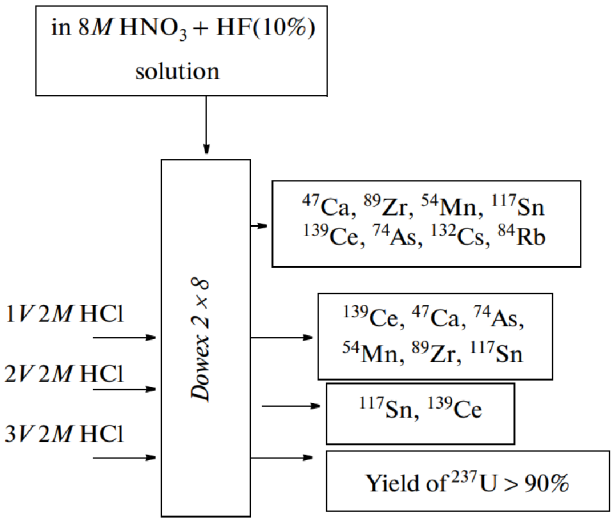

Fig. 19 Scheme of radiochemical separation of elements from fly ash and their resolution [142]

3 GOALS OF WORK

Hlavním cílem této práce je nalezení způsobů, jak dosáhnout maximální efektivity procesu separace majoritních prvků z vedlejších energetických produktů. Tohoto bude dosaženo pomocí výzkumu použití vhodných metod a postupů používaných v běžných odvětvích zpracování tradičních komodit – hydrometalurgických procesů. Dále pak bude prozkoumána a blíže objasněna možnost různých způsobů a možností modifikace popílků, ať už vysokoteplotních, či fluidních pro docílení vysoké míry efektivity celého separačního procesu.

Klíčovým parametrem pro posouzení vhodnosti experimentálně navržených řešení bude zejména parametr vyluhovatelnosti (rozpuštění do roztoku) hliníku, železa a titanu.

Cíle práce lze rovněž vyjádřit v v bodech následovně:

1) Literární rešerše shrnující původ a vlastnosti popílků, jejich stávající způsoby zpracování s přesahem o potenciální aplikace jako zdroje surovin.
2) Analýza složení vstupních surovin.
3) Studium způsobů zisku vybraných komodit pomocí hydrometalurgických procesů.
4) Modifikace vstupních surovin a parametrů aktivace extrakce pro dosažení co nejvyšší míry efektivity procesu.
5) Diskuze a shrnutí podstatných výsledků výzkumu.

The main goal of this work is to find ways to achieve the maximum efficiency of the process of separating major (macro-concentrated) elements from coal combustion products. This will be achieved by researching the appropriate methods and procedures used in traditional commodity processing industries, such as hydrometallurgical processes. Furthermore, various techniques and possibilities of ash modification, either high-temperature or fluidised-bed ashes, will be explored and clarified to achieve high efficiency in the entire separation process.

The key parameter for assessing the suitability of experimentally designed solutions will be the leachability parameter (dissolution into solution) of aluminium, iron and titanium.

1) Literary research summarizing the origin and properties of fly ash, their existing processing methods with an overlap of potential applications as a source of raw materials.
2) Analysis of the input raw materials composition.
3) Possibilities of selected commodities recovery using hydrometallurgical processes.
4) Modification of input materials and parameters of activation and extraction to maintain the most effective form of the recovery process.
5) Discussion and summary of the main research results.

4 EXPERIMENTAL

The experimental section of this thesis focuses primarily on identifying effective methods for activating fly ash to maximise the leaching of aluminium, followed by iron and potentially titanium, within a reasonable experimental timeframe. This was achieved through the application of conventional techniques and protocols, specifically the prevalent hydrometallurgical process involving leaching with a suitable reagent (specific type and concentration), optimisation of the solid-to-liquid phase ratio, reaction conditions (i.e. temperature and time)…

4.1 Summary of utilised samples and input materials

Various ash samples were chosen to extract macro-concentrated elements, specifically aluminium, titanium, and iron. These samples were obtained from the energy industry's production in multiple countries, including the Czech Republic, Poland, Turkey, and India. Additionally, the experiment encompassed the examination of ashes of natural origin, specifically volcanic ash from the Sicilian region.

HTFA from the CR: Počerady, Tušimice, TDK, Prunéřov, Ledvice, Dětmarovice, Opatovice, Paskov, Tisová, Vřesová, Orlen, ‘ŽĎÁS, TTR.

FBA/FFA from the CR: Ledvice, Poříčí, Hodonín, Tisová.

HTFA other countries: Rybnik, Opole (Poland); Sarni, Angul (India); non-specified locality Turkey.

Natural FA from Italy, Sicilia: Etna Silvester’s craters, Stromboli

Other chemicals and reagents: finely ground limestone from Štramberk and Vitošov, concentrated solutions of mineral acids such as sulphuric, phosphoric, nitric, and hydrochloric (p.a., Lachner), hydrogen peroxide, ammonia (p.a. Penta), anhydrous sodium, potassium, and calcium chlorides, citric acid anhydrous (p.a. Lachner), sodium and potassium carbonates (p.a. Lachner), sucrose, chelate III, sodium and potassium hydroxides, murexide, phenolphthalein (p.a. Penta) and demineralised water (FCH BUT).

4.2 Methods of laboratory analysis

4.2.1 Determination of moisture

All samples of CCPs used in the study were dried to a constant weight at 105 °C for HTFA and 65 °C for FFA and FBA before manipulation. The lower drying temperature for FFA and FBA is due to the expected presence of gypsum, a by-product of the dry flue gas desulphurisation process, to prevent its decomposition into hemihydrate, etc. This is how the moisture content of the samples was determined.

4.2.2 Determination of loss on ignition

Furthermore, the loss on ignition was determined in accordance with ČSN EN 72 2071 [143] in ceramic crucibles in a muffle furnace with a ramp of 5 °C/min to a temperature of 1,000 °C and a duration of 60 min, followed by controlled cooling with a ramp of 5 °C/min to a temperature of 150 °C, after which the samples were removed and left to cool to room temperature in a desiccator.

4.2.3 Determination of the free (reactive) calcium oxide content

The determination of the free (reactive) calcium oxide content was conducted for FFA and FBA and samples subjected to a thermal activation reaction with $CaCO_3$ reagents. The reactive part of CaO was quantified using the sucrose method following the guidelines of ČSN EN 72 2080. [144] This involved using a sample weight of 0.5 g, along with 15 g of sucrose and 50 g of demineralised water in a 250 mL plastic Erlenmeyer flask. The mixture was shaken horizontally on a laboratory shaker for 15 minutes. Subsequently, calcium saccharide was titrated with standard HCl solution, with phenolphthalein serving as a visual colourimetric indicator of the equivalence point.

4.2.4 Complexometric determination of calcium

The calcium content in the aqueous solution of the samples subjected to thermal activation reaction using $CaCl_2$ was determined by complexometric analysis. To initiate the analysis, a 2 g sample dose was mixed with 50 mL of demineralised water in a 250 mL Erlenmeyer flask. The flask was then placed on a laboratory shaking machine with horizontal movement for a duration of 30 minutes. Following this, 2.5 mL of 5 M KOH was added to the aliquot to adjust the pH to a highly alkaline level and precipitate magnesium hydroxide. The resulting mixture was subsequently titrated using a standard solution of chelate III, with murexide serving as a visual colourimetric indicator to determine the equivalence point. For the dilution of Ca^{2+} ions in Chapter 5.4.3, washing with citric acid was used due to the combination of $CaCO_3$ and $CaCl_2$ in the sample.

4.3 Methods of instrumental analysis

Various instrumental or structural analysis techniques were employed to characterise the input components, activated precursors, solutions during the extraction processes, or the resulting products obtained. The subsequent sections will concisely overview sample preparation procedures and characterisation conditions.

4.3.1 Phase composition – X-ray diffraction analysis

The powdered X-ray diffraction (XRD) technique has been extensively utilised to examine the phase/mineralogical composition of the input components and monitor phase changes in situ during high-temperature modification/activation reactions. The analysis involved processing a powder sample either by grinding in an agate bowl or using a vibrating mill in a zirconium bowl. Measurements were conducted using a copper anode ($K\alpha_1$ = 1.5406598 Å, $K\alpha_2$ = 1.544426 Å) with an excitation voltage of 40 kV and a current ranging from 5–90° 2θ, with a step size of 0.01313° 2θ on an Empyrean 2 instrument from Panalytical. Calcium fluoride served as a standard for quantitative Rietveld analysis, including the assessment of amorphous phase content. The collected data were evaluated using the software High Score plus.

4.3.2 Chemical composition – X-ray fluorescence spectrometry

Indicative values of the elemental composition of the samples were determined using X-ray fluorescence spectrometry (XRF) in the bulk state in a plastic vial with a thin PP foil (the sample was ground in an agate grinding bowl or ground in a vibrating mill and a zirconia bowl before measurement). The determination was carried out on an Olympus Vanta EDX-XRF stand with a 4 W Cu-anode at an excitation voltage of 40 kV, with a measurement time of 90 s for light and heavy elements.

4.3.3 Morphology and chemical composition – Scanning electron microscopy

Scanning electron microscopy (SEM) was used to monitor the morphology of the samples as well as the chemical composition. Before analysis, the sample was seduced by vaporising a layer of gold in an argon plasma environment. Secondary and backscattered electron imaging was used to monitor the morphology of the samples. An accelerating voltage of 10 or 15 kV was used depending on the nature of the analysis and a current of 100 pA to 2.5 nA (images/EDX analysis, WD 12 mm). Zeiss EVO LS 10 equipment was used. The EDX method (Oxford Instruments) analysed the elemental composition and evaluated it by AZtec software.

4.3.4 The determination of the specific surface area

The determination of the specific surface area of a material is crucial in assessing its reduction efficiency. N_2 adsorption/desorption behaviour was studied using the NOVA 2200 gas sorption analyser (Quantachrome). Samples were pre-treated by degassing them under the vacuum at 200 °C for 24 hours in case of HTFA samples and at 30 °C for 72 hours in case of FFA and

FBA samples. The multipoint BET (Brunauer-Emmett-Teller) method calculated total specific surface area from adsorption isotherm.

4.3.5 Particle size distribution determination

Laser diffraction was used to determine powdered samples' particle size and distribution. The particle size distribution was measured in a dry dispersion environment using a Venturi nozzle at a dispersion pressure of 2 bar and a vacuum of 10–50 mbar; the optical concentration of the sample was 3–5 % with an approximation to spherical particles (shape factor 1.00). The Fraunhofer diffraction model suppressing optical parameters was used for the evaluation. Measurements were made in the 0.1–1,750 μm range on a Helos KR instrument with a Rhodos dispersion system from Sympatec.

4.3.6 Thermal behaviour determination

Thermogravimetry and differential thermal analysis (TG-DTA) were utilised to investigate sample behaviour under increasing temperatures, detecting weight changes and differentiating individual thermal processes such as decomposition and crystallisation. A sample weighing 10–30 mg in a corundum crucible underwent analysis in an inert argon atmosphere with a flow rate of 100 ml/min and a heating rate of 5 °C/min up to a target temperature of 1,000 °C for 60 minutes, followed by cooling at 5 °C/min to 600 °C. The analysis was conducted using the SDT Q 650 instrument from TA Instruments.

Thermal microscopy involved observing changes in the sample's silhouette shape at a temperature rate of 5 °C/min up to a target temperature of 1,350°C. A picture of the sample's silhouette was taken after each 10 °C temperature increase, allowing for the evaluation of volume changes resulting from reactions like decomposition or sintering. An incandescent microscope Hesse Instruments EM-201 in a horizontal arrangement was employed for this analysis.

4.3.7 Inductively coupled plasma optical emission spectrometry

While other methods focused on characterising the solid state of samples and raw materials, ICP-OES was explicitly used to determine the exact content of individual components (elements) before and during the extraction process.

To prepare the samples for analysis, they were first converted from a solid to a liquid phase by melting them on a gas melter. This was achieved by using a mixture of propane-butane, oxygen, and air, along with lithium fluxes tetraborate and metaborate in a weight ratio of 3/1 and lithium bromide as a wetting agent. The sample weighed 0.5 g, while the flux mixture and wetting agent weighed 7.5 g and 0.5 g, respectively. The resulting homogeneous melt was then dissolved in 150 mL of nitric acid diluted in an acid/water ratio of 1/2, and this solution was stirred at 80 °C for 30 minutes using a teflon beaker and stirrer.

After the extraction process, samples of the resulting mixtures were taken at specific time intervals and the solid part was separated from the liquid using a centrifuge. The liquid portion was then subjected to analysis using ICP-OES.

ICP-OES uses argon plasma to atomize the sample. The sample is introduced into the nebuliser via a peristaltic pump and then mixed with argon before entering the plasma torch. The analysis is based on linear calibration curves. The measurements were performed using Ultima 2 device manufactured by Horiba.

4.4 Sample pre-treatment before extraction

4.4.1 Homogenization

The dried fly ash samples were mixed with the activator (or their blend) in plastic sealable containers, filling them up to 25 % of the container volume. Zirconium balls with a diameter of 10 mm were then added in an appropriate quantity. The homogenisation process lasted for 24 hours on a laboratory shaker of the "head/heel" type, operating at a speed of 2 s head-to-head.

4.4.2 High-temperature activation reaction

The high-temperature reaction between fly ash and selected activating agents occurred either in vertically positioned tablets or in fireclay cups ranging from 5 mL to 250 mL in volume. This process took place in a muffle furnace, following a heating mode of 5 or 10 °C until reaching the desired temperature range of 800–1,100 °C, with a maximum duration of 180 min. Subsequently, controlled cooling at a rate of 5 °C/min was applied until reaching a temperature of 150–600 °C, or alternatively, uncontrolled rapid cooling to room temperature was implemented.

4.4.3 Extraction process

The hydrometallurgical process was used as the primary mechanism for obtaining targeted elements from fly ash samples. Leaching of the samples under various conditions: in an acidic environment using different concentrations, equimolar amounts, L/S ratio, type of extractant and temperatures (concentration 5–20 wt: % or 0.5–2 M; mol eq. 0.4-1.4; L/S ratio 10–20; ambient to boiling point); in beakers made of borosilicate glass of suitable volume (filling up to 50 % of the container volume), the mixture was homogenised over time using a magnetic stirrer with a length of 30–60 % of the container diameter at speed optimised against sedimentation of the solid portion, as well as the formation of a vortex or spraying of the mixture. For mixtures exceeding the volume of 1,000 mL of extraction agent, a glass radial stirrer and a laboratory stand mixer were used in combination with a plastic container of suitable volume and diameter according to the amount of mixture (2.5–30 L)

The experiment road map in Fig. 20 can simplify the continuity of individual chapters to achieve a universal process of activation and extraction applicable to a wide range of samples.

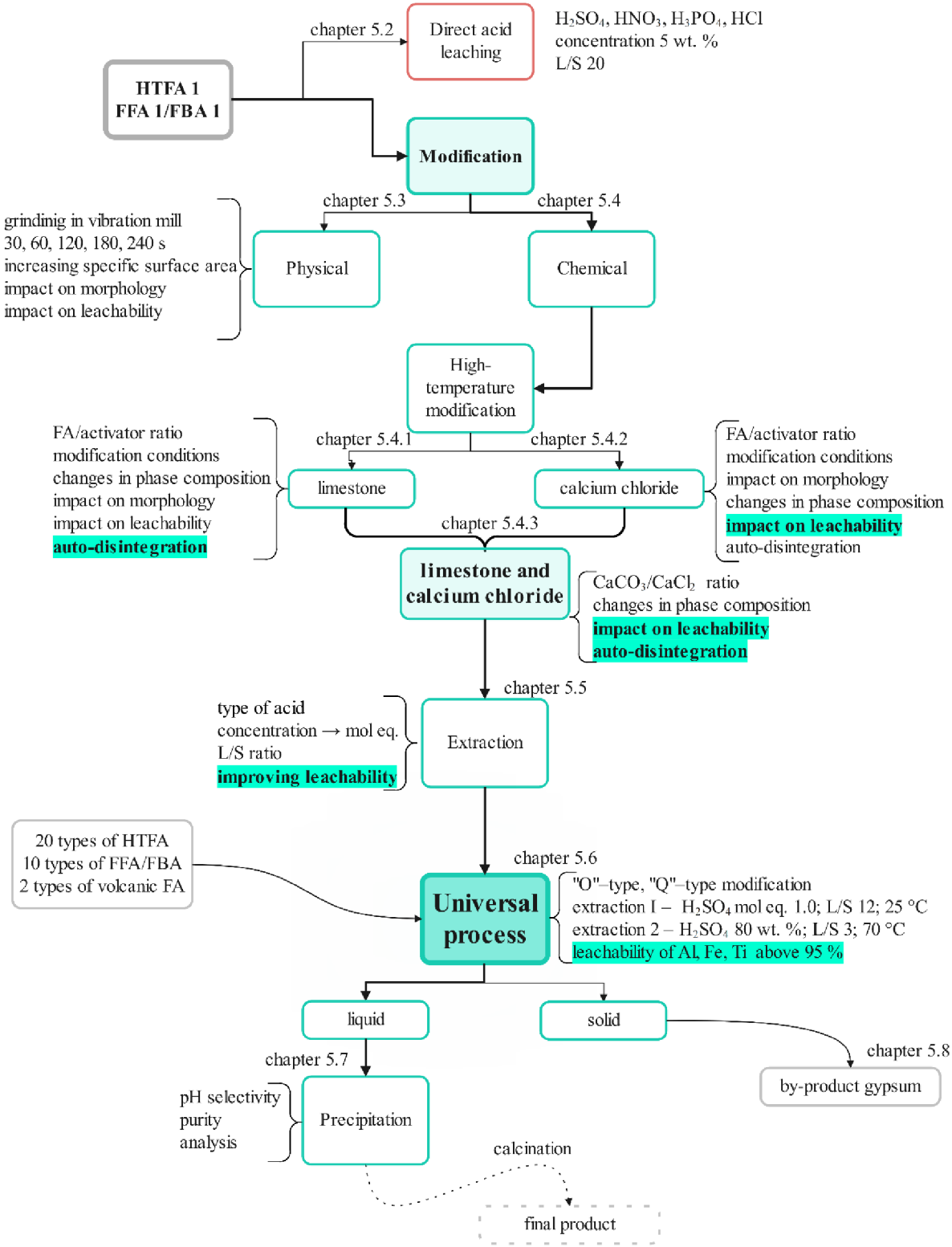

Fig. 20 Flow chart of the doctoral thesis experiment

5 RESULTS AND DISCUSSION

The upcoming chapter will provide a comprehensive overview and discussion of the outcomes obtained from experimental research in the asset/modification of used FA, modification options, and the leaching process.

5.1 Characterization of raw materials

Analysis of the raw materials input is crucial for the accurate extraction process, adjustment of modification parameters, and determining leachability/ (i.e., conversion of the solid part into a solution). The precise characterisation of the input raw materials was conducted through XRD Rietveld analysis, with the internal standard to ascertain the content of the crystalline and the amorphous phase. Furthermore, the chemical composition was identified using XRF. The results pertaining to the primary input samples (HTFA Počerady and FFA/FBA Ledvice) for these analyses can be found in Table 11–Table 13. The phase and elemental composition of other FA used later in a final experiment in chapter 5.6 can be found in the appendix.

Table 11 Phase composition (XRD) of HTFA 1 Počerady

Content (wt. %)						
Amorphous	**Quartz**	**Mullite**	**Magnetite**	**Hematite**	**Anatase**	**Rutile**
52.8	11.8	**34.8**	0.2	0.1	0.1	0.1

Table 12 Phase composition (XRD) of FFA and FBA Ledvice

	Content (wt. %)					
	Amorphous	**Quartz**	**Calcite**	**Magnetite**	**Hematite**	**Lime**
FFA1	**64.2**	10.5	1.4	0.1	1.9	7.8
FBA 1	**54.7**	10.3	–	0.1	0.4	11.0
	Anhydrite	**Anatase**	**Muscovite**	**Albite**	**Orthoclase**	**Åkermanite**
FFA 1	7.3	1.0	–	5.4	0.3	0.1
FBA 1	15.7	0.1	1.5	0.5	–	1.5

Table 13 Chemical (elemental) composition of HTFA 1, FFA1 and FBA 1

	Content (wt. %)							
	Al_2O_3	**Fe_2O_3**	**TiO_2**	**MgO**	**CaO**	**SiO_2**	**K_2O**	**SO_3**
HTFA 1	27.12	6.67	1.5	0.75	2.27	53.58	1.67	0.53
FFA1	20.17	4.32	2.29	0.19	17.25	33.11	0.35	11.47
FBA 1	15.73	6.42	1.89	0.38	29.15	26.79	0.13	11.56

Based on the phase composition results, the primary distinction between HTFA and FFA/FBA is the presence of free lime or portlandite and calcium carbonate as a desulphurisation reagent, respectively. The HTFA samples, resulting from the dry method of flue gas desulphurisation, contain mullite due to the higher temperature during the combustion process. Mullite is the primary source of aluminium in HTFA and could be relatively resistant to mineral acids. The focus of research in enhancing the leachability of metal-based elements from fly ash seems to be on modifying the phase composition, particularly by reducing the amorphous phase

content and chemically transforming mullite into other less resistant calcium and aluminium-based phases.

The input materials utilised in this study were HTFA Počerady (referred to as HTFA 1) and FFA and FBA Ledvice (referred to as FFA 1 and FBA 1). Samples were chosen due to their chemical and mineralogical composition (Table 11–Table 13). The remaining FA samples were employed towards the end of the experiment to evaluate the universality of the process established through comparison in Chapter 5.6.

Additionally, the applied industrial chemicals were analysed for phase and chemical composition. Finely ground limestone exhibited a high purity level (iron and magnesium impurities not exceeding 0.5 %), as evidenced by the contents of the individual components listed in Table 14. Table 15 then summarises other essential characteristics of the used CCPs for further experiments.

Table 14 Basic characterisation of used limestone Vitošov and Štramberk

	Content (wt. %)						
	Calcite	**Dolomite**	**Quartz**	**Al_2O_3**	**Fe_2O_3**	**MgO**	**K_2O**
Vitošov	99.8	0.1	0.1	–	0.1	0.	0.2
Štramberk	99.9	0.1	–	–	0,1	0.1	0.2

Table 15 Basic parameters of used CCPs

	Parameter/Content					
	Density ($kg \cdot m^{-3}$)	**Blaine** ($m^2 \cdot kg^{-1}$)	**BET** ($m^2 \cdot g^{-1}$)	**Free CaO** (%)	**LOD** (%)	**LOI** (%)
HTFA 1	2 249	315	9.624	–	0.29	1.12
FFA1	2 716	633	6.624	4.76	0.47	2.42
FBA 1	2 724	548	7.252	4.69	0.29	3.19

5.2 Direct acid leaching

Since the possibilities of using the direct leaching method were dealt with in earlier experiments in previous research [49, 113], in particular the leaching of unmodified fly ash in various mineral acids environment of various concentrations, were prepared for completeness of the comparison for HTFA 1, FFA 1 and FBA 1. Solutions of acids of 5 wt. % and L/S ratio of 20 were used. In Fig. 21a shows the leachability of Al from HTFA 1 in the environment of different mineral acids, while the graph in Fig. 21b shows the same values from FFA 1 and FBA 1.

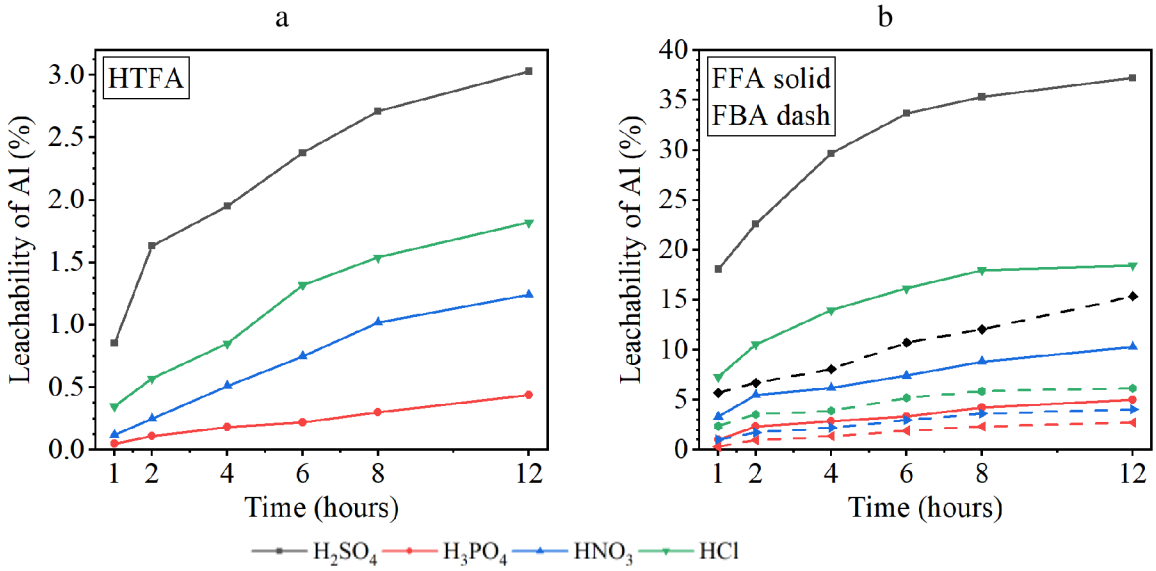

Fig. 21 Comparison of the leachability of Al at direct acid leaching: a) HTFA, b) FFA and FBA

For sample HTFA 1, the type or concentration of used acids did not have a significant impact, likely due to the unique combination of morphology and chemistry of HTFA, as was also examined by the authors [107]. Spherical particles covered with a large amount of glassy phase with a minimum of pores, as could be seen in the previous SEM image (see Fig. 5a), provided a poor opportunity to react with the extraction agent, and even if it penetrates the particle, it was not able to decompose the mullite present. In the case of FFA 1 and FBA 1, the situation was slightly different, mainly due to the morphology of the FFA ash. The absence of a significantly chemically resistant glassy phase is evident from the SEM image in Fig. 5b. The aluminium leachability was determined, and as can be seen from the results, the highest leachability occurred in a sulphuric acid environment, which was also confirmed by the published reactivity of base metals with acids [145]. Of course, the situation in FA samples is much more complicated, since there is no direct reaction of metallic Al with acid, but reaction with certain compounds, phases or alloys. Determining the reactivity in such a complex system is not entirely accurate, as evidenced by [117, 146, 147]. Nitric and hydrochloric acids reacted mainly with alkali content and CaO particles, which was also used as a modification of the ash before the main leaching in the previous work [97,119]. These findings conclusively demonstrated that adjusting or activating the input material is necessary to increase the leachability of the components.

5.3 Mechanical activation

Mechanical treatment with targeted particle size reduction is offered. As the size of the particles decreases, the size of the specific surface increases, increasing the number of places where the reaction can take place.

For this purpose, a series of mechanically activated HTFA 1, FFA 1, and FBA 1 samples were prepared. During the grinding time, the particle size, particle size distribution, specific surface area, and, last but not least, reactivity were analysed after leaching in a sulphuric acid solution (L/S 10, mol eq. 1.2 of the theoretical amount according.

In the case of HTFA 1, there is a very effective reduction of the part in the first minute of milling on the vibrating mill when the size of the medium particle x_{50} decreases from the original almost 50 µm to 18 and 12 µm, as well as the size of the largest particle x_{99} gradually decreases from 334 to 50 µm, as evidenced by the particle size distribution plot in Fig. 22. Mechanical activation resulted in a very effective change in the particle size distribution. Still, the specific surface areas increased only by approximately 18 %, as shown in Table 16.

Table 16 Specific surface area (BET) of the sample HTFA 1 Počerady

	Milling time (s)					
	raw	**30**	**60**	**120**	**180**	**240**
Specific area (m^2/g)	9.624	9.740	10.347	10.815	10.836	11.297

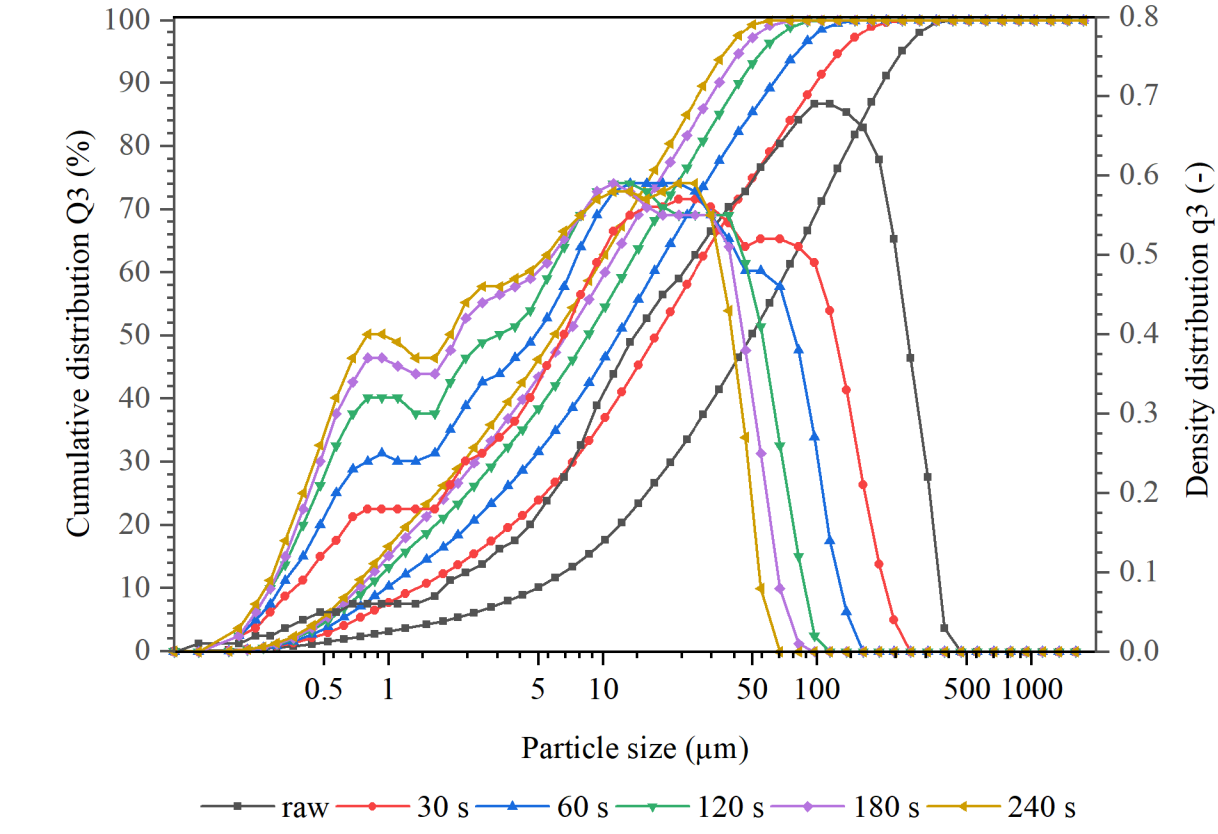

Fig. 22 Particle size distribution for various milling times, HTFA 1

After subjecting the sample to leaching in a sulphuric acid environment (L/S 10, mol eq. 1.2), it was evident that there was no significant enhancement in the efficiency of the leaching process, as could be seen in the graph in Fig. 23. While there was an overall increase ranging from several tens to hundreds of per cent, the absolute improvement did not surpass 5 % of the aluminium leachability. However, despite these sub-optimal results, it could be argued that the leachability of Al increases as the milling time increases, resulting in a higher specific surface area of the material. The most notable distinction can be observed when comparing the raw HTFA 1 with the sample ground for 30 seconds, which is consistent with the observed shift in particle distribution.

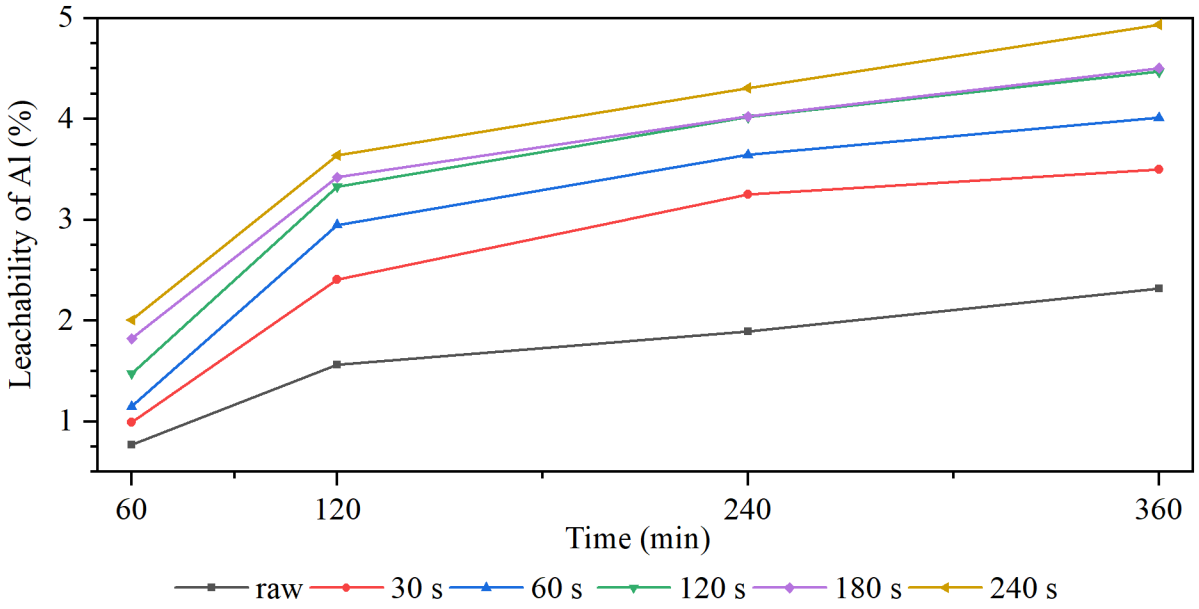

Fig. 23 Comparison of the leachability of Al; HTFA 1 at different milling times

These findings indicated that the conventional method of activating the sample through grinding was not suitable for the specific type of FA, as the particle morphology remains largely unchanged. This was further supported by the SEM image in Fig. 24, which revealed that despite an increase in the quantity of smaller particles in the grounded HTFA 1 sample compared to the unground sample, these particles still retained a spherical shape and minimal visible porosity. Although grinding resulted in the fragmentation of some particles, a significant amount of the larger particles still consisted of an agglomerate of smaller ones.

a b

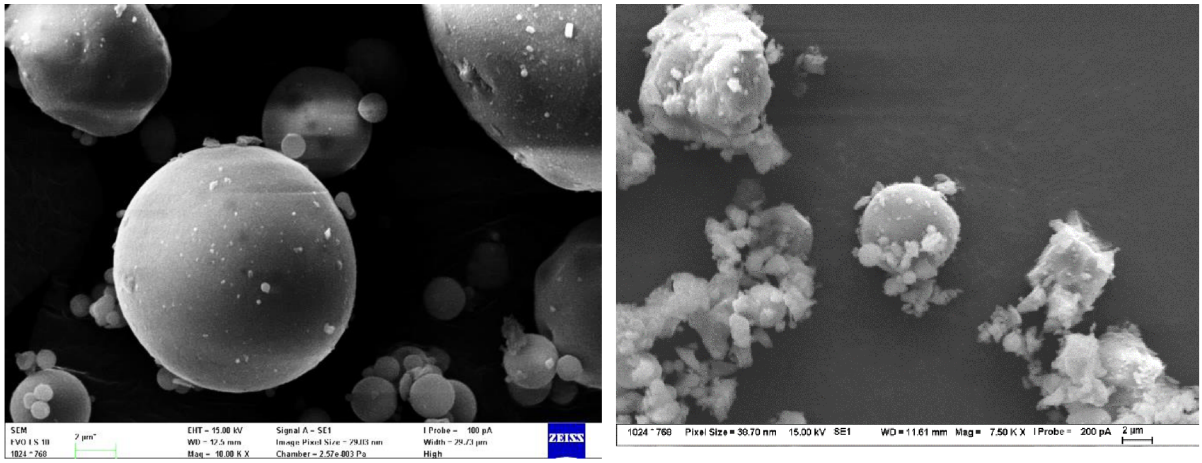

Fig. 24 SEM images of the HTFA 1 morphology, (a) raw HTFA; (b) milled for 240 s

The mechanical activation of FFA 1 and FBA 1 exhibited a slightly distinct nature. Initially, during the grinding process, the material underwent partial comminution, as depicted in the particle size distribution, Fig. 25 and Fig. 26. However, at a certain point, the particles started to adhere to each other once again, leading to an unexpected increase in their size. The measurement of the specific surface size of the particles in Table 17 further supported this phenomenon. This FFA 1 and FBA 1 property can probably be attributed to the presence of hemihydrate and portlandite. As the sample was ground, the temperature inside vessels increased and rose, causing partial decomposition of the hemihydrate and subsequent sticking of the particles, which can result in higher values of surface areas. Samples with a grinding time of 60 s were chosen for extraction. The achieved specific surface areas were more than 250 % (FBA 1) and 300 % (FFA 1) higher than the original material.

Table 17 Specific surface area (BET) of the sample FFA and FBA 1 Ledvice

		Milling time (s)					
		raw	**30**	**60**	**120**	**180**	**240**
FFA 1 Ledvice	**Specific area (m^2/g)**	6.624	9.940	19.974	19.973	17.333	17.426
FBA 1 Ledvice		7.252	10.037	18,361	17.573	17.761	17,328

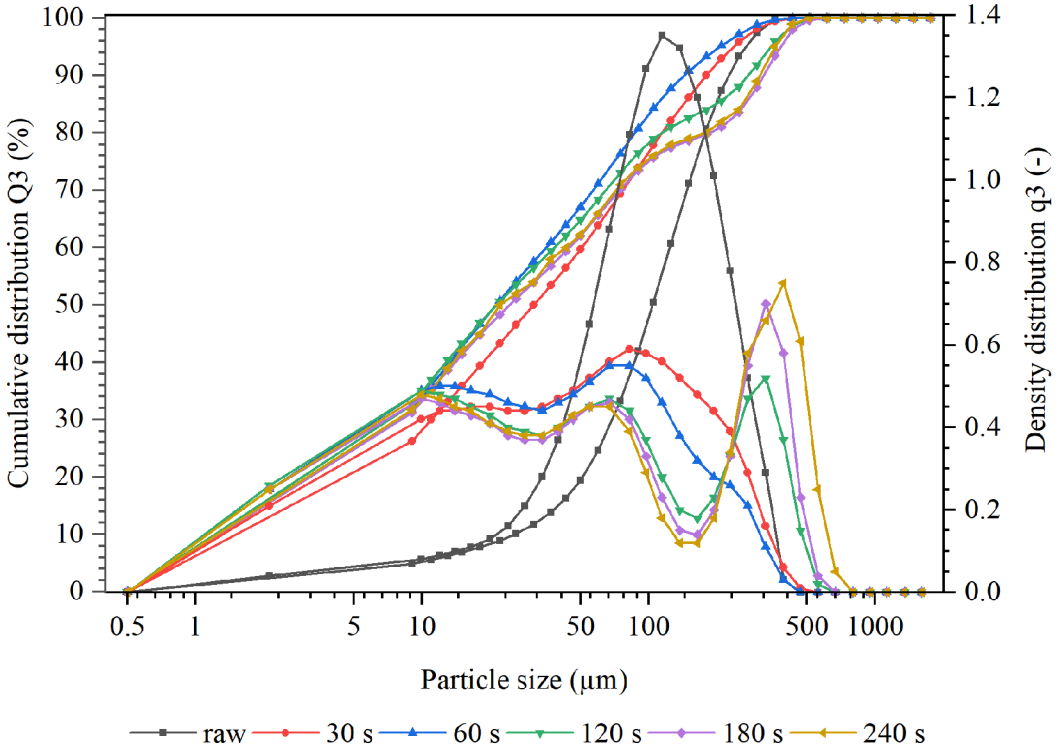

Fig. 25 Particle size distribution for various milling times, FFA 1

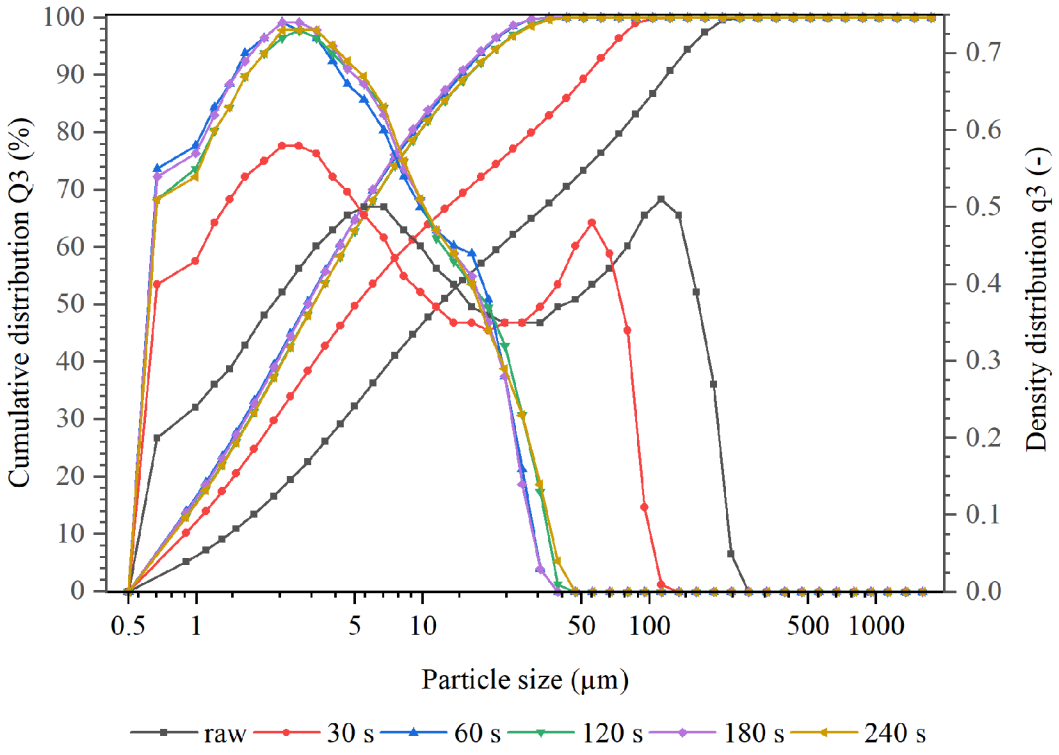

Fig. 26 Particle size distribution for various milling times, FBA 1

Despite the substantial increase in specific surface area, a control test of aluminium leachability under the same conditions as for the above sample revealed a rise in leachability of approx. 15–20 %, which is shown closely by the graphs in Fig. 27. Although this can be considered a positive result to some extent, the total leachability did not exceed 50 % for FFA 1 and 27 % for FBA 1.

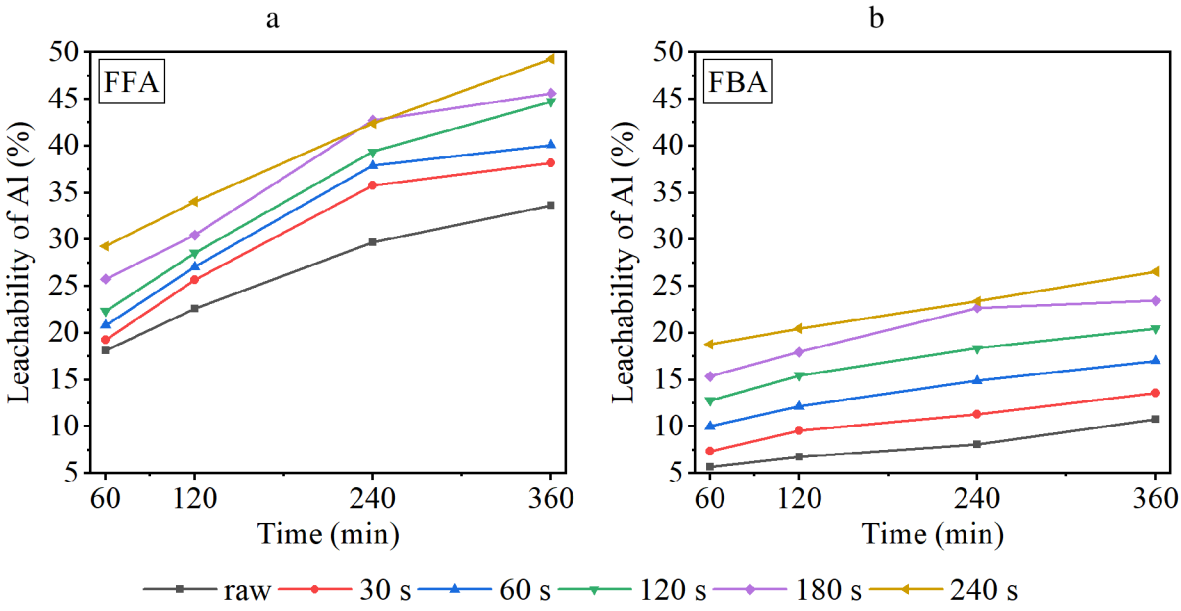

Fig. 27 Comparison of the leachability of Al; (a) FFA; (b) FBA at different milling times

The data in the graphs show that although there is a remarkable 2.5–3 times increase in specific surface area between the raw FFA 1/FBA 1 and the milled sample at 60 s, with no significant change or even decrease thereafter, in addition, Al leachability shows an approximately linear increase over time, in the case of sample FBA 1.

Based on the obtained results, the mechanical activation method is considered unsuitable for precise application on fluidised-bed CCPs.

5.4 Chemical activation

The following chapter can be considered as pivotal and the main part of this work and the entire multi-year research in this area. Only very few authors worldwide are dealing with the issue of obtaining specific components from FA, and an even smaller percentage of them are actually studying and describing the sequence of modification reactions.

However, the initial data from the previous work [113] already showed that the path to achieving maximum utilisation, especially of aluminium and HTFA, is possible. Therefore, this work mostly considers the individual modification parameters such as the ratio of activating/modifying substances or their mixtures, temperature, and the overall temperature regime of modification, cooling, and many others. In a very simplified way, chemical activation or the high-temperature modification of fly ash can be described as its reaction with a suitable agent at a temperature of several hundreds of degrees, which leads to a favourable change in the phase composition for leachability.

5.4.1 Activation with limestone

As a basic input experiment for modifying the phase composition of fly ash, a high-temperature reaction of fly ash with calcium carbonate was utilised [99, 100]. The experiment conducted in the context of this thesis involved a more intricate sample preparation method and an overall reaction model. In this model, the mass ratio between fly ash and the reagent was substituted by the molar equivalent ratio, which was determined based on the total amount of limestone needed to achieve the desired products as described in equations (21)–(27) in chapter 2.4.2., page 38.

Identifying the most suitable FA/activator ratio, temperature, and duration of the reaction

To begin with, samples were prepared with molar equivalent ratios ranging from 0.2 to 1.3, with an increment of 0.1 mol eq. The molar equivalent is understood as the sum of the molar equivalents of partial reactions leading to the formation of theoretical products according to the equations mentioned above. The elemental composition HTFA 1 is taken as the starting composition, i.e. the content of Al, Fe, Ti, Si, ... These samples were then subjected to a reaction at temperatures ranging from 800 to 1,100 °C, with a holding time of 30 to 180 minutes, followed by rapid cooling. In all the modified (HTFA 1 samples prepared using this method, with the addition of a modifying agent gradient, the quantity of free (reactive) CaO was determined using the titration method employing the carbohydrate method. Furthermore, the degree of conversion, or the rate of reaction, of the modifying agent was calculated based on obtained data. The summarised results of these calculations are presented in the graph in Fig. 28.

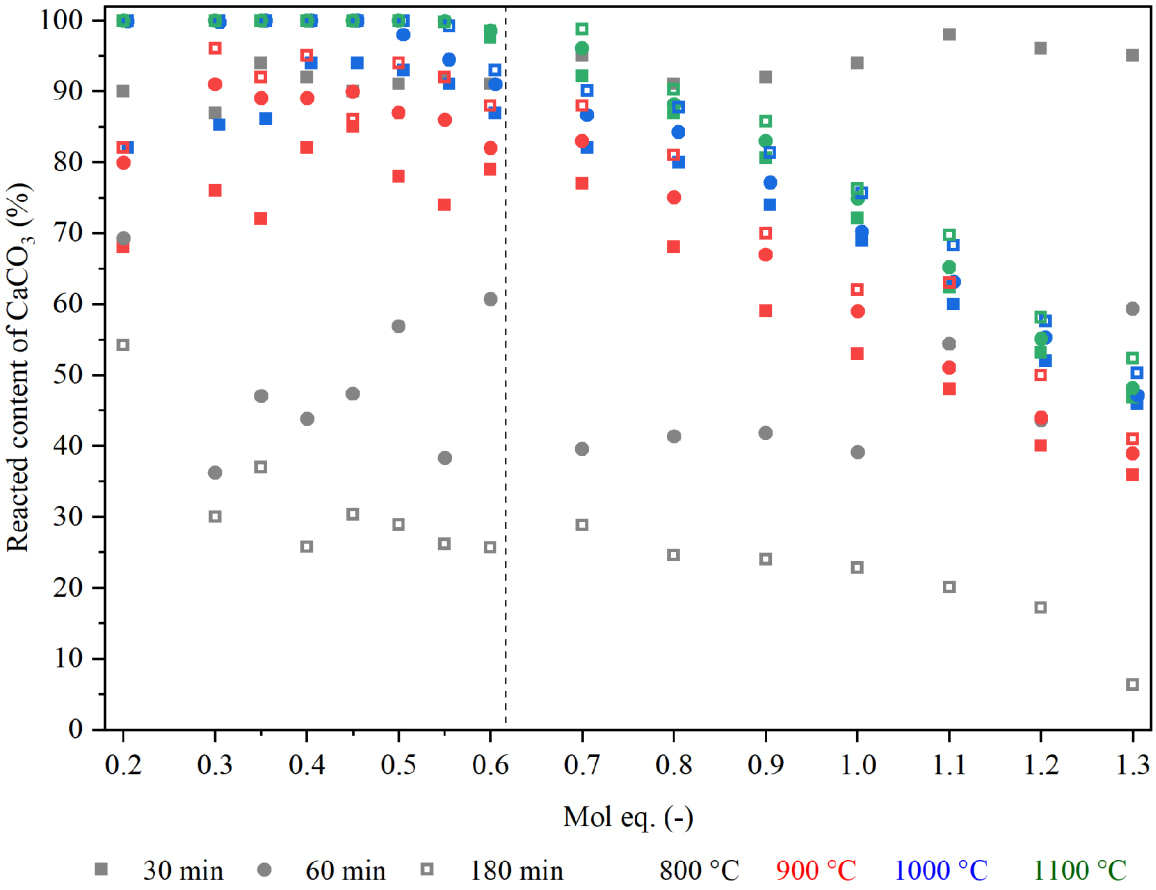

Fig. 28 Graph of the reacted amount of $CaCO_3$ with HTFA 1 as a function of reaction temperature and time

The results indicated that the HTFA 1 samples, which underwent the reaction at 800 °C (shown grey in the Fig. 28), displayed high initial conversions after 30 minutes of reaction but rapidly declined with prolonged temperature exposure. This phenomenon can be attributed to the absence of decomposition of the potentially reactive carbonate in addition to the HTFA 1 sample, which had the shortest reaction time due to the lowest temperature profile. Samples treated at 900 °C exhibited a certain trend, with a higher rate of reacted modifying agent at higher temperatures, which aligns with the theory of reaction activity. Moreover, the experimental data showed no significant increase in reaction degree with longer reaction times. The data also implied that addition exceeding 0.6 mol eq. may not result in a substantial modification of the input material, as was indicated by the gradual increase in unreacted CaO content above this ratio in the HTFA 1 sample (see dashed line in Fig. 28).

Hence, the FA/$CaCO_3$ ratio range of 0.3–0.6 mol eq. appeared to be the most potentially useful interval. To further refine this range and determine the optimal dosage of the modifying agent, additional amounts of 0.35, 0.45, and 0.55 mol eq. were added to the series. The results indicated that for the two highest temperatures, namely 1,000 °C and 1,100 °C (highlighted in blue and green in Fig. 28, the optimal conversion of the modifying agent occurred within the range of addition up to 0.55 mol eq. Therefore, for samples fired at 1,100 °C, a temperature

holding time of 30 minutes was recommended, while for samples subjected to treatment at 1,000 °C, a holding time of 60 minutes was suggested.

A higher addition of more than 0.6 mol eq. did not result in any additional modification of the material highlighted in theoretical reactions.

An essential inquiry arises: what are the products generated from the activation reaction, and more importantly, can the activation of FA through temperature modification and calcium carbonate be deemed appropriate.

To address this, the HTFA 1 samples underwent controlled leaching in an acidic environment, and the progression of the reaction was further elucidated using alternative analytical methods.

The samples across various reaction temperatures, durations, and limestone content exhibited an auto-disintegrating nature upon cooling to room temperature in the laboratory. Consequently, no sintering of the material or the development of a dense morphology was noted (Fig. 30). However, it was feasible to easily remove most of the samples from the ceramic container. In some cases, a self-supporting structure was formed, and it could be crushed by applying manual pressure.

The auto-disintegration phenomenon experienced during high-temperature modification could potentially yield significant benefits for future applications by eliminating the necessity for additional processing, such as energy-intensive grinding of sintered FA. This phenomenon will be discussed further later.

The impact of activation conditions on leachability

In order to evaluate the effectiveness of HTFA 1 modification using limestone in enhancing the leachability of macro-concentrated elements, esp. aluminium, a laboratory experiment was carried out. The primary objective of this study was to assess the leachability of aluminium over a specific period of time using extraction in a sulphuric acid environment at laboratory temperature. The experiment employed an L/S ratio of 10 and a quantity of acid equivalent to mol eq. 1.2, which corresponded to the products of the reaction mechanism described by the sequence of reactions (13)–(20) in chapter.2.4.1, page 35.

The results from the experiments conducted on modified HTFA at temperatures of 1,000 °C and 1,100 °C with reaction durations of 30 and 60 minutes at the specified temperatures demonstrated favourable outcomes when compared to unmodified HTFA 1 in the control assessment of aluminium leachability. The data presented in Fig. 29 highlighted two key observations derived from the investigations. Firstly, it can be observed that the aluminium leachability achieved was similar for samples subjected to firing processes at both temperatures mentioned, as well as for those with a reaction time of 60 minutes. Conversely, a group of HTFA 1 samples exposed to a lower reaction temperature and shorter duration (30 minutes) exhibited reduced leachabilities, approximately at 32 %, while the remaining sample groups under different conditions attained aluminium leachabilities of up to 48 %.

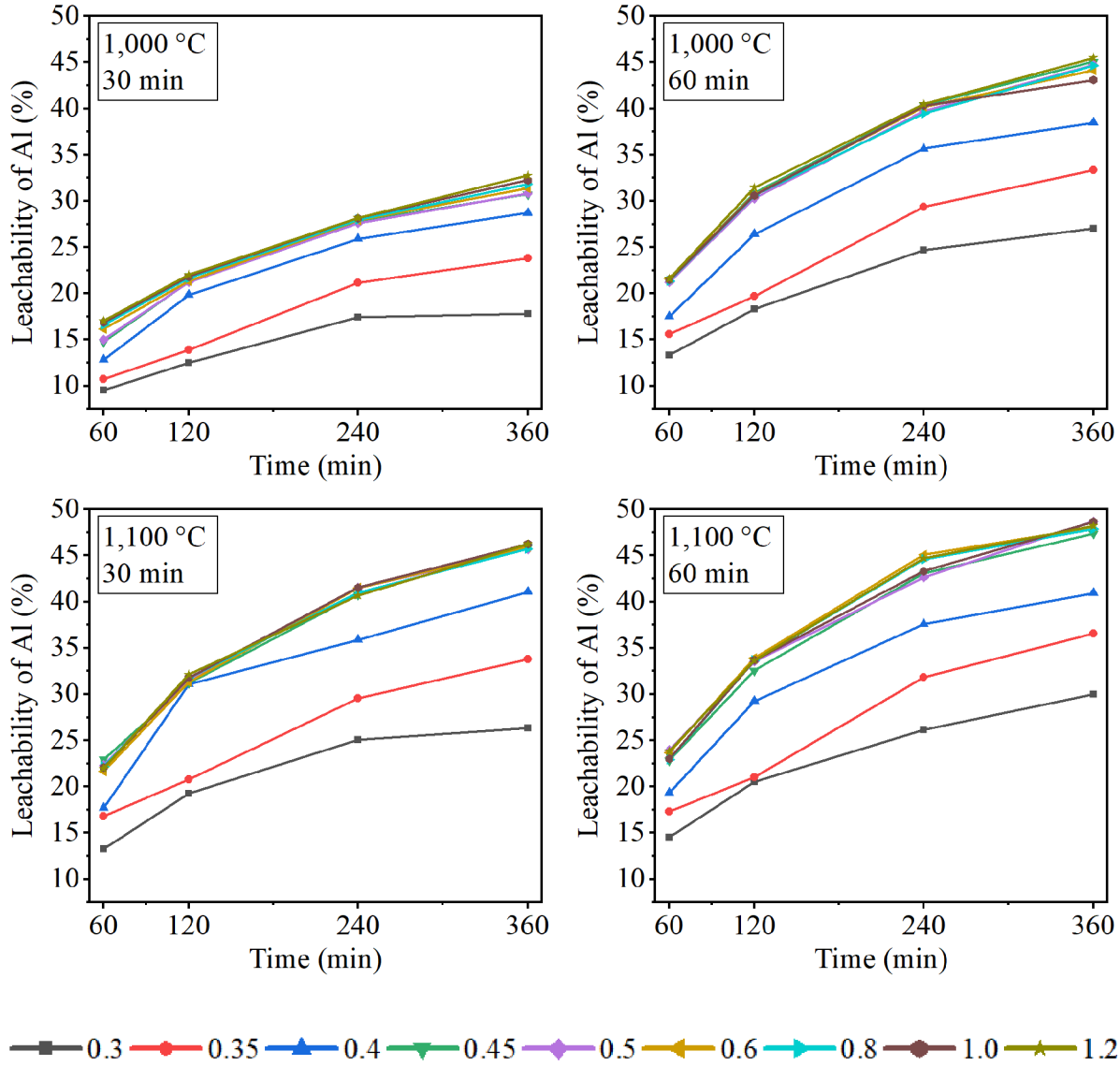

Fig. 29 Comparison of the leachability of Al; HTFA 1 modified with the addition of limestone at various dosages of the reagent, temperature, and reaction time

Simultaneously, this experiment has verified that the inclusion of quantities surpassing 0.6 mol eq. not only failed to yield additional reaction products and a greater extent of modification, but most importantly, all samples with limestone addition exceeding 0.6 mol eq. exhibited the same leachability. Based on the findings derived from this experiment, it can be concluded that the addition **of 0.45 mol eq. of limestone** was optimal in order to achieve the highest Al yield. Furthermore, the reaction was conducted at a higher temperature of **1,000 °C for 60 minutes** or at 1,100 °C with half the reaction duration. Subsequent experiments were performed at a reduced temperature.

Monitoring changes in HTFA during high-temperature modification reaction

Given the complexity of the high-temperature activation of FA using various reagents and the likely desired method for processing input materials in the future, as well as the lack of relevant publications describing or characterising the actual reaction sequence and products to date, it is necessary to attempt to solve this challenging task within the scope of research.

For these experiments, samples with the addition of 0.45 mol eq. $CaCO_3$ to HTFA 1 were utilised.

The heating microscopy technique was used to evaluate the sample body's volume changes and shape alterations as the temperature increased. This method was crucial in determining the theoretical reaction temperature limit before the sample underwent melting or sintering. The analysis revealed a deformation range of 1,220–1,250 °C and a material spreading limit temperature of 1,250–1,340 °C.

The images depicting the surface of the samples are illustrated in Fig. 30. It was observable that the sample's volume decreased gradually up to a temperature of 900 °C, primarily due to the compaction of the structure following the decomposition of limestone. Subsequently, at temperatures beyond 1,000 °C, there was a progressive increase in the sample's volume until it reached the melting point. This phenomenon can be further elucidated by plotting the sample's area size and shape factor against temperature, with the area expansion region being denoted by a dashed line (Fig. 31).

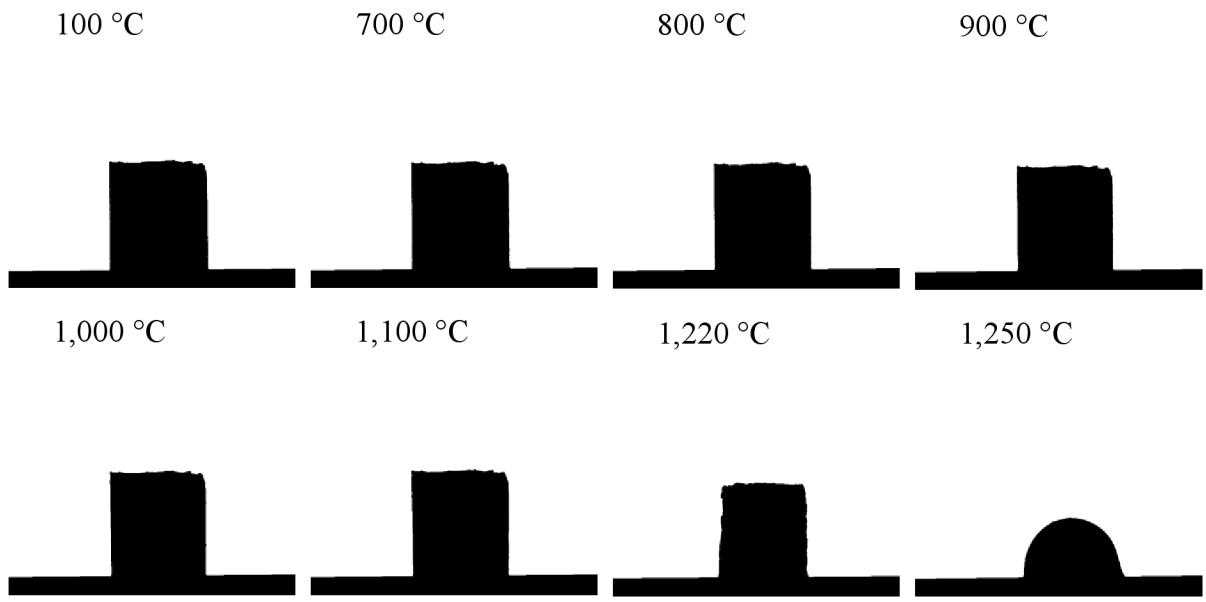

Fig. 30 Images of the shadow area of sample HTFA 1 mixed with limestone, mol eq. 0.45 as a function of temperature

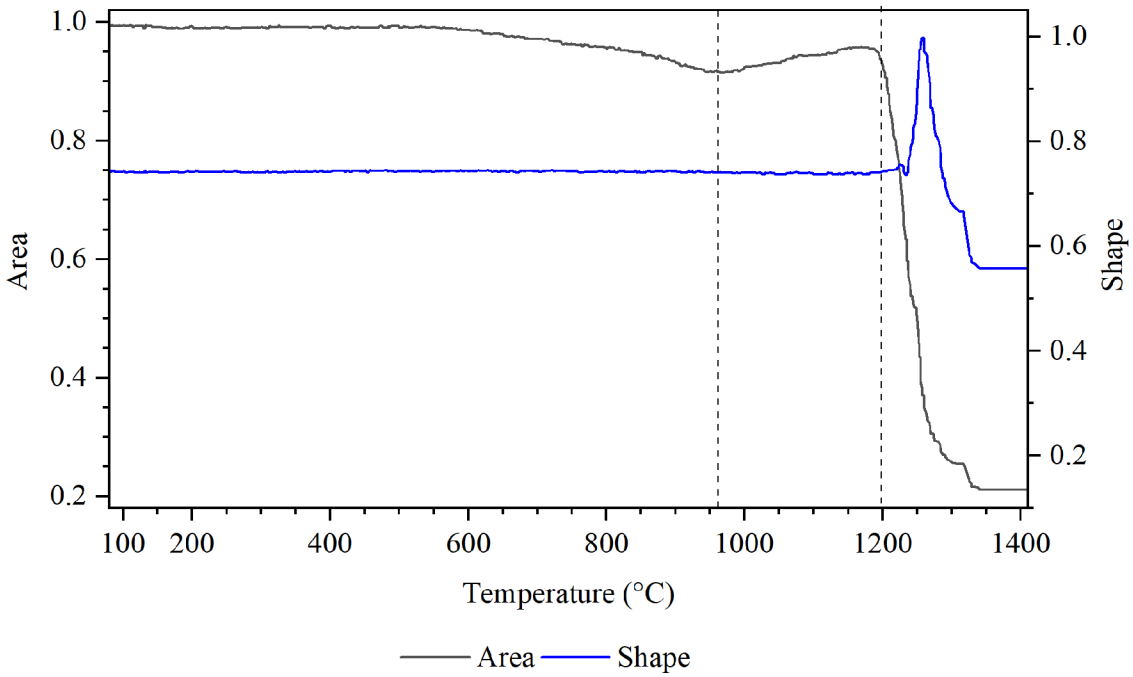

Fig. 31 The dependence of shadow surface area and shape on temperature as a function of temperature, sample HTFA 1 mixed with limestone, mol eq. 0.45

During the firing process, a simultaneous TG/DTA was utilised to simulate weight changes and monitor heat flow. This method aimed to approximate the temperature range at which various steps of the high-temperature modification reaction take place, including the formation of certain products. The TG/DTA examination was carried out on the HTFA 1 sample containing limestone in mol eq. 0.45, achieving a reaction temperature of 1,000 °C and a reaction duration of 60 minutes to ensure consistency in conditions during the high-temperature alteration process for the actual sample within the furnace. To simulate the conditions, the results (see Fig. 32) showed that the decomposition of $CaCO_3$ started around 680 °C and continued to almost 800 °C. Based on the heat flow data, it can be inferred that could be possible physical changes in state occurring at temperatures around 800 °C. However, this conclusion seems highly improbable considering that CaO has a melting point of 2,570 °C [146], while typical HTFA has a range of melting in temperature interval 1,400-1,500 °C [148]. Moreover, the resulting products, which will be discussed further, were expected to have similar properties, making it unlikely for there to be a change in crystallographic modifications based on the phases present. Therefore, it can be deduced that a chemical reaction between CaO and HTFA 1 takes place at these temperatures (approx. 1000–1200 °C) and can be seen from both thermal analyses. However, it is not possible to distinguish individual steps of this reaction using the current method. The discontinuity observed in the heat flux curve around 1,000 °C is attributed to the calibration response during mode switching. Therefore, it is not possible to definitively confirm the occurrence of the high-temperature modification reaction.

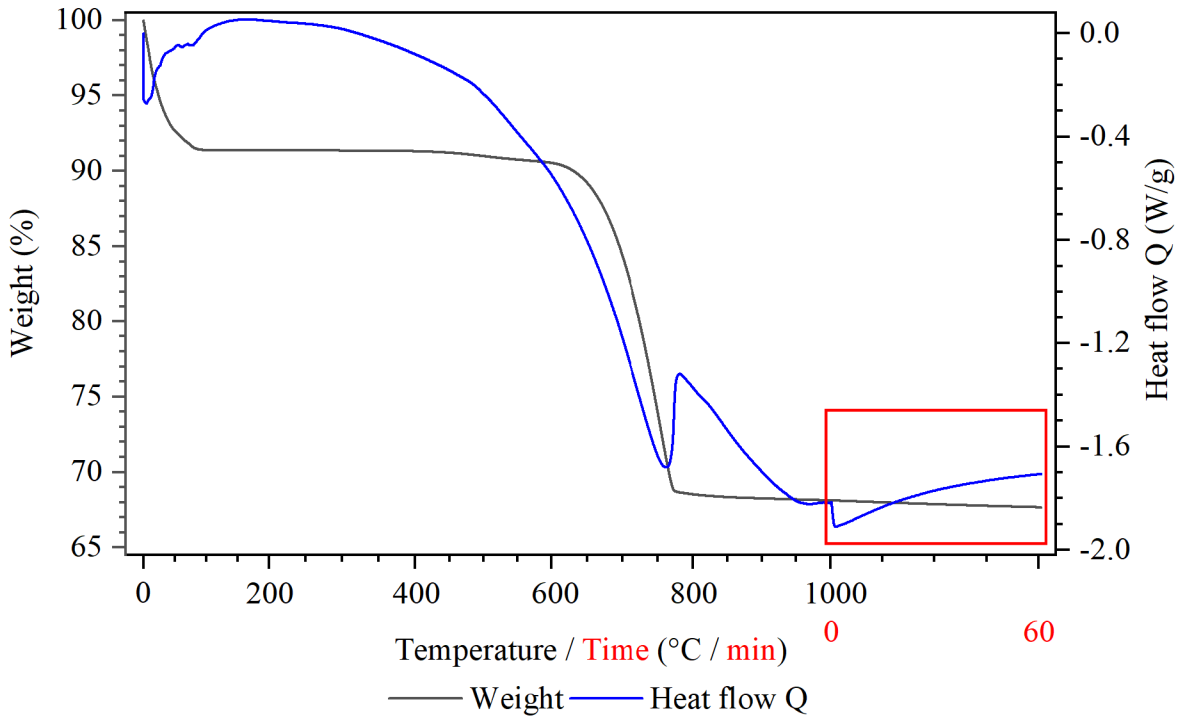

Fig. 32 TG/DTA curves of changes in the sample HTFA 1 mixed with limestone, mol eq. 0.45 under reaction mode

The in situ XRD high-temperature analysis provided a more detailed analysis of changes in the phase composition resulting from chemical reactions. In this study, a sample was subjected to heating according to a specific firing mode, and the phase composition was determined at regular intervals of 25 °C starting from a temperature of 500 °C. The duration of each temperature point was 10 minutes. The findings were then presented on the cut-out of the 3D graph in Fig. 33.

The results (see Fig. 33) indicate that the decomposition of limestone was observable until a temperature approximately 675 °C, which is consistent with the observations from TG/DTA and HM analyses. Additionally, from the initial temperature of the measurement, the formation of albite (sodium calcium aluminium silicate) or its analogue substituted by calcium ion was evident. The content of this phase gradually increased with rising temperature and reaction time. At 850 °C, the albite decomposed into gehlenite, and from 900 °C, gehlenite (G) and dicalcium silicate (C_2S) – larnite began to form gradually. Wollastonite (Wo) also gradually formed from these temperatures. Interestingly, the diffraction of mullite (M) did not decrease significantly, indicating the absence of a reaction between mullite and lime leading to the formation of new phases. Similarly, the content of quartz (Q) did not decrease either. It is highly likely that the formation of new phases occurs from the amorphous phase. The presence of a substantial proportion of lime (L), which remained relatively stable throughout the reaction, contributed to this phenomenon. No further adjustments in the phase composition, like the creation of new phases or adjustments in the content of current ones, took place despite prolonging the reaction time while keeping the temperature at 1,000 °C for 3 hours.

Unfortunately, it was not feasible to determine the amorphous fraction in-situ due to the potential reaction between the standard and the sample. Moreover, the specific experimental conditions, frequent isotherms, and the small weight of the mixture may not accurately reflect the processes that take place during the firing of the material in a bulk sample within a furnace.

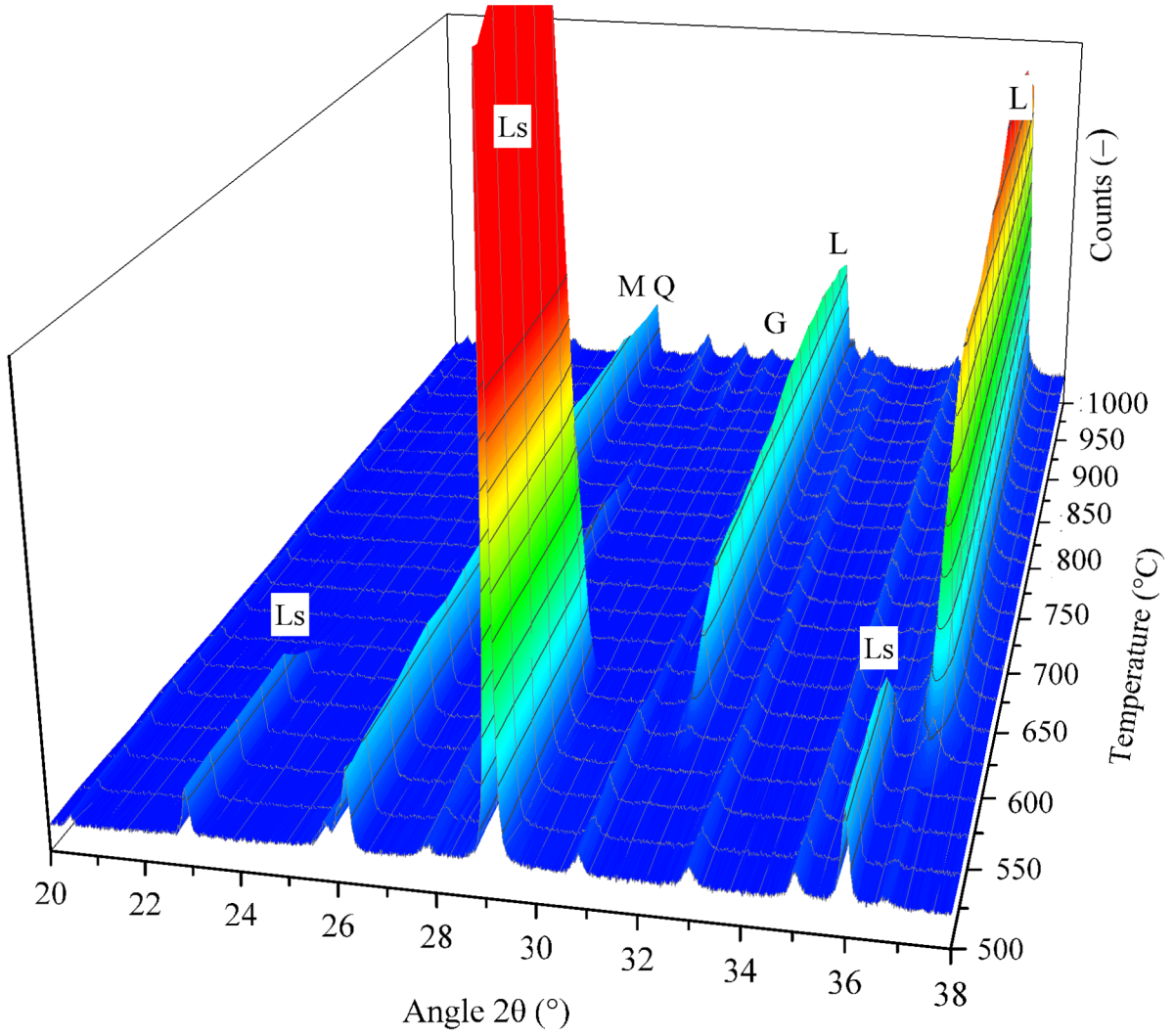

Fig. 33 3D graph of phase changes for sample HTFA 1 with limestone, mol eq. 0.45

Analysis of furnace-fired samples

In order to analyze the changes in phase composition of a real samples that were fired in ceramic crucibles within a muffle furnace, certain factors such as rapid cooling, sample handling, and the time delay between sample preparation and measurement need to be considered. To address this, a series of HTFA 1 samples were prepared using modification agent limestone and mol eq. 0.45, the same as mentioned in all the previously described methods, was maintained. These samples underwent a sequence of reactions at temperatures ranging from 800 to 1,100 °C, with a reaction time spanning from 0 to 180 minutes. The phase composition within the range of 2θ 20–38° is depicted in Fig. 34–Fig. 37.

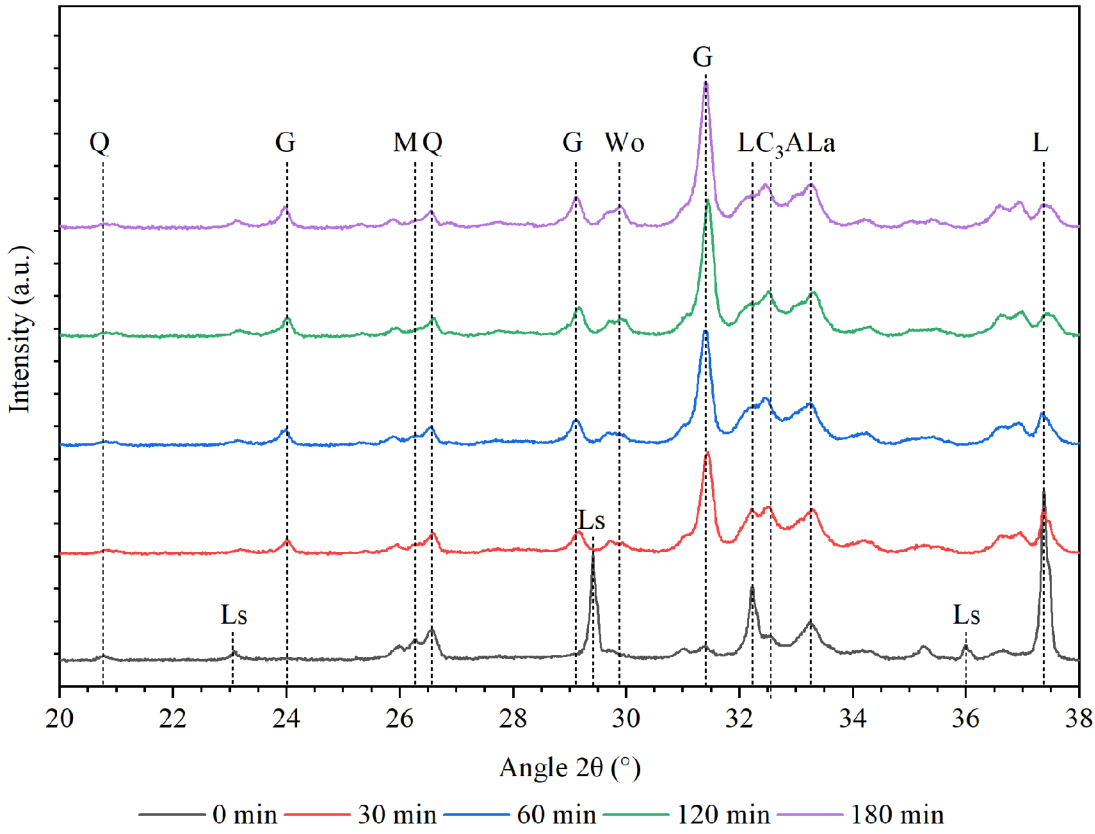

Fig. 34 Diffractogram of 2θ 20–38°range, sample HTFA 1 with limestone, mol eq. 0.45, 800 °C

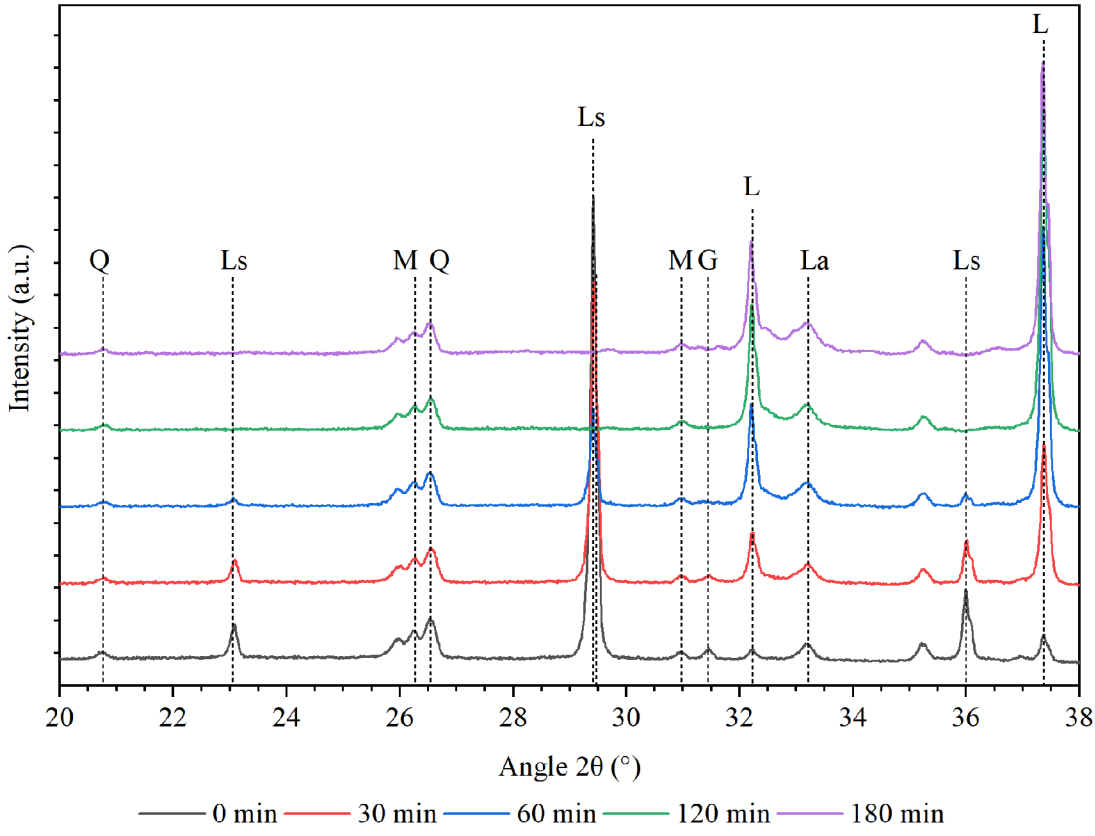

Fig. 35 Diffractogram of 2θ 20–38°range, sample HTFA 1 with limestone, mol eq. 0.45, 900 °C

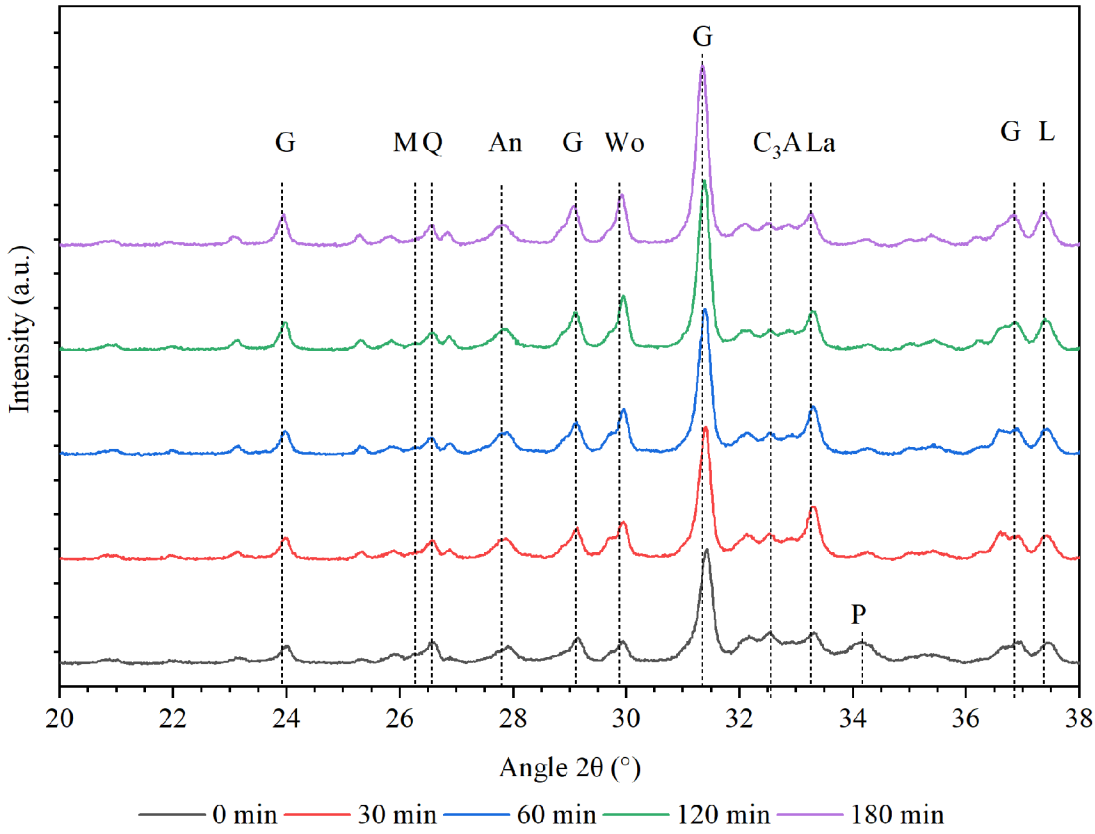

Fig. 36 Diffractogram of 2θ 20–38°range, sample HTFA 1 with limestone, mol eq. 0.45, 1,000 °C

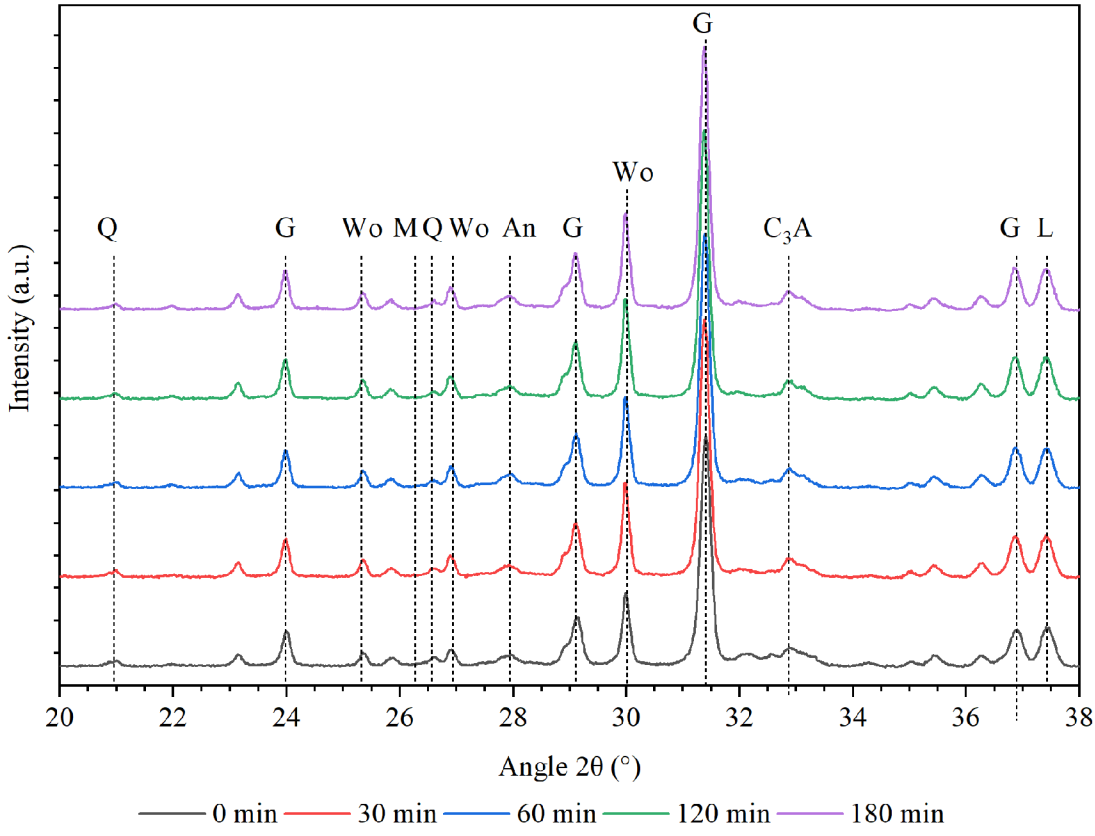

Fig. 37 Diffractogram of 2θ 20–38°range, sample HTFA 1 with limestone, mol eq. 0.45, 1,100 °C

In full accordance with the findings of prior trials, it can be affirmed that the onset of the high-temperature alteration reaction with limestone (Ls) commences at 800 °C, where the gradual emergence of novel phases becomes apparent. Yet, the overall completion of the reaction does not achieve noteworthy levels, given the substantial presence of unreacted lime (L) in the sample. Simultaneously, these outcomes indicate that the individual reactions take place at elevated temperatures compared to the scenario in a high-temperature chamber, as it is evident that the temperature at the surface and within the sample can be several hundred degrees lower due to heat transfer. The collection of samples subjected to a reaction temperature of 800 °C only exhibited a minor formation of larnite, specifically dicalcium silicate, larnite (La), with no alteration in the quantities of mullite (M) and quartz (Q).

Upon reaching the reaction temperature of 900 °C, a noticeable amount of undecomposed limestone (Ls) remained in the reaction mixture. However, after 30 minutes, this undecomposed limestone disappeared, leading to the formation of gehlenite (G), larnite (La), and tricalcium aluminate (C_3A) phases. Subsequently, after 120 minutes, there was a slight reduction in phase G and the emergence of wollastonite (Wo). Even after 180 minutes, a small quantity of unreacted L remained in the sample, consistent with the titration analysis for free lime as discussed earlier. Notably, unlike the sample at 800 °C, there was a significant decline in mullite (M) content, almost reaching the detection limit, along with a considerable decrease in quartz (Q). This suggests that the formation of gehlenite, wollastonite, as well as larnite and C_3A, was not solely derived from the non-crystalline fraction but also involves the crystalline phases.

By elevating the reaction temperature to 1,000 °C, the occurrence of undissolved limestone diminishes once the desired temperature was achieved. Furthermore, even after attaining the temperature of 1,000 °C, the proportions of gehlenite, wollastonite, larnite, C_3A, and anorthite (An) persisted. The representation of larnite increased as the reaction time extended, alongside gehlenite and wollastonite. Notably, the concentration of C_3A remained unaltered once the reaction reached completion, pushing the limits of the detection capability of the employed measurement method. The phase of mullite was visible solely at the onset of the measurement, and after 30 minutes of reaction time, mullite ceased to be detected. Additionally, the amount of quartz, which reacts with the available lime to form larnite, decreased. Larnite attained its highest abundance after 30 minutes of reaction time, subsequently experiencing a gradual reduction as it reacted to produce wollastonite and gehlenite. The detected presence of portlandite (P) is attributed to the handling and storage of the sample during the interval between firing and measurement. The cumulative quantity of unreacted lime was already minimal after 60 minutes of reaction time and remained constant thereafter. This finding aligns with the determination of free CaO using the titration method.

The utilisation of the sintering (high-temperature modification) method at the highest monitored temperature, which stands at 1,100 °C, exhibited notable distinctions when compared to the samples subjected to lower firing temperatures. Specifically, there was a

discernible decrease in the overall content of C_3A and a complete absence of larnite. On the other hand, the representation of G surpasses that of all other samples, while wollastonite experienced an increase at the expense of anorthite. Additionally, a minimal residue of mullite was only visible at the initial stage of the reaction, along with the presence of quartz.

This confirms that as the temperature increases, the degree of modification in the physical composition (morphology, etc.) also increases. However, in order to achieve maximum leachability of aluminium, it is not necessary to create perfect stoichiometric phases of the gehlenite and wollastonite type. This is evident from the leachability results, which show that there is no longer a significant difference between the samples at 1,000 °C with a reaction time of 60 minutes and those at 1,100 °C. The main changes in phase composition have an impact also on the morphology and properties of the modified FA, but it is not necessary for these changes to be clearly and necessarily reflected in the formation of detected phases.

Studies [149 and 150] have previously examined the reactions between FA and limestone. However, their focus was not on modifying the composition of FA to enhance leachability of its components. Instead, these studies aimed at creating belitic cements. It is worth noting that these sources also acknowledged the possibility of larnite formation through low-temperature sintering at 700–950 °C. However, this process required significant excess of calcium components as reactants, melt formation intensifiers, and a distinct temperature regime. Furthermore, the studies confirmed the presence of $C_{12}A_7$ and its derivative C_3A in their analyses.

Auto-disintegration of the modified FA

As mentioned earlier on preceding pages, the samples that underwent a high-temperature modification reaction exhibited a phenomenon known as auto-disintegration or self-disintegration. This implies that upon being cooled to room temperature, the sample spontaneously expanded, or its resulting shape mirrored the dimensions of the container in which it was placed. Moreover, the sample, once fired, could be easily crushed into a powder by applying slight pressure using two fingers.

The occurrence of this phenomenon does not involve the presence of a liquid phase during the reaction itself, nor does it require the sintered material to reach its threshold. The outcome of the auto-disintegration reaction has a beneficial impact on simplifying the overall process of modification and subsequent extraction. Notably, there is no need to adjust the particle size or reduce the material through grinding, a process that consumes significant amounts of energy. The auto-disintegration process occurs during the polymorphic transformation of dicalcium silicate β–γC_2S [151], or due to volumetric changes during the formation of gehlenite [152].

Fig. 38 has been included to evaluate alterations in particle size based on variations in reaction temperature between HTFA 1 and limestone. Additional graphs outlining the duration of reactions are included in the appendix. When analysing different firing conditions in terms of particle size and distribution, discrepancies are evident starting from the samples exposed to

a reaction temperature of 800 °C in comparison to the packing temperatures. Specifically, at 800 °C, a bimodal pattern is noticeable in the graph illustrating the distribution of particles in total, with the initial segment of the pattern corresponding to the unreacted lime. With an increase in temperature, a reduction in the peak at the smaller end of the curve is observed due to the consumption of CaO in reacting with other components, potentially forming bonds between the finest particles, or reacting with other substances. The partly narrowing of the distribution can also be identified as the temperature rises, although the average particle size remains relatively consistent both across varying crucible temperatures and in comparison, to the fly ash sample.

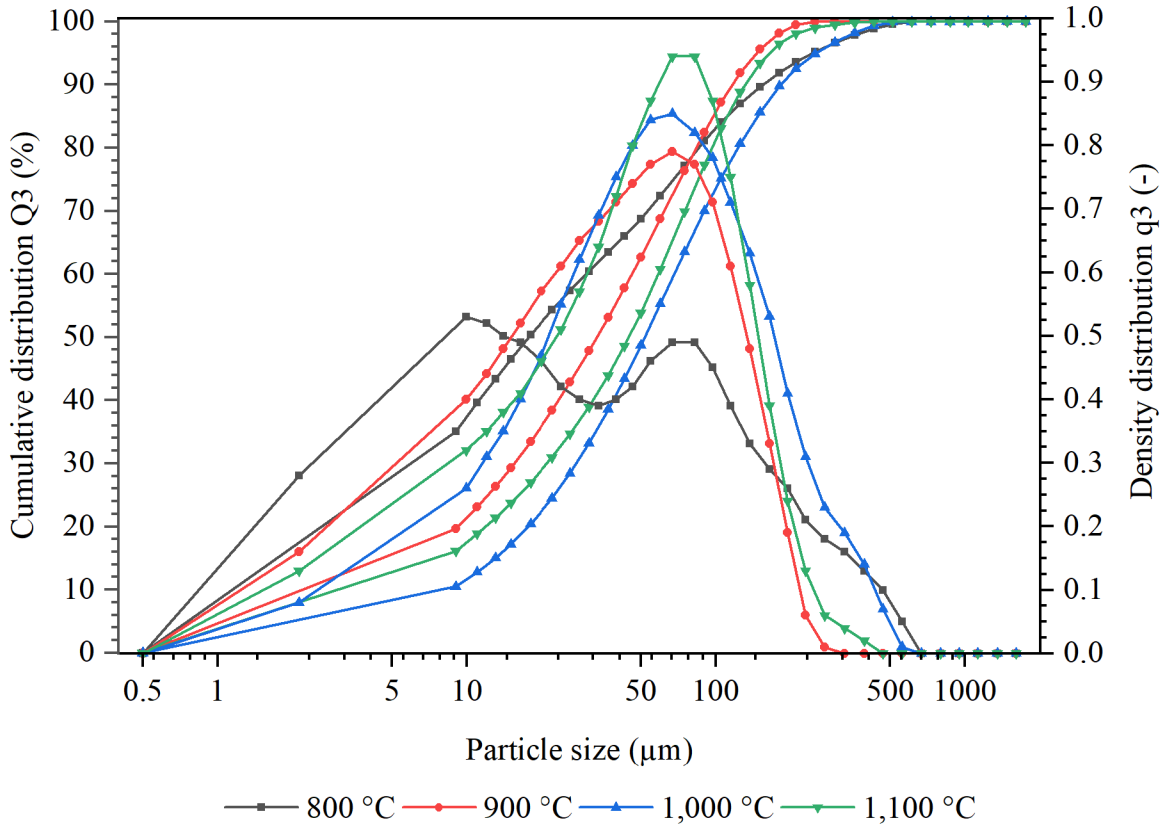

Fig. 38 Comparison of particle size distribution, HTFA 1 with limestone mol eq. 0.45, reaction temperature 800–1,100 °C for 60 min

Alterations in the morphology of particles FA modified by limestone

The high-temperature modification reaction of Fa with limestone involves a series of complex chemical processes that result in the formation of new compounds, phases and structures described above. The monitoring of these changes is crucial in understanding the transformation of the material and its potential applications.

The SEM images in Fig. 39 visually represent the changes that occur during the high-temperature reaction. The spherical grain of HTFA 1 remains intact, indicating that the original morphology of the material is preserved. However, the surface of the grain is covered with seedings of high-temperature reaction products, which exhibit a fine crystalline structure. These new products essentially grow from the surface of the original FA grain, indicating a

transformation of the material at a molecular level. This transformation can have significant implications for the material's properties and behaviour, as well as its leachability during extraction processes. Overall, the high-temperature modification reaction of FA with limestone is a complex process that requires careful monitoring and analysis to fully understand its effects. The SEM images Fig. 39 provides valuable insight into the changes that occur during this reaction, shedding light on the potential applications and implications of this process. The images depict the initial spherical particle of HTFA 1, with new phases beginning to form on its surface. Nevertheless, it is evident that, in terms of morphology, there is no indication of pores or break into the original glass shell.

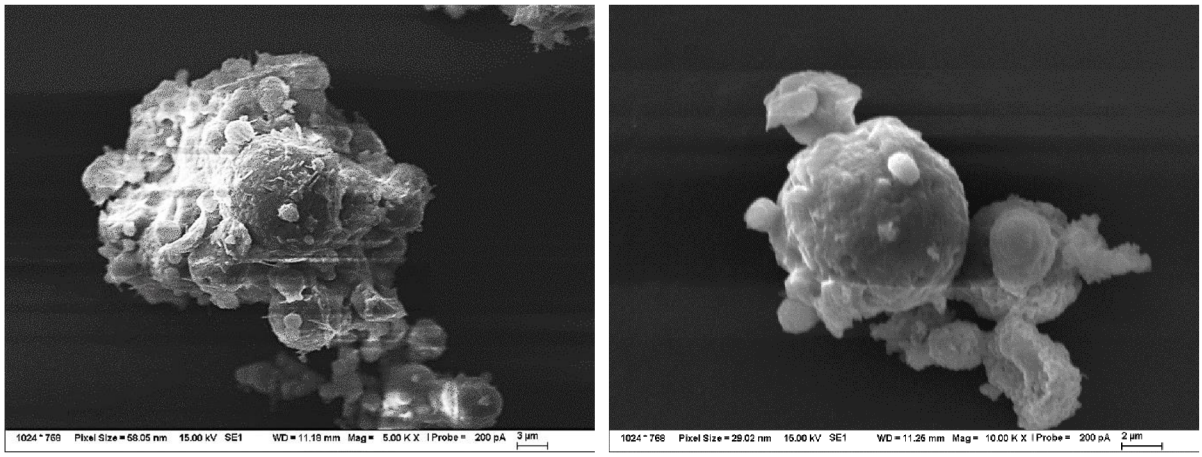

Fig. 39 SEM images of morphology, HTFA 1 with limestone, mol eq. 0.45, reaction at 1,000 °C for 60 min

The morphology of the modified HTFA 1 plays a crucial role in determining the optimal dose of the modifying agent. The surface area and morphology of the particles influences how effectively the modifying agent can interact with the FA, leading to a lower optimal dose than what would be theoretically calculated. This also explains why the modified HTFA 1 has up to 20 times higher leachability compared to the raw HTFA 1 (up to 50 % in case of modified HTFA 1 vs 2.5 % for raw HTFA 1), as the modified particles are more susceptible to leaching due to their altered morphology.

However, it is important to recognize that the modification process does not occur uniformly throughout the entire volume of the original FA. This means that the leachability of the modified HTFA 1cannot reach its maximum potential, as there are still areas within the particles that remain unmodified.

The alkaline environment during the high-temperature reaction does have some impact on transforming the products on the particle's surface, but it is not sufficient to achieve complete transformation. This limitation suggests that while the sintering method of FA with limestone may be a very interesting approach, it may not be universally applicable or feasible in a real-world industrial process. Further research and development are needed to optimise the modification process and fully understand the implications of the morphology of the modified HTFA 1 on its properties and behaviour.

5.4.2 Activation with calcium chloride

In the preceding chapter, it will be discussed how calcium chloride can be used as an activator to modify HTFA 1. Building upon the preliminary experiment conducted in study [104], the research in this thesis aims to provide a more comprehensive examination of the potential of calcium chloride as an activator for FA modification. To understand the chemical reactions involved in the formation of calcium-aluminate and calcium-silicate products, the equations (43)–(45) were elucidated (see chapter 2.4.2, page 41. These equations demonstrate the reactions that occur when calcium chloride is introduced to HTFA, resulting in the formation of calcium-aluminate and calcium-silicate compounds. The understanding these reactions, can better comprehend the mechanisms behind the modification process.

Moreover, the efficacy of calcium chloride as a modifying agent has been verified in earlier investigations [97]. Previous studies have shown that the addition of calcium chloride to FA can significantly enhance its properties, such as improving its change in morphology, sticky character, improved leachability. These findings further support the potential of calcium chloride as an activator for FA modification.

Considering the previous research, a theoretical framework of this part is employed to delve deeper into the potential of calcium chloride as an activator for modifying HTFA 1. By conducting a more comprehensive examination, researchers aim to gain a better understanding of the effects of calcium chloride on FA properties. Overall, the use of calcium chloride as an activator for modifying HTFA 1 holds great promise. Through a thorough investigation of the chemical reactions involved and the verification of its efficacy in earlier studies, this research aims to contribute to the advancement of FA modification techniques and the development of improved construction materials.

Identifying the most suitable FA/activator ratio, temperature, and duration of the reaction

In a manner similar to the prior experiment, the essential parameters of the high-temperature activation reaction were explored and defined. A collection of HTFA 1 samples, featuring different doses of $CaCl_2$ as a modifier in terms of molar equivalence, were produced following an identical process. The molar equivalent is understood as the sum of the molar equivalents of partial reactions leading to the formation of theoretical products according to the equations mentioned above. The elemental composition HTFA 1 is taken as the starting composition, i.e. the content of Al, Fe, Ti, Si, ...The expected values, established based on the provided reaction sequence, were ascertained within the range of 0.2–1.3, with an increment of 0.1. Furthermore, the consequences of a reduction in conversion degree following 0.05 mol eq., firing temperatures spanning 800–1,100 °C, and dwell times 30–180 minutes at the same temperature were scrutinised. The samples underwent firing in petite ceramic crucibles with a capacity of 10 mL, utilising a muffle furnace. At specific intervals, the samples were retrieved and permitted to naturally cool to room temperature without controlled rapid cooling. Subsequently,

the unreacted amount of the activator was quantified by means of complexometric titration of the aqueous leachate, subsequent to dispersion in an agate friction dish. The resultant data, demonstrating the fraction of the activator that reacted concerning the addition, temperature, and reaction duration, is delineated in Fig. 40.

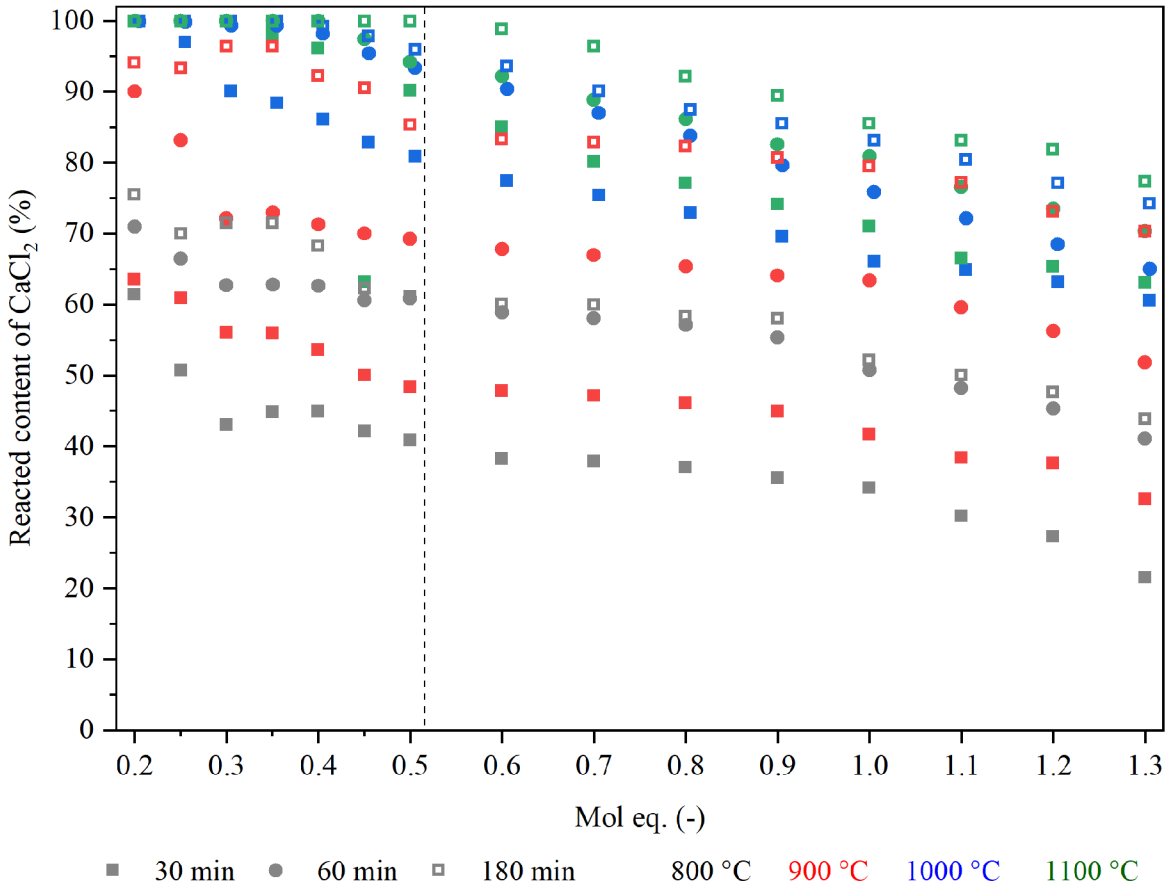

Fig. 40 Graph of the reacted amount of $CaCl_2$ as a function of reaction temperature and time

Following the prior experience with activation discussed in the preceding section, it is unsurprising that a lower amount than mol eq is needed to activate FA or a specific type of modification reaction, falling within the range of 0.25–0.5. The outcomes illustrated in Fig. 40 further demonstrate that the mixtures undergoing the response at 800 °C exhibit a less-trendoid trajectory, even if less pronounced than in the case of the reaction involving limestone. This observation can likely be attributed to the insufficient temperature for the reaction. Samples exposed to higher temperatures exhibit enhanced conversion rates and a trending nature. In contrast to the experiment with limestone, nearly 100 % of the reaction occurs at a temperature of 900 °C, albeit after a 3-hour reaction period. Substantial conversion rates of the reactant are achieved at a temperature of 1,000 °C within just 30 minutes. Furthermore, the trend is nearly identical compared to the counterpart undergoing the reaction at 1,100 °C. Notably, conversion rates manifest significantly earlier compared to the reaction with limestone, both in terms of lower reaction temperature and duration, as well as with a reduced ratio of reagent to FA.

Additionally, the addition rate of 0.25–0.5 ensures that the FA maintains its integrity while still benefiting from the properties of the $CaCl_2$. Overall, these findings suggest that careful control of both the addition rate and temperature is crucial in achieving the desired results in the modification process. Further experimentation and analysis are necessary to fully optimise these parameters for the best possible outcome. Consistent with the results of the precast modifier, a temperature of 1,000 °C appears to be the most suitable.

The impact of activation conditions on leachability

In order to maximise the leachability of macro-concentrated elements, the primary focus of this study is to explore various activation methods. As part of this investigation, an essential experiment was conducted to control the leaching process of litter that was prepared with modified HTFA 1. This experiment involved using $CaCl_2$ in a sulphuric acid environment, with a molar ratio of 1.2 times the theoretical amount required for the sequence of reactions. It is worth noting that this experiment mirrored the one conducted in the previous chapter and maintained the same L/S ratio of 10.

To assess the leachability, we once again chose samples with a high-temperature reaction mode, specifically at temperatures of 1,000 and 1,100 °C, and reaction durations of 30 and 60 minutes. Similar to the previous chapter, a portion of the liquid mixture obtained during the extraction process was analysed using ICP-OES. The obtained results of this analysis are then plotted in Fig. 41, where the leachability levels are presented as a function of time under various high-temperature modification conditions. This graphical representation aims to provide a clear understanding of the different degrees of leachability for each condition.

Compared to the limestone experiment, using calcium chloride for activation yields a leachability of aluminium that is twice as high, surpassing 95 %. This level of leachability can be considered the maximum and is highly valued in terms of results. The same outcomes are observed for both FA modification cases, whether conducted at a temperature of 1,000 °C for 60 minutes or at 1,100 °C for 30 minutes. These results are practically indistinguishable. On the other hand, the sample subjected to a reaction regime of 1,000 °C for 30 minutes exhibits a slightly lower leachability.

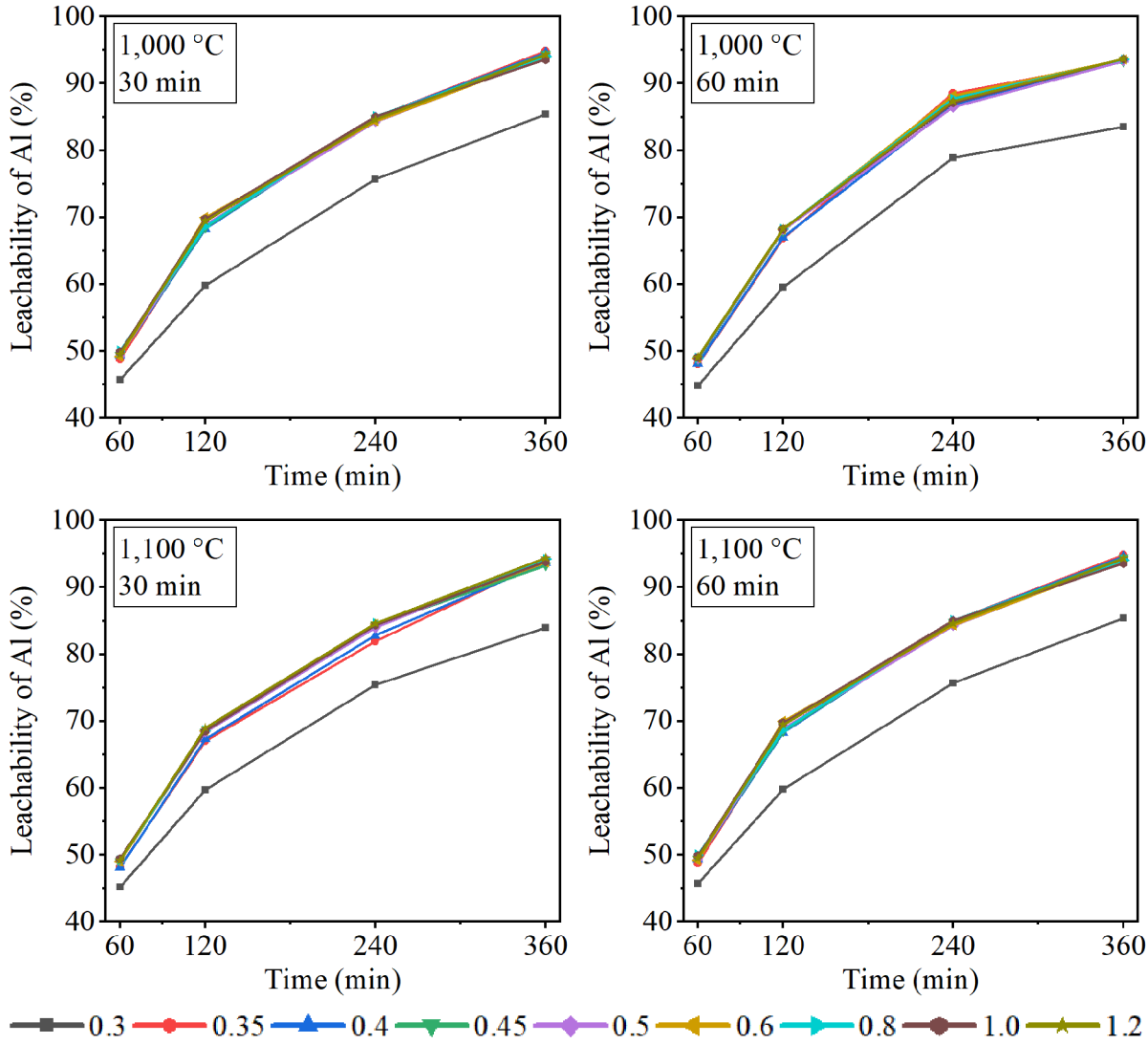

Fig. 41 Comparison of the leachability of Al; HTFA 1 modified with the addition of $CaCl_2$ at various dosages of the reagent, temperature, and reaction time

Growing the amount of reacting $CaCl_2$ in the reaction with FA from values of 0.5 results in nearly identical levels of success in converting aluminium into the acid solution. Therefore, it can be determined that the optimal addition of the modifying agent **$CaCl_2$** is **0.35 mol eq.** based on this dataset. At a reaction temperature of **1,000 °C for 60 minutes** (similar leachability could potentially be achieved even with a slightly shorter reaction time) or 1,100 °C for 30 minutes, it is more suitable to use the lower temperature due to energy consumption and temperature resistance considerations. In the study conducted by the author [104], comparable ratios of activator to fly ash were published. Nevertheless, the reagent was applied based on the weight of raw FA ash with an ideal mass ratio of 1/1, and the fly ash composition differed from HTFA 1 in their investigation. However, the determined mass ratio of $CaCl_2$/FA 1/1 in their study after conversion corresponds to approximately 0.375 mol eq. for the case of this dissertation results.

Monitoring changes in HTFA during high-temperature modification reaction

The absence of pertinent publications elucidating or characterising the precise reaction sequence and resulting products thus far posed a challenge. Therefore, it became imperative to unravel this formidable task within the realm of research. In these particular experiments, samples of HTFA 1 were prepared with the addition of 0.35 mol eq. of $CaCl_2$. The incorporation of this agent was hypothesised to significantly impact the reaction kinetics and the resulting products.

On the other hand, the heating-microscopy experiment was also performed for the observation of any phase transformations that occurred within the sample activated by calcium chloride as it was subjected to increasing temperatures. This provided valuable insights into the thermal stability of the sample and how it may behave under different heating conditions. Additionally, the heating-microscopy experiment helped to understand further the relationship between temperature and volume changes in the modified sample. By carefully monitoring the sample as it was heated, the ability to track any expansion or contraction that occurred, providing important data on the thermal expansion properties of the material could be observed and described.

The outcomes of heating-microscopy revealed that when $CaCl_2$ was added, a reduction in volume was observed starting from 550 °C due to the decomposition of reactants, the modification reaction itself, and subsequently, at temperatures exceeding 1,000 °C, sintering and gradual rounding of sample edges became apparent. Substantial shrinkage was noted from temperatures of 1,220 °C onwards, with the onset of the drip phase occurring within the range of 1,265–1,268 °C, and complete sample creep at 1,300 °C. The alterations in the shadow area of the samples are illustrated in Fig. 42. In contrast, the graphical relationship between the change in shadow area and sample shape is presented as a function of temperature in Fig. 43.

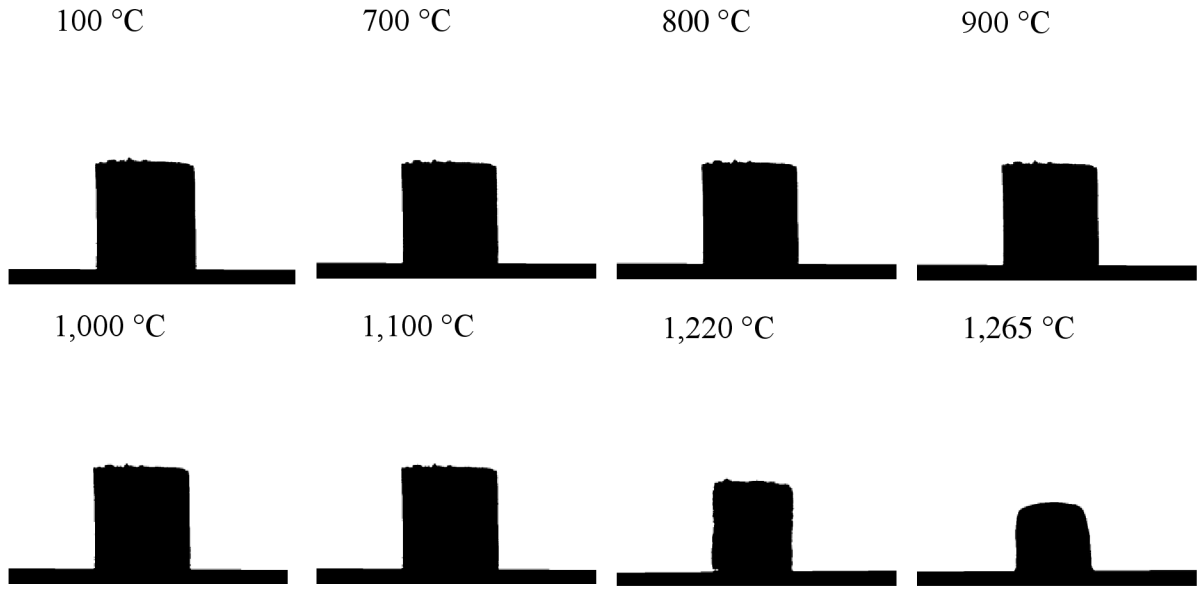

Fig. 42 Images of the shadow area of sample HTFA 1 mixed with $CaCl_2$, mol eq. 0.35 as a function of temperature

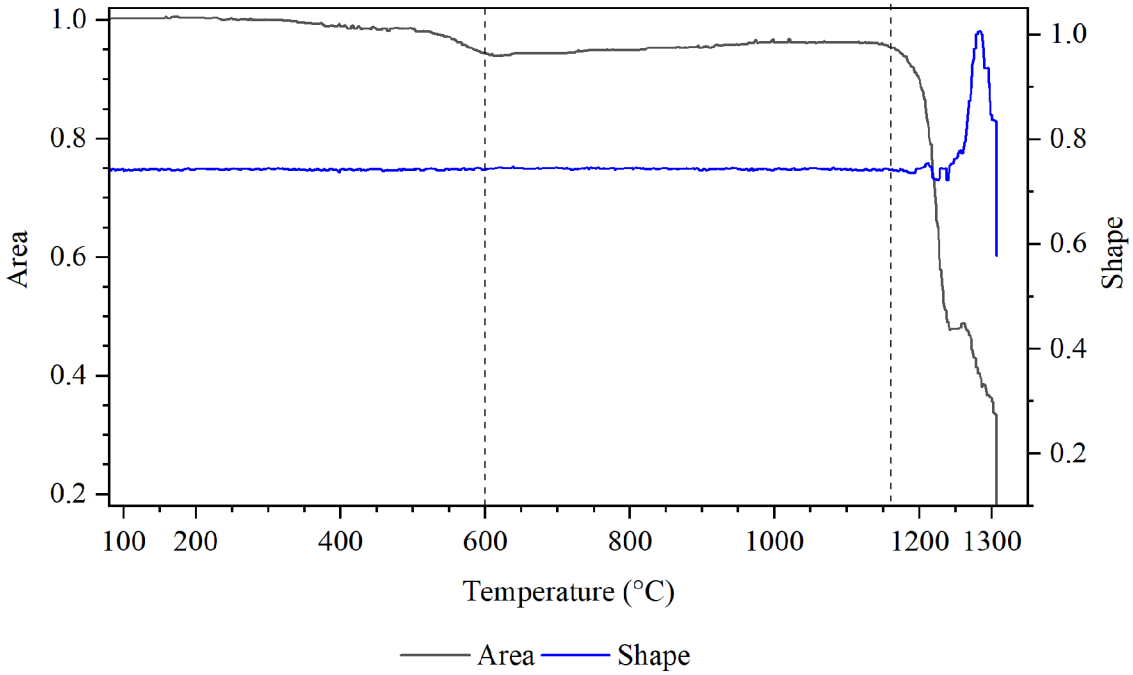

Fig. 43 The dependence of shadow surface area and shape on temperature as a function of temperature, sample HTFA 1 mixed with $CaCl_2$, mol eq. 0.35

In order to observe variations in weight based on temperature and heat flow, TG/DTA was once again employed. This allowed for the determination of the initiation temperature, which refers to the temperature at which the modifying agent decomposes and the reaction with HTFA 1 potentially begins, as well as the identification of other heat flow regions where sample conversion could be detected. In line with the previous findings, the optimal ratio of HTFA 1 and $CaCl_2$ was utilised, and the measurement conditions were adjusted to align with the temperature firing mode in the furnace, reaching a temperature of 1,000 °C, followed by a 60-minute isotherm at the same temperature. The graph in Fig. 44 illustrates the relationship between the change in mass and the heat flow in the simulated mode of the high-temperature modification reaction.

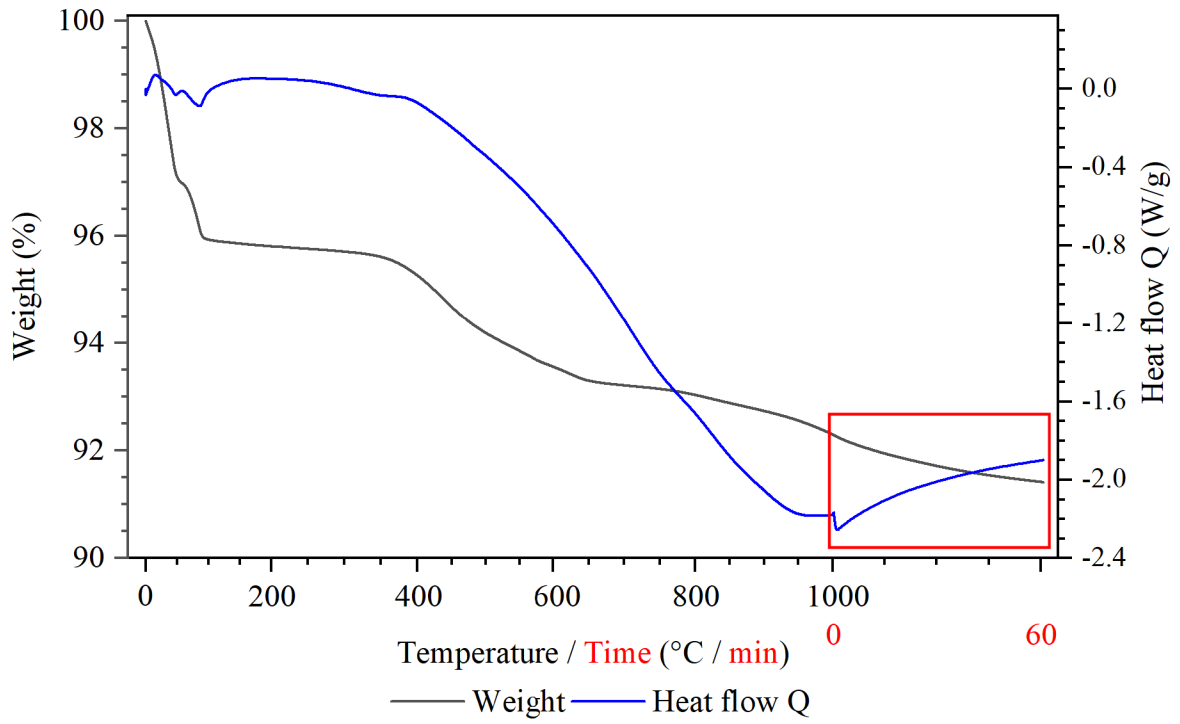

Fig. 44 TG/DTA curves of changes in the sample HTFA 1 mixed with $CaCl_2$, mol eq. 0.35 under reaction mode

The results obtained from the data as mentioned above clearly indicate that the reaction between HTFA 1 and $CaCl_2$ exhibits distinct characteristics compared to the reaction with limestone. During the experiment, it is observed that water or moisture evaporates from the mixture up to a temperature of 150 °C, moisture caused by handling, sample preparation, storage, etc. or water evaporation potentially due to the decomposition of calcium chloride hydrate (sinjarite). Subsequently, a break in the curve is evident in the temperature range of 400–600 °C, indicating changes in HTFA 1, such as the burning of organic residue and decomposition of carbonates caused by landfilling. A gradual weight loss is observed throughout the remaining process, although the change in sample weight is only 2 wt. %. This finding suggests that one of the reaction products between HTFA 1 and $CaCl_2$ neither confirms nor denies the fact of gaseous HCl or Cl_2. However, it is important to note that both gases can readily attack surrounding structures and cause etching, potentially leading to the penetration of reactants through the enamel on the surface of the FA grain and further into the particle's core.

Further analysis regarding the formation of new phases, their rate of formation, and the impact on the microstructure of the modified sample will be discussed in more detail later, particularly in relation to the XRD and SEM results.

By utilising an XRD high-temperature chamber, the sequence of reactions and the corresponding changes in phase composition during a high-temperature reaction were closely monitored. The sample was analysed at specific isotherms, temperature intervals of 25 °C,

ranging from 600°C to 1,000 °C. The 3D graph in Fig. 45, focusing on the region of 2θ 20–38°, provides a detailed visualisation of the phase composition evolution.

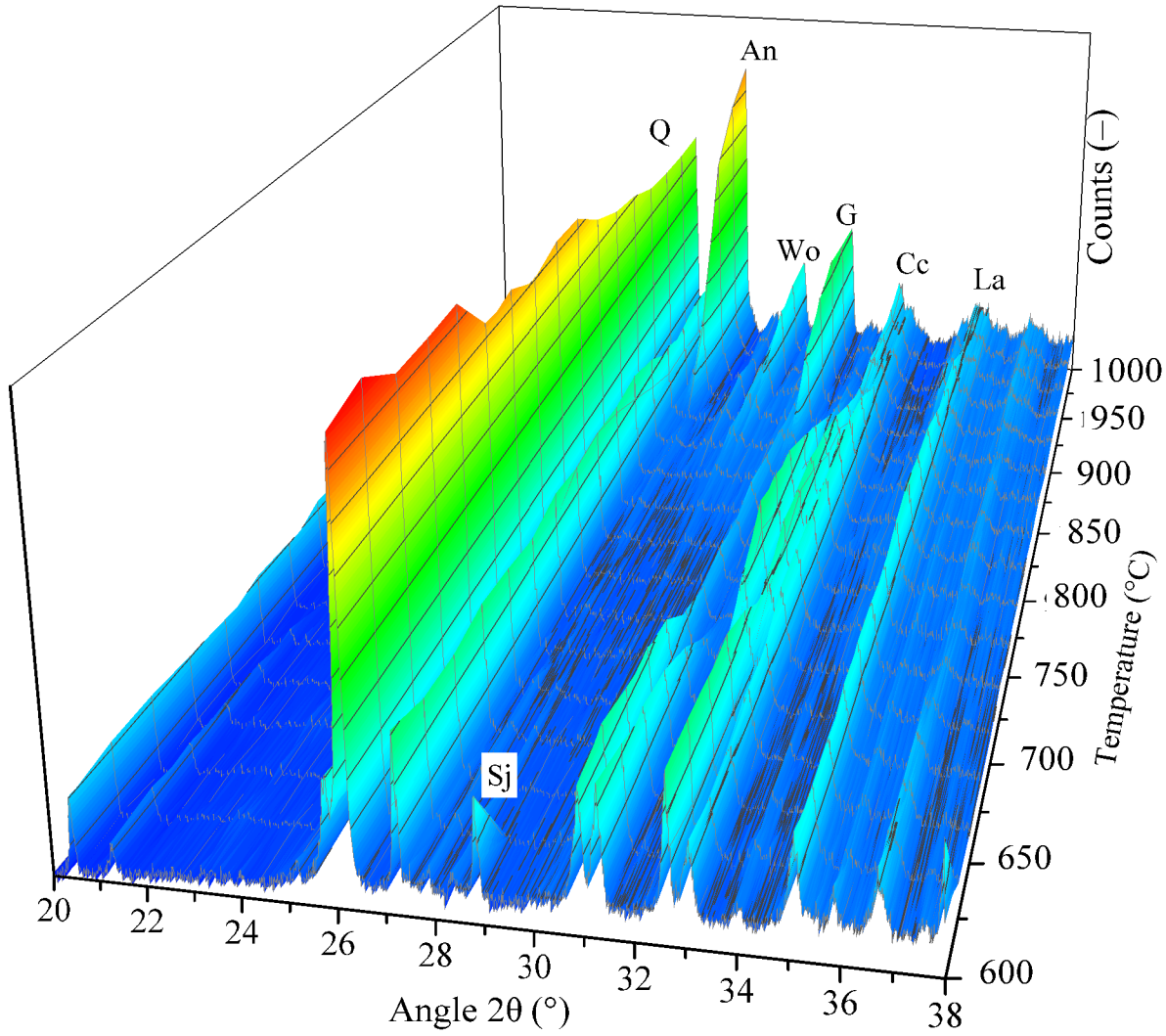

Fig. 45 3D diffractogram of 2θ 20–38°of phase changes during temperature, sample HTFA 1 with $CaCl_2$, mol eq. 0.35

The graph above clearly shows that at temperatures below 700 °C, unreacted $CaCl_2$ (Sj) was still present in the mixture. Additionally, a small possibility of larnite (La) forming was present, although this cannot be definitively confirmed due to the overlapping diffraction positions of both substances.

As the temperature increases to 850 °C, there was a slight decrease in the levels of mullite (M) and quartz (Q), while the emergence of gehlenite (G), wollastonite (Wo), and anorthite (An) becomes visible. The quantities of these three phases continued to increase as the temperature rose.

Compared to the sample that underwent reaction with limestone, there is a significant difference in the predominance of phase anorthite as the primary phase. In this case, phase anorthite surpasses phase gehlenite by a large margin, and the wollastonite content is also a bit higher. This indicates that the reaction with $CaCl_2$ follows a distinct path and has a more

pronounced and selective influence on the modification of HTFA 1. Interestingly, the content of quartz decreased only minimally, and the reaction to larnite occurred to a limited extent when $CaCl_2$ was involved. Moreover, this further highlights the unique effects of $CaCl_2$ on the composition of the phases.

Furthermore, maintaining a temperature of 1,000°C for several hours did not lead to any further changes in the phase composition or the content of individual phases. This was further evident from comparing diffractograms measured once an hour three times, which showed no additional diffraction positions or intensity in counts.

The reaction mechanism suggested in the publication [104] assumes the formation of gaseous hydrogen chloride, which is less likely at the given temperature, as the presence of water vapour is highly debatable if the reaction is not carried out in an autoclave. However, authors [153] exclude such a product during the electrolytic reaction of solid Al_2O_3 with $CaCl_2$.

Hence, in the event that the reaction was to yield HCl, gaseous Cl_2, or even $Cl^{\cdot}$, it would create a considerably aggressive environment that could potentially enhance the etching process of the glass phase in the FA. This would increase porosity and allow the extraction agent to penetrate even deeper into the FA grain. Consequently, this would account for the rapid escalation in Al leachability during the extraction process. If any of the aforementioned gaseous reaction products are indeed formed, they would swiftly reach the surface of the sample and diffuse out of the material. Therefore, samples fired in a ceramic crucible with sufficient height would facilitate a higher rate of activation product formation.

Analysis of furnace-fired samples

In the previous study on Fa activation through the use of limestone, HTFA 1 and $CaCl_2$ samples were combined in an optimal ratio and subjected to firing in a muffle furnace within ceramic crucibles. The firing procedure involved heating the samples to a temperature range of 800 to 1,100 °C for a variable reaction time of 0 to 180 minutes. This process allowed the samples to undergo the necessary chemical reactions and transformations. After the firing process, the samples were rapidly cooled to room temperature. The samples were ground into a fine powder using an agate grinding bowl after the cooling process. This step ensured that the samples were in a suitable form for further analysis because the samples activated with $CaCl_2$ did not show the ability to self-disintegrate.

The XRD technique was employed to analyse the phase composition of the samples. Fig. 46–Fig. 50, specifically within the 2θ 20–38° range, were utilised to visually represent the observed alterations in diffractograms for each set of samples. These diffractograms effectively demonstrated the changes in diffraction patterns, providing a clear understanding of the variations in phase composition.

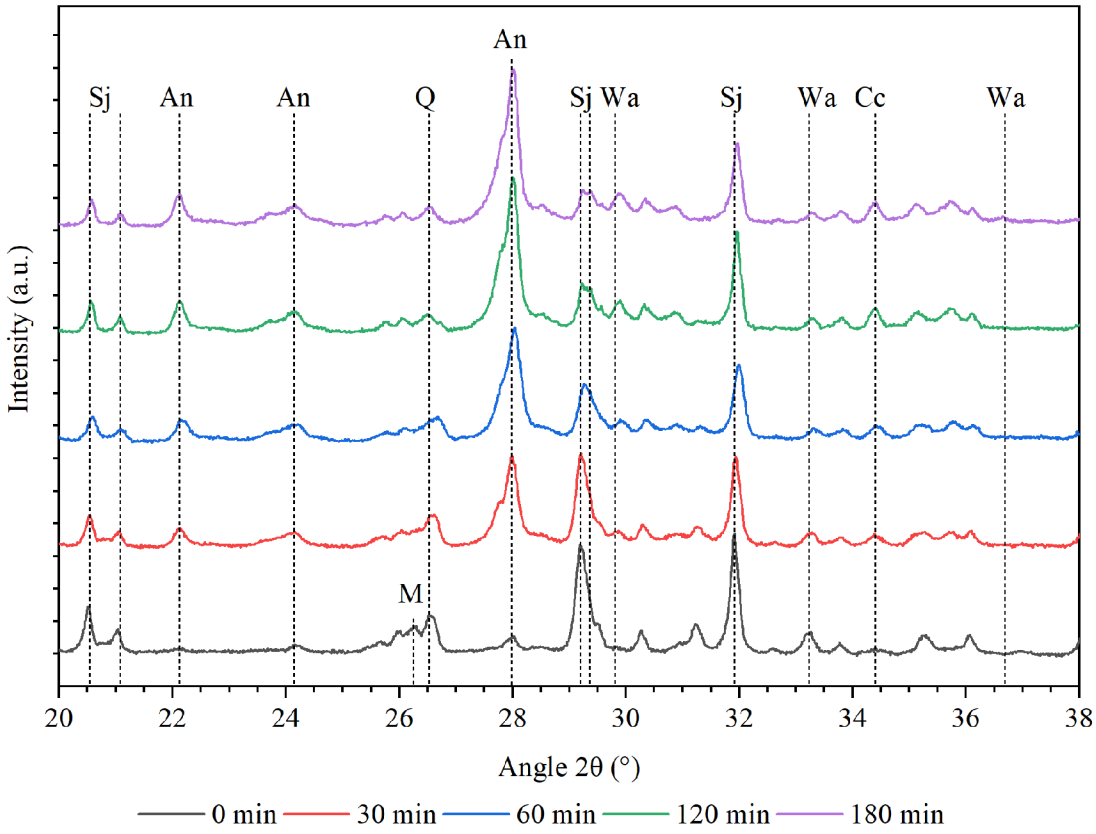

Fig. 46 Diffractogram of 2θ 20–38°range, sample HTFA 1 with $CaCl_2$, mol eq. 0.35, 800 °C

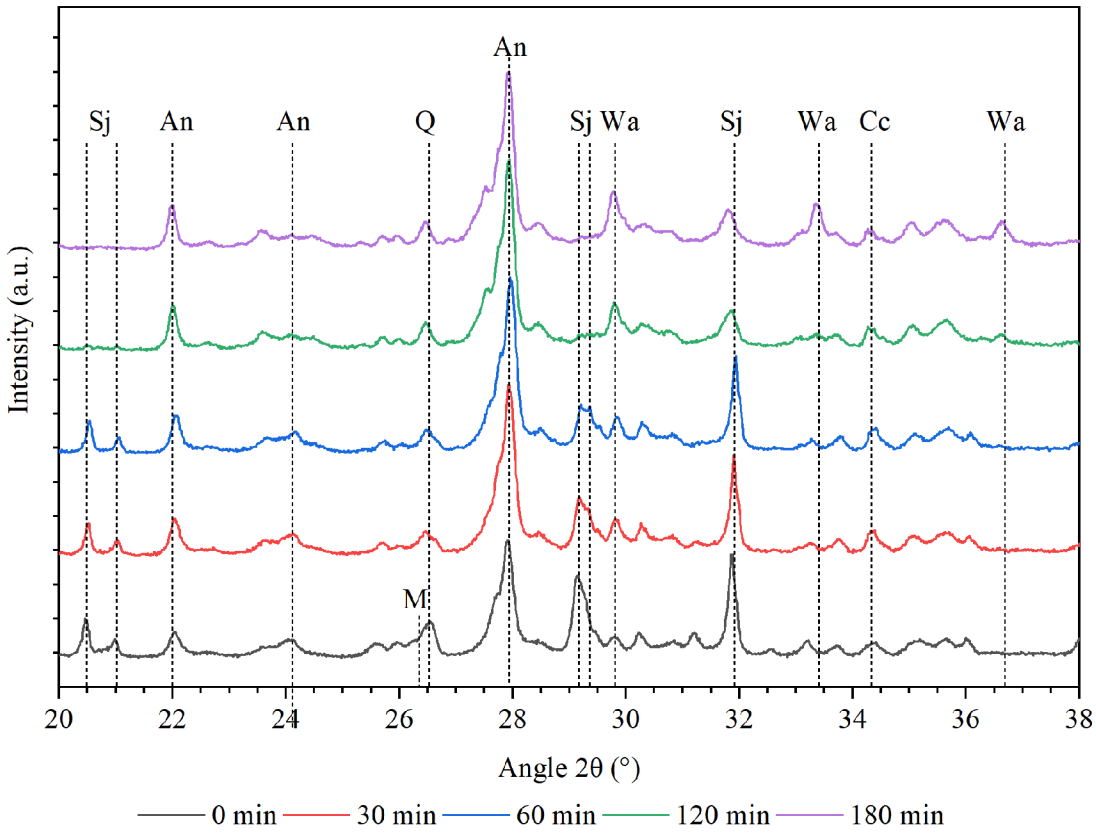

Fig. 47 Fig. 48 Diffractogram of 2θ 20–38°range, sample HTFA 1 with $CaCl_2$, mol eq. 0.35, 900 °C

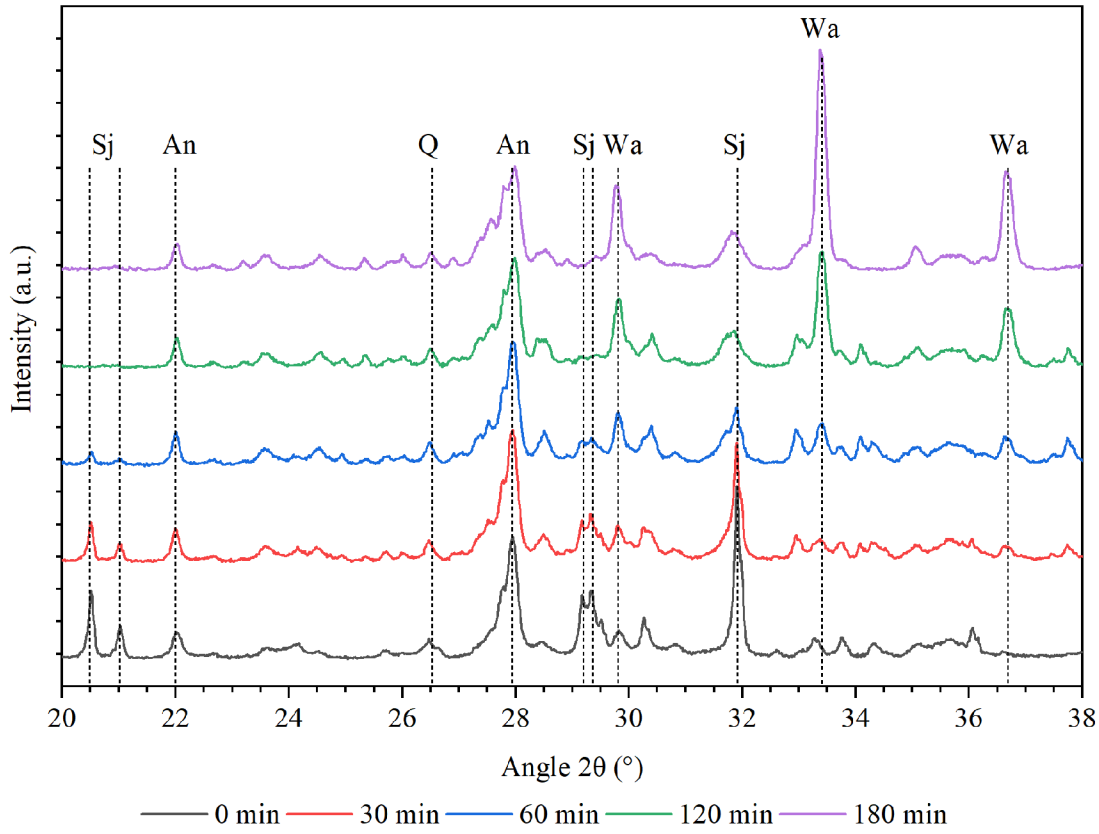

Fig. 49 Diffractogram of 2θ 20–38°range, sample HTFA 1 with $CaCl_2$, mol eq. 0.35, 1,000 °C

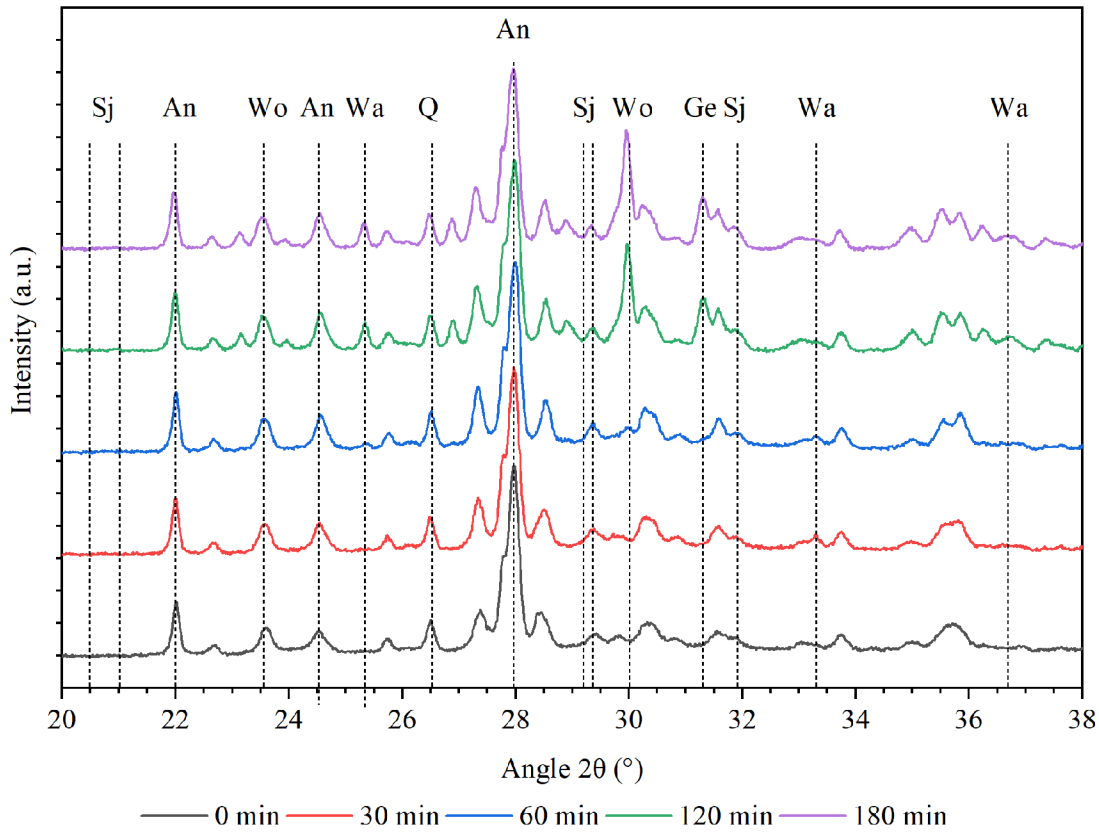

Fig. 50 Diffractogram of 2θ 20–38°range, sample HTFA 1 with $CaCl_2$, mol eq. 0.35, 1,100 °C

The diffractograms provide clear evidence supporting the initial hypothesis regarding the interaction between the by-product of the $CaCl_2$ and FA reaction with the material. The diffractograms indicated the presence of a distinct chlorocalcite phase (Cc) KCaCl3 in all samples. This suggests that the by-product of the $CaCl_2$ and FA reaction interacts with the material in a way that forms the chlorocalcite phase. The presence of this phase in all samples further strengthens the validity of the initial hypothesis. It suggests that the interaction between the by-product and the material is consistent and reproducible.

The presence of unreacted sinjarite (Sj – calcium chloride hydrate) in the sample exposed to the reaction at 800 °C indicates that there were issues with the cooling process, sample handling, and the time between synthesis and analysis. Despite these challenges, the formation of sodian anorthite (An – sodium-calcium-aluminium silicate) and wadalite (Wa – calcium-magnesium-aluminium-iron silicate-chloride) was still observed at the beginning of the reaction. The presence of mullite was only detected in the initial stages of the reaction, with mullite levels dropping below detection limits as the reaction progressed.

Interestingly, the quartz content in the sample fired at 800 °C exhibited a different trend compared to samples subjected to higher reaction temperatures. At 800 °C, the quantity of quartz decreased rapidly, suggesting a unique reaction pathway or kinetics at this specific temperature. Further analysis and experimentation will be necessary to fully understand the complex dynamics of this reaction and the role of each component involved.

Raising the temperature to 900 °C yields no discernible differences compared to the previous sample processed at a lower temperature. Even after 60 minutes of reaction, a similar amount of unreacted Sj is observed, and the overall concentrations of anorthite and wadalite remained relatively constant, mirroring those of the samples processed at 800 °C. Substantial alterations in the phase composition were only evident after 120 or 180 minutes of reaction at 900 °C, characterised by a notable decrease in Sj levels and a corresponding rise in anorthite and wadalite concentrations. Furthermore, a reduction in chlorocalcite content was accompanied by increased wadalite content. The presence of the mullite phase was only detectable at the initial stages of the reaction. At the same time, the total quartz content exhibited minimal variation throughout the reaction process. which partially confirms the theoretical reaction sequence according to the literature [104] (the case of the gradual reaction of mullite). Still, unlike the theoretical aspects, the activation in this experiment is more selective and the La phase (reaction with Si) is not formed.

From the beginning, the reaction carried out at 1,000 °C also shows a similar character, where after 30 min of reaction, the Sj content can still be described as high, with its subsequent decrease from 60 min of the reaction, and the formation of wadalite occurred. The content of wadalite increased with the duration of the reaction, later also at the expense of anorthite. The maximum amount of wadalite was reached after 180 min of reaction. It is important to note that when the temperature is increased to 1,100 °C, the presence of wadalite in the mixture becomes practically nonexistent. Right from the beginning of the experiment, the content of wadalite is

already below the detection limit, meaning it cannot be detected. On the other hand, the content of quartz remains relatively unchanged throughout the reaction. Furthermore, at this higher temperature, there was also a rapid decline in the content of the compound chlorocalcite. Initially, chlorocalcite can be detected at the start of the reaction. Still, after 60 minutes, its content falls below the detection limit, indicating no longer present in the mixture.

The absence of the wadalite phase in the experiment conducted at 1,100 °C was a significant finding that set it apart from the previous part. The initial presence of the wadalite in minimal quantities within the first 30 minutes of the reaction indicated a unique reaction pathway at this highest temperature. The absence of mullite or residual Sj in the sample was already in accordance with the previous trends. Interestingly, the quartz content in the sample remained relatively constant throughout the reaction, suggesting a stable composition despite the changing phases, and better selectivity of the activation process. Overall, it can be said that from the beginning of the reaction, a large amount of anorthite was contained in the mixture, but the content gradually decreased slightly. From 120 min of the reaction, wollastonite started to appear, as in the case of a single mixture of FA activated with $CaCl_2$.

The gradual decrease in the representation of mullite in the sample during the high-temperature modification reaction of the furnace-fired samples partially confirms the theoretical sequence of the reaction according to the literature [104] (a case of gradual reaction of mullite). However, contrary to theoretical aspects, the activation in this experiment is more selective and the La phase (by reaction with Si present) is not formed. This may be due to the reaction mechanism, when an acidic environment - rich in chlorine particles - more easily attacks particles richer in base metals.

The presence of anorthite in the samples not only has a demonstrably positive effect on the leachability of Al. This is because anorthite consists of structures that are easily hydrolysable [154], even in solutions of weaker acids or mineral acids with low concentrations. Hydrolysis of anorthite releases calcium and aluminium ions, which can then be easily leached out from the samples. On the other hand, the presence of wollastonite is not entirely desirable according to theoretical assumptions. This is because wollastonite is considered relatively inert and resistant to acids. [155] Its resistance to acid attack hinders the leaching process and makes it more challenging to extract desired elements from the samples.

Alterations in the morphology of particles FA modified by $CaCl_2$

The examination of the morphology of FA, which has been modified with $CaCl_2$, reveals that the modification reaction has a significantly more significant impact on the sample compared to the limestone activator. This is evident from the SEM images (Fig. 51), which show a completely different morphology, i.e. an absence of typical FA spherical particles in the material, unlike the first used modifying agent - limestone. Instead, the morphology of the modified FA is highly reacted and compact, exhibiting a highly porous nature. Interestingly, the modification process leads to the formation of structures resembling flower petals characterised by thin plate-like formations covered with tiny needles.

Further analysis using energy-dispersive X-ray spectroscopy (EDX) point analysis confirms the presence of several elements in these particles. Specifically, aluminium, silicon, calcium, a small quantity of sodium and potassium, and chlorine are detected. However, the stoichiometry of these elements does not correspond to a specific mineralogical analogue. This discrepancy arises from the XRD analysis, which reveals that the modification reaction results in the formation of two phases, namely anorthite and wadalite. Nevertheless, even these phases may not exhibit complete stoichiometry and could potentially contain atoms that have been substituted differently.

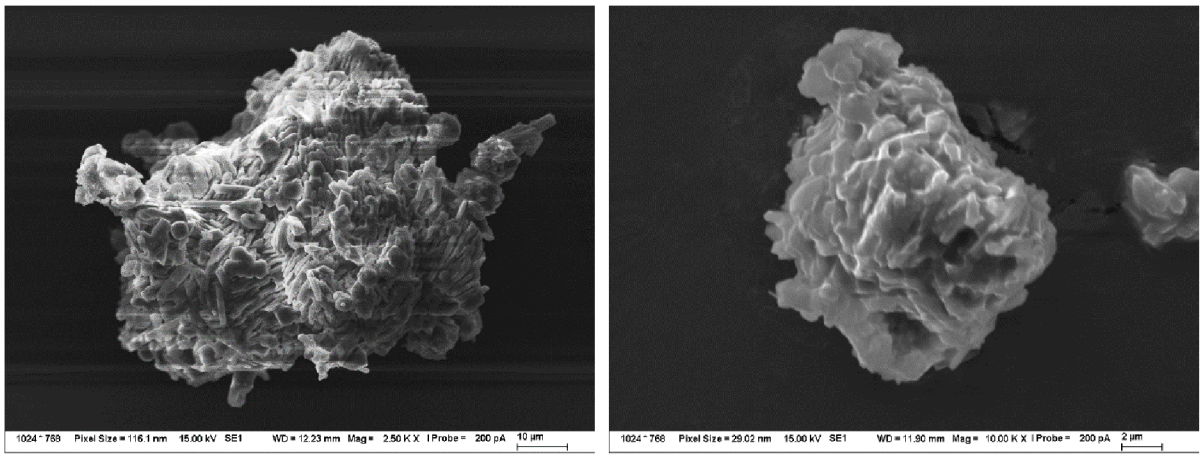

Fig. 51 SEM images of morphology, HTFA 1 with $CaCl_2$, mol eq. 0.35, reaction at 1,000 °C for 60 min

5.4.3 Activation with combination of limestone and $CaCl_2$

By considering the two previous reactions involving high-temperature modifications, there exists a possibility of employing a mixture of $CaCl_2$ and limestone for the purpose of activation. Through a detailed selection of suitable combinations of these substances, it becomes feasible to attain the intended results. Activation with $CaCl_2$ can result in products that facilitate a high level of leachability of macro-concentrated elements during the extraction process. At the same time, the presence of limestone can promote an auto-disintegrating nature (win-win strategy of synergy). Ideally, the advantages of both modification methods would be synergistically integrated.

Identifying the most suitable $CaCO_3/CaCl_2$ ratio in order to leachability and auto-disintegration

A series of HTFA 1 samples were meticulously prepared to achieve this objective using a carefully optimised ratio of 0.45 mol eq. $CaCO_3$ and 0.35 mol eq. $CaCl_2$. The ratio between $CaCO_3/CaCl_2$ was deliberately varied from 0.9/0.1 to 0.1/0.9, with a consistent increment of 0.1 in the ratio difference. Subsequently, all samples underwent a high-temperature reaction at 1,000 °C, maintaining the required temperature for 60 minutes. Based on the outcomes from the prior experiments involving the individual components, it is evident that these conditions were indeed satisfactory. Following the completion of the high-temperature reaction process, the samples were swiftly cooled to room temperature in an uncontrolled manner. The auto-disintegration capability was then evaluated, and the reaction conversion rate was determined through leaching in an excess of 1% citric acid. Subsequent alkalisation allowed for the determination of the reaction's conversion rate through complexometric titration.

Table 18 summarises the findings from the evaluation of self-disintegration capability based on the ratio of the two solvents employed. Initially, when transitioning from a $CaCO_3/CaCl_2$ ratio of 0.4/0.6 towards a higher chloride content, there is a noticeable decrease in self-disintegration ability. This is evidenced by the creation of sharp particles of approximately millimetres in size. As the amount of chloride is further increased, the particles gradually grow in size until a solid structure is formed, necessitating crushing or grinding starting from a ratio of 0.2/0.8.

Table 18 Ability to auto-disintegrate at different $CaCO_3/CaCl_2$ ratio

$CaCO_3/CaCl_2$ ratio								
0.9/0.1	**0.8/0.2**	**0.7/0.3**	**0.6/0.4**	**0.5/0.5**	**0.4/0.6**	**0.3/0.7**	**0.2/0.8**	**0.1/0.9**
+	+	+	+	±	± –	± – –	–	–
+ positive a-d		± partly a-d ≥ 50 %		± – partly a-d < 50 %		– negative a-d		

The auto-disintegration process can also be characterised by determining the particle size and particle size distribution using laser diffraction. This is captured in the graph shown in Fig. 52. As can be observed in more detail, the results correspond to visual observations. It is also evident from the achieved results that the particle size distribution of the modified HTFA 1 particle using both Ca-based agents is significantly narrower.

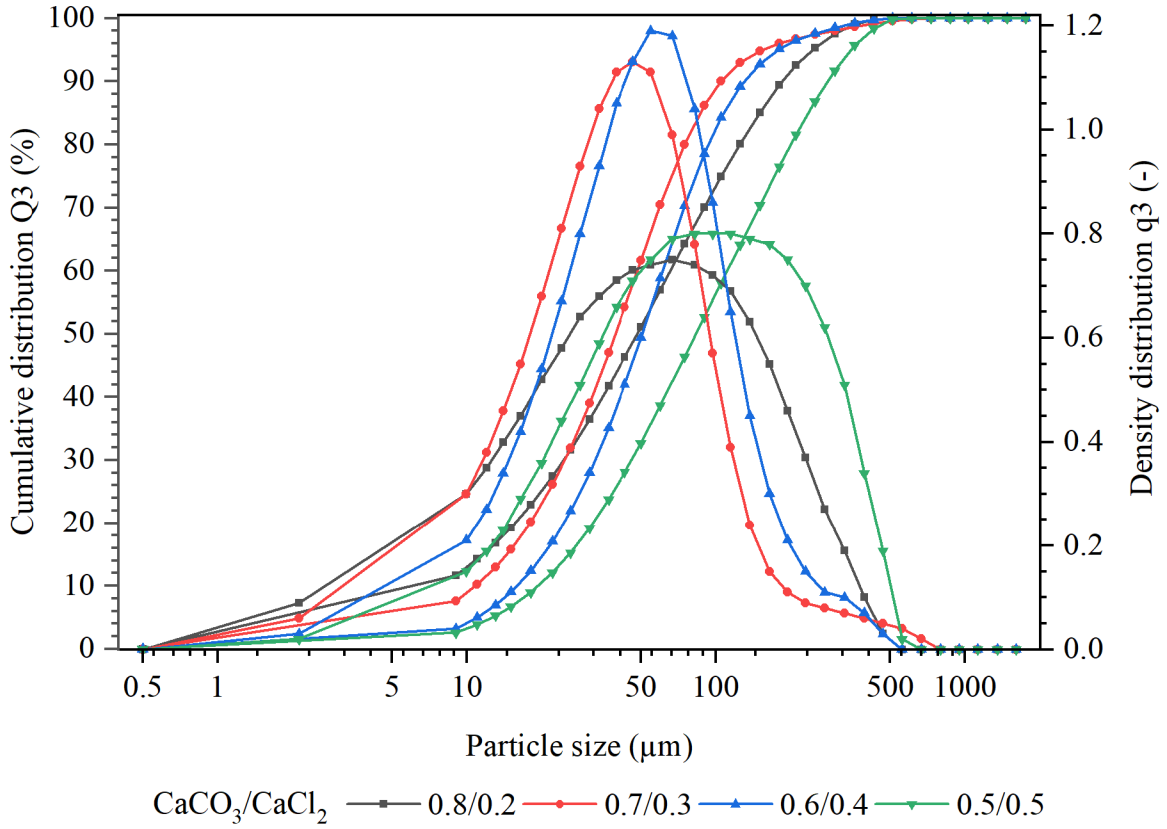

Fig. 52 Comparison of particle size distribution, HTFA 1 modified with different ratio of $CaCO_3/CaCl_2$

To evaluate the type of activation and its consequences, an alternative approach involves comparing the colour transformation of the product resulting from the process.

Fig. 53 illustrates the colour change based on the $CaCO_3/CaCl_2$ ratio. This straightforward observation reveals that when a higher proportion of limestone is added (ratios of 0.9/0.1 and 0.8/0.2), the predominant colour tones shift towards shades of grey, resembling the activation solely by $CaCl_2$. However, as the $CaCl_2$ content in the mixture further increases, the colour transitions from yellow to orange to rust brown, indicating activation solely by $CaCl_2$. Additionally, the colour gradually shifts towards shades of orange, and eventually, the sample loses its auto-disintegration characteristics.

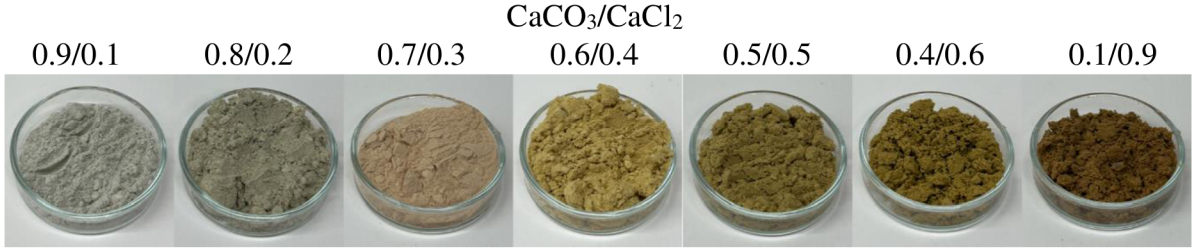

Fig. 53 Colour changes in HTFA 1 modification of different $CaCO_3/CaCl_2$ ratio addition

The graph in Fig. 54 provides a summary of the conversion of modification reactions with these combined activators – limestone and $CaCl_2$, specifically in relation to the assessment of the reaction extent of calcium components. It is noteworthy that nearly all of the modification agents exhibit reactivity in all mixtures, resulting in conversions surpassing 95 %.

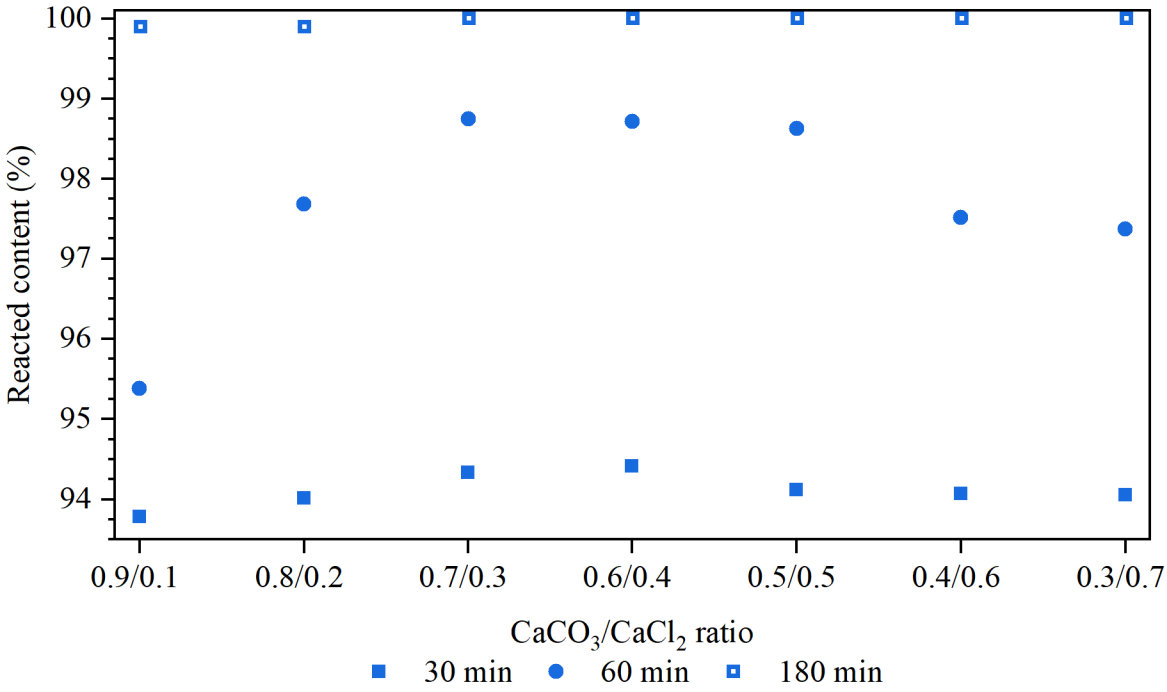

Fig. 54 Graph of the reacted amount of Ca based agents as a function of reaction time at 1,000 °C

The new findings align with the conclusions drawn from the earlier research, which meticulously examined the reactions of $CaCO_3$ and $CaCl_2$ in isolation. This consistency in results lends support to the idea of utilising a blend of these substances, as it appears that the order in which the modification reactions occur remains unaffected. This additional evidence strengthens the case for exploring the combined use of $CaCO_3$ and $CaCl_2$ in future studies and applications.

The impact of combined activation conditions on leachability

If the earlier findings demonstrated a beneficial impact of both substances on the alteration reactions across all concentrations, the critical element in establishing the correct carbonate-to-chloride ratio for FA activation is undoubtedly an investigation that consolidates the aluminium leachability. Subsequently, all the blends that were created were exposed to a reaction within a sulphuric acid setting at a mol eq. of 1.2 and a L/S ratio of 10. The collective aluminium leachability is subsequently plotted in Fig. 55.

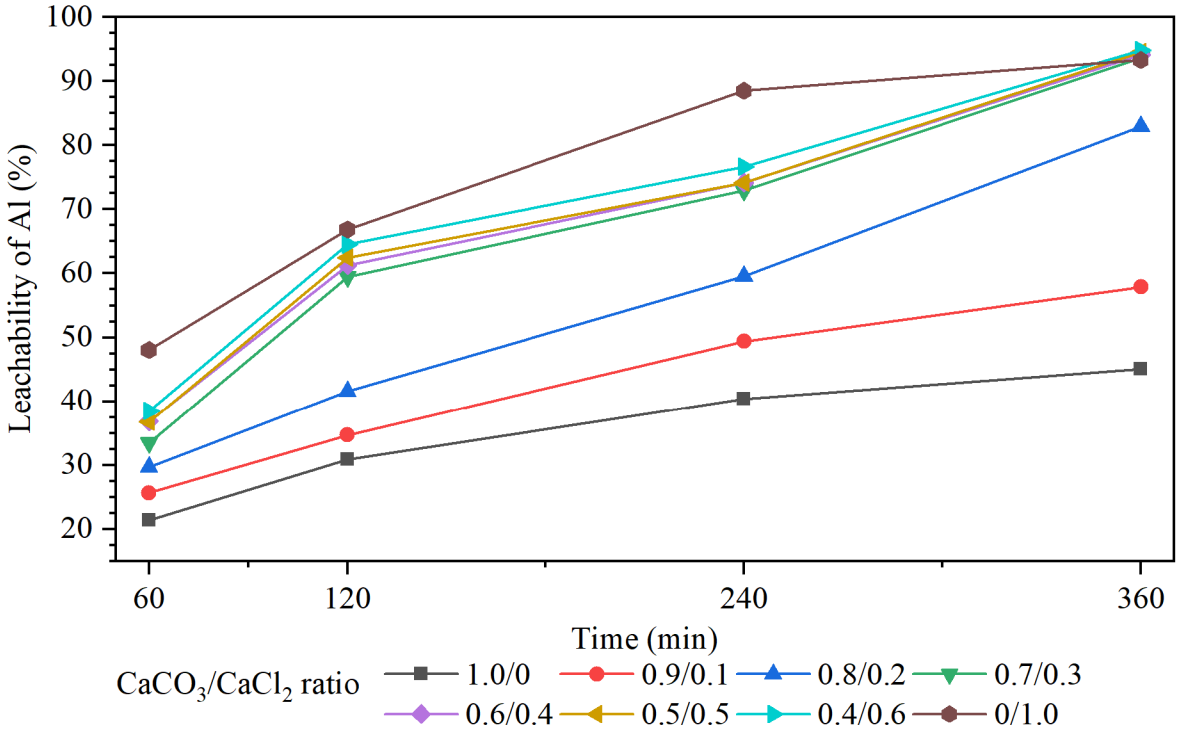

Fig. 55 Comparison of the leachability of Al; HTFA 1 modified with the addition of $CaCO_3$ and $CaCl_2$ at various ratio

Upon initial observation, the outcomes appear to be quite favourable, given that combinations containing varying proportions of both reagents significantly enhance the leachability of aluminium, thereby altering the initial HTFA input in a positive manner. In simple terms, it can be stated that leachability rises with an increase in chloride content. Notably, leachability already surpasses 90 % for a blend with a ratio of 0.7 $CaCO_3$/0.3 $CaCl_2$, and subsequent mixtures, such as ratio of 0.6 $CaCO_3$ to 0.4 $CaCl_2$ up to a ratio of 0/1.0, yield practically indistinguishable leachability levels, ranging from 90 % to 95 %. This outcome is highly encouraging. Simultaneously, a synergistic outcome was observed due to the combined influence of the modifying agents and the overlapping interval region where both the self-disintegration phenomenon and the optimal leachability of Al take place. The **$CaCO_3$/$CaCl_2$** ratio of **0.7/0.3** ("O"-type) **or 0.6/0.4** ("Q"-type) seems to be the most appropriate choice.

If the high-temperature modification reaction is combined with a controlled **cooling** regimen, specifically a ramp **of 5 °C/min until** reaching **600 °C**, the self-disintegration properties of the modified HTFA 1 are maintained. Furthermore, there is an increased level of Al leaching, both overall and within a shorter timeframe. The optimal outcome is the formation of a mixture consisting of **$CaCO_3$/$CaCl_2$** in a ratio of **0.7/0.3**.

The impact of combined activation conditions on phase content

The utilisation of a combination of Ca-based modifiers has been shown to effectively activate FA, with the addition of $CaCl_2$ in small quantities relative to limestone having a notable impact on leachability. Consequently, it is anticipated that the resulting products from this reaction will align more closely with the phase composition observed during the modification of FA with chloride. To investigate this further, various ratio of both reagents were examined to identify the presence of distinct phases. All samples underwent preparation through a high-temperature reaction at 1,000 °C for 60 minutes, followed by a gradual controlled cooling to 600 °C, and finally a rapid uncontrolled cooling to room temperature. The analysis of the phase composition of the crystalline fraction is presented within the 2θ 18–38° range in Fig. 56.

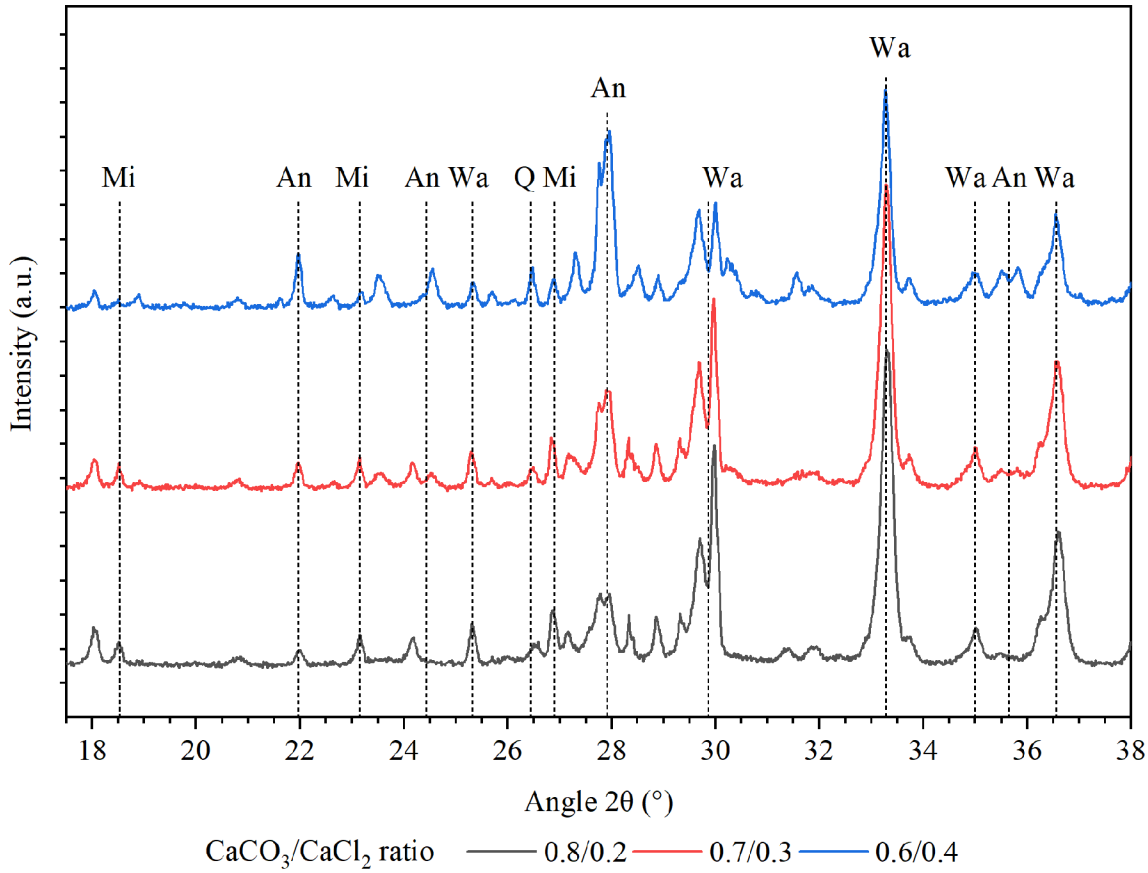

Fig. 56 Diffractogram of 2θ 18–38°range, sample HTFA 1 with different $CaCO_3/CaCl_2$ ratio, reaction at 1,000 °C

The XRD analysis results clearly indicate that the products formed due to phase modification by the combination of Ca-based agents, even with a low $CaCl_2$ ratio of 0.2, are similar to those obtained through activation with $CaCl_2$. The main phases of wadalite and anorthite are observed, with the Wa content corresponding to a reaction time of 180 minutes with $CaCl_2$. A noticeable trend is observed in the different ratios, where an increase in additional $CaCl_2$ to limestone leads to a higher representation of anorthite at the expense of wadalite. Moreover, as the chloride content in the mixture rises, the selective reaction involving quartz also increases, resulting in more quartz remaining in the mixture with higher $CaCl_2$ content. Phase of mullite

is not detected in any ratio of the reagents. Additionally, a new microsommite (Mi) phase is identified in all samples, which is a potassium-sodium-calcium-aluminium chloride-silicate, representing a non-stoichiometric intermediate product of activated aluminosilicate with chlorine. The presence of microsommite and wadalite phases further supports the idea that the chlorine by-product resulting from activation can interact with the surrounding structures to form chloro-silicates.

Alterations in the morphology of particles FA modified by combination of $CaCO_3$ and $CaCl_2$

The resemblance between the particle morphology activated solely by $CaCl_2$ and the high-temperature modification reaction of HTFA 1 with a combination of Ca–based agents in a $CaCO_3/CaCl_2$ ratio of 0.7/0.3, supplemented by controlled cooling at 600 °C, is a significant finding in the field of materials science. This similarity suggests that the use of $CaCl_2$ as an activating agent can produce results similar to those of a more complex modification process involving multiple Ca–based agents. The SEM image, Fig. 57, provides visual evidence of this resemblance, showing crystalline products forming thin plate-like formations with some adorned with small needles – left side. This indicates a high degree of structural similarity between the two processes. However, the modified sample also contained particles that exhibited morphological characteristics consistent with activation by limestone. An illustrative example of such particles can be observed on the Fig. 57a. Nevertheless, it is important to note that their presence can be classified as either borderline or infrequent.

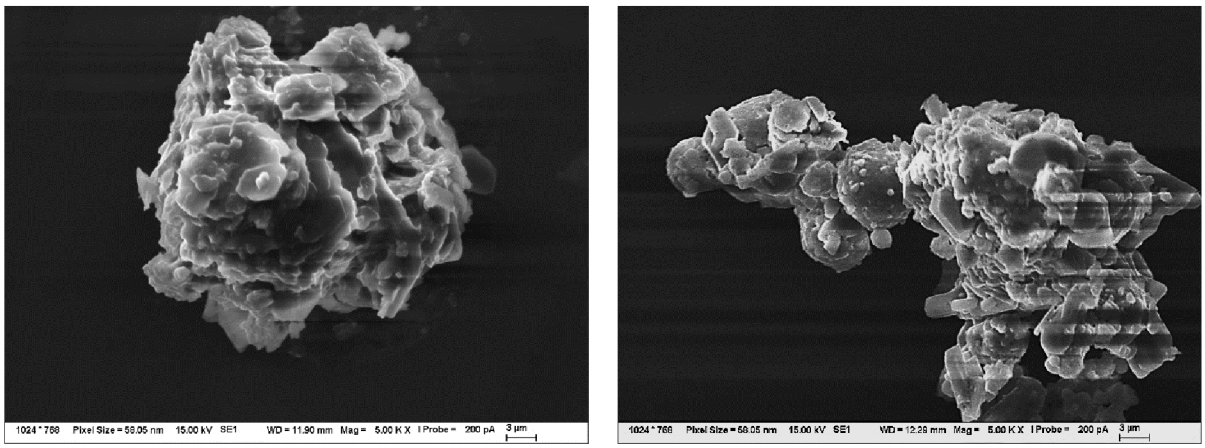

Fig. 57 SEM images of morphology, HTFA 1 with $CaCO_3/CaCl_2$, 0.7/0.3

5.4.4 Activation with combination of limestone and NaCl or KCl

In the subsequent chapter, concerning the outcomes, a brief report will be made regarding the potential of an alternative approach to FA modification. If the utilisation of FA through a blend of limestone and calcium chloride proves to be an effective technique in altering the phase composition of FA, the inquiry emerges regarding the potential substitution of $CaCl_2$ with other, more readily available and cost-effective chlorides such as NaCl or KCl. To investigate this, a small-scale experiment was conducted wherein $CaCl_2$ was replaced with NaCl in one instance and KCl in another, while maintaining the chloride content with an equally optimal dosage of

$CaCl_2$. In the initial group of samples, an addition of limestone equivalent to 0.45 mol eq. was retained. Following the ideal ratio established in section 5.4.1, the subsequent group contained a reduced quantity, corresponding to a $CaCO_3$ ratio of 0.32 mol eq., equal to 0.7 $CaCO_3$ as the ideal ratio in conjunction with chloride in section 5.4.3. The mixtures were subjected to firing in ceramic crucibles within a muffle furnace at a temperature of 1,000 °C. The extent of reaction conversion was ascertained through gravimetry and EDX analysis of the aqueous leachate. The proportion of the reacted component is delineated in Fig. 58.

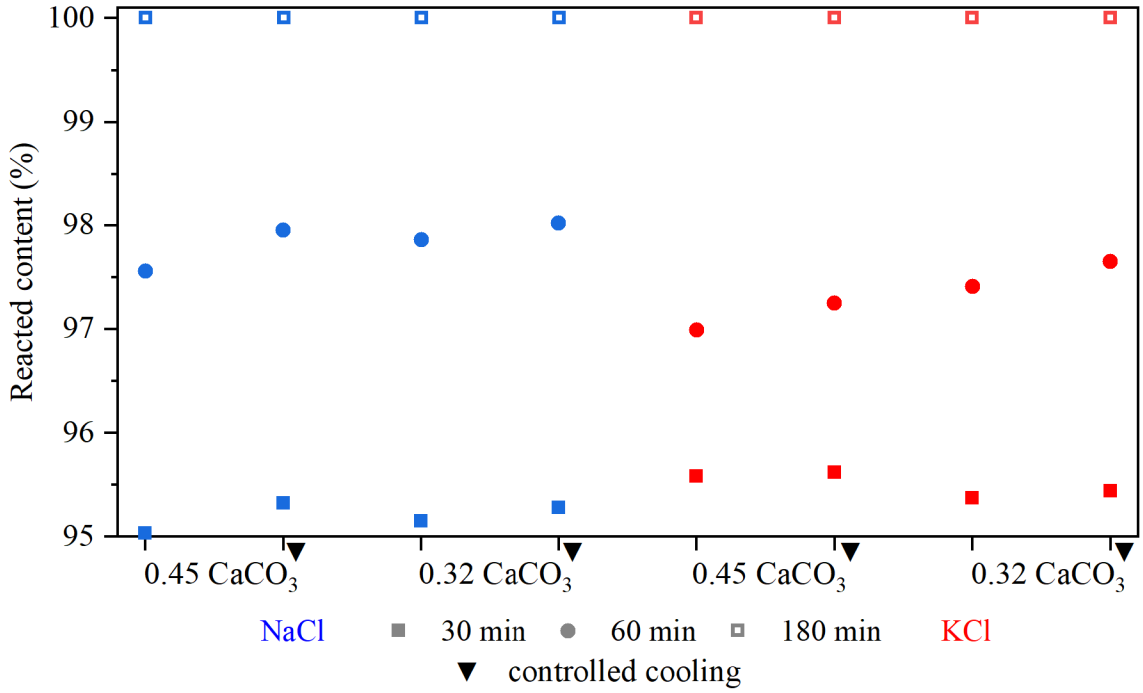

Fig. 58 Graph of the reacted amount of modification agents as a function of reaction time at 1,000 °C

The conversion rate of all samples is uniform due to the combination of methods utilised, surpassing 95 %. It was further noted that samples exposed to a regulated gradual cooling procedure attained a marginally further transformation. This can be attributed to an extended duration at an elevated temperature, during which the substance undergoes partial hardening even amidst the slow cooling process, while the addition of 0.32 or 0.45 mol eq. of limestone did not affect the conversion. All calcium components were reacted according to the complexometric titration within 30 minutes. Furthermore, the modified FA no longer displays its auto-disintegrating characteristics in both types of chlorites used, irrespective of the inclusion of $CaCO_3$ additions or the cooling process applied to the samples. Prior to further experiments and analyses, the samples underwent grinding in an agate grinding wheel to achieve a fineness corresponding to the D_{50} of the auto-disintegrated samples.

The impact of combined $CaCO_3$ and NaCl/KCl conditions on leachability

All pre-prepared combinations of HTFA 1 and adjusting agents, as detailed in the preceding section on taste, were exposed to controlled leaching in a sulphuric acid solution with mol eq.

1.2 and a L/S ratio of 10, mirroring the conditions of the control leaching experiments conducted in earlier sections.

The graphs in Fig. 59 summarise the results, illustrating the impact of NaCl modification on the leachability of aluminium on the left side. At the same time, the potassium counterpart of the modifying agent is depicted on the right side. Samples treated with NaCl or KCl during the initial phases of the extraction process demonstrate comparable outcomes and trends when contrasted with previously mentioned modification techniques. The presence of the symbol ▼ signifies that the sample has undergone a meticulously regulated gradual cooling process. In contrast, its absence suggests that the sample has been rapidly and non-controlled cooled to room temperature. Despite a significant proportion of individual components reacting, the leachability of aluminium from FA treated in this manner does not meet expectations of leachability results when modifying HTFA 1 with $CaCl_2$ and $CaCO_3$. Irrespective of the type of modifying chloride, carbonate addition, or cooling mode, all samples fall short when compared to the experiment involving FA activation using a combination of Ca-based agents, namely carbonate and chloride. The leachability of HTFA modified with a combination of NaCl and $CaCO_3$ does not exceed 85 %, while the combination of KCl and $CaCO_3$ reaches a maximum of less than 75 %. Although all the chlorides used have a melting point within the range of 770–800 °C, the reaction method in conjunction with $CaCO_3$ is likely to differ significantly from that of the calcium system.

Due to the comparatively limited leachability of aluminium activated through the use of FA and the lack of an auto-disintegration mechanism, no additional blends were formulated or fine-tuned. The effects of the addition of the mentioned chlorides on the phase composition were also not monitored using the XRD method. Nevertheless, it is plausible that sodium or potassium feldspars could develop in configurations altered with NaCl or KCl. These compounds exhibit low solubility in acidic environments. [156, 157]

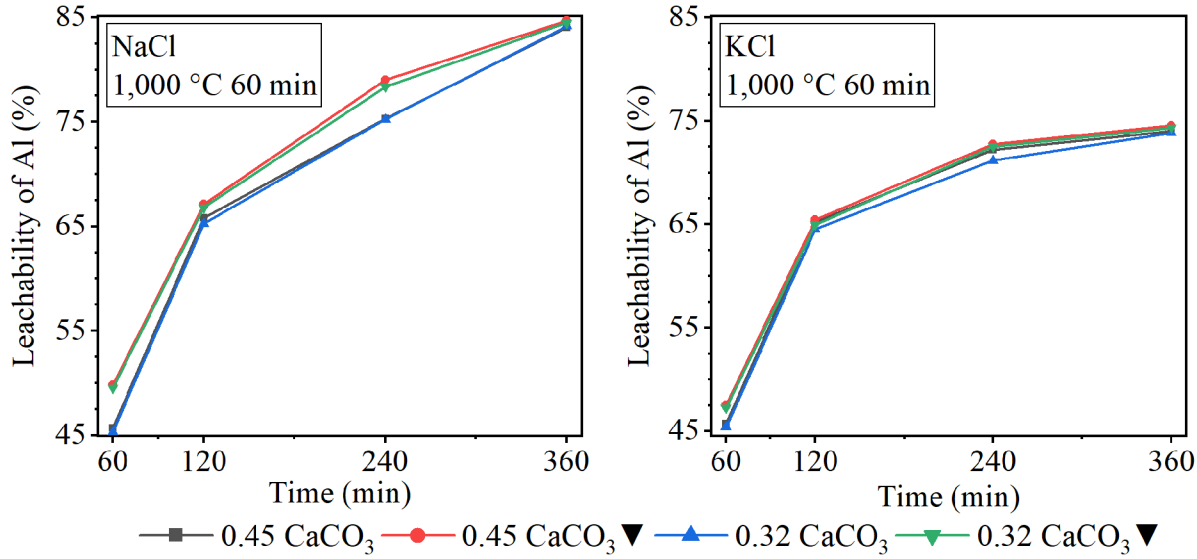

Fig. 59 Comparison of the leachability of Al; HTFA 1 modified with the addition of $CaCO_3$ and NaCl or KCl

5.5 Extraction of macro-concentrated elements

Upon successfully implementing effective methods for activating the input material to enhance leachability, this doctoral dissertation also aims to optimise the extraction procedure by considering factors such as the reagent type and concentration, L/S ratio, extraction duration, temperature, homogenisation techniques, and more. This endeavour seeks to identify the most comprehensive approach feasible for both universal and industrial utilisation.

A modified HTFA 1 mixture was employed to assess the various parameters and track their fluctuations in terms of aluminium leachability. This modification involved the addition of 0.45 mol eq. of $CaCO_3$ and 0.35 mol eq. of $CaCl_2$, with a mass ratio of 0.7/0.3 for both reagents. The high-temperature modification reaction proceeded as follows: a gradual increase in temperature at a rate of 10 °C/min until reaching 800 °C, followed by a slower ramp of 5 °C/min until reaching 1,000 °C followed by isotherm for 60 minutes at this temperature. The cooling process involved a gradual decrease in temperature at a rate of 5 °C/min until reaching 800 °C, followed by a faster cooling rate of 10 °C/min until 600 °C. Finally, the mixture was rapidly and uncontrollably cooled to room temperature within a few minutes. Collectively, this modified HTFA 1 mixture can be denoted as **"O"-modified HTFA 1**.

5.5.1 Type of extraction agent

The extraction agent plays a crucial role in the overall process, being the key factor among all influencing elements. Due to the products being insoluble in water or having minimal reactivity with water, as well as in alkaline conditions with aqueous solutions of carbonates or hydroxides [158–160], potentially leading to the formation of various insoluble byproducts, the utilisation of such environments seems highly unsuitable.

On the contrary, acid has a contrasting impact on these structures [157, 158]. In evaluating the appropriateness and efficacy of modification reactions to enhance leachability in preceding sections, sulphuric acid was employed as an extraction solvent owing to its widespread applicability and favourable outcomes in prior experiments, commonly referred to as direct acid leaching. However, the phases resulting from the modification of HTFA 1 using the sequence of reactions described in the previous chapters can undergo reactions in the environment of other acidic solutions.

In order to make a comparison, we utilised sulphuric, hydrochloric, nitric, and phosphoric acid solutions. These solutions were prepared with a high (L/S) ratio of 50, and the acid concentrations were set at 0.5 and 1.0 M. These acid concentrations ensured an ample excess of acid for the complete dissolution of all components, considering Al, Fe, Ti, Ca, Na, K, and Mg. The presence of Ti in the components renders them unreactive under these specific conditions. However, the remaining alkalis and base metals will undergo reactions. The effectiveness of the entire process was monitored under laboratory conditions, i.e. atmospheric pressure and a temperature of 25 °C. The efficiency of the complete procedure was observed in a laboratory setting, specifically at standard atmospheric pressure and a temperature of 25 °C.

The magnetic stirrer with a Teflon-coated stir bar was utilised, with the speed adjusted visually to prevent vortex formation and avoid sedimentation of the mixture at the bottom.

The findings of this experiment have been briefly presented in the two graphs depicted in Fig. 60. The graph on the left illustrates the yield of extraction under the conditions of 0.5 M solutions. In contrast, the graph on the right showcases the impact of 1 M solutions of the same reagents.

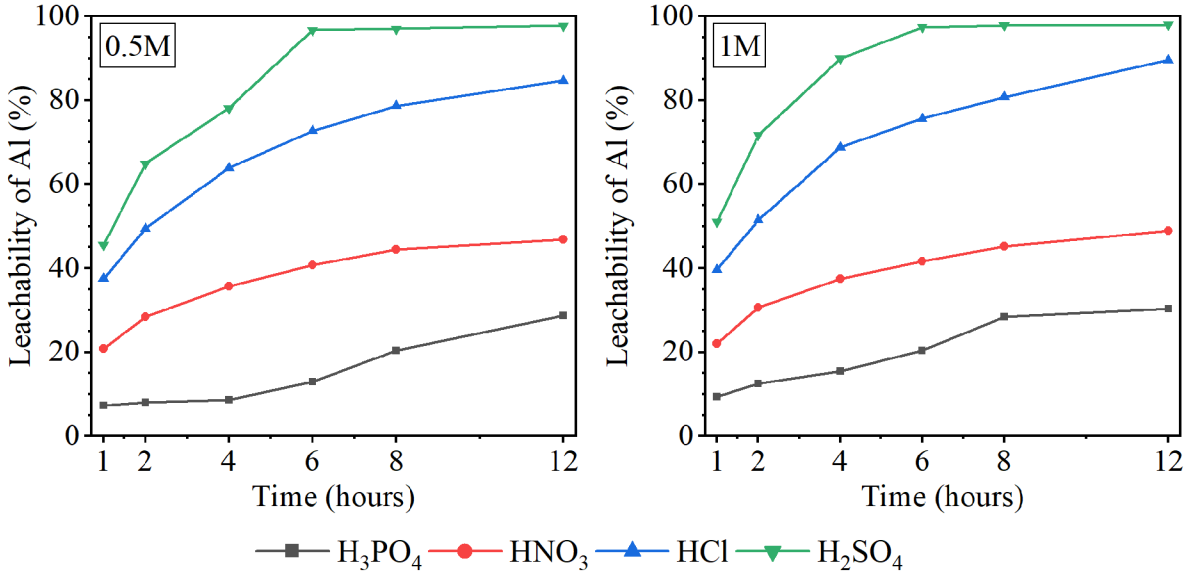

Fig. 60 Comparison of the leachability of Al in different acid solutions; "O"-modified HTFA 1

Unsurprisingly, only a minimal quantity of aluminium is dissolved into the phosphoric acid environment. This can be attributed to the fact that aluminium exhibits limited reactivity when subjected to such a low acid concentration. Consequently, it is highly improbable for any reaction to occur between the aluminium and the current Wa or An, as indicated by [161]. Hence, phosphoric acid is deemed unsuitable for the intended application.

Nitric acid appears to yield marginally improved outcomes in relation to the leaching of Al; however, the leaching efficiency remains below the 50 % threshold. The attainment of equilibrium is swift, with extended durations of exposure to "O"-modified HTFA 1 failing to enhance process efficiency significantly. In addition, the use of nitric acid is not entirely optimal, even with regard to the nitrous gases produced.

Extraction in hydrochloric acid results in significantly higher Al leachability values, with a leachability close to 85 % even at a lower concentration of 0.5 M, and nearly 90 % at a higher concentration of 1 M. These values are indicative of the reaction between the acid and feldspar minerals.

The most optimal outcomes, however, are attained through the use of sulphuric acid. Even with a lower acid concentration solution, the leachability exceeds 95 % within 4-6 hours of the extraction reaction. This demonstrates the versatile applicability of sulphuric acid, akin to other hydrometallurgical methods. Furthermore, hydrochloric acid achieves significantly higher leachability in a shorter timeframe.

The results obtained show that **sulphuric acid** is highly effective, even when used at a lower concentration of **0.5 M** and a reaction time of **6 hours**.

5.5.2 L/S ratio and concentration of extraction agent

Balancing the suitable L/S ratio is crucial for optimising the entire process. This is essential to maintain the efficiency of the extraction process as much as possible, while minimising the liquid volume in consideration of the reactor volume. The L/S ratio is a crucial parameter that influences the access of reactants to the material, the removal of products into the solution, and the rheology of the mixture.

L/S ratio

In order to find a suitable L/S ratio, a laboratory experiment was carried out using sulphuric acid as an extraction reagent at a concentration of 1,0 M with a differing L/S ratio of 6–20. The results, summarised in the graph depicted in Fig. 61, of this analysis is presented, similar to the entirety of the study, as the extractability of aluminium during the extraction process.

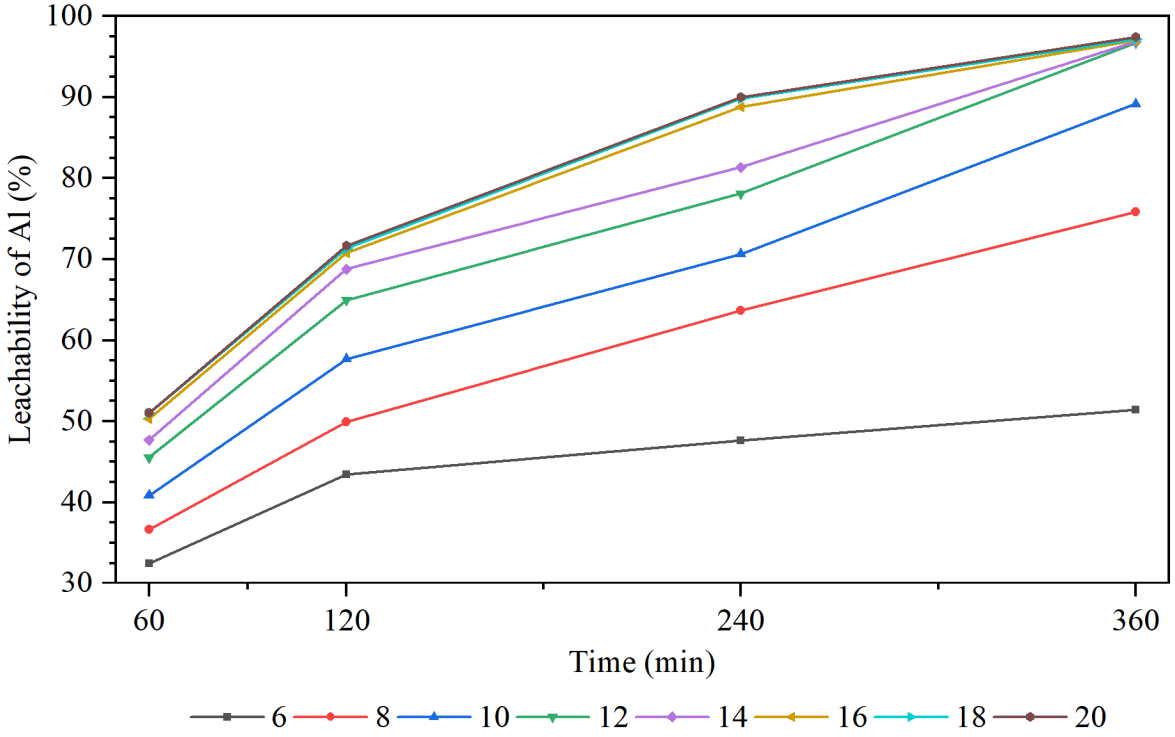

Fig. 61 Comparison of the leachability of Al at different L/S ratio, 1M H_2SO_4; "O"-modified HTFA 1

The results clearly indicate that the leachability of Al in the extraction process is significantly influenced by the L/S ratio. In the case of mixtures with L/S ratios of 6 and 8, limited mixing was observed due to the increased density of the mixture during extraction. The extraction process in sulphuric acid produces insoluble gypsum as a by-product, which requires approximately 2.6 g of water per 1 g of Ca for the reaction, based on the Ca content in "O"-modified HTFA. Consequently, up to 50 % of the water present in the mixture at a low L/S ratio is consumed for this reaction. The formation of gypsum has a significant impact on the results. Furthermore, the L/S determination model used in this study does not consider the

minimum amount of extractant required for the reaction of all components. As a result, it is clear from the calculations that mixtures with an L/S ratio of 10 and below lack adequate acid content. As the acid concentration surpasses the optimal level, the reaction rate during the latter stages is also influenced. This is due to the heightened likelihood of successful acid precipitation with the solid component, as the precipitation reaction theory postulates.

The next experiments of this study must substitute the current model with one that takes into account the molar equivalence of the extraction agent utilised in relation to all resultant products.

For the subsequent trial, an **adjusted model** is substituted for the model mentioned earlier, encompassing the **molar equivalent** of the extraction agent employed to ensure reproducibility and facilitate result comparison. The subsequent model relies on an acid content equivalent to 1.0 mol eq, which is essential for the reaction of all the existing components comprising Al, Fe, Ti, Ca, Na, and Mg to form stoichiometric sulphates. Consequently, the concentration of the acid employed in the experiment varies. Precisely, it corresponds to a concentration of 1.63 M (15 wt. %) for a mixture with an L/S ratio of 6, and subsequently decreases to 0.49 M (5 wt. %) for an L/S ratio of 20.

The results of the leachability of aluminium in this mode of the extraction process are presented by the course of the curves in the graph in Fig. 62. These experimental data better reflect the actual influence of the L/S ratio on the entire extraction process. It is evident that this model is much more suitable for describing the efficiency of the process, as a solid degree of leachability is observed in all monitored mixtures. For low L/S ratios (L/S 6 and 8), the leachability is approximately 10 % lower compared to the remaining mixtures. This is due to the high viscosity of the mixture during the extraction process. Viscosity, in this case, is perceived as resistance to mixing evaluated optically. This is both due to the thickening of the mixture due to the formation of gypsum, as well as the wetting of a relatively fine sample and, last but not least, the formation of amorphous silicic acid in the form of a gel. A significant leachability of 93 % is achieved in the mixture with an L/S ratio of 10, where the thickening of the mixture, which hinders the effective influence of the mixtures, is not as apparent as in the previous two cases. However, even more peculiar results are obtained when using an L/S ratio of 12 and higher, where the leachabilities are comparable and range from 97–98 %. At the same time, the curves corresponding to the L/S ratio are already similar. The most suitable option appears to be using **L/S 12 or 14** with H_2SO_4 mol eq. 1.0.

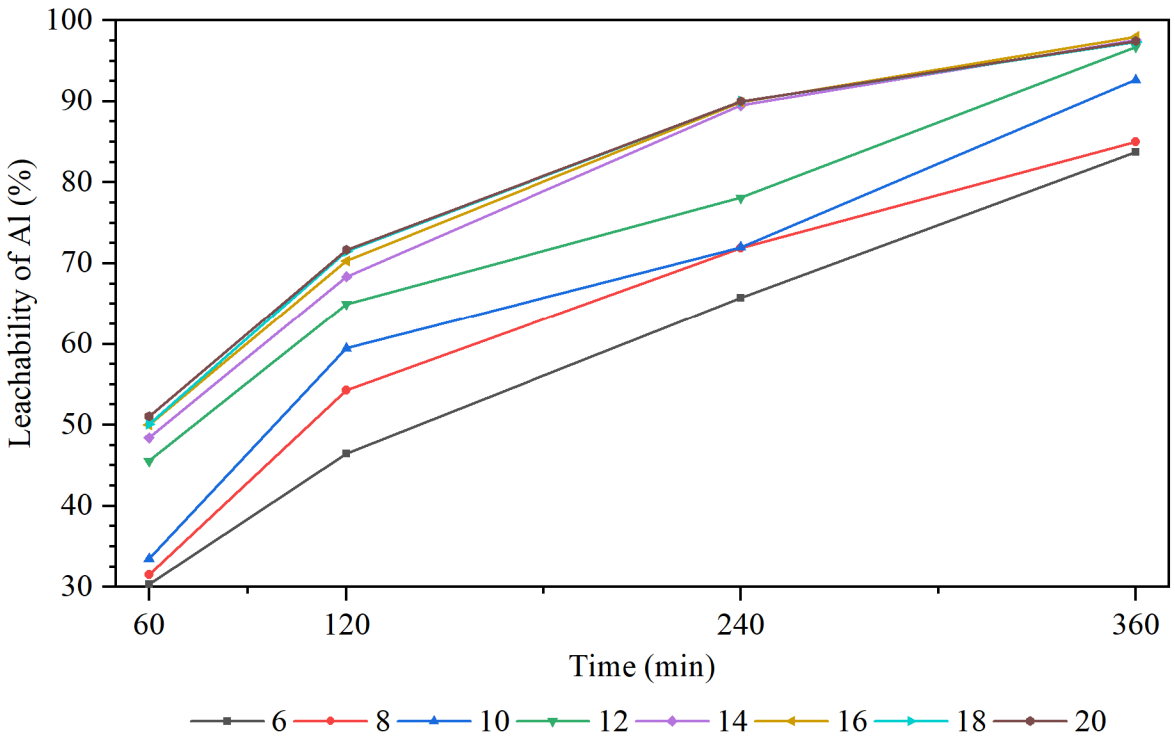

Fig. 62 Comparison of the leachability of Al at different L/S ratio, H_2SO_4 mol eq..1.0; "O"-modified HTFA 1

Molar equivalent

Once the optimal L/S ratio has been achieved, it becomes feasible to adjust the extraction agent to observe the impact of varying mol eq. H_2SO_4 on the leachability of Al. The mol eq was altered for mixtures with L/S H_2SO_4 12 and 14 within the range of 0.6–1.4. The mass and molar concentration of the extraction agent used in the reaction with "O"-modified HTFA 1 are detailed in Table 19 to provide a comprehensive overview of all laboratory experiment parameters. The results regarding aluminium leachability are depicted in two graphs in Fig. 63, with the progression of the experiment using a lower L/S ratio shown on the left side.

Table 19 Molar and wt. % concentration of H_2SO_4 used for extraction at mol eq. 0.6–1.4

		H_2SO_4 mol eq.				
		0.6	**0.8**	**1.0**	**1.2**	**1.4**
L/S 12	M	0.49	0.65	0.82	0.97	1.14
	wt. %	4.91	6.47	7.99	9.43	10.96
L/S 14	M	0.42	0.56	0.70	0.84	0.98
	wt. %	4.32	5.56	6.83	8.11	9.23

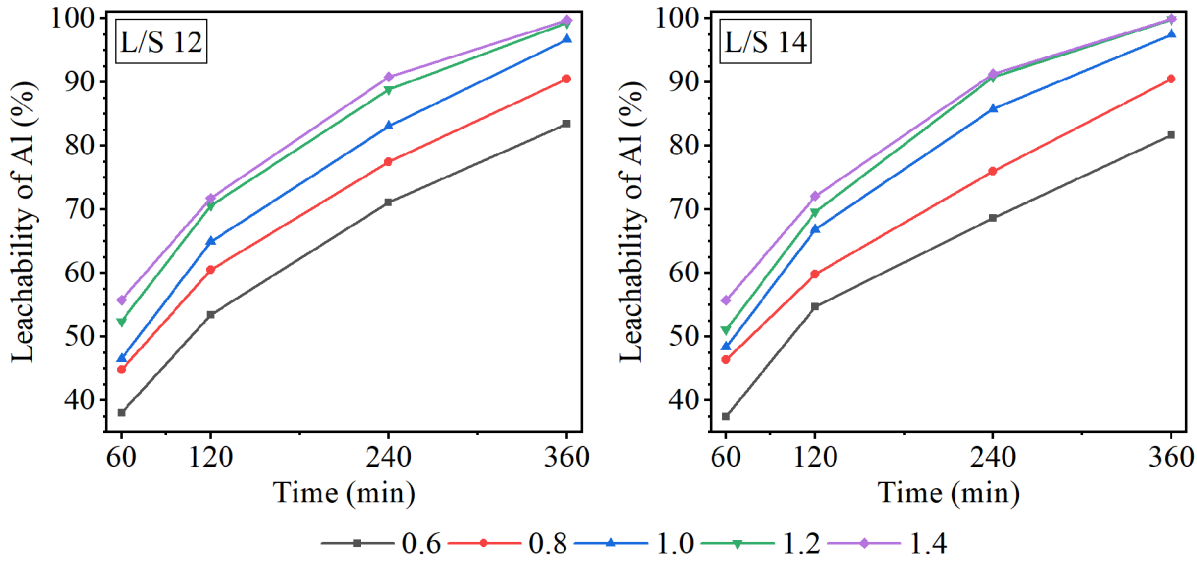

Fig. 63 Comparison of the leachability of Al at different H_2SO_4 mol eq.; "O"-modified HTFA 1

The findings from Fig. 63 indicate a minimal disparity in the impact of L/S 12 and 14 on the efficiency of the extraction process, as observed through the leachability of aluminium. However, the leachability is affected by the variation in the mol eq of the extraction agent utilised. It is evident and can be proven through the experiment that a ratio below mol eq 1.0 does not result in the conversion of the existing aluminium into the solution, leading to the premature termination of the extraction due to the depletion of the reaction groups of the extraction agent. Simultaneously, the experiment demonstrates that the aluminium reacts at a similar rate to the other components, as evidenced by the comparable shifts in the individual curves of mol eq. 0.6, 0.8, and 1.0 relative to each other. When employing a mixture with **mol eq. 1.0**, the dissolution is only a bit less than **97 %** for the chosen lower L/S and 97.5% for L/S 14 within a reaction time of 6 hours. **Mol eq. 1.2 and 1.4** already exhibit practically identical progress, achieving leachability of **99.5 %** and higher.

Thus, a suitable L/S ratio and mol eq. demonstrably affect the overall leachability of the extraction agent used, while its concentration does not. This only affects the course of the curve, and as the concentration of the reagent increases, its steepness is initially higher. According to this model, a high concentration of the extractant is a high mol eq. They certainly provide experimentally exciting data, but from the point of view of potential industrial application, they are not very desirable.

5.5.3 Combination of extraction agents

The study described in the subsequent paragraphs examined the impact of different extraction media combinations, precisely the combination of sulphuric acid and hydrochloric acid, sulphuric acid and hydrogen peroxide, and all three substances together. The purpose of the experiment was not to enhance the leachability of Al, but rather to determine if the combination of these agents could result in the maximum leachability within a shorter time frame.

The influence of the three substances was once again observed on "O"-modified HTFA 1, with sulphuric acid L/S 12 and mol eq. 1.0 with the addition of HCl or/and H_2O_2 – mixtures A-G. Table 20 presents a summary of the individual contributions of agents, encompassing the levels of the specified components in the extraction mixture. A comparison of the influence of individual mixtures on the leachability of aluminium is then shown in the graph in Fig. 64.

Table 20 Molar and wt. % concentration of extraction agents in mixtures A-G

		Concentration of extraction agents		
Mixture	**Concentration**	**H_2SO_4**	**HCl**	**H_2O_2**
A	M	0.82	–	0.17
	wt. %	7.99	–	0.55
B	M	0.82	–	0.35
	wt. %	7.94	–	1.08
C	M	0.82	–	0.70
	wt. %	7.81	–	2.15
D	M	0.82	0.20	–
	wt. %	7.93	0.69	–
E	M	0.82	0.41	–
	wt. %	7.87	1.37	–
F	M	0.82	0.82	–
	wt. %	7.76	2.69	–
G	M	0.82	0.82	0.70
	wt. %	7.58	2.64	2.09

The overall leachability of the aluminium content has been previously indicated to have reached a maximum and consistent value of approximately 97 % across all mixtures utilised in the experiment. A notable deviation in leachability is observed in mixture G, which contains the highest concentration of peroxide and hydrochloric acid, resulting in a significantly favourable aluminium leachability of 92 % after only 4 hours of the extraction process.

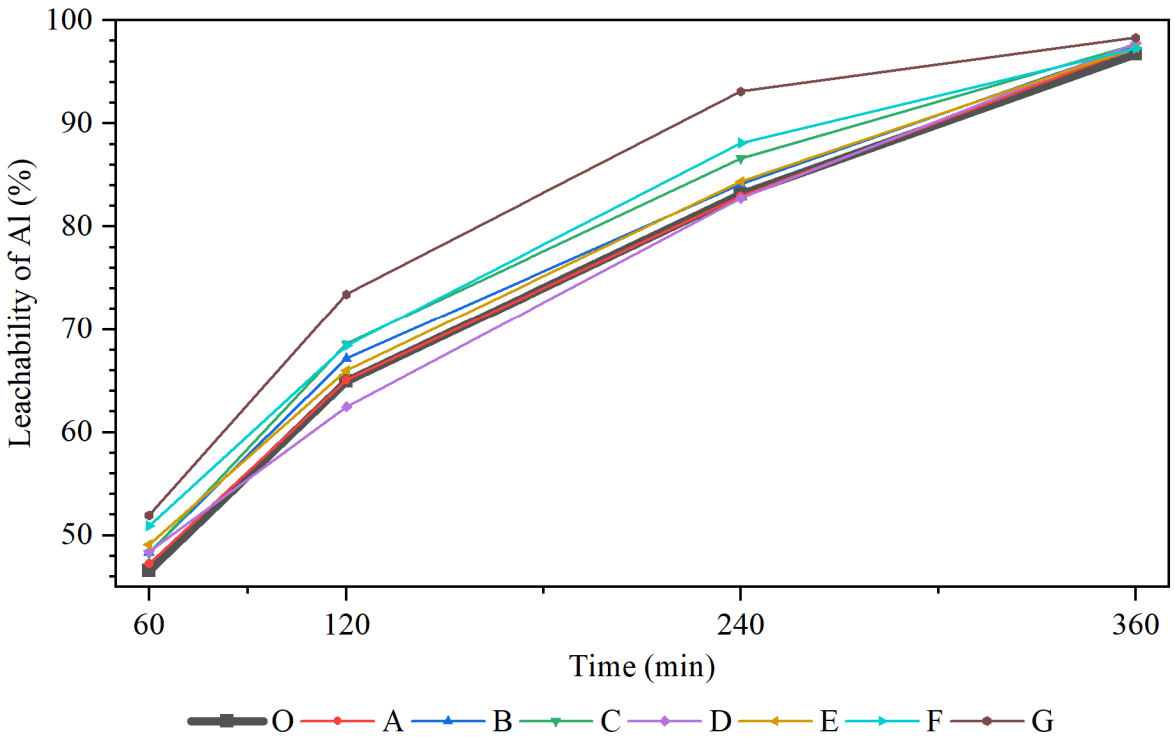

Fig. 64 Comparison of the leachability of Al at different extraction agent addition with H_2SO_4 mol eq. 1,0, L/S 12; "O"-modified HTFA 1

Based on the experimental data, it is evident that mixtures labelled A, B, and D, E, which contain lower amounts of peroxide or hydrochloric acid, do not have a positive impact on the aluminium leachability process. Their results are comparable to a mixture without these additions, as indicated by the bold line on the graph. The highest leachability is only achieved when the maximum amount of each reagent is added, specifically with mixture C and F, resulting in a total aluminium leachability of 4–5% after 4 or 6 hours, respectively. However, it is important to note that the addition of hydrochloric acid increases the total mol eq. extraction agent, or concentration, which may have a slightly favourable effect on the leachability process.

In summary, this experiment yielded no adverse outcomes; however, the amalgamation of these extraction agents did not result in a substantial advancement.

5.5.4 Extraction temperature

Temperature has consistently been recognised as a significant factor influencing various reactions. Elevated temperatures not only impact the solubility of products, diffusion rates, and penetration of extraction agents, but also accelerate chemical reactions. Previous studies have demonstrated that the extraction of aluminium in a 5 wt. % H_2SO4 environment at its boiling point is rapid and effective, even in the presence of FFA. [113].

In order to achieve this objective, an experiment was conducted using "O"–modified HTFA 1 in an H_2SO_4 solution, with a mol eq. of 1.0 and a L/S ratio of 12. To assess the impact of temperature on both the reaction rate and the leachability of aluminium itself, the experiment was replicated at various temperatures 25, 45, 55, 75 and 95°C, as well as at the boiling

temperature of the mixture. At a specific acid concentration and sample type, the boiling temperature reached a range of 107–109 °C. The findings regarding the influence of temperature are presented in the graph depicted in Fig. 65.

An increase in temperature evidently results in a notable alteration in leachability over a period of time. The impact of rising temperature on the leachability progression is clearly discernible, particularly within the initial two hours of the trial, where the leachability of aluminium doubles compared to the experiment conducted at room temperature. However, this augmentation is solely observed at a temperature of 95 °C. While utilising a lower temperature does lead to achieving a leachability exceeding 95 % in a shorter timeframe compared to room temperature, the reduction in extraction time is only around 1–1.5 hours, which may not be deemed practical considering the energy consumption required to heat the mixture to its optimal level.

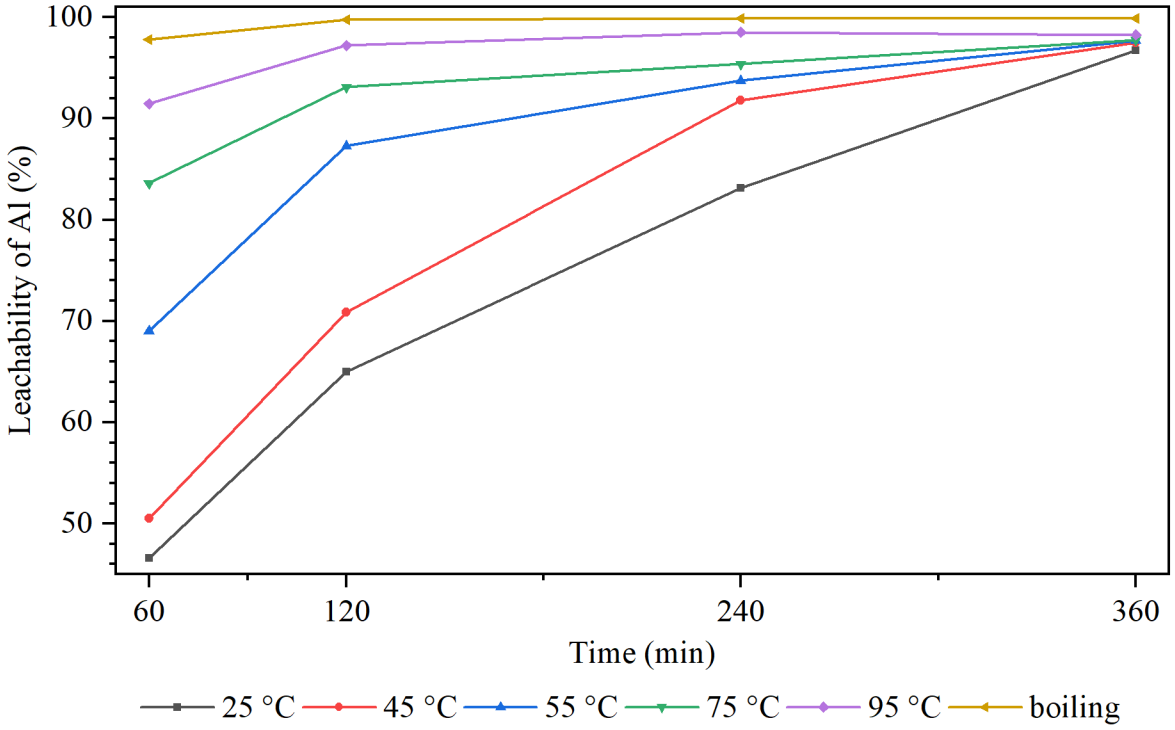

Fig. 65 Comparison of the leachability of Al at different temperatures, H_2SO_4 mol eq. 1,0, L/S 12; "O"-modified HTFA 1

Therefore, a preliminary inference can be drawn that the utilisation of heightened temperature can be unequivocally advocated in terms of reducing the duration of the extraction process. However, of greater significance is the fact that optimal leachability can be attained even at ambient temperature, underscoring its paramount importance.

5.5.5 Upscale experiment

The larger-scale extraction experiments allowed for a more accurate representation of potential industrial processes, as the increased volume and mixing techniques provided a more realistic simulation of industrial conditions. The results obtained from these experiments will be crucial in determining the feasibility and efficiency of scaling up the extraction process for industrial applications. Furthermore, using different mixing techniques allowed for a comparison of efficiency and effectiveness in extracting the desired compounds from the sample. To achieve this objective, the reaction volumes were gradually augmented to a total of 30 L for the extraction mixture. The mixing technique was accordingly modified, where the mixture in the 5 L reactor was stirred using a magnetic stirrer equipped with a Teflon stirrer. Additionally, for the purpose of efficiency comparison, a radial glass stirrer and a stand mixer were also employed. This mixing approach was also implemented for the largest reaction vessel depicted in Fig. 66. Overall, the expansion of the extraction experiments to larger scales has provided valuable insights into the potential industrial implications of the extraction process.

150 mL 1,000 mL 5,000 mL 50 L

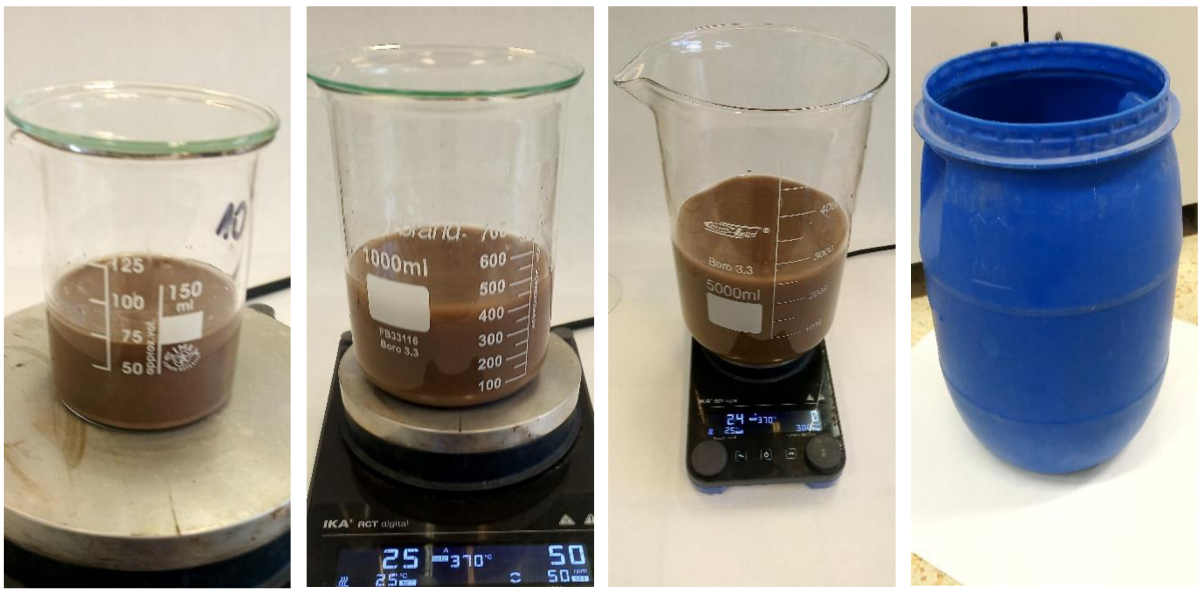

Fig. 66 Photos of the reaction vessels in the experiment

Upon experimenting with an expanded reaction volume, the temperature of the reaction mixture was observed concurrently with the leachability of aluminium as time progressed. Fig. 67 illustrates a comparison of the leachability of aluminium on the left side while measuring temperature on the right. The investigation was conducted utilising “O”-modified HTFA 1, within an sulphuric acid environment. The experiment employed L/S ratio of 12 and a mol eq. of extraction agent of 1.0.

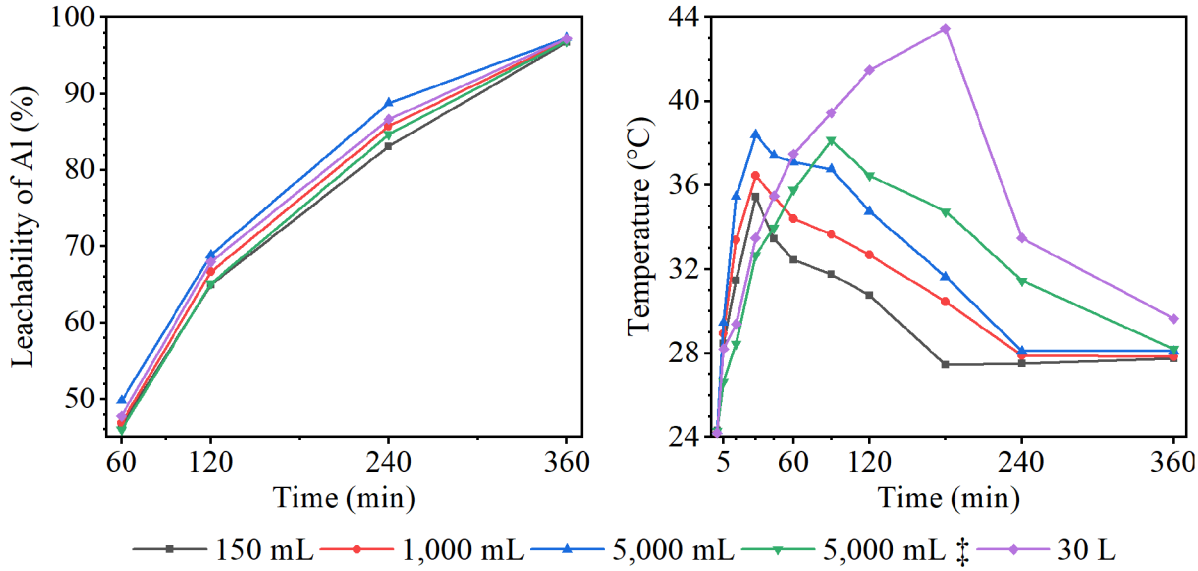

Fig. 67 Comparison of the leachability of Al and reaction temperature at different volumes of vessel, H_2SO_4 mol eq. 1,0, L/S 12; "**O**"-modified HTFA 1

The results obtained from this experiment can be characterised as highly successful, as the leachability during the gradual increase in reaction volume remained consistent with the original experiment. A minor discrepancy was observed during the extraction process. It is clear that, due to the larger scale of the experiment, there were slight variations in reaction temperature, both overall and in the time taken before a decrease was recorded. This phenomenon results from the increased volume of the reaction mixture and, consequently, the higher heat capacity of the entire system, where heat transfer to the surroundings primarily occurs through the wall of the reaction glass vessel. Another minor difference observed during the extraction process was the transition from using a magnetic stirrer with a Teflon stirrer to shaft stirring with a radial glass stirrer, denoted by the symbol ‡. In the initial stages of the process, there was a noticeable delay and a slight deceleration in the reaction, as evidenced by the lower temperature of the mixture in the first 60 minutes, along with the peak temperature of the reaction mixture being reached 45 minutes later compared to the magnetic stirrer setup. The impact on leachability was only significant in the first two hours of the experiment, where the efficiency of the reaction homogenised by mixing ‡ was 2–3 % lower. However, in the later stages of the experiment, the outcomes were consistent. The most significant difference in temperature trends during the experiment, as well as in the initial leachability of aluminium, was observed in the case of the largest reaction vessel used with a 30 L extraction medium volume. In this scenario, the influence of the stirrer's geometry, specifically a single-row stirrer with two blades of rectangular cross-section, 30 mm in height and 125 mm in length, with blades angled at 30° relative to the rotation axis and immersed in the lower third of the reaction mixture .The reaction in this experiment was delayed due to the unique geometry of the mixing process in comparison to previous mixtures. Factors contributing to this delay include the start of the stirrer's engine, stirring of the mixture, the time required for the mixture to achieve

homogenisation, friction against the walls of the reaction container (which is made of plastic HDPE rather than glass), and other related variables. Additionally, the total reaction temperature in this experiment was 6 °C higher than that of the smaller mixture. This temperature variation can be attributed to the higher heat capacity of the system and the heat transfer coefficient through the wall of the reaction vessel, which is significantly lower in the case of HDPE as opposed to glass.

5.5.6 The influence of extraction conditions on the leachability of macro-concentrated elements

Up to this point of the study, the appropriateness of the conditions of the individual experiments has been evaluated as a factor affecting the leaching of aluminium, which is the most economically significant macro-element. However, HTFA 1 is a multi-elemental material that also includes Fe, Ti, or Si, which belong to the group of macro-concentrated elements. During the experimental conditions, the "O"-modified HTFA 1 exhibited a leachability of these other components as well when extracted in sulphuric acid with L/S 12 and mol eq. 1.0.

Based on the findings of the leachability study of the macro-concentrated elements mentioned, as depicted in three distinct graphs in Fig. 68, it is evident that the extraction process employed in this particular method exhibits a higher degree of selectivity towards aluminium, with a maximum of 60 % of the Fe content and up to 5 % of Ti being dissolved in the solution.

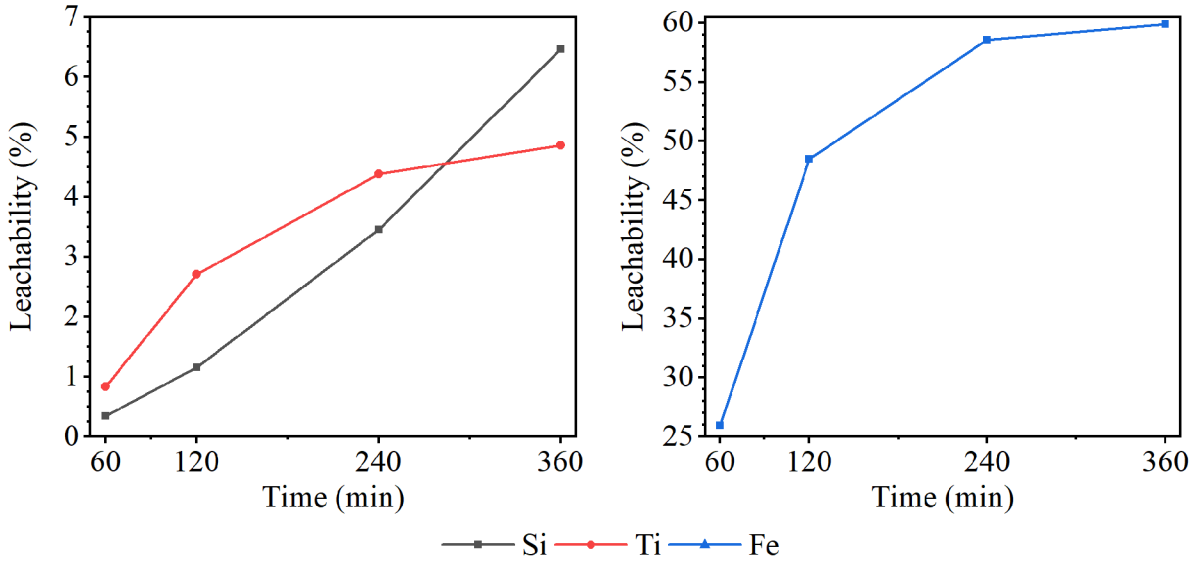

Fig. 68 Comparison of the leachability of Si, Ti and Fe in H_2SO_4 mol eq. 1,0, L/S 12; "O"-modified HTFA 1

The dissolution of Si in the extraction medium is not factored into the molar equivalent calculation. Including the extraction agent used is noteworthy, as this reaction is atypical; however, in terms of the breakdown of aluminium-silica constituents, its presence may potentially result in the partial formation of amphoteric or colloidal silicic acid. The correlation between Si concentration and its leachability into the solution shows that this reaction indeed occurs in a partial capacity. The impact of silicic acid or other soluble silicon compounds in

this setting will be further explored in the subsequent chapter 5.7, particularly in relation to their influence on the stability of the extracted liquid component.

Extraction of the remaining amount of Fe and Ti present can then be carried out using the second extraction step, namely by reaction with sulphuric acid with a concentration of 80 % at an elevated temperature of 70 °C at L/S 2–3 using a stand mixer with a glass radial stirrer. The conditions for the second extraction step are taken from extensive study [162]. The results for the leachability of Fe and Ti are then shown in the graphs in Fig. 69.

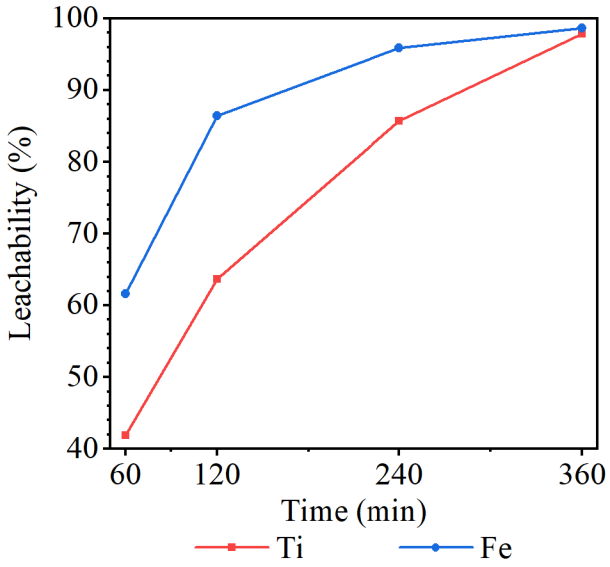

Fig. 69 Leachability of Fe and Ti, 2nd extraction in H_2SO_4 80 wt. %, L/S 3, 70 °C

In the second extraction, carried out with concentrated acid and high temperature, nearly 98 % of the titanium and more than 98.5 % of iron in the experiment were successfully transferred into the solution. The results of this reaction align perfectly with the theoretical predictions as reported in the publication [162]. The quantity of silicon found in the solution indicated that less than 2 % of the total amount had been leached.

These findings suggest that employing a two-step extraction process, with the addition of a second stage that aligns with the reaction conditions of concentrated sulphuric acid (at least 80 %) and elevated experimental temperature (at least 70 °C) at low L/S 3, results in the dissolution of all remaining macro-concentrated elements except for Si. The undissolved Si-based structures, along with the by-product gypsum, form an insoluble residue that may have the potential for further applications. The composition of the extraction residue and its potential uses will be examined in a separate chapter 5.8.

5.6 Assessment of modification and extraction methods as a potentially universal process

The optimisation of conditions leading to changes in the phase composition, along with enhancements in the extraction process, has proven to be effective when dealing with one specific type of sample - HTFA 1. Given the significant similarity in phase composition among individual samples, applying the most appropriate conditions to other samples within the experiment becomes feasible. A total of 33 FA samples from various regions including the Czech Republic, Poland, Turkey, India, as well as samples of natural volcanic ash were carefully chosen for this investigation. This selection represents a diverse array of samples necessary for evaluating the effectiveness of the overall process. Specifically, 21 distinct types of HTFAs were obtained from different sources such as Tušimice, TDK, Prunéřov, Ledvice, Dětmarovice, Mělník, TTR Prunéřov, Ždár nad Sázavou, Paskov, Tisová, Opatovice, Vřesová, Orlen, Rybnik, Opole, Sarni, Angul, along with two samples with unidentified origins within Turkey; 10 types of FFA and FBA sourced from Ledvice, Tisová, Hodonín, Poříčí, also with ash from biomass combustion from Poříčí K8; and two volcanic ashes from the Silvestre Craters region of Etna, as well as ash from Stromboli.

The entire range of samples was then subjected to a high-temperature modification reaction of type "O" and "Q". The ability of self-disintegration and subsequent leachability of Al in a sulphuric acid medium at mol eq. 1.0 and L/S 12 under laboratory temperature were evaluated for all FA modified in this way. Additionally, a second extraction stage was carried out for selected mixtures, using sulphuric acid with a concentration of 80 wt. %, at a temperature of 70 °C and L/S 3.

Overall, the leachability test results of the modified "O" type samples showed distinct trends based on their HTFA and FFA/FBA categorisations. The HTFA samples consistently tended to auto-disintegration, while the behaviour of fluidised-bed ashes varied between FA and BA samples. FA samples showed similarity to HTFA in terms of disintegration, while BA samples required physical crushing by mortar and pestle, though they did not exhibit high strength. The FFA and FBA samples resulting from biomass combustion formed clusters of 2–3 mm particles, also requiring crushing. The colour change in the modified samples was uniform for all except FFA and FBA from biomass, showing yellowish particles, with some samples displaying a more orange hue, likely due to higher Fe content.

To present leachability of Al in a more transparent and more organised manner, the results were segregated into separate Fig. 70 and Fig. 71. This division offered better clarity in understanding the distinct behaviours exhibited by the different sample types.

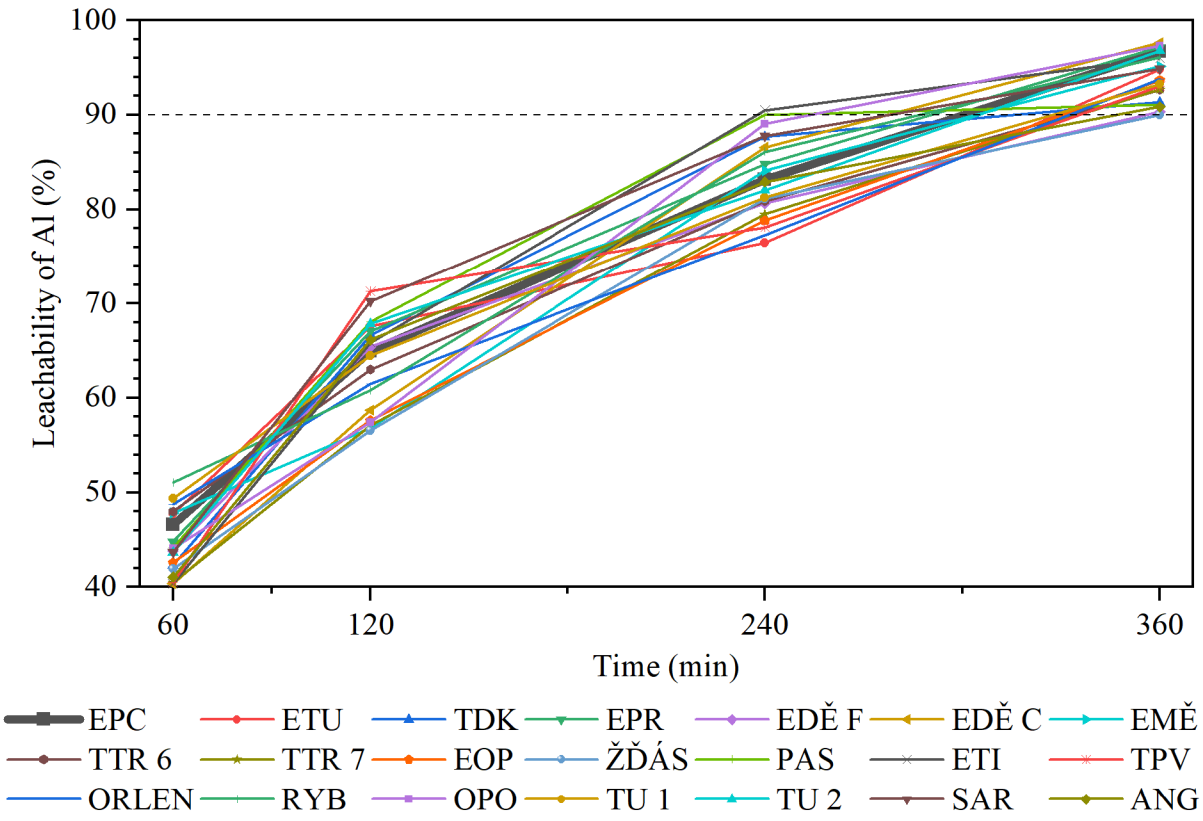

Fig. 70 Comparison of Al leachability on different types of "O"-modified HTFA in H_2SO_4 mol eq. 1,0, L/S 12

Based on the summary provided by the Al leachability graph presented in Fig. 70, it is evident that **successful activation occurred across all types of HTFA** utilised due to the high-temperature modification reaction. Furthermore, the extraction conditions during processing were optimally set, with the Al leachability exceeding 90 % for all samples studied after a 6-hour reaction with sulphuric acid. While the leachability trends over time mimic those of the reference sample HTFA 1 (EPC – Počerady), the values recorded during the experiment fluctuated within a 5 % range above and below the corresponding value of HTFA 1. Nevertheless, it was observed that samples with a higher aluminium content, necessitating a greater amount of modifier, tended to exhibit excessively high viscosity levels, potentially affecting leachability. As previously discussed in Chapter 5.5.2, it might be advisable to consider employing L/S 14 or higher ratios for improved processing and potentially enhanced leachability. However, even under the combination of all the implemented experiment conditions, we can talk about very positive results.

The extraction by-product exhibited a predominantly white colour in most mixtures, with only the ashes containing higher Fe content (Angul, Tušimice, Opatovice) displaying a yellowish hue.

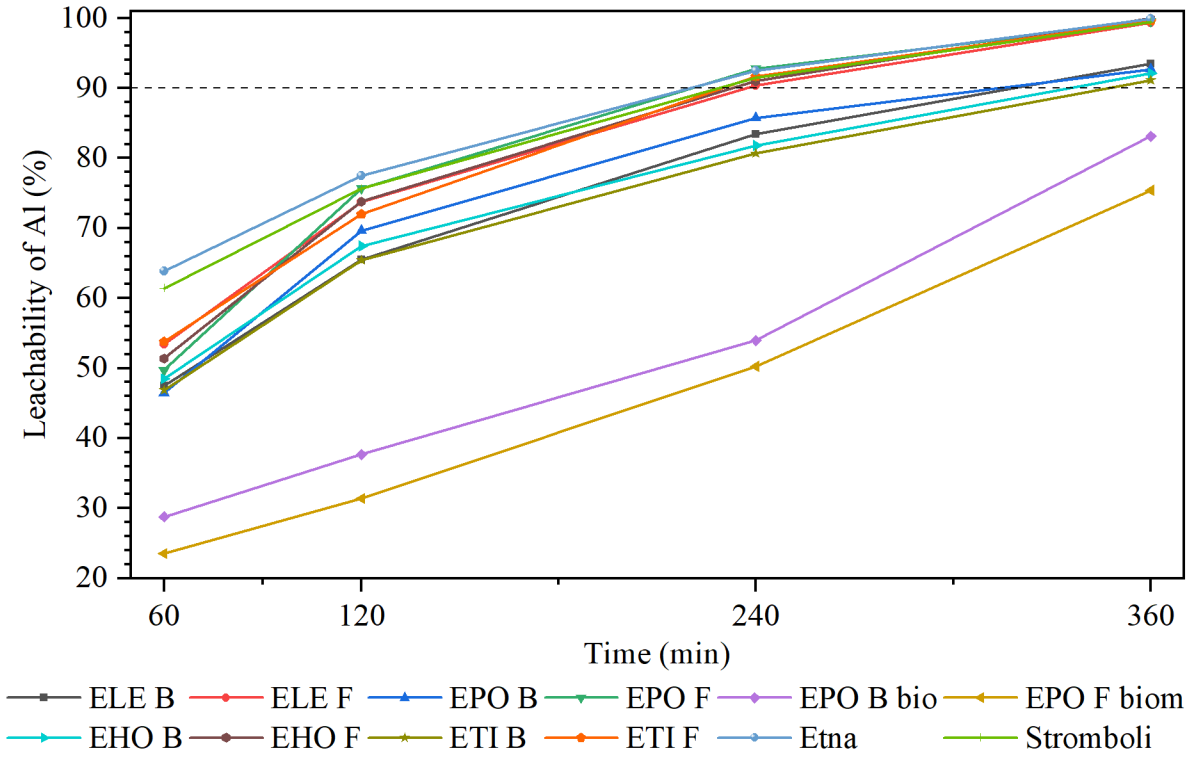

Fig. 71 Comparison of Al leachability on different types of "O"-modified FFA, FBA and volcanic FA in H_2SO_4 mol eq. 1,0, L/S 12

A similar pattern of aluminium leachability is also observed in the case of FFA and FBA, as illustrated in Fig. 71. Initially, there appears to be a slight discrepancy in the leachability of FFA and FBA, with FFA exhibiting an aluminium leachability exceeding 99 %, whereas FBA reaches up to 93 %. This variance may be attributed to differences in morphology, as FBA often forms distinct agglomerates due to higher concentrations of gypsum and unreacted free lime. Nevertheless, FFA and FBA derived from biomass-burning boilers lag significantly behind all other samples in terms of aluminium leachability. This discrepancy is likely due to the substantial alkali content present in the fly ash, leading to the premature formation of a melt with the generation of 2–3 mm lumps, which hinders adequate activation. Volcanic ash samples achieve a leachability of up to 99.5 % post-modification. Compared to other HTFA, FFA, and FBA samples, they also exhibit superior aluminium leachability in the initial hours of extraction.

The graph in Fig. 72 summarises the leachability of Al from the modified samples of "Q" type. The variations between the samples are negligible, with HTFA, FFA, FBA, and volcanic ash all achieving process efficiency above 97 % (97–99.9 %), except for FFA and FBA from biomass burning. The leachability of samples from biomass shows an increase, reaching a maximum of 80 %.

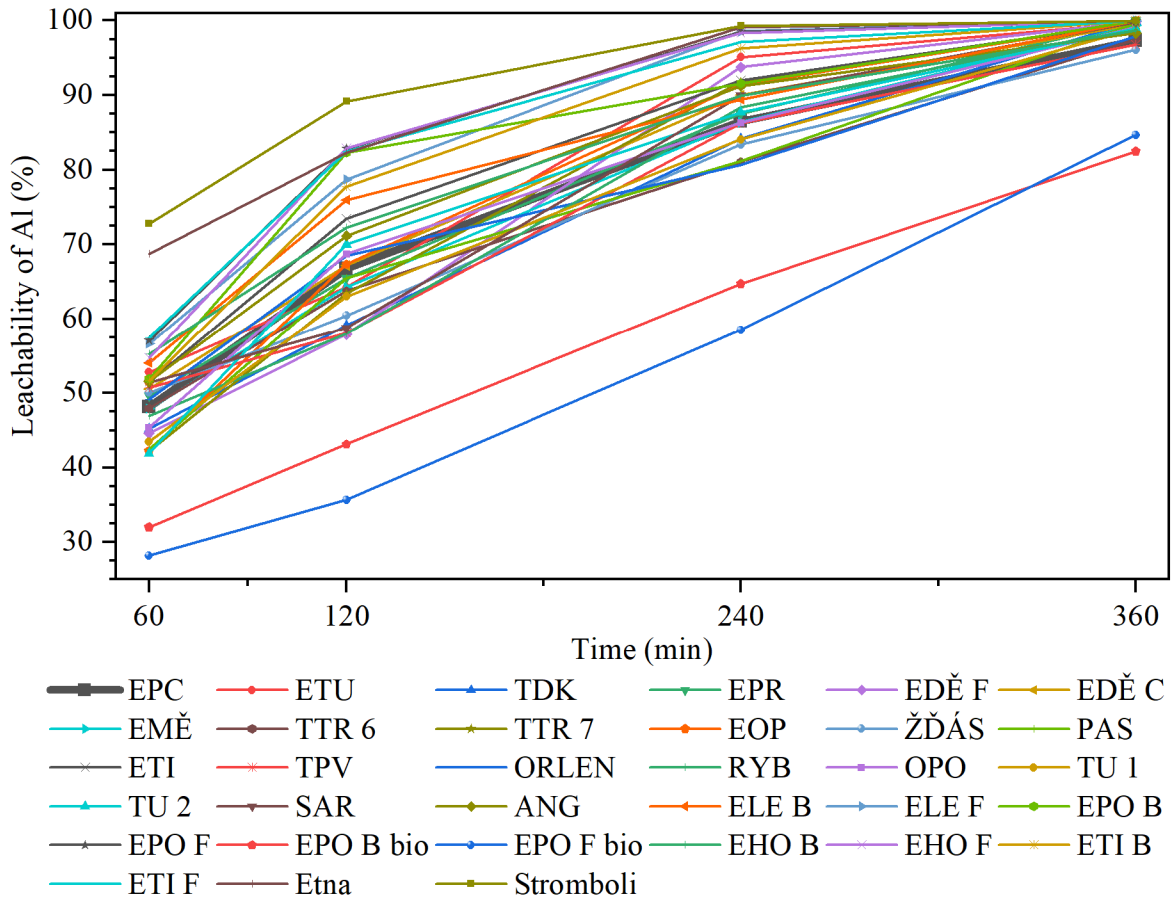

Fig. 72 Comparison of Al leachability on different types of "Q"-modified HTFA, FFA, FBA and volcanic FA in H_2SO_4 mol eq. 1,0, L/S 12

In order to evaluate the effectiveness of the second leaching step of the total process in maximising the leachability of titanium and iron from the "O"-modified FA, individual samples were taken from both FFA and FBA, as well as three samples from HTFA which had the highest titanium content in its initial state. The leachability of iron from these samples is visually represented in the graph located on the left side of Fig. 73. At the same time, the dissolution efficiency of titanium is illustrated in the graph on the right side.

Following the second leaching process, the by-products extracted from the monitored mixtures appeared entirely white post-filtration, showing no indication of the existence of Fe ions.

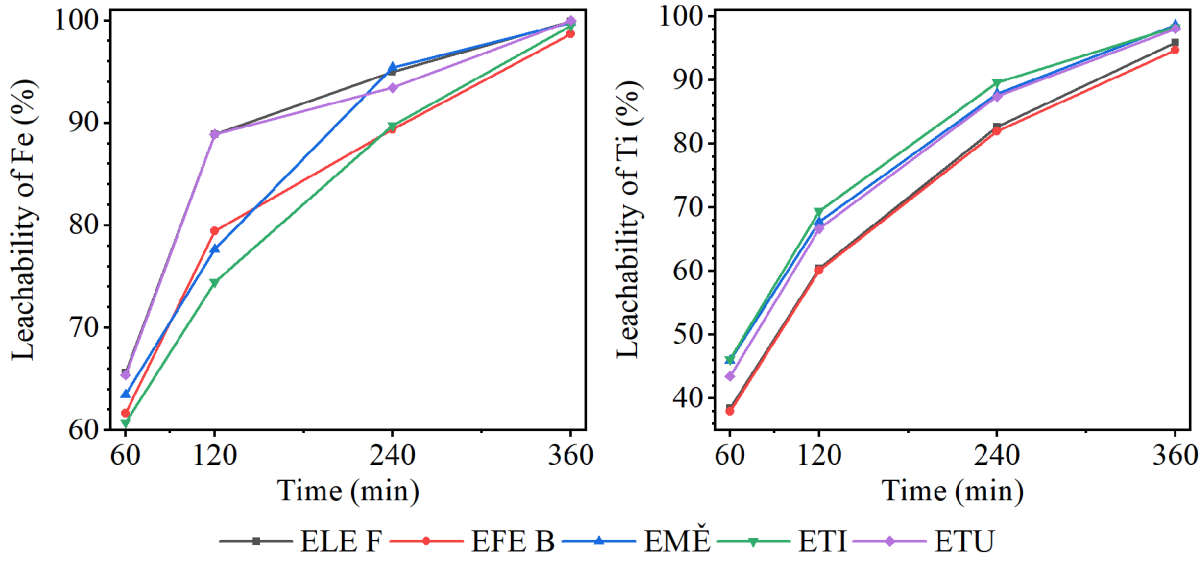

Fig. 73 Comparison of Fe and Ti leachability on different types of "Q"-modified HTFA, FFA and FBA; 2nd extraction in H_2SO_4 80 wt. %, L/S 3, 70 °C

Based on the data depicted in the above graphs, it is evident, although unsurprising, that when subjected to "O" type modification under conditions different from the optimised initially HTFA 1, both Fe and Ti have notably comparable leaching behaviours into a sulphuric acid solution. In fact, the cumulative leachability of these elements exceeds 95 %.

Upon comparing the leachability of Al, Ti, and Fe in various sample types, including FFA and FBA from biomass, it is evident that the activation technique involving a high-temperature modification reaction utilising a blend of chloride and calcium carbonate followed by an extraction process in a two-step approach within a sulphuric acid setting is suitable for different HTFA samples as well as FFA and FBA. This perspective confirms the versatility of the experimental procedure's application in this context.

5.7 Methods of selective separation of macro-concentrated elements from leachates

In the preceding sections, optimising the complete reaction sequence led to attaining the highest leachability of macro-concentrated elements. Subsequently, these elements could be differentially isolated from the mixture by manipulating the pH of the solution. Special attention was given to reducing the surplus of extracting agents in order to minimize the usage of precipitating agents and prevent the wastage of acids in the leaching process.

This section provides an overview of the fundamental characteristics of leachate and its stability and subsequently delves more deeply into the relationship between the solubility of Al, Fe, and Fe and the pH value in terms of pH solubility curves. Additional findings are then presented regarding the analysis of precipitated fractions and the potential for their further utilisation or treatment.

5.7.1 Stability and fundamental properties of leachate

The acidic leachate, which had been stored in a sealed plastic container, exhibited a notable shift in rheological properties and the development of a gel-like substance within 7–14 days. Following a meticulous process of mixing and centrifugation, a finely ground fraction was isolated, revealing a mass composition of 20.1 % Si, 0.3 % Al, 3.5 % Ca, 0.2 % K, and 2.6 % S as determined by XRF analysis, with the remaining 73.3 % attributed to light elements (Na, H, O, C, ...). This composition aligns with that of silicic acid. It is worth noting that this particular product, constituting only 0.41 % of the total leachate weight, was not subjected to further analysis using alternative methodologies.

Following the separation process, the leachate exhibits stability for at least 30 days, with only sporadic elimination of a minimum of aluminium sulphate flakes. The resulting flakes, which underwent centrifugation, were found to have a composition corresponding to aluminium sulphate (14.2 % Al, 25.4 % S, and the remaining portion attributed to LE) upon XRF analysis.

The pH level recorded using a pH meter falls within the range of –0.5–0.5 for this acidic leachate. Depending on the extraction conditions, it remains constant throughout the monitoring timeframe. The density of the initial leachate fluctuates between 1.12–1.19 but decreases to 1.10–1.15 after the separation of the silicic acid fraction, and then remains stable for the duration of the storage period under observation.

5.7.2 Effect of pH on the solubility of extract components

To sustain the selectively separate macro-concentrated elements that were converted into the solution during the extraction process, the initial step involved monitoring their solubility or concentration in the solution as the pH value gradually increased. Experimental determination of these curves for the macro-concentrated elements under study was crucial since there was a lack of available literature discussing their solubility variations with pH changes under conditions similar to those employed in the experiment. The solubility had to be examined in a

sulphuric acid solution containing all these elements together, with pH adjustments achieved by adding an ammonia solution. This study chose an ammonia solution to mimic industrial processes, whereas an aqueous NH_3 solution is preferred due to its simple regeneration capabilities. This decision aimed to mirror the practices seen in industrial setups, thereby enhancing the relevance and practical implications of the research findings.

The concentration curves for Al and Fe vary based on the excess pH resulting from introducing an aqueous ammonia solution. These curves are depicted in Fig. 74. A concentration of 1 at the start represents the initial concentration of the respective element in the acid leachate. The dependence of Ti solubility on the pH value in the first extract might not reflect reality due to its low concentration; Ti is then excluded from the second extract by diluting the solution, analogous to the production of TiO_2 by the sulphate method, along with the process discussed in publication [163].

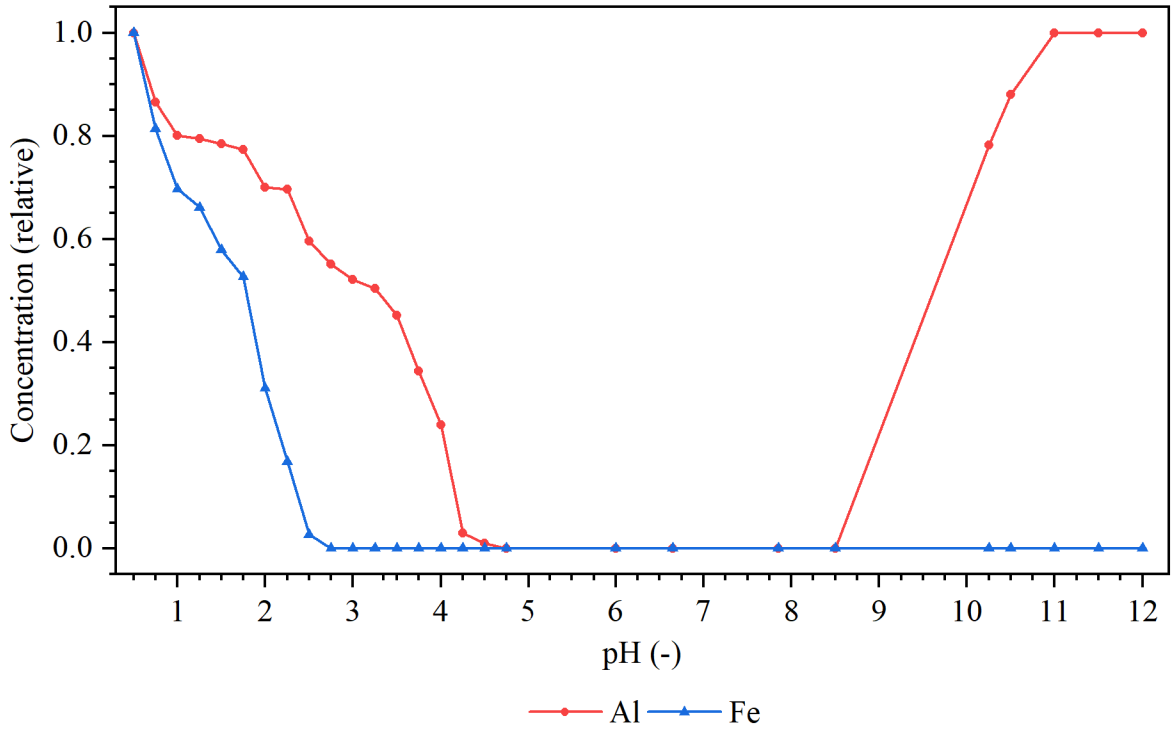

Fig. 74 Al and Fe precipitation curve using NH_3 from H_2SO_4 acidic leachate

Based on the experimental findings, it was established that complete precipitation of iron occurs from the solution until pH 2.75, with 30 % of the aluminium present being co-precipitated at this pH level. Therefore, it is imperative to separate these two components further. Aluminium is subsequently precipitated from the solution until pH 4.5. In contrast to iron, which remains precipitated within the subsequent pH range, aluminium experiences further dissolution above pH 9.5, leading to complete dissolution at pH 10.5 and beyond.

In relation to the experimental data, fractions that precipitated at a pH of 2.75 were prepared and analysed further; 2.75–4.5 and then 0.5–10. The resulting precipitates were separated from the mixture through centrifugation and, after being washed with water, they were dried at

105 °C. From the XRD analysis perspective, it was impossible to distinguish these precipitated fractions further, as only a small amount of crystalline fraction was found in their content. From the XRF perspective, the fraction between pH 0.5–3.0 contained 0.1 % Ti, 16.8 % Fe, 14.4 % S and the rest to LE), the mixture at pH interval 3.0–4.5 then 1.3 % Fe, 7.6 % Al, 23.6 % S and the rest LE; the composition of the mixture of pH interval 0.5–10 then corresponded to the composition of the first mixture, without the presence of Ti.

The concentration of the precipitating agent can meticulously regulate the dimensions of the resulting flakes utilised and the mixing speed. Excessive mixing intensity can result in prompt particle aggregation and the creation of a gelatinous clump, which can be exceedingly challenging to cleanse.

Fig. 75 enhances the description and morphology of the separated gel-like part of the acidic leachate. In the image from the elemental map (on the right), particles containing Si are visible, while the rest of the product corresponds to the residue of the excluded extraction by-product—calcium sulphate. The highly delicate morphology indicates the presence of a fine fraction resulting from coagulation or other physical aspects.

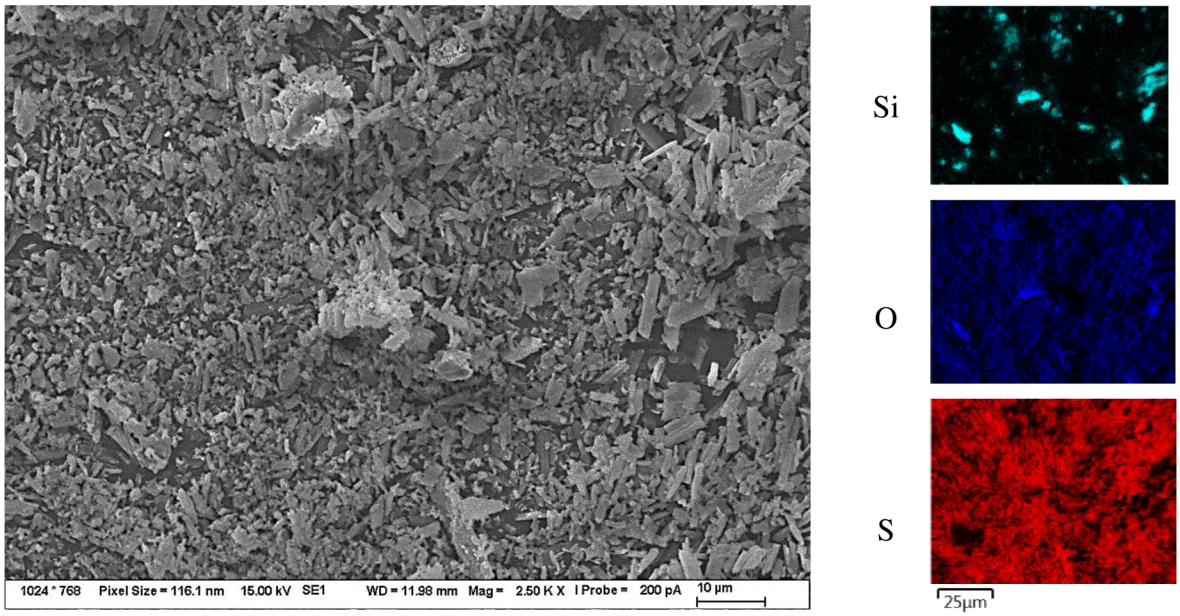

Fig. 75 SEM image of the morphology of the separated fraction from the leachate after 7 days, EDX map on the left

Fig. 76 depict SEM images of fractions separated at pH 3.0 on the left (a) side and pH 4.5 on the right (b). There is no apparent change in morphology, as the resulting fine flakes of the precipitated products were agglomerated during processing, such as centrifugation, washing, and drying. However, the EDX analysis revealed a composition consistent with the XRF measurement, with the first fraction containing both Fe and Al and the second fraction containing only Al. These fractions can also be visually distinguished, with the first fraction appearing yellow-orange due to the presence of Fe, while the second fraction is more whitish with a slight yellow tinge.

a b

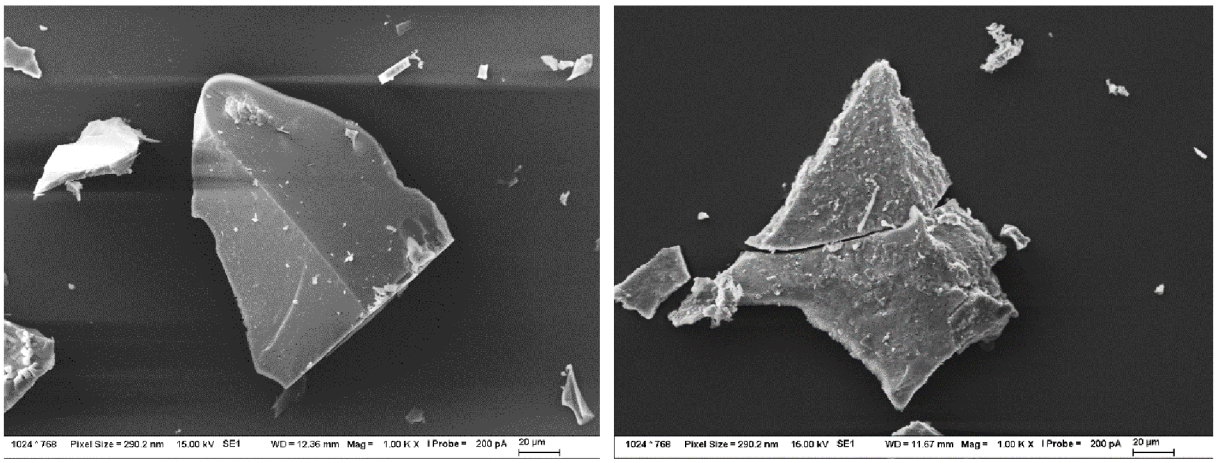

Fig. 76 SEM images of the fraction precipitated to pH 3.0 (a) and to 4.5 (b)

In order to capture the morphology of the newly forming small flakes of Fe and Al fractions, the precipitation of the droplet of the extract with several drops of the reagent directly on the sample holder was carried out. The morphology corresponds to a very fine clustering of platelets and is visually very similar for both fractions, as shown in the SEM images in Fig. 77.

a b

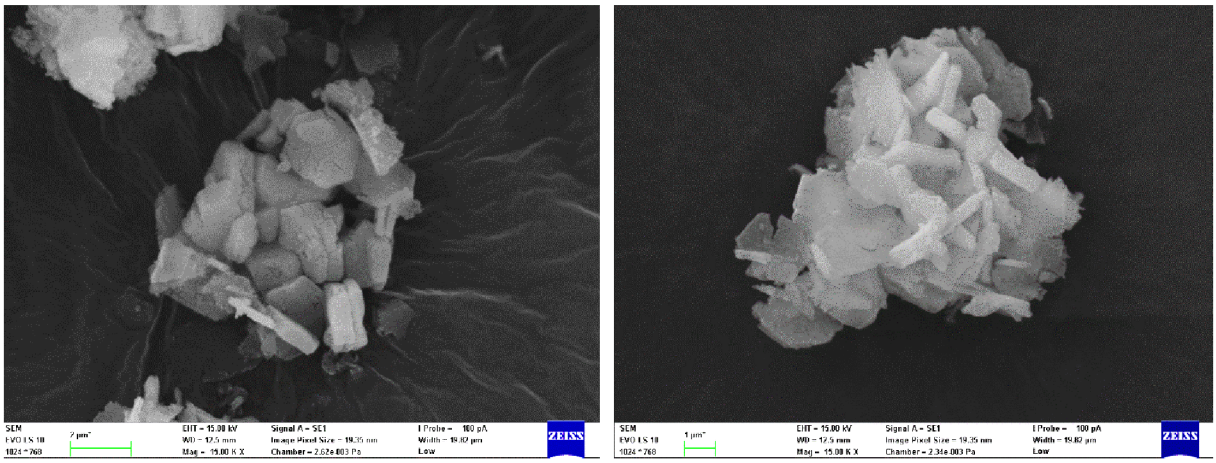

Fig. 77 SEM images of the flakes precipitated to pH 3.0 (a) and to 4.5 (b)

5.8 Extraction by-product

A comprehensive and meticulous analysis of the by-product extraction must be carried out to fully understand the process sequence. The interaction between Ca-based elements present in the sulphuric acid extraction solution triggers the creation of either gypsum, hemihydrate gypsum, or anhydrite. The resultant by-product manifests as a fine, white powdery substance, as confirmed by the particle size distribution chart in the appendix and the morphology observed in the SEM images in Fig. 78.

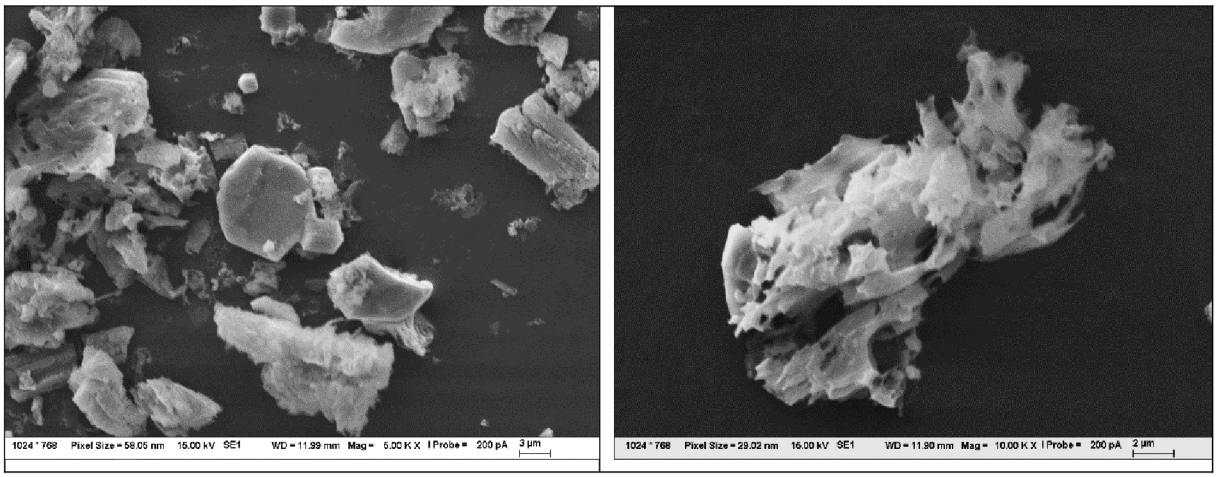

Fig. 78 SEM image of by-product morphology

The proportion of hemihydrate and anhydrite in this material varies based on the washing and drying methods employed, similar to regular gypsum. Through X-ray diffraction analysis, the product was determined to be a combination of hemihydrate and anhydrite. Following the initial extraction, the by-product may show remnants of undissolved An, Wa, or Ge based on the process parameters. In the by-product obtained from the most optimal extraction method, the Ti component is concentrated, specifically the rutile present. Upon completion of the second extraction, the sample only exhibits hemihydrate and anhydrite as identifiable crystalline phases.

This product can thus be subjected to conventional methods of processing gypsum plasters into gypsum products and applied, for example, in the production of plasterboard boards or as an additive to regulate the initial setting of cement.

6 CONCLUSION

The primary objective of this doctoral thesis was to address the convergence of two growing challenges in contemporary times: the management of secondary by-products generated from coal combustion in thermal power plants or heating plants, known as coal combustion products CCP, and the need to address the scarcity of new, appropriate raw material sources while ensuring self-sufficiency and independence in commodities. Despite the increasing efforts to utilise CCP, the focus has predominantly been on incorporating different fly ash forms into various technologies. However, a limited number of research publications globally explore the true potential of these secondary products as a viable source of raw materials.

The author's final theses [113, 164] have already primarily indicated that the critical factor for the possible application of CCPs and especially HTFA and also FFA or FBA as a potential source of raw materials is the methods of classic hydrometallurgical processes. However, in order to achieve a high level of efficiency of such a process, it is necessary to pre-adjust – modify or activate the FA.

The activation methods of FA before the extraction process were the lengthiest, most challenging, and most intricate aspect of the entire study, in both time and experimentation. After reviewing a limited number of scientific papers, a series of modification reactions involving calcium compounds were utilised to potentially produce calcium-aluminate or calcium-silicate phases, which could be readily dissolved in the subsequent acid hydrometallurgical process under sulphuric acid conditions.

It has been demonstrated that the activation of HTFA 1 can occur through a high-temperature modification reaction with limestone. Through optimisation techniques, maximum Al leachability of over 48 % was achieved, representing a more than 20-fold increase compared to the leachability of raw HTFA 1. Adding 0.45 mol eq. was identified as the optimised modification procedure, with a reaction temperature of 1,000 °C and a duration of 60 minutes at the same temperature. Further composition analysis revealed that the high-temperature modification reaction not only yields products according to the theoretical sequence of reactions, such as larnite or tricalcium-aluminate, but also gehlenite and wollastonite phases, and a limited extent, anorthite. Additionally, the samples modified in this manner demonstrated the ability to self-disintegrate, which provides a significant benefit throughout the process. Samples showing this phenomenon do not need to be ground during processing.

The experimental setup and procedure were replicated using calcium chloride as the modifying agent. Through the optimisation of the modification process, a leachability of Al from HTFA 1 exceeding 90 % was subsequently achieved, representing a more significant advancement than that observed with limestone activation. Adding 0.35 mol eq. was the optimal condition for the modification process, along with a reaction temperature of 1,000 °C and a duration of 60 minutes. Despite the absence of products according to the theoretical reaction mechanism, the modified samples contained chloro-calcite phases, with limited amounts of

larnite, gehlenite, and wollastonite, but a high representation of anorthite and wadalite. The modified samples did not exhibit the characteristic of auto-disintegration.

This study introduces a novel approach not found in the author's literature, which involves the combination of modifying agents to achieve a 90 % leachability of aluminium while preserving its auto-disintegrating properties. This was accomplished by utilising a **limestone and chloride ratio of 0.7/0.3 or 0.6/0.4** while maintaining a mol eq. $CaCO_3$ of 0.45 and mol eq. $CaCl_2$ of 0.35. As part of the optimisation process, the high-temperature reaction mode involved heating at a rate of 10 °C/min to 800 °C, followed by heating at 5°C/min to 1,000 °C, a duration of 60 min, and controlled cooling at 5 °C/min to 600 °C, followed by rapid uncontrolled cooling to room temperature. This optimisation resulted in an increase in the **leachability of aluminium up to 95 %**.

Finally, a considerable part of the experimental work focused on enhancing the hydrometallurgical process, specifically the extraction process. Numerous trials demonstrated that the highest rate of aluminium dissolution into the solution was achieved in a **sulphuric acid environment, with an optimised L/S ratio of 12 or 14 with mol eq. of H_2SO_4.1.0 or1.2.** This ratio allowed for the release of all reactive components in the solution, corresponding to 1.0 to 1.2, which equates to 0.7–0.8 M acid in the given HTFA 1 composition, resulting in the leaching of over 97 % of aluminium. Moreover, increasing the reaction temperature to 55 °C and above significantly accelerated the reaction process, with 90 % of aluminium leached out after just 4 hours of extraction (or 2 hours at 95 °C). Conversely, adding hydrogen peroxide or hydrochloric acid to the extraction mixture alongside sulphuric acid did not yield substantial changes in leachability over time.

Consequently, a nearly indistinguishable degree of Al solubility was attained during the initial extraction phase in the upscale experiment, employing 30 L of extraction agent. After the first extraction, the residual quantities of iron, titanium, and aluminium were fully transferred to the solution in the second leaching process, facilitated by 80 wt. % sulphuric acid with L/S 3 and a reaction temperature of 70 °C.

The primary and most significant outcome of the study involves implementing the modification reaction and extraction under optimised conditions on an additional 20 samples of HTFA and 10 samples of FFA/FBA. This achieved Al leachability levels ranging from 90 % to 99 % by modifying $CaCO_3$/$CaCl_2$ in ratios of 0.7/0.3 or 0.6/0.4 based on mol eq. $CaCO_3$ 0.45 and mol eq. $CaCl_2$ 0.35. The extraction process was conducted in a sulphuric acid medium with mol eq. 1.0 and L/S 12 for 6 h.

Another discovery from the study involves identifying the solubility curve of Al and Fe based on the pH of the solution in actual samples. This information can be used to separate leached elements. Additionally, there is potential for using extraction by-products containing varying ratios of hemihydrate and anhydrite of calcium sulphate, depending on the drying circumstances. This by-product could be incorporated into gypsum products or as an additive to control the initial setting of cement.

7 Lists

7.1 References

1 FEČKO, Peter. Fly ash. Ostrava: VŠB-Technical University of Ostrava, 2005. ISBN 978-802-4808-369.

2 OREM, W.H. a FINKELMAN, R.B. Coal Formation and Geochemistry. Online. *Treatise on Geochemistry*. 2003, s. 191-222. ISBN 9780080437514. Available at: https://doi.org/10.1016/B0-08-043751-6/07097-3.

3 VAN KREVELEN, D. W. Coal: Third Edition: Typology – Physics – Chemistry – Constitution (Coal Science & Technology. 3rd. Elsevier Science, 2013. ISBN 978-0444895868.

4 ROUBÍČEK, Václav. Uhlí: zdroje, procesy, užití. Ostrava: Montanex, 2002, 173 s. Odborné publikace. ISBN 80-722-5063-9.

5 ATTAR, A. Sulphur Groups in Coal and Their Determinations. Analytical Methods for Coal and Coal Products [online]. Elsevier, 1979, 1979, 585-624. DOI: 10.1016/B978-0-12-399903-0.50025-8. ISBN 9780123999030. Available at: https://linkinghub.elsevier.com/retrieve/pii/B9780123999030500258.

6 Minerals in coal. Organic Matter and Mineralisation: Thermal Alteration, Hydrocarbon Generation and Role in Metallogenesi. Dordrecht: Springer, 2000, s. 315–332. ISBN 978-94-015-9474-5.

7 KOPPERJAN, Jaap a VAN LOO, Sjaak. Biomass Fuel Properties and Basic Principles of Biomass Combustion. In: *Handbook of Biomass Combustion and Co-firing*. London: Earthscan, 2010, s. 7-50. ISBN 9781849711043.

8 OBERNBERGER, I; BRUNNER, T a BARNTHALER, G. Chemical properties of solid biofuels—significance and impact. Online. *Biomass and Bioenergy*. 2006, vol. 30, vol. 11, s. 973-982. ISSN 09619534. Available at: https://doi.org/10.1016/j.biombioe.2006.06.011.

9 TORTOSA MASIÁ, A.A.; BUHRE, B.J.P.; GUPTA, R.P. a WALL, T.F. Characterising ash of biomass and waste. Online. *Fuel Processing Technology*. 2007, vol. 88, vol. 11-12, s. 1071-1081. ISSN 03783820. Available at: https://doi.org/10.1016/j.fuproc.2007.06.011.

10 HAVLÍČKOVÁ, Kamila. *Zhodnocení ekonomických aspektů pěstování a využití energetických rostlin: vědecká monografie*. Průhonice [Praha]: Výzkumný ústav Silva Taroucy pro krajinu a okrasné zahradnictví, https://www.mobile.de/cz/Osobn%C3%AD-v%C5%AFz/Mercedes-Benz-E-220-d-7-Sitze,-AMG,-LED,-GLSD/vhc:car,srt:price,sro:asc,ms1:17200_48_amg,frn:2018,prx:35000,ful:diesel,mln:30000,mlx:125000,exc:beige!silver!blue,dmg:false,vcg:estatecar/pg:vipcar/352536101.html2007. ISBN 978-80-7040-948-0.

11 RITCHIE, Hannah a ROSADO, Pablo. Fossil Fuels. Online. *{Our World in Data*. Vol. 2017. Available at: https://ourworldindata.org/fossil-fuels.

12 *Infographic - How is EU electricity produced and sold?* Online. Eurpean Council; Council of the European Union. 2022. Available at: https://www.consilium.europa.eu/en/infographics/how-is-eu-electricity-produced-and-sold/.

13 BALÁŠ, Marek, Martin LIŠÝ and Jiří MOSKALÍK. Kotle – 2. část. TZB-info [online]. 2012. Available at: http://vytapeni.tzb-info.cz/kotle-kamna-krby/8438-kotle-2-cast.

14 YIN, Chungen, Lasse A. ROSENDAHL and Søren K. KÆR. Grate-firing of biomass for heat and power production. Progress in Energy and Combustion Science [online]. 2008, 34(6), 725-754. DOI: 10.1016/j.pecs.2008.05.002. ISSN 03601285. Available at: https://linkinghub.elsevier.com/retrieve/pii/S0360128508000245.

15 WILLIAMS, A.; POURKASHANIAN, M. a JONES, J.M. Combustion of pulverised coal and biomass. Online. *Progress in Energy and Combustion Science*. 2001, vol. 27, vol. 6, s. 587-610. ISSN 03601285. Available at: https://doi.org/10.1016/S0360-1285(01)00004-1.

16 HURSKAINEN, Markus and Pasi VAINIKKA. Technology options for large-scale solid-fuel combustion. Fuel Flexible Energy Generation [online]. Elsevier, 2016, 2016, 177-199. DOI: 10.1016/B978-

1-78242-378-2.00007-9. ISBN 9781782423782. Available at: https://linkinghub.elsevier.com/retrieve/pii/B9781782423782000079.

17 BUHRE, B.J.P., L.K. ELLIOTT, C.D. SHENG, R.P. GUPTA and T.F. WALL. Oxy-fuel combustion technology for coal-fired power generation. Progress in Energy and Combustion Science [online]. 2005, 31(4), 283-307. DOI: 10.1016/j.pecs.2005.07.001. ISSN 03601285. Available at: https://linkinghub.elsevier.com/retrieve/pii/S0360128505000225.

18 KHODAEI, Hassan, Yasir M. AL-ABDELI, Ferdinando GUZZOMI and Guan H. YEOH. An overview of processes and considerations in the modelling of fixed-bed biomass combustion. Energy [online]. 2015, 88, 946-972. DOI: 10.1016/j.energy.2015.05.099. ISSN 03605442. Available at: https://linkinghub.elsevier.com/retrieve/pii/S036054421500701X.

19 Fluidní spalování. In: ČEZ [online]. 1999. Available at: https://www.cez.cz/edee/content/file/static/encyklopedie/vykladovy-slovnik-energetiky/hesla/fluid_spal.html.

20 OKA, S. and E. J. ANTHONY. Fluidised-bed combustion. New York: M. Dekker, c 2004. Mechanical engineering (Marcel Dekker, Inc.), 162. ISBN 08-247-4699-6.

21 SARKAR, Dipak K. Fluidised-Bed Combustion Boilers. Thermal Power Plant [online]. Elsevier, 2015, 2015, 159-187. DOI: 10.1016/B978-0-12-801575-9.00005-6. ISBN 9780128015759. Available at: https://linkinghub.elsevier.com/retrieve/pii/B9780128015759000056.

22 Ramachandran, R., P. SIVAKUMAR, N. PRASANNA and A. M. VASAN. Development of an optimum CFBC Cyclone separator with REPDS for low pressure drop and denudation rates using CFD. International Journal of Applied Engineering Research [online]. 2015, 10 (13), 580-588. Available at: https://www.researchgate.net/publication/283756834_Development_of_an_optimum_CFBC_cyclone_separator_with_REPDS_for_low_pressure_drop_and_denudation_rates_using_CFD.

23 NOSKIEVIČ, Pavel. Spalování uhlí. 2. vyd. Ostrava: VŠB-Technická univerzita, 2002. ISBN 80-248-0204-X.

24 OSAKA, Yugo, Takuya TSUJIGUCHI, Akio KODAMA and Hongyu HUANG. Improvement of dry desulphurisation performance using activated calcium carbonate by amorphous citric acid complex method for diesel gas purification. Journal of Material Cycles and Waste Management [online]. 2020, 22(2), 470-478. DOI: 10.1007/s10163-019-00942-1. ISSN 1438-4957. Available at: http://link.springer.com/10.1007/s10163-019-00942-1.

25 NOLAN, Paul S. Flue Gas Desulphurisation Technologies for Coal-Fired Power Plants. In: Coal-Tech 2000 International Conference [online]. Jakarta, 2000, s. 148–160. Available at: http://plainsjustice.org/files/ElkRun/Elk_Run_References/Flue%20Gas%20Desulphurisation%20Technologies%20for%20Coal-fired%20Power%20Plants.pdf.

26 IBLER, Zdeněk. Technický průvodce energetika. Praha: BEN – technická literatura, 2002. ISBN 80-730-0026-1.

27 Mokrá vápencová vypírka spalin. In: ČEZ [online]. Praha. Available at: https://www.cez.cz/edee/content/file/static/encyklopedie/encyklopedie-energetiky/02/vypirka_5.html.

28 Odsiřování spalin v elektrárnách skupiny ČEZ. Praha, 2006. Available at: https://www.cez.cz/edee/content/file/investori/odsirovani.pdf.

29 Wet Limestone Scrubbing Process Description. In: Powermag [online]. Available at: https://www.powermag.com/advanced-process-control-for-optimizing-flue-gas-desulphurisation.

30 GRYCMANOVÁ, Markéta and Rostislav ZBIEG. 2010. Metody dosažení emisních limitů emisí NOx kotlů velkých výkonů. In: *Energetika a biomasa 2010, sborník přednášek z konference*. Praha: ČVUT Praha. ISBN 978-80-01-04523-7.

31 ZHENG, Jingfan, Jing WANG, Fengling YANG, Zhiping DU and Fangqin CHENG. 2023. Adsorption and catalytic oxidation of residual NH3 on coal ash after selective non-catalytic reduction in coal-fired boilers. *Chemosphere* [online]. **317**. DOI: 10.1016/j.chemosphere.2023.137765. ISSN 00456535. Available at: https://linkinghub.elsevier.com/retrieve/pii/S0045653523000310.

32 HELA, Rudolf and Martin ŤAŽKÝ. 2018. Effect of SNCR on the Properties of Fly Ash in Terms of its Applicability to Concrete. *Solid State Phenomena* [online]. **272**, 107-114. DOI: 10.4028/www.scientific.net/SSP.272.107. ISSN 1662-9779. Available at: https://www.scientific.net/SSP.272.107.

33 SOKOL, Pavel. Vedlejší energetické produkty a jejich využití. Praha, 2012. Available at: http://www.top-expo.cz/domain/top-expo/files/spsb-2012/prednasky/sokol_pavel.pdf.

34 JAMES, Jijo and Kasinatha PANDIAN. Soil Stabilization as an Avenue for Reuse of Solid Wastes: A Review. Civil Engineering & Architecture [online]. 2015, 1(58), 50-76. Available at: file:///D:/Michal/moje%20plocha/%C5%A1kola/konference%20a%20%C4%8Dl%C3%A1nky/Agloporit/literatura/Soil_Stabilization_as_an_Avenue_for_Reus.pdf.

35 STYSZKO-GROCHOWIAK, Katarzyna, Janusz GOŁAŚ, Henryk JANKOWSKI and Stanisław KOZIŃSKI. 2004. Characterization of the coal fly ash for the purpose of improvement of industrial on-line measurement of unburned carbon content. Fuel [online]. 83(13), 1847-1853. DOI: 10.1016/j.fuel.2004.03.005. ISSN 00162361. Available at: https://linkinghub.elsevier.com/retrieve/pii/S0016236104000845.

36 Chapter 2: Fly Ash. RAMEZANIANPOUR, A. A. Cement replacement materials. New York: Springer, 2014, s. 47–156. ISBN 978-3-642-36720-5.

37 PAGE, A. L., Ahmed A. ELSEEWI and I. R. STRAUGHAN. Physical and chemical properties of fly ash from coal-fired power plants with reference to environmental impacts. Residue Reviews [online]. New York, NY: Springer New York, 1979, 1979, 83–120. DOI: 10.1007/978-1-4612-6185-8_2. ISBN 978-1-4612-6187-2. Available at: http://link.springer.com/10.1007/978-1-4612-6185-8_2.

38 BHATT, Arpita, Sharon PRIYADARSHINI, Aiswarya ACHARATH MOHANAKRISHNAN, Arash ABRI, Melanie SATTLER and Sorakrich TECHAPAPHAWIT. Physical, chemical, and geotechnical properties of coal fly ash: A global review. Case Studies in Construction Materials [online]. 2019, 11. DOI: 10.1016/j.cscm. 2019.e00263. ISSN 22145095. Available at: https://linkinghub.elsevier.com/retrieve/pii/S2214509518303735.

39 IVANOV, A I, A Yu STOLBOUSHKIN, M V TEMLYANSTEV, V A SYROMYASOV and O A FOMINA. Structure formation of aerated concrete containing waste coal combustion products generated in the thermal vortex power units. IOP Conference Series: Earth and Environmental Science [online]. 2016, 45. DOI: 10.1088/1755-1315/45/1/012019. ISSN 1755-1307. Available at: https://iopscience.iop.org/article/10.1088/1755-1315/45/1/012019.

40 COPELAND, Kevin. Fly Ash Properties and Uses. In: Construction [online]. 2011. Available at: https://www.monolithic.org/blogs/construction/fly-ash-properties-and-uses.

41 MALHOTRA, V a P MEHTA. High-performance, high-volume fly ash concrete: materials, mixture proportioning, properties, construction practice, and case histories. 2nd ed. Ottawa: Supplementary Cementing Materials for Sustainable Development, 2005, xi, 120 s. ISBN 09-731-5072-6.

42 BAYKAL, Gökhan and A. Gürhan DÖVEN. Utilization of fly ash by pelletization process: Theory, application areas and research results. Resources, Conservation & Recycling [online]. 2000, (30), 59-77. Available at: https://www.academia.edu/26395598/Utilization_of_fly_ash_by_pelletization_process_theory_application_areas_and_research_results.

43 Výzkum a vývoj ekologického pojiva na bázi geopolymerních struktur se schopností imobilizace potenciálně nebezpečných látek z velkoobjemově produkovaných průmyslových odpadů a jeho následné aplikace ve stavebnictví: VSTUPNÍ ANALÝZY SUROVIN. Brno, 2008.

44 RISDANARENI, Puput, Poppy PUSPITASARI, Ekaputri JANUARTI JAYA, M.A.B. ABDULLAH, S.Z. ABD RAHIM, M.E. MUHAMMAD SUANDI, M.N. MAT SAAD and M.F. GHAZALI. Chemical and Physical Characterization of Fly Ash as Geopolymer Material. MATEC Web of Conferences [online]. 2017, 97. DOI: 10.1051/matecconf/20179701031. ISSN 2261-236X. Available at: http://www.matec-conferences.org/10.1051/matecconf/20179701031.

45 UPADHYAY, Ankur and MANISH KAMAL. Characterisation and Utilization of Fly Ash [online]. ROURKELA, 2007. NATIONAL INSTITUTE OF TECHNOLOGY.

46 AHMARUZZAMAN, M. A review on the utilization of fly ash. Progress in Energy and Combustion Science [online]. 2010, 3(36), 327–363. DOI: 10.1016/J.PECS.2009.11.003. Available at: http://linkinghub.elsevier.com/retrieve/pii/S0360128509000604.

47 SCHEETZ, Barry E and Russell EARLE. Utilization of fly ash. Current Opinion in Solid State and Materials Science [online]. 1998, 5(3), 510–520.DOI: 10.1016/S1359-0286(98)80017-X. ISSN 1359-0286. Available at: http://linkinghub.elsevier.com/retrieve/pii/S135902869880017X.

48 ALTERARY, Seham S. and MAREI, Narguess H., 2021. Fly ash properties, characterization, and applications: A review. Online. *Journal of King Saud University - Science*. Vol. 33, vol. 6, s. 1-19. Available at: https://doi.org/10.1016/j.jksus.2021.101536.

49 MARKO, Michal. Elektrárenský popílek jako surovinová základna pro budoucnost. In: Druhotná surovina. 2018, s. 1-16.

50 PELLANT, Chris. Horniny a minerály. 1. vyd. Martin: Osveta, 1992, 256 s. ISBN 80-217-0563-9.

51 ÖZÇELIK, V. Ongun and Claire E. WHITE. 2016. Nanoscale Charge-Balancing Mechanism in Alkali-Substituted Calcium–Silicate–Hydrate Gels. *The Journal of Physical Chemistry Letters* [online]. **7**(24), 5266-5272. DOI: 10.1021/acs.jpclett.6b02233. ISSN 1948-7185. Available at: https://pubs.acs.org/doi/10.1021/acs.jpclett.6b02233.

52 FAROOQUE, KN, Z YEASMIN, S ALAM, AMS ALAM and M ZAMAN. Pozzolanic Activity of Fly Ash. Bangladesh Journal of Scientific and Industrial Research [online]. 2011, 45(4), 303-308. DOI: 10.3329/bjsir.v45i4.7326. ISSN 2224-7157. Available at: https://www.banglajol.info/index.php/BJSIR/article/view/7326.

53 GOLEWSKI, Grzegorz Ludwik, 2022. The Role of Pozzolanic Activity of Siliceous Fly Ash in the Formation of the Structure of Sustainable Cementitious Composites. Online. *Sustainable Chemistry*. Vol. 3, vol. 4, s. 520-534. Available at: https://doi.org/10.3390/suschem3040032.

54 HEIKAL, M., H. EL-DIDAMONY, I. M. HELMY and F ABD EF-RAOOF. Pozzolanic activity of fly ash. Silicates Industriels [online]. 2003, 68(9-10), 117-117. Available at: https://www.researchgate.net/publication/296805510_Pozzolanic_activity_of_fly_ash.

55 VILLAR-COCIÑA, Ernesto, Loic RODIER, Holmer SAVASTANO, Manuel LEFRÁN and Moisés Frías ROJAS. A Comparative Study on the Pozzolanic Activity Between Bamboo Leaves Ash and Silica Fume: Kinetic Parameters. Waste and Biomass Valorization [online]. 2020, 11(4), 1627-1634. DOI: 10.1007/s12649-018-00556-y. ISSN 1877-2641. Available at: http://link.springer.com/10.1007/s12649-018-00556-y.

56 BIBORA, Petr. Energosádrovec, anhydrit a možnosti jejich využití. Odpadové fórum [online]. 2010, (4), 27–28. Available at: http://www.odpadoveforum.cz/upload/pageFiles/4-2010-pdf.pdf.

57 KORALEGEDARA, Nadeesha H., Patricio X. PINTO, Dionysios D. DIONYSIOU and Souhail R. AL-ABED. Recent advances in flue gas desulphurisation gypsum processes and applications – A review. Journal of Environmental Management [online]. 2019, 251. DOI: 10.1016/j.jenvman.2019.109572. ISSN 03014797. Available at: https://linkinghub.elsevier.com/retrieve/pii/S0301479719312903.

58 Energy-gypsum. Silotransport [online]. 2020. Available at: https://www.silotransport.cz/energy-gypsum.

59 VEJVODA, Josef, Pavel MACHAČ and Petr BURYAN. Technologie ochrany ovzduší a čištění odpadních plynů. Praha: Vysoká škola chemicko-technologická v Praze, 2003. ISBN 80-708-0517-X.

60 AMERICAN COAL ASH ASSOCIATION, 2022. *Coal Combustion Products Production & Use Reports*. Online. American Coal Ash Association. Available at: https://acaa-usa.org/wp-content/uploads/2023/12/2022-Production-and-Use-Charts.pdf.

61 *Ecoba - fly ash utilisation*, 2022. Online. EUROPEAN COAL COMBUSTION PRODUCTS ASSOCIATION. Ecoba. Available at: https://www.ecoba.com/ecobaccputil.html.

62 LUO, Yang; WU, Yinghong; MA, Shuhua; ZHENG, Shili; ZHANG, Yi et al., 2021. Utilization of coal fly ash in China: a mini-review on challenges and future directions. Online. *Environmental Science and Pollution Research*. Vol. 28, vol. 15, s. 18727-18740. Available at: https://doi.org/10.1007/s11356-020-08864-4.

63 ESKOM, 2020. *Ash manegement in Eskom*. Online. Eskom. Available at: https://www.eskom.co.za/Pages/Landing.aspx.

64 D. LUTZE. [EDS.]. Handbook on fly ash in concrete: principles of production and use. 2. ed. Düsseldorf: Bau Technik, 2010. ISBN 978-376-4005-276.

65 EN 197-1 Cement – Part 1: Composition, specifications and conformity criteria for common cements. European Committee for Standardization, 2012.

66 MADHAVI, T. Ch.; SWAMY RAJU, L. a MATHUR, D. Durabilty and Strength Properties of High Volume Fly Ash Concrete. Online. *Journal of Civil Engineering Research*. 2014, vol. 4, vol. 2A, s. 7-11. ISSN 2163-2340. Available at: https://doi.org/10.5923/c.jce.201401.02.

67 PIMRAKSA, K., S. HANJITSUWAN and P. CHINDAPRASIRT. Synthesis of belite cement from lignite fly ash. Ceramics International [online]. 2009, 35(6), 2415-2425. DOI: 10.1016/j.ceramint.2009.02.006. ISSN 02728842. Available at: https://linkinghub.elsevier.com/retrieve/pii/S0272884209000625.

68 SAHU, Sadananda and Ján MAJLING. Preparation of sulfoaluminate belite cement from fly ash. Cement and Concrete Research [online]. 1994, 24(6), 1065-1072. DOI: 10.1016/0008-8846(94)90030-2. ISSN 00088846. Available at: https://linkinghub.elsevier.com/retrieve/pii/0008884694900302.

69 WANG, Wenlong, Wenlong WANG, Zhongyang LUO, Zhenglun SHI and Kefa CEN. Experimental study on cement clinker co-generation in pulverised coal combustion boilers of power plants [online]. 2016, 24(3), 207-214. DOI: 10.1177/0734242X06063892. ISSN 0734-242X. Available at: http://journals.sagepub.com/doi/10.1177/0734242X06063892.

70 GUERRERO, A., S. GOÑI and V.R. ALLEGRO. Durability of class C fly ash belite cement in simulated sodium chloride radioactive liquid waste: Influence of temperature. Journal of Hazardous Materials [online]. 2009, 162(2-3), 1099-1102 . DOI: 10.1016/j.jhazmat.2008.05.151. ISSN 03043894. Available at: https://linkinghub.elsevier.com/retrieve/pii/S0304389408008558.

71 GUERRERO, A., S. GOÑI, I. CAMPILLO and A. MORAGUES. Belite Cement Clinker from Coal Fly Ash of High Ca Content. Optimization of Synthesis Parameters [online]. 2004, 38(11), 3209-3213. DOI: 10.1021/es0351589. ISSN 0013-936X. Available at: https://pubs.acs.org/doi/10.1021/es0351589.

72 PALOMO, A., M.W. GRUTZECK and M.T. BLANCO. Alkali-activated fly ashes. Cement and Concrete Research [online]. 1999, 29(8), 1323-1329. DOI: 10.1016/S0008-8846(98)00243-9. ISSN 00088846. Available at: https://linkinghub.elsevier.com/retrieve/pii/S0008884698002439.

73 PACHECO-TORGAL, Fernando, João CASTRO-GOMES and Said JALALI. Alkali-activated binders: A review: Part 1. Historical background, terminology, reaction mechanisms and hydration products. Construction and Building Materials [online]. 2008, 7(22), 1305–1314. DOI: 10.1016/j.conbuildmat.2007.10.015. Available at: http://linkinghub.elsevier.com/retrieve/pii/S0950061807002462.

74 PACHECO-TORGAL, Fernando, João CASTRO-GOMES and Said JALALI. Alkali-activated binders: A review. Part 2. About materials and binders manufacture. Construction and Building Materials [online]. 2008, 7(22), 1315–1322. DOI: 10.1016/j.conbuildmat.2007.03.019. Available at: http://linkinghub.elsevier.com/retrieve/pii/S0950061807000918.

75 SHI, Caijun, A. Fernández JIMÉNEZ and Angel PALOMO. New cements for the 21st century: The pursuit of an alternative to Portland cement. Cement and Concrete Research [online]. 2011, 41(7), 750-763. DOI: 10.1016/j.cemconres.2011.03.016. ISSN 00088846. Available at: https://linkinghub.elsevier.com/retrieve/pii/S0008884611000925.

76 SARKAR, A., R. RANO, K. K. MISHRA and A. MAZUMDER. Characterization of Cenospheres Collected from Ash-pond of a Super Thermal Power Plant. Energy Sources, Part A: Recovery, Utilization, and Environmental Effects [online]. 2007, 30(3), 271-283. DOI: 10.1080/00908310600713883. ISSN 1556-7036. Available at: http://www.tandfonline.com/doi/abs/10.1080/00908310600713883.

77 DANISH, Aamar and Mohammad Ali MOSABERPANAH. Formation mechanism and applications of cenospheres: a review. Journal of Materials Science [online]. 2020, 55(11), 4539-4557. DOI: 10.1007/s10853-019-04341-7. ISSN 0022-2461. Available at: http://link.springer.com/10.1007/s10853-019-04341-7.

78 KOLAY, Prabir K. and Sudha BHUSAL. Recovery of hollow spherical particles with two different densities from coal fly ash and their characterization. Fuel [online]. 2014, 117, 118-124. DOI: 10.1016/j.fuel.2013.09.014. ISSN 00162361. Available at: https://linkinghub.elsevier.com/retrieve/pii/S0016236113008430.

79 HANIF, Asad, Zeyu LU and Zongjin LI. Utilization of fly ash cenosphere as lightweight filler in cement-based composites – A review. Construction and Building Materials [online]. 2017, 144, 373-384 . DOI: 10.1016/j.conbuildmat.2017.03.188. ISSN 09500618. Available at: https://linkinghub.elsevier.com/retrieve/pii/S0950061817305792.

80 LEHKÉ UMĚLÉ KAMENIVO URČENÉ PRO STAVEBNICTVÍ. Agloporit [online]. Brno, 2018. Available at: http://agloporit.cz/lehke-umele-kamenivo/.

81 MARKO, Michal, Matěj LÉDL, Tomáš OPRAVIL, František ŠOUKAL, Jiří MÁSÍLKO and Petr HRUBÝ. Possibilities of High-temperature Fly Ash Application in Light-weight Mortars with Crushed Agloporite and Degradation Resistance. 2020, s 1–9.

82 SUKKAE, Rinyapat, Somkeat SUEBTHAWILKUL and Benya CHERDHIRUNKORN. Utilization of coal fly ash as a raw material for refractory production. Journal of Metals, Materials and Minerals [online]. 2018, 28(1), 116-123. DOI: 10.14456/jmmm.2018.16. Available at: https://www.researchgate.net/publication/326404724_Utilization_of_coal_fly_ash_as_a_raw_material_for_refractory_production.

83 LUO, Yang, Shuhua MA, Shili ZHENG, Chunli LIU, Dajie HAN and Xiaohui WANG. Mullite-based ceramic tiles produced solely from high-alumina fly ash: Preparation and sintering mechanism. Journal of Alloys and Compounds [online]. DOI: 10.1016/j.jallcom.2017.09.179. Available at: http://linkinghub.elsevier.com/retrieve/pii/S0925838817332280.

84 OTERO, J. Gonzalez, F. BLANCO, M.P. GARCIA and J. AYALA. Manufacture of refractory insulating bricks using fly ash and clay. British Ceramic Transactions [online]. 2013, 103(4), 181-186. DOI: 10.1179/096797804225018714. ISSN 0967-9782. Available at: http://www.tandfonline.com/doi/full/10.1179/096797804225018714.

85 KOTOVA, Olga B.; IGNATIEV, Grigory V.; SHUSHKOV, Dmitry A.; HARJA, Maria a BROEKMANS, Maarten A. T. M. Preparation and Properties of Ceramic Materials from Coal Fly Ash. Online. *Minerals: Structure, Properties, Methods of Investigation*. Springer Proceedings in Earth and Environmental Sciences. 2020, s. 101-107. ISBN 978-3-030-00924-3. Available at: https://doi.org/10.1007/978-3-030-00925-0_16.

86 O, Y. Preparation of ceramic membrane filters, from waste fly ash, suitable for hot gas cleaning. Waste Management [online]. 1996, 14(3), 281–295. DOI: 10.1006/wmre.1996.0027. ISSN 0734242x. Available at: http://linkinghub.elsevier.com/retrieve/pii/S0734242X96900270.

87 SALAH, Numan, Attieh A. AL-GHAMDI, Adnan MEMIC, Sami S. HABIB and Zishan H. KHAN. Formation of Carbon Nanotubes from Carbon-Rich Fly Ash: Growth Parameters and Mechanism. Materials and Manufacturing Processes [online]. 2015, 2(31), 146–156. DOI: 10.1080/10426914.2015.1025975. Available at: http://www.tandfonline.com/doi/full/10.1080/10426914.2015.1025975.

88 YASUI, Akihiro, Yasuhiro KAMIYA, Shota SUGIYAMA, Shingo ONO, Hidetomo NODA and Yo ICHIKAWA. Synthesis of Carbon Nanotubes on Fly Ashes by Chemical Vapor Deposition Processing. IEEJ Transactions on Electrical and Electronic Engineering [online]. 2009, 4(6), 787-789. DOI: 10.1002/tee.20481. ISSN 19314973. Available at: http://doi.wiley.com/10.1002/tee.20481.

89 What is the difference between single walled and multi walled carbon nanotubes? In: Quora [online]. 2016. Available at: https://www.quora.com/What-is-the-difference-between-single-walled-and-multi-walled-carbon-nanotubes.

90 ROVATTI, M., A. PELOSO and G. FERRAIOLO. Susceptibility to regeneration of fly ash as an adsorbent material. Resources, Conservation and Recycling [online]. 1988, 2(1), 137–143. DOI: 10.1016/0921-3449(88)90050-X. Available at: http://linkinghub.elsevier.com/retrieve/pii/092134498890050X.

91 BAYAT, Belgin. Comparative study of adsorption properties of Turkish fly ashes. Journal of Hazardous Materials [online]. 2002, (95), 251–273. DOI: 10.1016/S0304-3894(02)00140-1. Available at: http://linkinghub.elsevier.com/retrieve/pii/S0304389402001401.

92 DAI, Shifeng, Ian T. GRAHAM and Colin R. WARD. A review of anomalous rare earth elements and yttrium in coal. International Journal of Coal Geology [online]. 2016, 159, 82-95. DOI: 10.1016/j.coal.2016.04.005. ISSN 01665162. Available at: https://linkinghub.elsevier.com/retrieve/pii/S016651621630115X.

93 DAI, Shifeng and Robert B. FINKELMAN. Coal as a promising source of critical elements: Progress and future prospects. International Journal of Coal Geology [online]. 2018, 186, 155-164. DOI: 10.1016/j.coal.2017.06.005. ISSN 01665162. Available at: https://linkinghub.elsevier.com/retrieve/pii/S0166516217304007.

94 KOLÁŘ, Ladislav. 1969. Popílky a možnost jejich využití. 1. vyd. Praha: Práce, 92 s.

95 WANG, Zhen, Shifeng DAI, Jianhua ZOU, David FRENCH and Ian T. GRAHAM. Rare earth elements and yttrium in coal ash from the Luzhou power plant in Sichuan, Southwest China: Concentration, characterization and optimised extraction. International Journal of Coal Geology [online]. 2019, 203, 1-14. DOI: 10.1016/j.coal.2019.01.001. ISSN 01665162. Available at: https://linkinghub.elsevier.com/retrieve/pii/S0166516218310097.

96 MORENO, N, X QUEROL, J ANDRES, K STANTON, M TOWLER, H NUGTEREN, M JANSSENJURKOVICOVA a R JONES. Physico-chemical characteristics of European pulverised coal combustion fly ashes. Fuel [online]. 2005, 84(11), 1351-1363. DOI: 10.1016/j.fuel.2004.06.038. ISSN 00162361. Available at: https://linkinghub.elsevier.com/retrieve/pii/S0016236104003394.

97 MARKO, M, T OPRAVIL, J MASILKO and J PORIZKA. Possibilities of fly ash activation in alumina recovery process. IOP Conference Series: Materials Science and Engineering [online]. 2019, 583 . DOI: 10.1088/1757-899X/583/1/012003. ISSN 1757-899X. Available at: https://iopscience.iop.org/article/10.1088/1757-899X/583/1/012003.

98 YAO, Z.T., M.S. XIA, P.K. SARKER and T. CHEN. A review of the alumina recovery from coal fly ash, with a focus in China. Fuel[online]. 2014, 120), 74–85. DOI: 10.1016/j.fuel.2013.12.003. ISSN 00162361. Available at: http://linkinghub.elsevier.com/retrieve/pii/S001623611301140X.

99 DING, Jian, Shuhua MA, Shirley SHEN, Zongli XIE, Shili ZHENG and Yi ZHANG. Research and industrialization progress of recovering alumina from fly ash: A concise review. Waste

management [online]. 2017, (60), 375–387. DOI: 10.1016/j.wasman.2016.06.009. ISSN 0956-053X. Available at: http://linkinghub.elsevier.com/retrieve/pii/S0956053X16303142.

100 WANG, Xiao Huan, Bao Dong WANG, Yong Feng XIAO, Xiao Ting LIU, Li Jun ZHAO, Geng Zhi YU and Qi SUN. The Optimization of Sintering Process for Alumina Extraction from Fly Ash. Advanced Materials Research [online]. 2014, (878), 264–270 .[DOI: 10.4028/www.scientific.net/AMR.878.264. ISSN 1662-8985. Available at: http:/www.scientific.net/AMR.878.264.

101 BERANOVA, D, L GALVANKOVA, J MASILKO and P PTACEK. The products of a high temperature reaction of fly ash with lime and soda. IOP Conference Series: Materials Science and Engineering [online]. 2019, 583. DOI: 10.1088/1757-899X/583/1/012026. ISSN 1757-899X. Available at: https://iopscience.iop.org/article/10.1088/1757-899X/583/1/012026.

102 LIU, Dandan, Li FANG, Yanxia GUO, Kezhou YAN, Cong YAO and Fangqin CHENG. Effects of calcium oxide and ferric oxide on the process of alumina extraction of coal fly ash activated by sodium carbonate. Hydrometallurgy [online]. 2018, 179, 149-156. DOI: 10.1016/j.hydromet.2018.04.017. ISSN 0304386X. Available at: https://linkinghub.elsevier.com/retrieve/pii/S0304386X17310265.

103 CALCIUM CHLORIDE. Toxnet [online]. 2012. Available at: https://toxnet.nlm.nih.gov/cgi-bin/sis/search2/f?/temp/~gzciuP:3.

104 SUN, Yinglong, Zhenkai LIANG and Fangyan SUN. Recovery of Alumina from Coal Fly Ash by CaCl2 Calcination Followed by H2SO4 Leaching. Journal of Environmental & Analytical Toxicology [online]. 2017, 7(427). DOI: 10.4172/2161-0525.1000427. ISSN 2161-0525. Available at: https://www.omicsonline.org/open-access/recovery-of-alumina-from-coal-fly-ash-by-cacl2-calcination-followed-byh2so4-leaching-2161-0525-1000427.php?aid=84655.

105 LI, Laishi, Xinqin LIAO, Yusheng WU and Yingying LIU. Extracting Alumina from Coal Fly Ash with Ammonium Sulfate Sintering Process. Light Metals 2012 [online]. Hoboken, NJ, USA, 2012, 2012-05-23, 213-217 . DOI: 10.1002/9781118359259.ch38. ISBN 9781118359259. Available at: http://doi.wiley.com/10.1002/9781118359259.ch38.

106 WU, Yusheng, Ping XU, Jiao CHEN, Laishi LI and Mingchun LI. Effect of Temperature on Phase and Alumina Extraction Efficiency of the Product from Sintering Coal Fly Ash with Ammonium Sulfate. Chinese Journal of Chemical Engineering [online]. 2014, 22(11-12), 1363-1367. DOI: 10.1016/j.cjche.2014.09.008. ISSN 10049541. Available at: https://linkinghub.elsevier.com/retrieve/pii/S1004954114001153.

107 SHEMI, A., R.N. MPANA, S. NDLOVU, L.D. VAN DYK, V. SIBANDA and L. SEEPE. Alternative techniques for extracting alumina from coal fly ash. Minerals Engineering [online]. 2012, 34, 30-37. DOI: 10.1016/j.mineng.2012.04.007. ISSN 08926875. Available at: https://linkinghub.elsevier.com/retrieve/pii/S0892687512001574.

108 Extraction of Alumina from Coal Fly Ash with Sulphuric Acid Leaching Method. The Chinese Journal of Process Engineering[online]. 2011, 11(2), 254–258. DOI: 1009-606x. ISSN 1009-606X. Available at: http://www.citeseerx.ist.psu.edu/viewdoc/download?doi=10.1.1.472.6625&rep=rep1&type=pdf.

109 NAYAK, Niva and Chitta R. PANDA. Aluminium extraction and leaching characteristics of Talcher Thermal Power Station fly ash with sulphuric acid. Fuel [online]. 2010, 89(1), 53-58. DOI: 10.1016/j.fuel.2009.07.019. ISSN 00162361. Available at: https://linkinghub.elsevier.com/retrieve/pii/S0016236109003494.

110 SEIDEL, A. and Y. ZIMMELS. Mechanism and kinetics of aluminium and iron leaching from coal fly ash by sulphuric acid. Chemical Engineering Science [online]. 1998, 53(22), 3835-3852. DOI: 10.1016/S0009-2509(98)00201-2. ISSN 00092509. Available at: https://linkinghub.elsevier.com/retrieve/pii/S0009250998002012.

111 TILLEY, G. S., R. W. MILLAR and O. C. RALSTON. Acid Processes For The Extraction Of Alumina [online]. Washington: Government printing office, 1927. Available at:

https://books.google.cz/books?id=DYrHLEfYUvgC&printsec=frontcover&hl=cs&source=gbs_ge_summary_r&cad=0#v=onepage&q&f=false.

112 SHIVPURI, Kandarp K., Lokeshappa B., Deepak A. KULKARNI and Anil Kumar DIKSHIT. Metal Leaching Potential in Coal Fly Ash. American Journal of Environmental Engineering [online]. 2011, 1(1), 21-27 DOI: 10.5923/j.ajee.20110101.04. ISSN 2166-4633. Available at: http://article.sapub.org/10.5923.j.ajee.20110101.04.html.

113 Marko, M. Vedlejší energetické produkty jako surovinová základna budoucnosti. Brno: Vysoké učení technické v Brně, Fakulta chemická, 2016. 77 s.

114 WEI, Cundi, Shan CHENG, Fujie ZHU, Xiaoling TAN, Wenqing LI, Peiping ZHANG and Shiding MIAO. Digesting high-aluminium coal fly ash with concentrated sulphuric acid at high temperatures. Hydrometallurgy [online]. 2018, 180, 41-48. DOI: 10.1016/j.hydromet.2018.07.004. ISSN 0304386X. Available at: https://linkinghub.elsevier.com/retrieve/pii/S0304386X17309842.

115 HUANG, Kai, Katsutoshi INOUE, Hiroyuki HARADA, Hidetaka KAWAKITA and Keisuke OHTO. Leaching behaviour of heavy metals with hydrochloric acid from fly ash generated in municipal waste incineration plants. Transactions of Nonferrous Metals Society of China [online]. 2011, 21(6), 1422-1427]. DOI: 10.1016/S1003-6326(11)60876-5. ISSN 10036326. Available at: https://linkinghub.elsevier.com/retrieve/pii/S1003632611608765.

116 ELOMAA, Heini; SEISKO, Sipi; LEHTOLA, Jenna a LUNDSTRÖM, Mari. A study on selective leaching of heavy metals vs. iron from fly ash. Online. *Journal of Material Cycles and Waste Management*. 2019, vol. 21, vol. 4, s. 1004-1013. ISSN 1438-4957. Available at: https://doi.org/10.1007/s10163-019-00858-w.

117 DAHAN, Al Mon E.; ALORRO, Richard D.; PACAÑA, Mona Lisa C.; BAUTE, Ronben M.; SILVA, Leaniel C. et al. Hydrochloric Acid Leaching of Philippine Coal Fly Ash: Investigation and Optimisation of Leaching Parameters by Response Surface Methodology (RSM). Online. *Sustainable Chemistry*. 2022, vol. 3, vol. 1, s. 76-90. ISSN 2673-4079. Available at: https://doi.org/10.3390/suschem3010006.

118 VALEEV, Dmitry; KUNILOVA, Irina; SHOPPERT, Andrei; SALAZAR-CONCHA, Cristian a KONDRATIEV, Alex. High-pressure HCl leaching of coal ash to extract Al into a chloride solution with further use as a coagulant for water treatment. Online. *Journal of Cleaner Production*. 2020, vol. 2020, vol. 276. ISSN 09596526. Available at: https://doi.org/10.1016/j.jclepro.2020.123206.

119 MARKO, Michal, Tomáš OPRAVIL, František ŠOUKAL and Jaromír POŘÍZKA. Ash – the raw material base for the future. Chemistry and Life .018, 116-124.

120 BAI, Guang-hui, Wei TENG, Xiang-gang WANG, Jin-guo QIN, Peng XU and Peng-cheng LI. Alkali desilicated coal fly ash as substitute of bauxite in lime-soda sintering process for aluminium production. Transactions of Nonferrous Metals Society of China [online]. 2010, 1(20), 169–175. DOI: 10.1016/S1003-6326(10)60034-9. ISSN 1003-6326. Available at: http://linkinghub.elsevier.com/retrieve/pii/S1003632610600349.

121 WANG, Ming Wei, Jing YANG, Hong Wen MA, Jie SHEN, Jin Hong LI and Feng GUO. Extraction of Aluminium Hydroxide from Coal Fly Ash by Pre-Desilication and Calcination Methods. Advanced Materials Research [online]. 2011, (396–398), 706–710. DOI: 10.4028/www.scientific.net/AMR.396-398.706. ISSN 1662-8985. Available at: http://www.scientific.net/AMR.396-398.706.¨

122 GONG, Yanbing, Junmin SUN, Shu-Ying SUN, Guozhi LU a Ting-An ZHANG. Enhanced Desilication of High Alumina Fly Ash by Combining Physical and Chemical Activation. Metals [online]. 2019, 9(4). DOI: 10.3390/met9040411. ISSN 2075-4701. Available at: https://www.mdpi.com/2075-4701/9/4/411.

123 NOWAK, B., A. PESSL, P. ASCHENBRENNER, P. SZENTANNAI, H. MATTENBERGER, H. RECHBERGER, L. HERMANN and F. WINTER. Heavy metal removal from municipal solid waste fly ash by chlorination and thermal treatment. Journal of Hazardous Materials [online]. 2010, (179), 323–331. DOI: 10.1016/j.jhazmat.2010.03.008. ISSN 0304-3894. Available at: http://linkinghub.elsevier.com/retrieve/pii/S0304389410003146.

124 L., Krejčiřík and Zahradník K. Získávání titanu z elektrárenských popelů. Chemický průmysl. 1966, (9).

125 SHABTAI, Yossef and Igor MUKMENEV. A combined chemical-biotechnological treatment of coal fly ash (CFA). Journal of Biotechnology. 1996, 51(3): 209–217 DOI: 10.1016/S0168-1656(96)01598-2. ISSN 01681656. Available at: http://linkinghub.elsevier.com/retrieve/pii/S0168165696015982.

126 IZQUIERDO, Maria and Xavier QUEROL. Leaching behaviour of elements from coal combustion fly ash: An overview. International Journal of Coal Geology [online]. 2012, 94, 54-66. DOI: 10.1016/j.coal.2011.10.006. ISSN 01665162. Available at: https://linkinghub.elsevier.com/retrieve/pii/S0166516211002230.

127 MIRAVET, Ricard, José Fermín LÓPEZ-SÁNCHEZ and Roser RUBIO. Leachability and analytical speciation of antimony in coal fly ash. Analytica Chimica Acta [online]. 2006, 576(2), 200-206. DOI: 10.1016/j.aca.2006.06.003. ISSN 00032670. Available at: https://linkinghub.elsevier.com/retrieve/pii/S0003267006012293.

128 CORNELIS, Geert, C. Anette JOHNSON, Tom Van GERVEN and Carlo VANDECASTEELE. Leaching mechanisms of oxyanionic metalloid and metal species in alkaline solid wastes: A review. Applied Geochemistry [online]. 2008, 23(5), 955-976. DOI: 10.1016/j.apgeochem.2008.02.001. ISSN 08832927. Available at: https://linkinghub.elsevier.com/retrieve/pii/S0883292708000693.

129 NORRIS, Pauline, Chien-Wei CHEN and Wei-Ping PAN. A technique for sequential leaching of coal and fly ash resulting in good recovery of trace elements. Analytica Chimica Acta [online]. 2010, 663(1), 39-42. DOI: 10.1016/j.aca.2010.01.033. ISSN 00032670. Available at: https://linkinghub.elsevier.com/retrieve/pii/S0003267010000930.

130 ZHANG, Siyu, Shifeng DAI, Robert B. FINKELMAN, Ian T. GRAHAM, David FRENCH, James C. HOWER and Xuewen LI. Leaching characteristics of alkaline coal combustion by-products: A case study from a coal-fired power plant, Hebei Province, China. Fuel [online]. 2019, 255. DOI: 10.1016/j.fuel.2019.115710. ISSN 00162361. Available at: https://linkinghub.elsevier.com/retrieve/pii/S0016236119310622

131 IZQUIERDO, Maria, Nikolaos KOUKOUZAS, Sofia TOULIOU, Kyriakos D. PANOPOULOS, Xavier QUEROL and Grigorios ITSKOS. Geochemical controls on leaching of lignite-fired combustion by-products from Greece. Applied Geochemistry [online]. 2011, 26(9–10), 1599–1606. DOI: 10.1016/j.apgeochem.2011.04.013. ISSN 08832927. Available at: https://linkinghub.elsevier.com/retrieve/pii/S0883292711002241.

132 OGATA, Fumihiko, Hisato TOMINAGA, Hitoshi YABUTANI, Atsushi TAGA and Naohito KAWASAKI. Recovery of molybdenum from fly ash by gibbsite. Environmental Chemistry/Technology [online]. 2011, 93(4), 635-642. DOI: 10.1080/02772248.2011.558508. ISSN 0277-2248. Available at: http://www.tandfonline.com/doi/abs/10.1080/02772248.2011.558508.

133 Calcium arsenate. In: PubChem [online]. USA, 2005. Available at: https://pubchem.ncbi.nlm.nih.gov/compound/Calcium-arsenate.

134 SAHOO, Prafulla Kumar, Kangjoo KIM, M. A. POWELL and Sk Md EQUEENUDDIN. Recovery of metals and other beneficial products from coal fly ash: a sustainable approach for fly ash management. International Journal of Coal Science & Technology [online]. 2016, 3(3), 267–283. DOI: 10.1007/s40789-016-0141-2. ISSN 2095-8293. Available at: http://link.springer.com/10.1007/s40789-016-0141-2.

135 MESHRAM, Pratima, B.D. PANDEY and T.R. MANKHAND. Extraction of lithium from primary and secondary sources by pre-treatment, leaching and separation: A comprehensive review. Hydrometallurgy [online]. 2014, 150, 192-208. DOI: 10.1016/j.hydromet.2014.10.012. ISSN 0304386X. Available at: https://linkinghub.elsevier.com/retrieve/pii/S0304386X14002278.

136 SANNA, Aimaro, Ili RAMLI and M. MERCEDES MAROTO-VALER. Development of sodium/lithium/fly ash sorbents for high temperature post-combustion CO 2 capture. Applied

Energy [online]. 2015, 156, 197-206. DOI: 10.1016/j.apenergy.2015.07.008. ISSN 03062619. Available at: https://linkinghub.elsevier.com/retrieve/pii/S0306261915008375.

137 ARROYO, Fátima, Constantino FERNÁNDEZ-PEREIRA, Joaquín OLIVARES and Pilar COCA. Hydrometallurgical Recovery of Germanium from Coal Gasification Fly Ash: Pilot Plant Scale Evaluation. Industrial & Engineering Chemistry Research [online]. 2009, 48(7), 3573-3579. DOI: 10.1021/ie800730h. ISSN 0888-5885. Available at: https://pubs.acs.org/doi/10.1021/ie800730h.

138 ARROYO, Fátima, Oriol FONT, Josep María CHIMENOS, Constantino FERNÁNDEZ-PEREIRA, Xavier QUEROL and Pilar COCA. IGCC fly ash valorisation. Optimisation of Ge and Ga recovery for an industrial application. Fuel Processing Technology [online]. 2014, 124, 222-227. DOI: 10.1016/j.fuproc.2014.03.004. ISSN 03783820. Available at: https://linkinghub.elsevier.com/retrieve/pii/S0378382014001003.

139 WANG, Tian, Jianmin WANG, Joel G. BURKEN, Heng BAN and Ken LADWIG. The Leaching Characteristics of Selenium from Coal Fly Ashes. Journal of Environment Quality [online]. 2007, 36(6), 1784-1792. DOI: 10.2134/jeq2007.0143. ISSN 1537-2537. Available at: https://www.agronomy.org/publications/jeq/abstracts/36/6/1784.

140 CHEN, Xiang-yang, Xin-zhe LAN, Qiu-li ZHANG, Hong-zhou MA and Jun ZHOU. Leaching vanadium by high concentration sulphuric acid from stone coal. Transactions of Nonferrous Metals Society of China [online]. 2010, 20, s123-s126. DOI: 10.1016/S1003-6326(10)60025-8. ISSN 10036326. Available at: https://linkinghub.elsevier.com/retrieve/pii/S1003632610600258.

141 VITOLO, Sandra, Maurizia SEGGIANI, Sara FILIPPI and Cristina BROCCHINI. Recovery of vanadium from heavy oil and Orimulsion fly ashes. Hydrometallurgy [online]. 2000, 57(2), 141-149. DOI: 10.1016/S0304-386X(00)00099-2. ISSN 0304386X. Available at: https://linkinghub.elsevier.com/retrieve/pii/S0304386X00000992.

142 MASLOV, O. D., Sh. TSERENPIL, N. NOROV, M. V. GUSTOVA, M. F. FILIPPOV, A. G. BELOV, M. ALTANGEREL and N. ENHBAT. Uranium recovery from coal ash dumps of Mongolia. Solid Fuel Chemistry [online]. 2010, 44(6), 433-438. DOI: 10.3103/S0361521910060133. ISSN 0361-5219. Available at: http://www.springerlink.com/index/10.3103/S0361521910060133.

143 ČSN 72 2071. Popílek pro stavební účely: Společná ustanovení, požadavky a metody zkoušení. Praha: Český normalizační institut, 2011.

144 ČSN 72 2080. Fluidní popel a fluidní popílek pro stavební účely – Společná ustanovení, požadavky a metody zkoušení. Český normalizační institut, 2011.

145 GREENWOOD, N. N. 1993. Hliník, gallium, indium a thallium. *Chemie prvků*. Praha: Informatorium, p. 262-316. ISBN 80-85427-38-9.

146 LIANG, Wang, Guang-wei WANG, Xiao-jun NING, Jian-liang ZHANG, Yan-jiang LI and Chun-he JIANG. 2020. Effect of CaO mineral change on coal ash melting characteristics. Journal of the Energy Institute [online]. 93(2), 642-648. DOI: 10.1016/j.joei.2019.06.001. ISSN 17439671. Available at: https://linkinghub.elsevier.com/retrieve/pii/S1743967119304714.

147 KIM, Taehwan, Masoud MORADIAN and M. Tyler LEY. 2018. Dissolution and Leaching of Fly Ash in Nitric Acid Using Automated Scanning Electron Microscopy. *Advances in Civil Engineering Materials* [online]. **7**(1), 291-307. DOI: 10.1520/ACEM20180016. ISSN 2379-1357. Available at: https://asmedigitalcollection.asme.org/civilengineeringmaterials/article/7/1/291/1173382/Dissolution-and-Leaching-of-Fly-Ash-in-Nitric-Acid.

148 LIN, Xiaoqing, Tieying MAO, Zhiliang CHEN, Jie CHEN, Sheng ZHANG, Xiaodong LI and Jianhua YAN. 2021. Thermal cotreatment of municipal solid waste incineration fly ash with sewage sludge: Phases transformation, kinetics and fusion characteristics, and heavy metals solidification. Journal of Cleaner Production [online]. 317. DOI: 10.1016/j.jclepro.2021.128429. ISSN 09596526. Available at: https://linkinghub.elsevier.com/retrieve/pii/S095965262102641X.

149 PIMRAKSA, K., S. HANJITSUWAN and P. CHINDAPRASIRT. 2009. Synthesis of belite cement from lignite fly ash. Ceramics International [online]. 35(6), 2415-2425. DOI: 10.1016/j.ceramint.2009.02.006. ISSN 02728842. Available at: https://linkinghub.elsevier.com/retrieve/pii/S0272884209000625.

150 MAZOUZI, W., L. KACIMI, M. CYR and P. CLASTRES. 2014. Properties of low temperature belite cements made from aluminosilicate wastes by hydrothermal method. Cement and Concrete Composites [online]. 53, 170-177. DOI: 10.1016/j.cemconcomp.2014.07.001. ISSN 09589465. Available at: https://linkinghub.elsevier.com/retrieve/pii/S0958946514001188.

151 PYZALSKI, Michał, Jarosław DĄBEK, Anna ADAMCZYK and Tomasz BRYLEWSKI. 2021. Physicochemical Study of the Self-Disintegration of Calcium Orthosilicate (β→γ) in the Presence of the C12A7 Aluminate Phase. Materials [online]. 14(21). DOI: 10.3390/ma14216459. ISSN 1996-1944. Available at: https://www.mdpi.com/1996-1944/14/21/6459.

152 PTÁČEK, Petr, Tomáš OPRAVIL, František ŠOUKAL, Jaromír HAVLICA and Radek HOLEŠINSKÝ. 2013. Kinetics and mechanism of formation of gehlenite, Al–Si spinel and anorthite from the mixture of kaolinite and calcite. Solid State Sciences [online]. 26, 53-58. DOI: 10.1016/j.solidstatesciences.2013.09.014. ISSN 12932558. Available at: https://linkinghub.elsevier.com/retrieve/pii/S1293255813002720.

153 SUZDALTSEV, A. V., A. P. KHRAMOV, Yu. P. ZAIKOV, A. A. PANKRATOV, E. G. VOVKOTRUB and B. D. ANTONOV. 2017. Reduction of Solid Al 2 O 3 with Electrolysis of CaCl 2 -Based Melt. Journal of The Electrochemical Society [online]. 164(8), H5183-H5188. DOI: 10.1149/2.0291708jes. ISSN 0013-4651. Available at: https://iopscience.iop.org/article/10.1149/2.0291708jes.

154 OELKERS, Eric H. and Jacques SCHOTT. 1995. Experimental study of anorthite dissolution and the relative mechanism of feldspar hydrolysis. Geochimica et Cosmochimica Acta [online]. 59(24), 5039-5053. DOI: 10.1016/0016-7037(95)00326-6. ISSN 00167037. Available at: https://linkinghub.elsevier.com/retrieve/pii/0016703795003266.

155 WEISSBART, Erich J and J.Donald RIMSTIDT. 2000. Wollastonite: Incongruent dissolution and leached layer formation. Geochimica et Cosmochimica Acta [online]. 64(23), 4007-4016. DOI: 10.1016/S0016-7037(00)00475-0. ISSN 00167037. Available at: https://linkinghub.elsevier.com/retrieve/pii/S0016703700004750.

156 OELKERS, Eric H. and Jacques SCHOTT. 1995. Experimental study of anorthite dissolution and the relative mechanism of feldspar hydrolysis. *Geochimica et Cosmochimica Acta* [online]. **59**(24), 5039-5053. DOI: 10.1016/0016-7037(95)00326-6. ISSN 00167037. Available at: https://linkinghub.elsevier.com/retrieve/pii/0016703795003266.

157 MA, Jiayu, Yanfang ZHANG, Yuanhang QIN, Zaikun WU, Tielin WANG and Cunwen WANG. 2017. The leaching kinetics of K-feldspar in sulphuric acid with the aid of ultrasound. *Ultrasonics Sonochemistry* [online]. **35**, 304-312. DOI: 10.1016/j.ultsonch.2016.10.006. ISSN 13504177. Available at: https://linkinghub.elsevier.com/retrieve/pii/S1350417716303455.

158 ENGSTRÖM, F., D. ADOLFSSON, C. SAMUELSSON, Å. SANDSTRÖM and B. BJÖRKMAN. 2013. A study of the solubility of pure slag minerals. *Minerals Engineering* [online]. **41**, 46-52. DOI: 10.1016/j.mineng.2012.10.004. ISSN 08926875. Available at: https://linkinghub.elsevier.com/retrieve/pii/S089268751200341X.

159 PAK, Tatyana M., Christoph A. HAUZENBERGER and Lukas P. BAUMGARTNER. 2003. Solubility of the assemblage albite K-feldspar andalusite quartz in supercritical aqueous chloride solutions at 650 °C and 2 kbar. *Chemical Geology* [online]. **200**(3-4), 377-393. DOI: 10.1016/S0009-2541(03)00211-0. ISSN 00092541. Available at: https://linkinghub.elsevier.com/retrieve/pii/S0009254103002110.

160 ROSELLE, Gregory T. and Lukas P. BAUMGARTNER. 1995. Experimental determination of anorthite solubility and calcium speciation in supercritical chloride solutions at 2 kb from 400 to 600°C. *Geochimica et Cosmochimica Acta* [online]. **59**(8), 1539-1549. DOI: 10.1016/0016-7037(95)00060-D. ISSN 00167037. Available at: https://linkinghub.elsevier.com/retrieve/pii/001670379500060D.

161 BOTHE, James V. and Paul W. BROWN. 1993. Reactivity of Alumina toward Phosphoric Acid. *Journal of the American Ceramic Society* [online]. **76**(9). DOI: 10.1111/j.1151-2916.1993.tb07776.x. ISSN 0002-7820. Available at: https://ceramics.onlinelibrary.wiley.com/doi/10.1111/j.1151-2916.1993.tb07776.x.

162 XIONG, Xunhui, Zhixing WANG, Feixiang WU, Xinhai LI and Huajun GUO. 2013. Preparation of TiO2 from ilmenite using sulphuric acid decomposition of the titania residue combined with separation of Fe3 with EDTA during hydrolysis. *Advanced Powder Technology* [online]. **24**(1), 60-67. DOI: 10.1016/j.apt.2012.02.002. ISSN 09218831. Available at: https://linkinghub.elsevier.com/retrieve/pii/S0921883112000118.

163 GÁZQUEZ, Manuel Jesús, Juan Pedro BOLÍVAR, Rafael GARCIA-TENORIO and Federico VACA. 2014. A Review of the Production Cycle of Titanium Dioxide Pigment. *Materials Sciences and Applications* [online]. **05**(07), 441-458. DOI: 10.4236/msa.2014.57048. ISSN 2153-117X. Available at: http://www.scirp.org/journal/doi.aspx?DOI=10.4236/msa.2014.57048.

164 Marko, M. *Popílky jako surovinová základna budoucnosti*. Brno: Vysoké učení technické v Brně, Fakulta chemická, 2018. 90 s.

7.2 List of abbreviations

An	Anortite
C_2S	Dicalcium silicate
C_3A	Tricalcium aluminate
Cc	Chloro-calcite
CCP	Coal combustion product
EDX	Energy dispersive X-ray analysis
FA	Fly ash
FBA	Fluidised-bed bottom ash
FFA	Fluidised-bed filter (fly) ash
Fig.	Figure
G	Gehlenite
HTFA	High-temperature fly ash
ICP-OES	Inductively coupled plazma optical emission spectrometry
L	Lime
L/S	Liquid to solid
La	Larnite
Ls	Limestone
M	Mullite
Mi	Microsommite
Mol eq.	Molar equivalent
Q	Quartz
SEM	Scanning electron microscopy
Sj	Sinjarite
TG-DTA	Thermogravimetry Differential Thermal Analysis
Wa	Wadalite
Wo	Wollastonite
XRD	X-ray diffraction analysis
XRF	X-ray fluorescence spectrometry

7.3 List of tables

7.4 List of figures

7.5 List of appendices

8 APPENDICES

8.1 Materials and samples info

Append. 1 Phase composition of HTFA

	Content (wt. %)						
	Amorphous	**Quartz**	**Mullite**	**Magnetite**	**Hematite**	**Anatase**	**Rutile**
ETU	58.9	7.9	29.8	2.0	1.0	0.3	–
TDK	72.4	7.7	13.2	0.8	1.0	–	–
EPR	66.8	5.1	25.5	1.9	0.7	–	–
ELE	61	3.8	34.5	0.1	0.5	–	–
EDĚ f	62.6	14.3	22.1	0.1	0.8	–	–
EDĚ c	69.2	19.9	10.1	0.5	0.1	–	–
EMĚ	54.2	7.7	34.1	0.3	1.3	1.3	1.3
TTR K6	73.3	7.3	18.2	0.1	0.3	0.4	0.4
TTR K7	59.3	5.4	34.5	0.2	0.5	–	–
EOP	57.2	5.5	34.7	1.7	0.7	–	–
ŽĎAS	54.2	12.4	32.2	0.4	0.6	0.1	
Paskov	55.6	18.8	24.6	0.4	0.5	0.1	
ETI	53.0	8.5	32.2	0.6	1.5	2.5	1.6
TPV	72.4	4.5	17.9	1.3	0.6	0.4	0.6
Orlen	57.7	7.1	34.6	0.2	0.4	–	–
Rybnik	57.1	18.2	22.5	1.3	0.8	0.1	0.1
Opole	58.1	8.6	31.7	0.7	0.7	0.1	0.1
Turkey 1	63.8	18.9	13.4	1.8	1.3	0.4	0.3
Turkey 2	43.8	21.4	33.2	0.3	0.9	0.2	0.1
Sarni In	46.9	22.9	28.9	0.6	0.5	0.3	–
Angul In	55.6	24.7	18.3	0.7	0.4	0.3	–

Append. 2 Phase composition of FFA and FBA

	Content (wt. %)												
	Amorphous	**Quartz**	**Calcite**	**Magnetite**	**Hematite**	**Lime**	**Anhydrite**	**Anatase**	**Muskovite**	**Albite**	**Ortoklase**	**Akermanite**	**Portlandite**
ELE BA	72.1	4.9	0.1	0.7	0.1	9.4	10.5	0.4	–	–	–	0.9	1.0
ELE FA	64.2	10.5	1.4	0.1	1.9	7.8	7.3	1.0	–	5.4	0.3	0.1	–
EPO BA	54.7	10.3		0.1	0.4	11.1	15.7	0.1	1.5	4.5	–	1.5	–
EPO FA	60.2	13.1	3.0	0.1	2.5	5.9	7	0.4	1.3	5.1	0.4	1	–
EPO FA biomas	44.4	23.4	1.0	0.3	0.4	3.4	1.9	0.1	6.0	18.3	0.5	0.4	–
EPO BA biomas	50.3	35.1	–	0.2	0.2	4.1	1.5	0.1	–	6.7	1.6	0.1	–
EHO BP	61.8	10.6	–	0.4	1.1	7.7	10.3	0.2	–	4.5	0.7	2.0	0.7
EHO Fp	42.5	20.5	3.9	0.4	0.6	5.9	7.6	0.3	1.8	12.1	2.4	2.1	–
ETI BP	57.1	9.0	0.1	0.2	0.4	14.7	13.0	2.2	–	11.8	1.0	0.2	0.2
ETI FP	62.7	7.6	3.1	0.3	2.1	10.4	9.0	0.5	1.4	–	–	2.3	0.6

Append. 3 Elemental composition of HTFA and FFA, FBA

	Content (wt. %)							
	Al_2O_3	**Fe_2O_3**	**TiO_2**	**MgO**	**CaO**	**SiO_2**	**K_2O**	**SO_3**
ETU	18.01	8.17	0.95	0.98	0.69	29.41	0.78	1.01
TDK	21.19	6.36	1.86	7.42	2.21	27.38	0.78	10.71
EPR	22.95	9.27	1.23	1.66	0.89	39.39	1.12	0.74
ELE	29.90	5.03	3.05	1.02	0.00	46.56	0.63	0.69
EDĚ f	23.40	6.55	1.22	2.17	0.88	46.63	2.37	0.70
EDĚ c	20.44	6.86	0.98	1.94	1.19	47.93	2.16	0.24
EMĚ	29.47	6.32	6.95	1.02	0.00	42.37	0.31	0.41
TTR K6	30.07	5.94	3.35	0.67	0.50	45.11	0.45	0.24
TTR K7	12.41	6.92	2.01	0.27	0.00	17.72	0.20	0.27
EOP	26.62	8.31	1.73	0.61	1.07	45.40	1.20	0.47
ŽĎAS	28.87	8.92	4.58	0.88	3.52	37.95	0.33	1.04
Paskov	5.81	2.86	0.44	4.94	8.34	38.88	3.25	3.85
ETI	27.90	7.25	7.37	0.44	1.04	39.21	0.37	0.80
TPV	17.00	7.26	4.07	0.00	2.06	23.15	0.19	0.45
Orlen	27.77	5.19	1.98	0.56	0.74	51.09	1.47	0.24
Rybnik	24.04	9.82	1.19	0.76	1.36	43.00	1.30	0.81
Opole	27.25	4.86	1.99	0.11	0.76	40,95	0.53	0.06
Turkey 1	24.4	56.5	6.1	4.5	2.2	2.2	0.7	0.9
Turkey 2	21.8	61.5	5.8	3.2	2.5	2.1	0.8	0.7
Sarni In	29.52	55.16	6.32	1.3	1.95	2.54	0.77	0.6
Angul In	27.13	55.45	7.28	2.74	2.55	1.9	1.2	0.55
ELE BA	20.27	4.45	3.07	17.39	0.63	28.50	0.14	14.97
ELE FA	26.54	4.73	3.05	12.36	0.00	40.24	0.32	5.74
EPO BA	13.48	3.80	1.64	24.71	1.25	19.32	0.40	21.04
EPO FA	23.75	6.56	1.90	15.06	1.26	37.11	0.81	6.95
EPO FA biomas	7.42	3.88	0.72	22.11	3.07	31.04	3.72	6.45
EPO BA biomas	3.83	0.79	0.15	8.71	2.96	17.13	1.17	2.73
EHO BP	16.39	4.36	1.29	19.85	1.71	34.23	2.40	7.76
EHO Fp	16.04	6.87	6.25	0.00	29.50	19.92	0.00	16.30
ETI BP	16.66	5.60	1.19	1.26	21.99	24.97	0.95	7.98
ETI FP	22.16	7.16	6.02	0.55	20.24	29.94	0.02	8.86

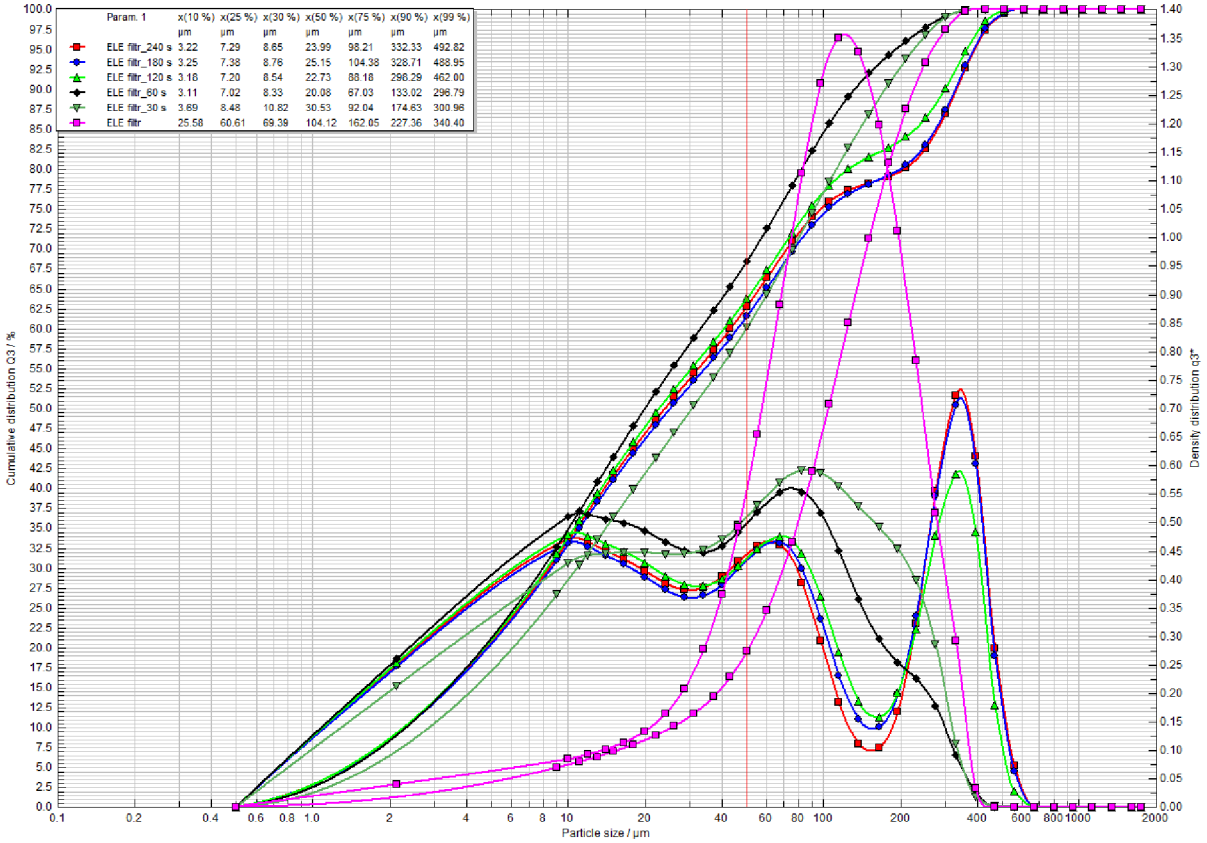

Append. 4 Particle size distribution of milled FFA 1

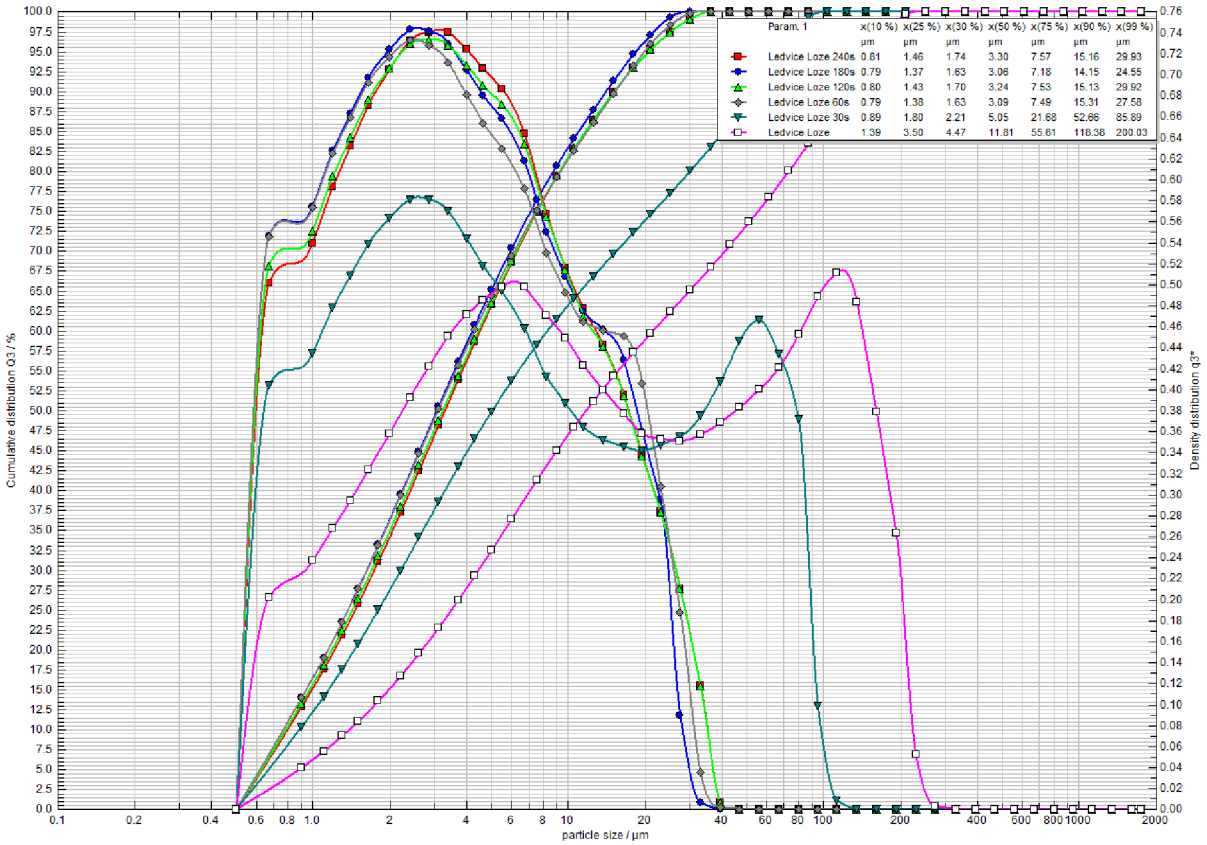

Append. 5 Particle size distribution of milled FBA 1

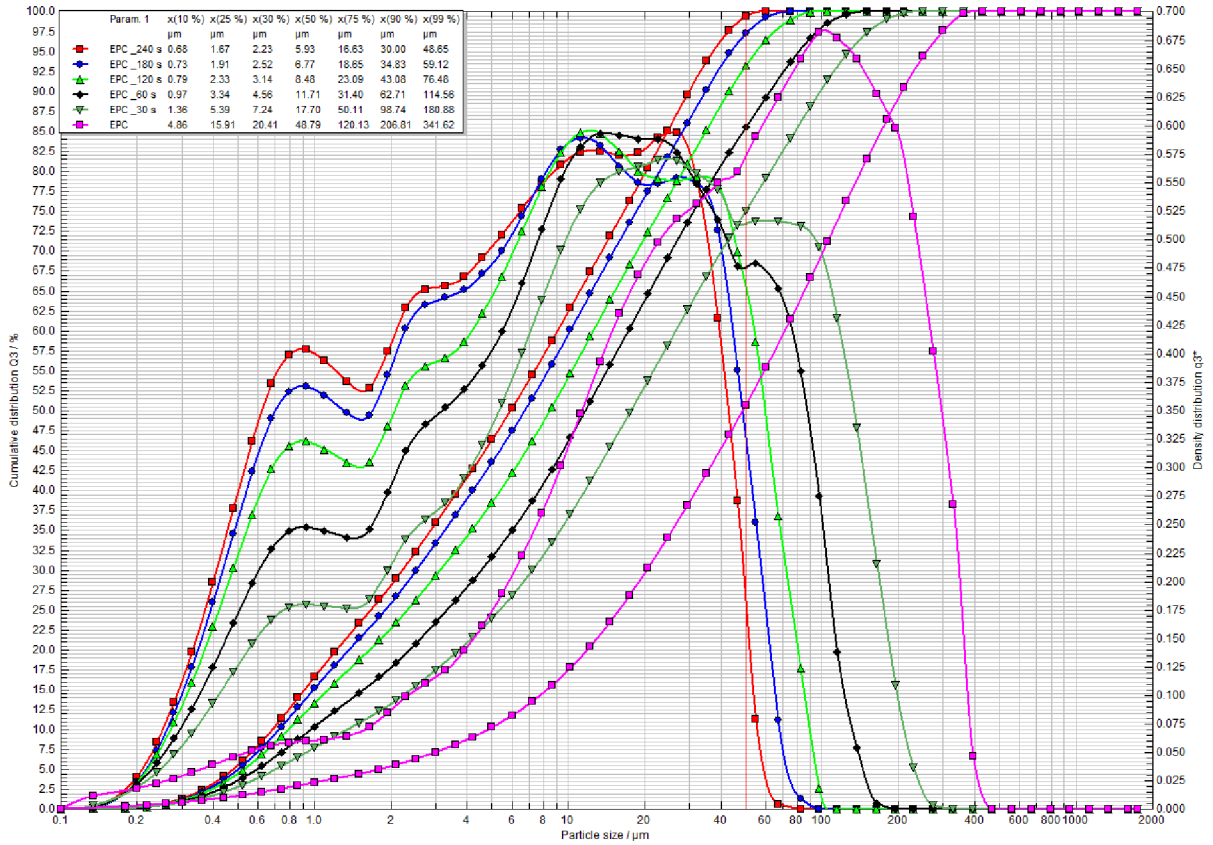

Append. 6 Particle size distribution of milled HTFA 1

a

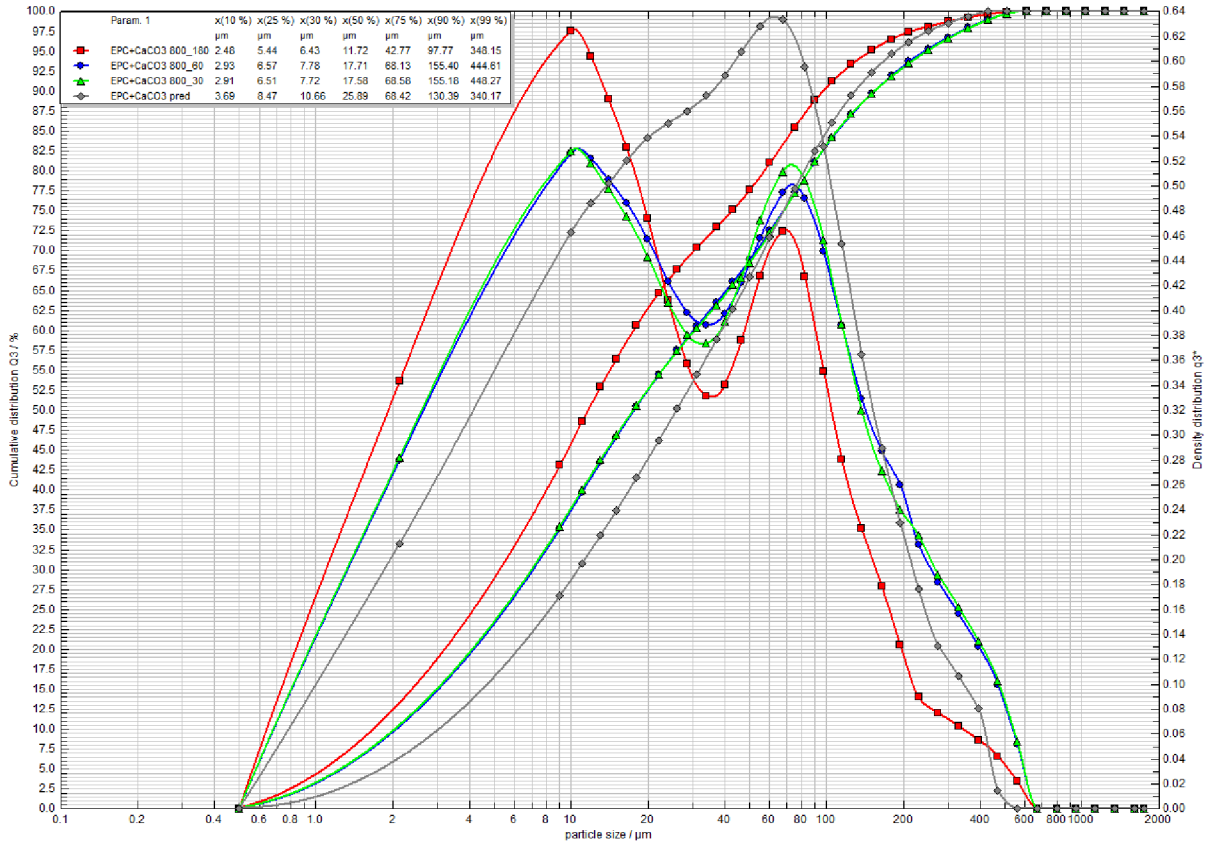

Append. 7 Particle size distribution of HTFA 1 modified with $CaCO_3$ at 800 °C

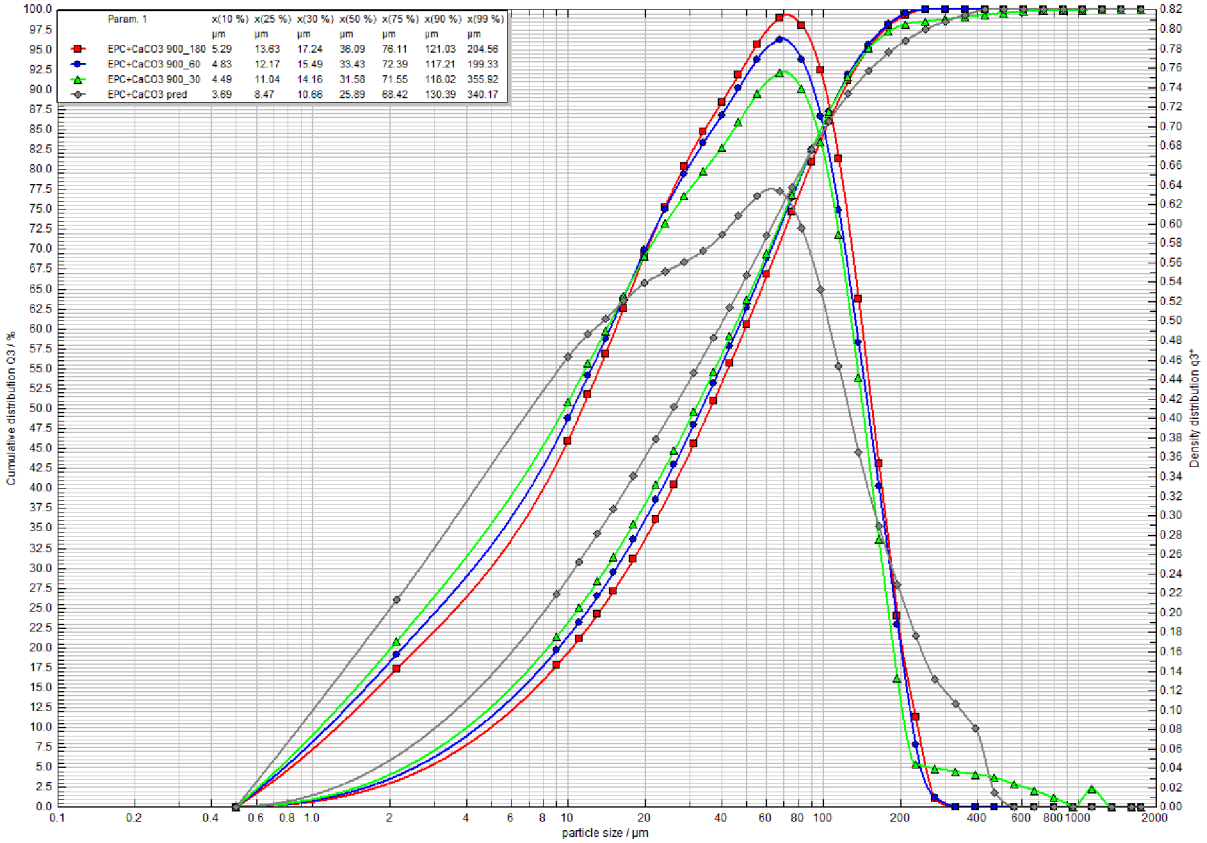

Append. 8 Particle size distribution of HTFA 1 modified with $CaCO_3$ at 900 °C

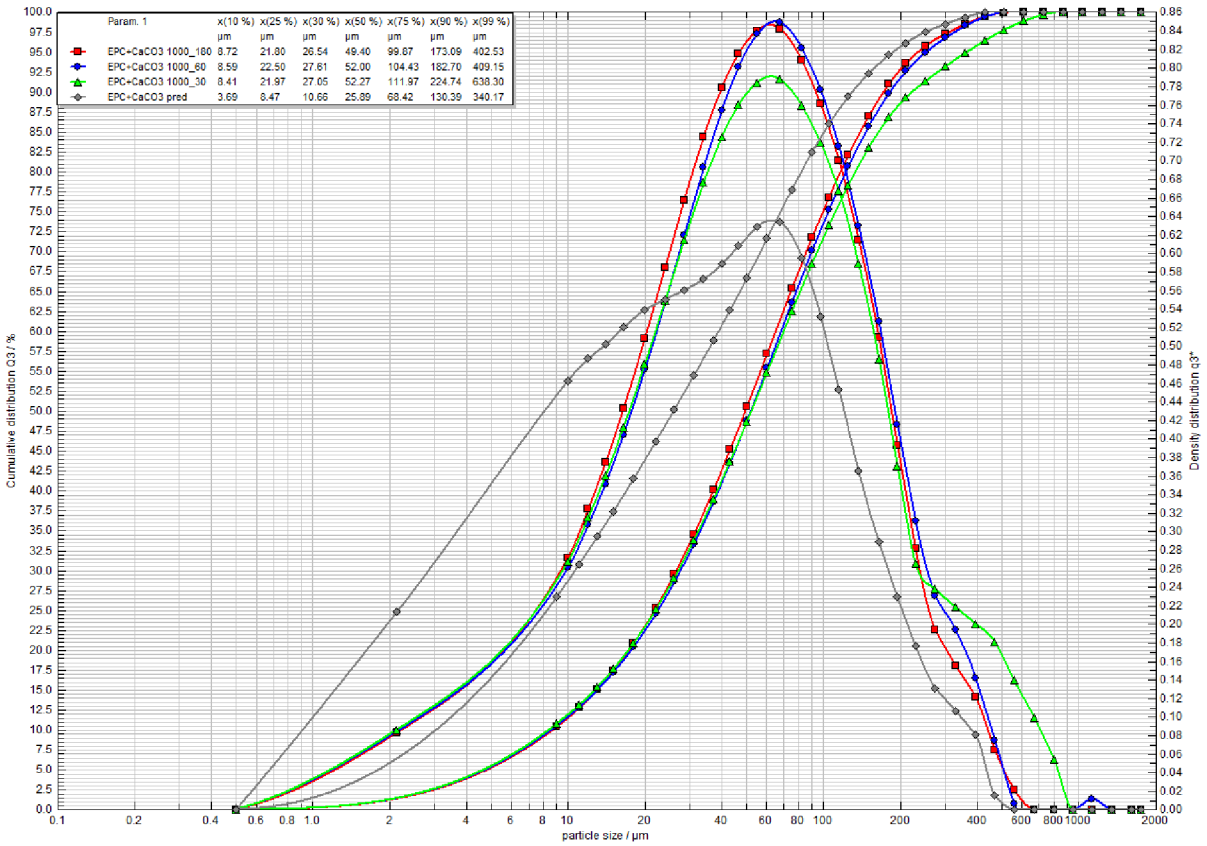

Append. 9 Particle size distribution of HTFA 1 modified with $CaCO_3$ at 1,000 °C

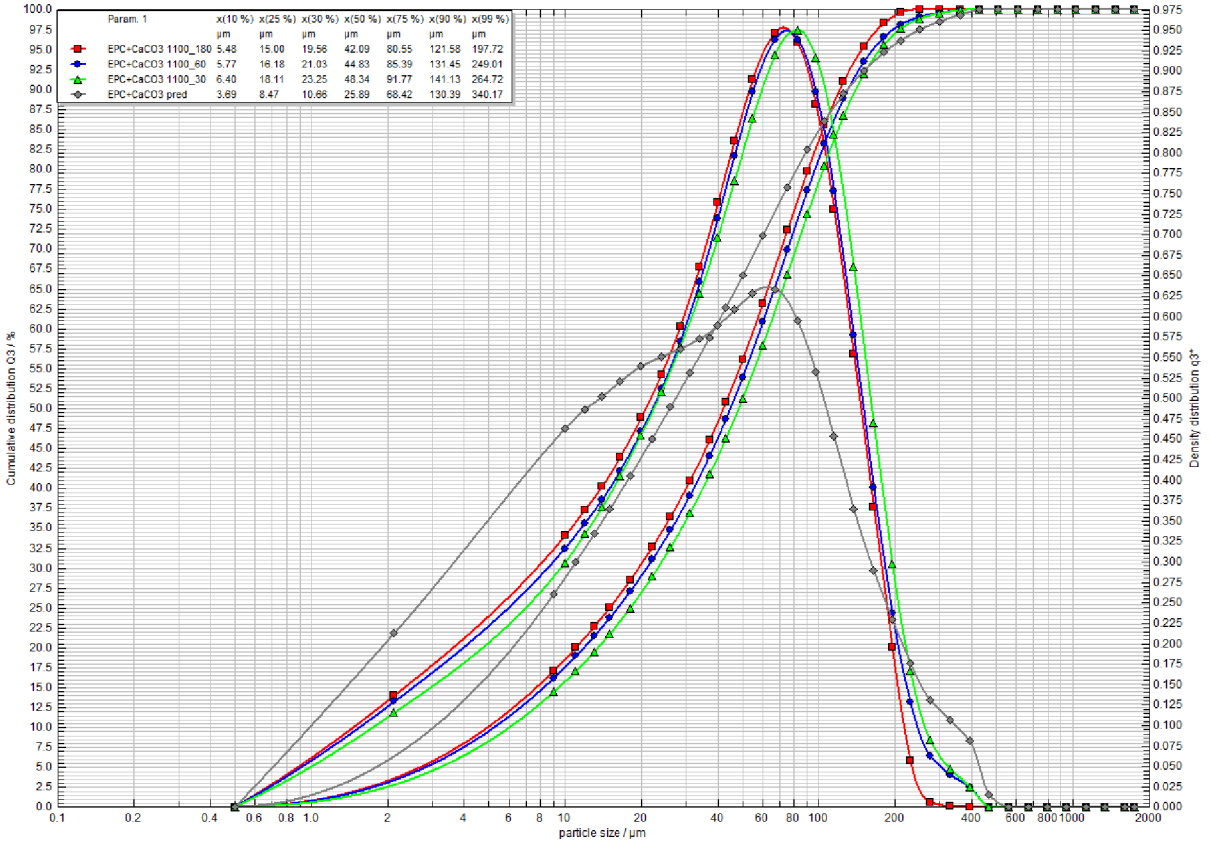

Append. 10 Particle size distribution of HTFA 1 modified with $CaCO_3$ at 1,100 °C

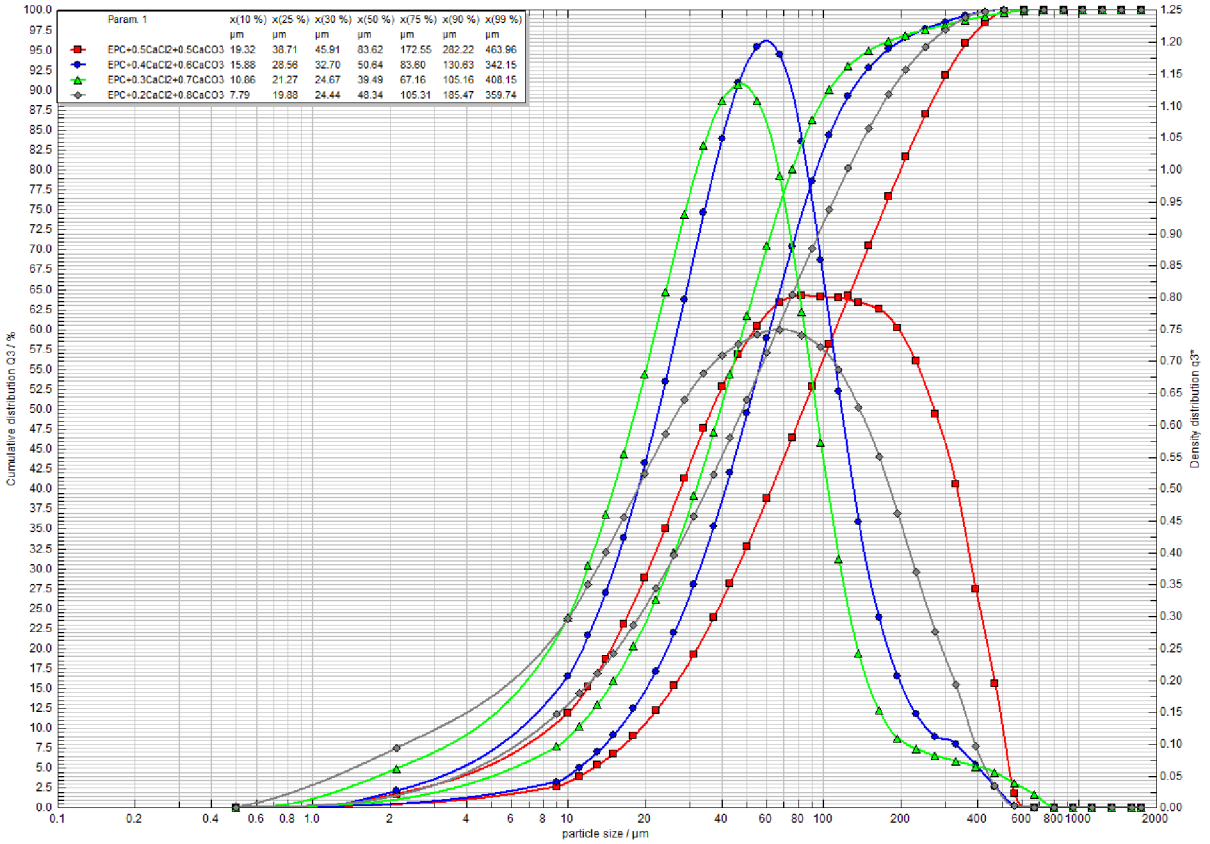

Append. 11 Particle size distribution of HTFA 1 modified with $CaCO_3$ and $CaCl_2$ combination at 1,000 °C

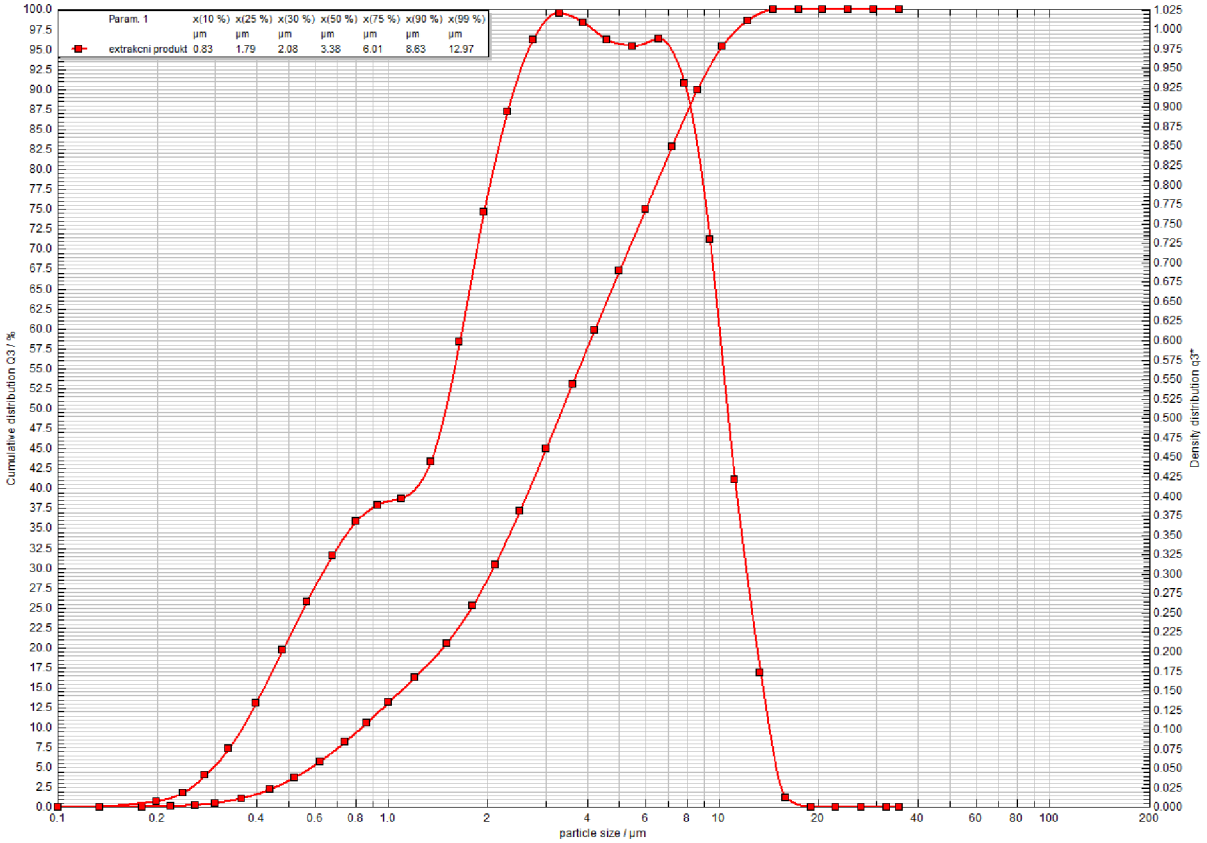

Append. 12 Particle size distribution of extraction by-product

8.2 Author's publish activity and projects participation

Publications in impact and Scopus journals

1 MARKO, M.; HRUBÝ, P.; JANČA, M.; KŘIKALA, J.; HAJZLER, J.; ŠOUKAL, F.; VOJTÍŠEK, J.; DOLEŽAL, M. Monitoring of Ion Mobility in the Cement Matrix to Establish Sensitivity to the ASR Caused by External Sources. *Materials,* 2022, y15, vol. 14, s. 1-19. ISSN: 1996-1944.

2 MARKO, M.; OPRAVIL, T.; MÁSILKO, J.; POŘÍZKA, J. Possibilities of fly ash activation in alumina recovery process. In *International Conference Building Materials, Products and Technologies. IOP Conference Series: Materials Science and Engineering.* IOP Conference Series: Materials Science and Engineering, 2019. s. 1-8. ISSN: 1757-899X.

3 BÍLEK, V.; HRUBÝ, P.; ILIUSHCHENKO, V.; KOPLÍK, J.; KŘIKALA, J.; MARKO, M.; HAJZLER, J.; KALINA, L. Experimental Study of Slag Changes during the Very Early Stages of Its Alkaline Activation. *Materials,* 2021, year 15, vol. 1, s. 1-21. ISSN: 1996-1944.

4 HRUBÝ, P.; BÍLEK, V.; TOPOLÁŘ, L.; KALINA, L.; MARKO, M.; ŠOUKAL, F.; DVOŘÁK, R.; HERČÍK, T. Decalcification resistance of various alkali activated materials. In *IOP Conference Series: Materials Science and Engineering. IOP Conference Series: Materials Science and Engineering.* Bristol: IOP Publishing, 2021. s. 1-8. ISSN: 1757-8981.

5 VOJTÍŠEK, J.; NOVOTNÝ, R.; BARTONÍČKOVÁ, E.; HRUBÝ, P.; MARKO, M.; JANČA, M. HPC Cement materials prepared by mixing under reduced pressure. In *IOP Conference Series: Materials Science and Engineering. IOP Conference Series: Materials Science and Engineering.* Telč: IOP Publishing, 2020. s. 1-11. ISSN: 1757-8981.

6 ŠILER, P.; KOLÁŘOVÁ, I.; BEDNÁREK, J.; HAJZLER, J.; MARKO, M.; ŠOUKAL, F.; OPRAVIL, T.; JANČA, M.; ZLÁMAL, M.; KOPLÍK, J.; MÁSILKO, J.; NOVOTNÝ, R.; MATĚJKA, L.; ŠVEC, J.; KUZIELOVA, E. Use of Isothermal and Isoperibolic Calorimetry to Study the Effect of Zinc on Hydration of Cement Blended with Fly Ash. *Materials,* 2020, year 13, vol. 22, s. 1-18. ISSN: 1996-1944.

7 ŠILER, P.; KOLÁŘOVÁ, I.; NOVOTNÝ, R.; MÁSILKO, J.; BEDNÁREK, J.; JANČA, M.; KOPLÍK, J.; HAJZLER, J.; MATĚJKA, L.; MARKO, M.; POKORNÝ, P.; OPRAVIL, T.; ŠOUKAL, F. Application of Isothermal and Isoperibolic Calorimetry to Assess the Effect of Zinc on Hydration of Cement Blended with Slag. *Materials,* 2019, year 12, vol. 18, s. 1-18. ISSN: 1996-1944.

Other publications

8 MARKO, M.; OPRAVIL, T.; KŘIKALA, J. *Using Sodium, Potassium and Calcium Carbonates as Fly Ash Activators to Achieve Higher Leachability of Aluminium.* Chémia a technológie pre život 25. celoslovenská študentská vedecká konferencia s medzinárodnou účasťou. Bratislava: Slovenská chemická knižnica, 2023. s. 92-93. ISBN: 978-80-8208-106-3.

9 MARKO, M.; OPRAVIL, T.; ŠOUKAL, F. *Recovery of Macro-elements From Fly Ash Using Combined Leaching Methods.* Chémia a technológie pre život. Bratislava: Slovenská chemická knižnica, 2022. ISBN: 978-80-8208-083-7.

10 MARKO, M.; HRUBÝ, P.; JANČA, M.; ŠOUKAL, F.; OPRAVIL, T. *THE EFFECT OF SODIUM IONS OF DEGRADING AGENTS IN CEMENTITIOUS COMPOSITES WITH REACTIVE AGGREGATE.* Chémia a technológie pre život. Bratislava: Slovenská chemická knižnica, 2021. ISBN: 978-80-8208-064-6.

11 HRUBÝ, P.; KALINA, L.; BÍLEK, V.; TOPOLÁŘ, L.; MARKO, M.; HERČÍK, T. *DEGRADATION RESISTANCE OF ALKALI-ACTIVATED BLAST FURNACE SLAG.* Chémia a technológie pre život. Bratislava: Slovenská chemická knižnica, 2021. ISBN: 978-80-8208-064-6.

12 JANČA, M.; OPRAVIL, T.; MARKO, M.; HRUBÝ, P.; VOJTÍŠEK, J.; DOLEŽAL, M. Studium uvolňování alkálií v pórovém roztoku. In *Vápno, cement, ekologie.* 1. Praha: Výzkumný ústav maltovin Praha, 2021. s. 79-84. ISBN: 978-80-906541-6-7.

13 MARKO, M.; OPRAVIL, T.; ŠOUKAL, F.; POŘÍZKA, J. *Wet Pre-treatment Methods in Macroelements Recovery from Fly Ash Combined with Acid Leaching.* Studentská odborná konference - CHEMIE JE ŽIVOT - sborník abstraktů. Brno: Vysoké učení technické v Brně, Fakulta chemická, Purkyňova 464/118, 612 00 Brno, 2020. s. 100-101. ISBN: 978-80-214-5920-0.

14 MARKO, M.; OPRAVIL, T.; ŠOUKAL, F.; POŘÍZKA, J. *Ash – the raw material base for the future.* 7th Meeting on Chemistry and Life 2018. Book of abstracts. 1st. 2018. s. 118-118. ISBN: 918-80-214-5488-0.

Creative activities

1 SOLNÝ, T.; TROJTLEROVÁ, L.; VAŘEJKA, Z.; ČERVINKA, P.; BÍLEK, V.; JANČA, M.; MARKO, M.; HAJZLER, J.: Lepidlo pro nepotravinářské využití; *Lepidlo pro nepotravinářské využití*. Provozovna firmy TOPCORE service s.r.o. Sušice 167, 571 01 Moravská Třebová, Česká Republika. (funkční vzorek).

2 SOLNÝ, T.; OPRAVIL, T.; TROJTLEROVÁ, L.; VAŘEJKA, Z.; HAJZLER, J.; JANČA, M.; MARKO, M.: Lepidlo se zohledněním ekonomických parametrů; *Lepidlo se zohledněním ekonomických parametrů výroby*. TOPCORE service s.r.o. Sušice 167 571 01 Moravská Třebová Česká Republika. (funkční vzorek).

3 SOLNÝ, T.; MARKO, M.; ČERVINKA, P.; VAŘEJKA, Z.; TROJTLEROVÁ, L.; HAJZLER, J.: Sypké směsi dextrinových lepidel rozmíchatelné za tepla; *Sypké směsi dextrinových lepidel rozmíchatelné za tepla*. Funkční vzorek je archivován v provozovně společnosti TOPCORE service s.r.o Adresa a kontakt na odpovědnou osobu: Ing. Zdeněk Vařejka, varejka@topcore.cz TOPCORE service s.r.o. Sušice 167 571 01 Moravská Třebová Česká Republika. (funkční vzorek).

Projects participation

1 Development of methodology for the monitoring of alkaline ions mobility in cementitious composites and assessment of the connection with the potential of the alkali-silicate reaction, zahájení: 01.02.2021, ukončení: 30.04.2022

2 Studium využití druhotných surovin pro lehké malty, zahájení: 01.03.2019, ukončení: 28.02.2020

3 Nové pokročilé materiály a materiálové technologie pro soudobé společenské potřeby, zahájení: 01.03.2023, ukončení: 28.02.2024.

4 Nové perspektivní materiály a materiálové technologie, zahájení: 01.03.2022, ukončení: 28.02.2023.

5 Příprava a charakterizace pokročilých materiálů, zahájení: 01.03.2021, ukončení: 28.02.2022

6 Pokročilé materiály a materiálové technologie, zahájení: 01.03.2020, ukončení: 28.02.2021.

7 Materiály a technologie pro 21. století , zahájení: 01.03.2019, ukončení: 28.02.2020.

8 CZ.01.01.01/01/2 2_002/0000869. Výzkum a vývoj elastického lepidla nové generacy. zahájení: 06.06.2023 ukončení: 31.12.2026.

9 SS06020247, Pucolány na bázi odpadní křemeliny, kalcinované břidlice a jílů a jejich aplikace, zahájení: 01.04.2023, ukončení: 31.12.2025.

10 FW01010021 – Prostředky pro zvýšení balistické ochrany vozidel a kritické infrastruktury, zahájení: 1. 1. 2020, ukončení: 31. 12. 2024.

11 FV40375, Cihly pokročilé koncepce s řízenými vlastnostmi, zahájení: 01.05.2019, ukončení: 31.12.2022

12 FV40379, VÝVOJ NOVÝCH EKOLOGICKÝCH LEPIDEL NA BÁZI DEXTRINU, zahájení: 01.05.2019, ukončení: 30.04.2022.

13 TH04010207, Zvýšení trvanlivosti cementobetonových krytů (CBK) pozemních komunikací omezením vlivu alkalicko křemičité reakce (ASR), zahájení: 01.01.2019, ukončení: 31.12.2022.

14 GA19-16646S Potlačení negativního vlivu zinku v Portlandském cementu pomocí akcelerátorů hydratace, zahájení: 01.01.2019, ukončení: 31.12.2022.

15 FW01010077 – Žáromateriály vyráběné sol gel technologií, zahájení: 1. 1. 2020, ukončení: 31. 12. 2022.

16 OP PIK Zvyšování bělosti kaolinu, zahájení: 01.03.2016, ukončení: 31.12.2019.